

Identification of Allosteric Ligands of *N*-methyl-*D*-aspartate receptor GluNR1: Potential Neuroprotective Treatment for Acute Ischaemic Stroke (AIS)

by

Arshnous Marandi

Thesis submitted for the degree of Doctor of Philosophy at
The University of Sheffield

30th of September 2021
Department of Neurology

Supervisors: Professor Arshad Majid, Professor Beining Chen and Dr Asad Fallah

Copyright declaration

This thesis is made available electronically by the online depository used by The University of Sheffield with permission of the authors. It can be copied and distributed on the circumstances that it is fully cited.

Date: 30st September 2021

Signature:

A handwritten signature in black ink, appearing to read 'Adam Zaid', written in a cursive style.

*Nothing is impossible,
the word itself says
"I'm possible"!*

- Audrey Hepburn

Acknowledgments

I would like to take this opportunity to thank all the individuals that have guided me through this astonishing research project and making this wonderful journey possible.

Foremost, I would like to express my sincere gratitude to my principal supervisor Professor Arshad Majid and secondary supervisor Professor Beining Chen for their constructive advice, guidance and engagement throughout the learning process of this project.

I would like to thank my industrial supervisors Dr Asad Fallah and Dr Ruhksana Quyoom for providing me with the opportunity of this PhD project at the University of Sheffield. I am forever grateful to them for opening my eyes to the world of drug discovery and encouraging me to reach for heights I did not know I could reach. I would also like to thank Dr Vishal Gulati for his insightful advice throughout the project.

Furthermore, I would also like to thank post-docs Dr Saurabh Jain and Dr Melina De felice, as well as PhD student Razan Alqarni for investing their precious time to train and mentor me during this research project.

A big thank you also goes to Professor Chen's research group, past and current members who have given me a wonderful learning experience, useful advice and long lasting friendships. In particular, Dr Antonio de la Vega de Leon, Dr Gian Marco Ghiandoni, Dr Philip Reeve, Dr Anthony Choi, Dr Luke Tattersall and James Webster.

Finally, I would like to thank my family and loved ones, who have supported me through the entire process; I am truly blessed and will be grateful forever for their love.

Abstract

Introduction: Acute ischaemic stroke (AIS) is a significant global health burden. Nearly 2/3 of stroke survivors leave hospital with a disability, costing billions of pounds per year. There is an urgent need for new therapies. Effective neuroprotective drugs can fill the significant unmet need for AIS therapies by protecting the brain during stroke and aiding recovery.

Glutamate is an important excitatory neurotransmitter in the brain that has many physiological functions including memory and cognition. It has many receptors with their own distinct signal transduction and secondary messenger systems. An important glutamate receptor is the *N*-methyl-*D*-aspartate (NMDA) ionotropic receptor which is essential for the normal physiological function of the central nervous system (CNS). During AIS, there is an excessive release of glutamate and overstimulation of NMDA receptors which leads to neural injury. Considerable preclinical data have been published demonstrating that blocking NMDA receptors with antagonists is neuroprotective. However, clinical studies have been unsuccessful partly due to unacceptable side effects caused by interference of normal physiological function of NMDA receptors. The NMDA receptor is composed of several subunits with distinct and varied function. When stimulated during ischemia, some NMDA subunits have a protective effect while others have a deleterious effect. Previous studies in our laboratory have shown that selective blockade of a short peptide region (designated P8) of NMDA subunit GluNR1 with antibodies generated by a vaccine are highly protective without side effects. However, vaccine development presents many challenges and small molecules offer simpler development pathways to the clinic. We hypothesised that targeted and selective inhibition of the same short region of subunit GluNR1 with small molecule inhibitors will also have a protective effect in AIS.

Aims: To use rational drug design and structure based virtual screening methods to identify small molecule inhibitors, which will target the short peptide sequence (P8) of the ligand binding domain of the NMDA receptor and to test these using *in vitro* and *in vivo* models.

Methodology: *In silico* methods were used to identify compounds that interact well with the peptide sequence P8 on the NMDA receptor. Several compounds were tested for their efficacy and safety profiles in a high throughput *in vivo* model of neurodegeneration using zebrafish that express mutant superoxide dismutase 1 (SOD1). An *in vitro* assay using primary cortical neurons from mice was also used to assess cell injury when exposed to NMDA excitotoxicity by the extent of lactate dehydrogenase (LDH) release. In addition, we used the high content imaging analysis system (Columbus) to assess nuclear morphology of the cells when exposed to different concentrations of the compounds in the presence of NMDA. A selection of the compounds was also tested for efficacy in a mouse middle cerebral artery occlusion model of stroke.

Results: Virtual screening was conducted on ~25,000 compounds from commercial vendors and in-house libraries. This collection was narrowed down using computational analysis to 24 compounds that interacted well with the novel site. No compounds exhibited protection in the zebrafish model and in the *in vitro* studies using primary cortical neurons from mouse. However, preliminary data for one of the *in silico* hits showed significant protection in the mouse *in vivo* stroke model.

Conclusion: The *in silico* hits selected failed to show significant neuroprotection in the zebrafish stress assay and in *in vitro* studies. However, we were able to identify an initial hit compound that exhibited marked protective effects in the *in vivo* model. The next stage will be to validate the effectiveness of the initial hit by testing the compound at different concentrations and its corresponding analogues in *in vitro* studies. Furthermore, experiments including binding assays as well as more extensive *in vivo* experiments to determine therapeutic time windows are also needed.

Table of contents

Copyright declaration	i
Acknowledgments.....	iii
Abstract.....	iv
List of figures	x
List of tables	xiii
List of equations.....	xiv
Abbreviations	xv
Chapter 1: Introduction: a literature overview on drug discovery for ischaemic stroke	1
1.1 The drug discovery process.....	1
1.2 Burden of Ischaemic Stroke	4
1.3 Pathophysiology of cell death.....	6
1.3.1 Oxidative stress.....	9
1.3.2 Inflammation processes	10
1.3.3 BBB breakdown in ischaemic stroke.....	12
1.4 Treatments for Ischaemic stroke	14
1.5 Role of NMDARs in stroke: function, regulation and initiation of excitotoxicity	15
1.5.1 Pharmacology of NMDAR	17
1.5.2 Dual nature of NMDAR	20
1.6 Small molecule inhibitors of NDMAR	25
1.7 The discovery of peptide P8 sequence on NMDAR and its significance as a potential binding site for NMDAR antagonists	33
1.8 Overall aims and objectives of the project.....	34
Chapter 2: Methods.....	39
2.1 In silico Studies	39
2.1.1 Fab model built via homology modelling	39
2.1.2 ZDOCK for P8-Fab docking.....	40
2.2 In silico docking studies.....	40
2.2.1 Protein preparation.....	42
2.2.2 Ligand preparation.....	42
2.2.3 Similarity Search with DS	43
2.2.4 ADMET	43
2.3 ZNStress Assay: Methods and Materials	45
2.4.5 The immunocytochemistry and immunofluorescence protocol for mouse primary cortical neurons	53
2.4.6 Synthesis of N-(4-fluorobenzyl)-2-(1H-indole-3-yl)-2-oxoacetamide (3000917).....	53
2.5. In vivo Methods and Material	54

2.5.1 Mice and anesthesia preparation	54
2.5.2 Solubility Methods.....	55
2.5.3 Dosage	56
2.5.4 Induction of tMCAO.....	57
2.5.5 Induction of pMCAO.....	57
Chapter 3: Computer aided drug design (CADD) to identify putative bioactive molecules for peptide 8 region of GluNR1	59
Part 1:- Predicting the interaction between peptide fragment (P8) on the GluNR1 with its polyclonal antibody via antigen-antibody docking.....	60
3.1 Introduction	60
3.1.1 Immunoglobulins (Ig): (monoclonal vs polyclonal antibody).....	61
3.1.2 Structural and physical features of Igs	62
3.1.3 Antigen-binding fragments (Fab)	65
3.1.4 Fab binding mode hypothesis	66
3.1.5 Computational approach for predicting Fab binding to P8 of GluNR1	67
3.2 Aims of part one	71
3.4 Results and discussion	71
3.4.1 Supporting studies for the antigen-Fab docking.....	71
3.4.2 Homology model: Alignment and identification of potential Fab templates	76
3.4.3 Homology model: 3D model	79
3.4.4 PP ZDOCK of the Fab model onto GluNR1	83
3.5 Limitations of antigen-Fab docking predictions and conclusion	90
Part 2:- SBVS campaign to identify small molecules compatible to the P8 region.	92
3.6 Introduction	92
3.6.1 Structure-based virtual screening (SBVS).....	92
3.6.2 Ligand-based virtual screening LBVS	93
3.6.3 Combined method: SBVS and LBVS.....	94
3.7 Docking algorithms.....	96
3.8 Scoring functions.....	98
3.8.1 Class 1: Force Field Based.....	99
3.8.2 Class 2: Empirical	100
3.8.3 Class 3: Knowledge Based	101
3.9 Aims of part two	102
3.10 Result and discussion	103
3.10.1 Selecting Crystal structure.....	103
3.11.2 Binding site identification.....	111
3.11.3 Ligand library preparation	113
3.12 Validation and supporting studies for the docking protocol.....	118
3.12.1 Quality of the docked poses.....	119
3.12.2 Performance of the scoring functions.....	125
3.13 Initial VS hits selection	135
3.13.1 Ensemble docking.....	138
3.13.2 ADMET of the molecules.....	151
3.13.3 Do Fab binding areas overlap with the binding sites of small molecules?	154
3.14 Limitations of the study	157
3.15 Conclusion.....	158
Chapter 4. Phenotypic screening <i>in vivo</i> using a high throughput zebrafish model.....	161
4.1 Introduction: Phenotypic screening	161

4.1.2 Advantages of using Zebrafish for HTS	162
4.1.3 The challenges of phenotypic screening using zebrafish	164
4.2 ZNstress assay: Zebrafish SOD1 G93R model	166
4.2.1 The role of heat shock proteins (HSPs)	167
4.3 HSP70 in ischaemic stroke.....	169
4.3.1 Screening out in silico hits using ZNstress assay	170
4.4 Aims and objectives.....	171
4.5 Results	171
4.5.1 DsRed SOD1 screen and percentage inhibition of the compounds	171
4.5.2 Measurement of toxicity in the ZNstress assay	174
4.6 Discussion	177
4.6.1 <i>In silico</i> compounds and NMDAR antagonists failed to show efficacy in the ZNstress assay.	178
4.6.2 How similar is the zebrafish GluNR1 to human GluNR1?	180
4.6.3 BBB permeability of the compounds in the ZNstress assay.....	181
4.6.4 How relevant is the toxicity reading of the zebrafish to humans?	183
4.7 Conclusion.....	186
Chapter 5. <i>In Vitro</i> assay using using primary cortical neurons.....	189
5.1 Introduction: In Vitro assay	189
5.1.1 Primary cortical neuronal cell cultures.....	190
5.1.2 Measurement of excitotoxicity in mammalian neuronal cells	194
5.2 Aims and objectives.....	195
5.3 Results	195
5.3.1 Dose response of NMDA induced excitotoxicity	195
5.3.2 Cytotoxicity of the compounds tested	197
5.3.3 Cell imaging.....	198
5.3.4 Efficacy of the in silico hits in NMDA induced cytotoxicity.	201
5.3.5 The dose response of nitrendipine, 3000917 and 3000608 against NMDA induced cytotoxicity	203
5.4 Discussion	206
5.4.1 The neuroprotection observed with nitrendipine	206
5.4.2 Selection of compounds for in vivo experimental stroke studies in mice	207
5.5 Challenges and limitations with NMDA induced cell cytotoxicity analysis	207
5.6 Conclusion.....	209
Chapter 6. Preliminary efficacy evaluation in experimental stroke	210
6.1 Rodent in vivo studies: Experimental Animal models of stroke	210
6.1.1 Impact of COVID on selection of compounds for in vivo testing.....	210
6.1.2 Blood supply of the brain	210
6.1.3 Middle cerebral occlusion (MCAO) model	211
6.1.4 Excitotoxicity and experimental stroke	213
6.1.5 Route of delivery, drug solubility and formulation	213
6.2 Solubility of our selected compounds	214
6.2.1 Nitrendipine	214
6.2.2 Diprophylline	214
6.2.3 Methocarbamol	214
6.2.4 Floxuridine	215
6.3 Safety assessment of drug formulations	215
6.4 Aims and objectives of in vivo studies in experimental stroke.....	215
6.5 Results	216

6.5.1 Nitrendipine	216
6.5.2 Diprophylline, methocarbamol and floxuridine	218
6.5.3 Efficacy against tMCAO	218
6.5.4 Efficacy against pMCAO	220
6.6 Discussion	221
6.6.1 Efficacy observed with vehicle Vc alone and in combination with nitrendipine.	222
6.7.2 Efficacy observed for compounds tested in vehicle Va	223
6.7 Limitation of the study	225
6.8 Conclusion.....	226
Chapter 7. Research limitations and future work.	228
7.1 Mechanism of action of the drugs and development of a specific binding assay.	228
7.2 The limitations of the models used and future experiments to elucidate mechanism of action of the drugs.	231
7.3 Experimental limitations.....	232
7.4 Conclusion.....	234
Chapter 8. References	235
Appendix.....	270

List of figures

Figure 1. 1 The drug development pipeline.	2
Figure 1. 2 Impact of stroke.....	5
Figure 1.3 Scheme of the pathways activated during ischaemic stroke.	8
Figure 1. 4 The barriers surrounding the brain.	13
Figure 1. 5 Structure of heterotetrameric GluNR1a/GluNR2b NMDA receptor.....	17
Figure 1. 6 The GluNR1 splicing sites	19
Figure 1. 7 Schematic representation of NMDA receptor function within normal cells and during excitotoxicity.....	23
Figure 1. 8 Antagonists developed for the NMDAR	26
Figure 1. 9 The sequences of the 18 polyclonal antibodies on the human GluNR1 subunit.....	34
Figure 2. 1. The protocol for the ZNstress assay used for the initial screening of the compounds.	48
Figure 2. 2 The solubility work flow.	56
Figure 2. 3 The MCAO models and staining of mouse brain slices from the in vivo experiment. ¹⁷⁹	58
Figure 3. 1 The differences between a monoclonal antibody (mAb) and polyclonal antibody (pAb).....	61
Figure 3. 2 The structure of immunoglobulin, PDB ID 1IGT	64
Figure 3. 3 A Fab region of the antibody (10A).....	66
Figure 3. 4 The binding of the mAb against chicken egg white lysozyme.	72
Figure 3. 5 The superimposed poses of docked confirmations with the reference bound mAb crystal structure.....	74
Figure 3. 6 The binding of query pAb with its target protein BG505 SOSIP	77
Figure 3. 7 The primary sequence of FV region of pAb query structure, templates and the homology models.....	78
Figure 3. 8 Superimposed structures of query models and homology models	80
Figure 3. 9 The Ramachandran chart of the query structure 5ACO and homology model. ..	82
Figure 3. 10 Demonstrating the 3 main clusters generated from ZDOCK.	84
Figure 3. 11 The top poses predicted for docking the 5ACO_M.M0012 binding to NR1 model 4PE5_C.	86
Figure 3. 12 The most stable predicted conformation of binding of FV to the P8 sequence of NR1 is from below.....	87
Figure 3. 13 Geometrical characteristics of top poses predicted when docking the 5ACO_M.M0012 binding to NR1 model 4PE5_C	89
Figure 3. 14 VS methods	94
Figure 3. 15 Sequence alignment and sequence identity clustering	106
Figure 3. 16 The calculated RMSD values of Human crystal structures LBD with full receptor.....	108
Figure 3. 17 Analysis of the crystal structures selected for docking studies.....	109
Figure 3. 18 Calculation of the binding sites in the human NMDAR LBD 5H8F.	111
Figure 3. 19 Analysis of the binding sites available at P8 GluNR1.....	113
Figure 3. 20 Pie charts representing of the number ligands within the libraries used for VS.	116
Figure 3. 21 Histogram graphs of molecular properties of the libraries.....	117

Figure 3. 22 Alignment of the docked glycine ligand with crystallographic ligand	120
Figure 3. 23 The RMSD values of the top 10 poses generated with Glycine molecule in DS	122
Figure 3. 24 Docking of glycerol molecule into the binding site around P8	124
Figure 3. 25 The first set of GluNR1 subunit competitive antagonists.....	127
Figure 3. 26 Results obtained from the small screening test with competitive antagonists at GluNR1.....	129
Figure 3. 27 Histograms showing the performance of the scoring functions in GOLD and DS on the kynurenic acid compound set.....	131
Figure 3. 28 The receiver operator curves generated for the analysis of scoring functions using the kynuric acid inhibitors assay.	133
Figure 3. 29 Multiple poses predicted for active and non-active molecules in the docking studies.	134
Figure 3. 30 The binding scores of the docked ligands in the four binding sites selected. .	135
Figure 3. 31 Clustering of the top scoring ligands.....	137
Figure 3. 32 Ensemble Docking procedure, align and superimpose the structures.....	138
Figure 3. 33 The binding scores obtained after the ensemble docking.	141
Figure 3. 34 The binding of 300-1113 and droperidol with GluNR1 P8 sites.....	142
Figure 3. 35 The binding of nitrendipine and 3000917 with GluNR1 P8 sites.	143
Figure 3. 36 The Binding energies of the top 27 <i>in silico</i> hits.....	144
Figure 3. 37 The ADMET absorption model.	151
Figure 3. 38 The heat map of the ADMET properties.	152
Figure 3. 39 Discovery trajectories of NMDAR antagonists. ³⁶⁸	154
Figure 3. 40 Five comparisons of how the protein interacts with the FV segment and with synthetic small molecules.....	156
Figure 3. 41 Work flow applied for P8 <i>in silico</i> hit identification. VS methods and the biological testing for identification of HIT molecules for P8.	160
Figure 4. 1 A superoxide dismutase mutant zebrafish larva at 6-day post fertilisation (dpf) after treatment with 0.1% DMSO.....	163
Figure 4. 2 A summary of the key advantages and disadvantages of using zebrafish in drug screening and toxicological studies	165
Figure 4. 3 The catalytic mechanism of intracellular Copper, Zinc SOD1 that is present in the cytoplasm of the cells.....	166
Figure 4. 4 Simple diagram showing the role of HSP70 in protein folding and protein degradation.	168
Figure 4. 5 Phenotypic screening using the mutated zebrafish (SOD1 G93R).....	169
Figure 4. 6 The efficacy of <i>in silico</i> hit molecules in the Zebrafish SOD1 Assay.	172
Figure 4. 7 No effect observed with Sc-172 at lower dose 1 μ M.....	173
Figure 4. 8 The known NMDAR modulators also failed to show any effect in the SOD1 zebrafish model.....	174
Figure 4. 9 The zebrafish larvae in the ZNstress assay.....	176
Figure 4. 10 3000-146 causing oedema in the swim bladder and yolk sac.	177
Figure 4. 11 The potential molecular mechanisms of riluzole.	180
Figure 4. 12 The BBB complex formation in three different species, human, mouse and zebrafish.	182
Figure 4. 13 The contrast between anatomical features of embryo development between the three species.	185

Figure 5. 1 A comparison of the human and mouse cortex areas.....	190
Figure 5. 2 The <i>In vitro</i> workflow demonstrates isolation, culture and assay development of cortical neurons.....	193
Figure 5. 3 The LDH assay mechanism of detection.	194
Figure 5. 4 The extent of cytotoxicity induced by NMDA in primary cortical neurons.	196
Figure 5. 5 Analysis of cytotoxicity of the test compounds in primary cortical neurons.	198
Figure 5. 6 Cell death analysis of cells tested with compounds using nuclei staining with Hoechst and PI staining techniques.	200
Figure 5. 7 Neuroprotective evaluation of <i>in silico</i> hits against NMDA induced cytotoxicity.	202
Figure 5. 8 The NMDA induced cytotoxicity assessment using nuclei staining.	203
Figure 5. 9 The nuclei count of the dose response with nitrendipine in NMDAR induced cytotoxicity assay.	204
Figure 5. 10 Nuclei count after NMDA induced excitotoxicity. Treatment with positive controls and nitrendipine at 10 μ M.....	205
Figure 6. 1 The Circle of Willis in both the human and mouse brain.	211
Figure 6. 2 Vehicle (Vc) and using nitrendipine.	220
Figure 6. 3 Infarct volumes in the pMCAO model.	221
Figure 6. 4 The proposed mechanism of NMP acting as scavenger for hydroxyl radicals	223
Figure 7.1 Schematic representation of pAb purification from serum and a competitive binding assay using ELISA assay	230

List of tables

Table 1. 1 Historically important NMDAR antagonist for ischaemic stroke.....	31
Table 1. 2 Challenges in successful vaccine development. ^{147,148}	35
Table 2. 1 The softwares used for P8-Fab docking.	39
Table 2. 2. List of software used.....	41
Table 2. 3 The ADMET descriptors used. ¹⁷⁰⁻¹⁷³	44
Table 2. 4 The compounds purchased for the screening.	45
Table 2. 5 The reagents and machines used in the ZNstress assay.....	46
Table 2. 6 Reagents and machines used for primary cortical cultures and their suppliers. ..	49
Table 2. 7 The volumes and concentrations.....	51
Table 2. 8 The concentration of NMDA from stock solution	51
Table 2. 9 The reagents and suppliers used.	54
Table 2. 10 The equipments used in the MCAO models and solubility test.	55
Table 3. 1 The different classes of Ig structures details. ²⁰¹⁻²⁰³	63
Table 3. 2 The antibodies selected for initial docking studies	71
Table 3. 3 RMSD Calculation of Reference 1MLC mAb versus the best docked mAb poses.	73
Table 3. 4 RMSD Calculation of reference 1MLC_E Antigen in the complex conformation versus the unbound antigen (1LZA) docked and in crystal structure.	75
Table 3. 5 The best matched templates identified for the pAb	79
Table 3. 6 The 20 homology models generated including their PDF and DOPE score values.	81
Table 3. 7 Docking scores, cluster groups and of the top four models for 5ACO_M.M0012 binding to NR1 model 4PE5_C	88
Table 3. 8 Analysing the protein interface of FV-NR1 ZDOCK poses.....	90
Table 3. 9 Scoring function for small molecule docking ²⁹⁴	99
Table 3. 10 Pairwise alignment of the human NMDAR GluNR1 with other species GluNR1	104
Table 3. 11 The seven crystal structures selected for docking studies and full receptor used as a reference.....	110
Table 3. 12 The co-ordinates of binding sites available in human NMDAR LBD (PDB:5H8F_B).....	112
Table 3. 13 Recommended range of molecular properties shown for CNS drugs ³³⁴	118
Table 3. 14 The poses generated and scored in GOLD	120
Table 3. 15.....	121
Table 3. 16 Superimposed RMSD and Number of Overlapped Residues (NRES) with respect to 5H8F used for ensemble docking	138
Table 3. 17 The <i>in silico</i> hit compounds from the VS campaign.	147
Table 5. 1 The advantage and disadvantage of common cell cultures used <i>in vitro</i> models for ischaemic stroke. ⁴⁶⁷	192
Table 6. 1 The solubility of the compounds selected for <i>in vivo</i> studies.....	217
Table 6. 2 Solvents used to dissolve higher dose of nitrendipine	217
Table 6. 3 The maximum amount of the compounds dissolved in Va solution.....	218
Table 6. 4 Compounds tested against MCAO.....	219

List of equations

Equation 2. 1.....	52
Equation 2. 2.....	56
Equation 3. 1.....	70
Equation 3. 2.....	99
Equation 3. 3.....	100
Equation 3. 4.....	102
Equation 3. 5.....	107

Abbreviations

Å	Ångström
ADMET	Absorption, distribution, metabolism, excretion, toxicity
AMD	Amino terminal domain
AMPA	α -amino-3-hydroxyl-5-methyl-4-isoxazolepropionic acid
ATP	Adenosine 5'-triphosphate
AUC	Area under the curve
BBB	Blood brain barrier
BDNF	Brain-derived neurotrophic factor
CADD	Computer Aided Drug Design
CaM	Calmodulin
CDR	Complementarity determining regions
CHARMM	Chemistry at HARvard Macromolecular Mechaniscs
clogP	Calculated octanol water coefficient
CNS	Central Nervous System
CREB	Adenylyl cyclase pathway (cAMP) response element binding protein
DIV	Days <i>in vitro</i>
DMSO	Dimethyl sulfoxide
DNA	Deoxyribonucleic acid
DOPE	Discrete Optimised Potential Energy score
EBI	The European Bioinformatics Institute
EC ₅₀	Half maximal effective concentration
ELISA	Enzyme-linked immunosorbent assay
EtOAc	Ethyl acetate
EtOH	Ethanol
Fab	Antigen binding fragment
FBD	Fragment based design
Fcs	Fragment crystallisable region (tail of antibody)
FDA	Food and drug administration
Fv	Variable fragment
GBMV	Generalized born with molecular volume
HBA	Hydrogen bond acceptor
HBD	Hydrogen bond donor
HMM	Hidden Markov Model
HPLC	High performance liquid chromatography
HSC70	Heat shock chaperone 70
HTS	High throughput screening
IC ₅₀	Half maximal inhibitory concentration
IgG	Immunoglobulin G
IL	Interlukine
IND	Investigational new drugs
iNOS	Induced nitric oxide synthase
i-PPI	Inhibitors protein-protein interactions
K _a	Acid dissociation constant
K _b	Base dissociation constant
K _i	The equilibrium dissociation constant
LBD	Ligand binding domain
LBDD	Ligand Based Drug Design
LBVS	Ligand-based virtual screening

LD50	Median lethal dose
LDH	Lactate dehydrogenase
mAb	Monoclonal antibody
MAPK	Mitogen activated protein kinase
MCAO	Middle cerebral artery occlusion
MHRA	Medicines and Healthcare products Regulatory Agency
MMPs	Matrix metalloproteinases
MPTP	Mitochondrial permeability transition pore
NADH	Nicotinamide adenine dinucleotide
NMDAR	<i>N</i> -methyl- <i>D</i> -aspartate receptor
NMP	<i>N</i> -Methyl pyrrolidone
NMR	Nuclear magnetic resonance
nNOS	Nitric oxide synthase
NO	Nitric oxide
Nrf2	Nuclear factor erythroid 2-related factor 2
NT	Neurotransmitter
°C	Celsius degrees
OH·	Hydroxyl radicals
pAb	Polyclonal antibody
PD	Pharmacodynamic
PDB	Protein data bank
PDF	Probability Density Function
PEG400	Polyethylene glycol 400
PIR	The International Protein Sequence Database
PK	Pharmacokinetic
pKa	The negative base10 logarithm of the acid dissociation constant of solution
pMCAO	Permanent middle cerebral artery occlusion
PSD	Post synaptic density
QSTR	quantitative structure-toxicity relationship
RMSD	Root mean square deviation
RO5	Lipinski's rule of 5
ROC	Receiver operating characteristic
ROS	Reactive oxygen species
SBD	Substrate binding domain
SBDD	Structure Based Drug Design
SBVS	Structure-based virtual screening
scFv	Single chain variable fragment
scFvs	single-chain variable fragment
SMILES	Simplified molecular input entry specification
2D and 3D	Two dimensional
TEG	Triethylene glycol
tMCAO	Transient middle cerebral artery occlusion
TMD	Trans membrane domain
tPA	Tissue plasminogen activator
Tween 80	Polysorbate 80
VEGF	Vascular endothelial growth factor
VH	Variable heavy chain
VL	Variable light chain
ΔG	Binding free energy

Chapter 1: Introduction: a literature overview on drug discovery for ischaemic stroke

1.1 The drug discovery process

Successful drug development of new medicines is complex, expensive, risky and a very lengthy process, often requiring a decade or longer.¹ Even with multidisciplinary efforts combining genomics, cheminformatics, chemistry and biology, it still has a very high attrition rate. The drug discovery pipeline is summarised in Figure 1.1. The drug candidate must demonstrate that the benefits outweigh any associated risks to be able to reach the commercial market and ultimately to the patients.

A drug discovery project starts with the understanding and characterisation of potential therapeutic targets that play a crucial part in the pathophysiology of the disease.² This also includes investigating the existing therapeutics for the target and forming the initial hypothesis that can meet the medical need for the disease. Therapeutic targets can be intracellular or on the membrane surface. Some of the most common targets include ion channel receptors, G protein coupled receptors, enzymes, transcription factors and protein-protein interactions.³ These can be identified through clinical observations and rational approaches using *in vitro* cell based mechanistic studies.

Genetic mutations in patients can also provide polymorphisms connected to the disease. Recently, data mining techniques using bioinformatics tools have been useful in identifying and prioritising potential disease targets.⁴ Target validation is performed next to demonstrate the direct link of the target to the disease pathophysiology and whether its modulation can be beneficial for patients. In some cases, this can be achieved through knock down or knock-in of particular genes in animals and examining the effect in the disease process. Other methods include RNA interference methods such as gene silencing using small interfering ribonucleic acid (siRNA) and silencing short hairpin RNA (shRNA). Other studies use knockout studies using clustered regularly interspaced short palindromic repeats (CRISPR) or zinc finger nucleases (ZFNs) and knock-in studies with viral transfections.⁵ Antibodies can also be developed for a specific target to inhibit its functions and this can allow analysis of the effect in downstream pathways.

Ultimately, target validation studies must demonstrate that modification of the target itself or its activity can influence the outcome of the illness.⁶

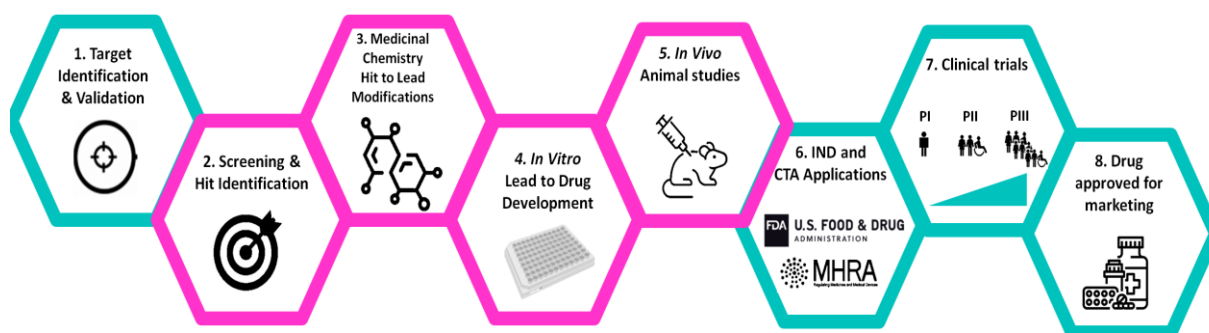


Figure 1. 1 The drug development pipeline.

The drug discovery projects initiate by gathering the current knowledge about the mechanism of the disease as well as examining the adequacy of existing therapeutics if there are any available. This will allow formation of specific hypotheses that can meet the medical need for the disease. The next step for the project would be to identify and characterise a molecule with relevant biological activity (hit molecule) in cell based studies (*in vitro*) and animal models of the disease (*in vivo*). The accumulated research data are combined to produce an Investigational New drug (IND) application for FDA or Clinical Trial Authorisation (CTA) form for Medicine and Healthcare Products Regulatory Agency (MHRA) in UK. The clinical trials are divided into three phases, Phase I (testing in healthy human volunteers for safety), Phase II (testing for efficacy in patients at different doses) and Phase III (larger trial for efficacy and safety). The combined data is once more accumulated and reviewed by the regulatory bodies prior to the approval of the drug into the market and given to doctors and the patients. (This study mainly focuses on the steps of hit identification, *in vitro* and *in vivo* studies (shown in pink)). Adapted from CMT research foundation.⁷

The screening process tests large and diverse libraries of chemicals to identify the active compounds (hits) at a given concentration. The size of the screening process can be varied depending on the objective of the project, from thousands of compounds to as many as millions, which can be tested using automated high throughput screening (HTS) procedures. The HTS can be applied for larger more drug-like ($MW \sim 500 \text{ g mol}^{-1}$) or with smaller, less complex and lower binding affinity fragments of compounds ($MW > 300 \text{ g mol}^{-1}$).⁸ These initial fragment hits can then be modified and grown into drug-like molecules through medicinal chemistry strategies, which consist of synthesising similar analogues of the initial hit molecule; to identify the pharmacophore structure of the compound and its key features that may be responsible for its biological effect.

These are the initial structure active relationship (SAR) experiments which links the chemical structure of a molecule to its biological activity.⁹ There are a diverse range of assays available to examine whether compounds can modulate their corresponding therapeutic target; 1. Phenotypic assay (measure modulation of physiological property of a cell or organism)¹⁰, 2. biophysical assays (fluorescence resonance energy transfer (FRET) for analysis of different interactions)¹¹, 3. biochemical assays (enzyme linked immune assay ELISA for detection of markers of interest) and 4. biological (cell based) assays which can measure many different features such as cell death, cell growth or morphological changes. These experiments alongside kinetic assays that examine binding affinities of the analogues of the initial hit molecules can provide data regarding potency, solubility and safety to allow further improvements that may be required for the hit to progress towards becoming a lead candidate.

Computational tools for drug design can also be utilised from hit identification to lead optimisation through initiating virtual screening of a large number of molecules against a specific biological target, discussed in detail in Chapter 3.¹² Ultimately, this screening process yields a handful of compounds with more promising activity to be investigated in more complex models that are more physiologically relevant. This process also aims to eliminate false positives, compounds that may bind to the target but fail to show any of the relevant biological effects at early stages of the drug development process.

The *in vitro* studies are cellular models performed outside of a living organism. These experiments are relatively throughput and allow evaluation of the initial lead compounds in controlled biological settings.¹³ It also provides a chance of examining the compounds efficacy and its safety at different doses. This will give an insight into the concentration at which the compound is most potent and the dose at which it is toxic.¹⁴ This data can provide the initial starting points for more complex animal testing where the drug would be exposed to a living organism (*in vivo* experiments). It is important to mention that after the identification of the *in vitro* hit molecule, further optimisations to the compound may also be introduced based on the structure activity relationship (SAR). This would allow the lead compound to be 'tailored' for maintaining or enhancing potency, efficacy and safety, which are all key features of a successful drug candidate.

The next stage is to examine if the biological effects observed in the *in vitro* model can be achieved in an appropriate *in vivo* model of the disease. The lead compound must satisfy multiple parameters such as acceptable pharmacokinetics with good absorption, distribution (e.g not a substrate for plasma binding proteins), metabolism (e.g examine if the compound is a substrate for hepatic enzymes (cytochrome P-450)), excretion rate (e.g appropriate elimination half-life) and reduced toxicity due to no off target interactions, (also known as ADMET).¹⁵ Once again, design and synthesis of new analogues of the compound may be required for optimisation of the above parameters. When successful, the accumulated research data are combined to produce an investigational new drugs (IND) application and submitted to regulatory bodies such as Medicines and Healthcare products Regulatory Agency (MHRA) in the UK or Food and Drug Administration (FDA) in US prior to initiation of clinical trials in human volunteers.¹⁶ The clinical trials in Phase I examine the drug candidate in healthy human volunteers for safety and toleration. In Phase II, the dose range and efficacy in patients are analysed. Phase III expands the trials to thousands of patients to obtain a greater amount of data for efficacy and safety. The combined data is once more accumulated and reviewed by the regulatory bodies prior to the approval of the drug into the market and given to doctors and the patients.

Overall, throughout the pipeline the researchers aim to demonstrate that the drug is able to interact with the intended target with great potency; it is not harmful to humans and is able to meet the medical needs of the targeted patients.

1.2 Burden of Ischaemic Stroke

Acute ischaemic stroke (AIS) is a devastating neurological disease. It is one of the leading causes of death and neurological disability in the world.¹⁷ In the UK it is responsible for 2/3 of patients developing a disability (Figure 1.2) and most often to an extent that they might require external care for daily tasks.¹⁷ Nearly 3/4 of all strokes occur in people over the age of 65, costing the NHS and social care £25.6 billion per year.¹⁸ Unfortunately, modern lifestyles and an ageing population further contribute to the burden of stroke.

The Aftermath of Stroke

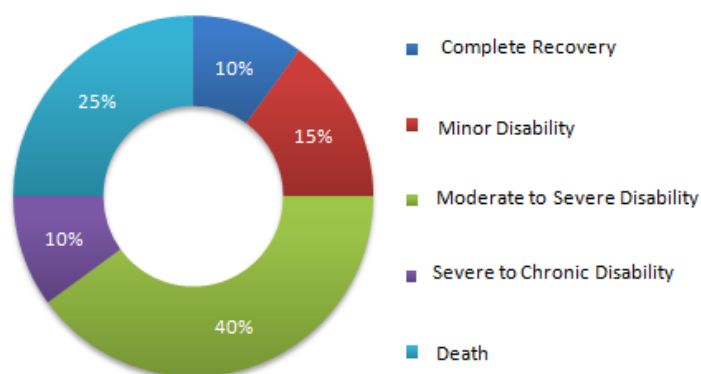


Figure 1. 2 Impact of stroke.

Stroke can result in a range of conditions and effects. This can be fatal in 25%, a severe to chronic disability in 10%, moderate to severe in 40%. Only 15% of cases result in a minor disability and only 10% result in complete recovery.^{19,20} This highlights the severity and mortality of the disease and the need for the development of novel compounds. Used with permission under the terms of the creative commons attribution licence (CC-BY).

Ischaemic stroke is the most common, accounting for 85% of cases²¹ caused by the obstruction of an artery in the brain that causes restriction of blood flow to that part of the brain.²² The remaining 15% of cases are due to haemorrhagic stroke which are caused by rupture of the artery within the brain causing bleeding around and into the brain tissue.²³

In both conditions, disruption of blood flow to the brain deprives neurons of adequate nutrients, such as oxygen and glucose that are necessary for cellular survival.²⁴ Neuronal cells are most vulnerable to ischaemic insults²⁵ compared to other supporting cells (glial and capillary cells). Ischaemic cell death is initiated within minutes of stroke onset and rapidly expands if blood flow is not restored.²⁶ The improved acute care in hospital settings and management of modifiable risk factors (e.g. hypertension, diabetes, obesity and smoking) across the western world has helped stroke mortality, from the third leading cause of death to fourth.²⁷ Although stroke death rates are in gradual decline, the incidence of stroke is still high across different age groups.²⁸ The risk of stroke multiplies each decade after the age of 55 and only 10% of the cases occur in young individuals.²⁹ Stroke is also a disease that

is influenced by multiple non-modifiable factors such as age, race, ethnicity and gender. Although these factors are uncontrollable, they allow the opportunity to identify which patients may be at more risk.³⁰

The exact symptoms of an ischemic stroke depend on what segment of the brain is affected. However, certain symptoms are common across many types of ischaemic strokes; including disturbance/loss of speech, disturbance/loss of vision and limb weakness/numbness. To reduce the chances of rapid progression and permanent brain damage from stroke, it is crucial to get treatment as soon as immediate symptoms are observed. The public and the ambulance service have been encouraged to use the acronym (FAST); Fallen Face, Arms- Inability to raise arms, Speech difficulty and Time to identify someone who is having a stroke. If these symptoms are identified, then the patient should be taken to hospital immediately with a suspected diagnosis of acute stroke.³¹

1.3 Pathophysiology of cell death

Stroke pathophysiology involves multiple cellular mechanisms. These include oedema, excitotoxicity, oxidative stress and inflammation all of which contribute to death of neurons via necrosis or apoptosis (programed cell death).³²⁻³⁴ These processes begin as soon as the cells are deprived of oxygen. The reduced oxygen levels disrupt production of adenosine triphosphate (ATP) molecules, which are crucial in many cellular functions particularly in the brain. This subsequently also leads to anaerobic glycolysis.³⁵

Initially as the amount of ATP is reduced in the cells the sodium/potassium ATPase pumps on the neuron axon stop functioning as they rely on ATP to be activated, and sodium ions accumulate in neurons. This results in water moving from extracellular space into the intracellular space into the neuron. This causes swelling of the neuron leading to cytotoxic oedema. As time progresses, the ischaemic injury can spread affecting neighbouring cells. The progression of stroke after minutes, hours and days are shown in Figure 1.3. The ischaemic penumbra region is the potentially salvageable region of the brain which is injured but is destined to die if blood flow is not restored or saved by other therapeutic means such as neuroprotection.³⁶

Excitotoxic pathways are activated by depolarisation of excitatory neurons,³⁷ which releases an excessive amount of the neurotransmitter (NT) glutamate into the synaptic cleft. In normal healthy cells, glutamate is known to contribute to learning, memory and higher functions of the CNS. It is mainly kept at restricted levels within the synaptic cleft with the presence of astroglial cell transporters excitatory amino acid transporter-2 (EAAT-2) that removes excess glutamate.

High levels of glutamate in synaptic cleft promotes activation of corresponding post-synaptic neurons. As a result, there is an increased influx of calcium ions (Ca^{2+}) through the intracellular membrane of the excitatory neurons. Excitotoxic pathways are known to contribute to early stages of stroke that result in most of the cell death.³⁸ The death of neurons can be immediate (mostly) or it can take a few days after the initial stroke insult as a result of excitotoxicity. This process also contributes to vasogenic oedema as neurons become permeable to other positively charged ions such as sodium (Na^+) and potassium (K^+) ions leading to disruption of ionic homeostasis, leading to cell death.³⁹ The influx of Ca^{2+} influx can also cause activation of downstream enzymes such as protein kinase C, cyclo-oxygenase, phospholipases and nitric oxide synthase (NOS). Subsequently, processes such as the hydrolysis of phospholipids into fatty acids, or other lipophilic substances and the breakdown of other important cellular proteins can occur.⁴⁰

Initial work of Kalia and colleagues⁴¹ demonstrated the link between glutamate and toxicity. Glutamate is the major neurotransmitter (NT) known to be released during an ischaemic insult. Glutamate is responsible for activation of the ionotropic receptors and metabotropic glutamate receptors (further details in section 1.5).

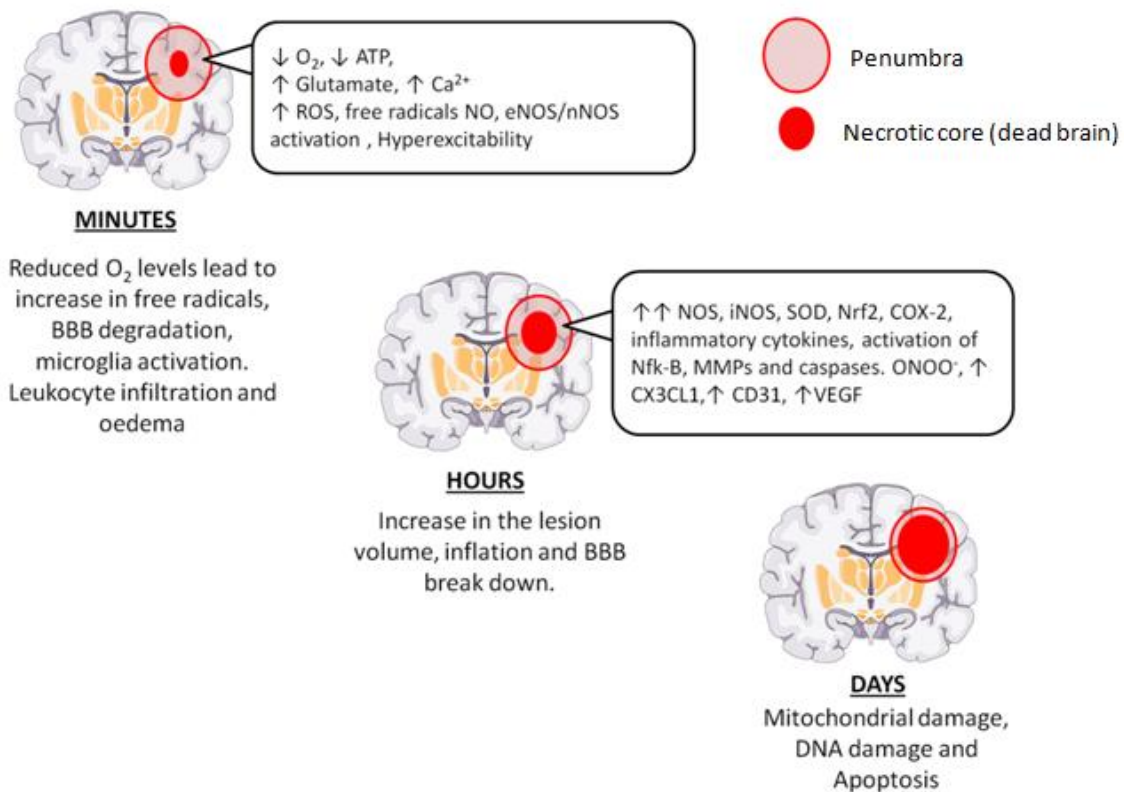


Figure 1.3 Scheme of the pathways activated during ischaemic stroke.

The different stages of a stroke involve activation of multiple cellular pathways that ultimately lead to cell death and occurs over a period of minutes, hours and days. A reduction of oxygen supply leads to reduction of ATP synthesis in the cells. There is release of glutamate which leads amongst other things, the excess Ca²⁺ influx through the NMDAR and other glutamate receptors causes activation of cell death pathways and production of free radicals. There is subsequent elevation of superoxide ions due to the mitochondrial dysfunction. During ischaemia superoxide's can also be produced from other sources such as uncoupled endothelial nitric oxide synthase (eNOS) and neuronal nitric oxide synthase (nNOS) thereby producing Nitric oxide (NO). As time progresses the inflammatory reaction is initiated and the inducible NOS (iNOS) are also elevated. An endogenous antioxidant defence mechanism can also be activated, nuclear factor erythroid-derived-2-like 2 (Nrf2) which counteracts the oxidative stress pathways in neurons, microglia and astrocytes in the penumbra, leading to some extent of protection in cerebral ischaemia by providing antioxidant and anti-inflammatory mediators for the cells in the penumbra. However, the blood brain barrier breaks down drastically due to the free radical production. Other reactive oxygen species (ROS) also activate the MMP molecules (MMP9, MMP2) that damage the basal lamina and contribute to the BBB breakdown. Image adapted from Villanueva, C⁴² and used with permission under the terms of creative commons attribution licence (CC-BY).

Ca^{2+} can act as a substrate for calmodulin (CaM) and cause activation of downstream cellular cascades, such as the synthesis of nitric oxide (NO) by neuronal nitric oxide synthase (nNOS).⁴³ NO can then contribute to large amounts of tissue damage by further reactions with superoxide radicals to produce reactive oxidants such as peroxynitrite (ONOO⁻). Other enzymes that are also triggered include proteases, calpains and calcineurins.^{43,44} Calpain has numerous substrates, for example B cell lymphoma-extra-large (Bcl-XL) that promotes apoptosis and Bax located in cytosol/mitochondria can diffuse into the mitochondria causing or resulting in release of the cytochrome c. This results in activation of the pro-apoptotic protein Bcl-2, which the disruption of the mitochondrial permeability. Thus resulting in release of cytochrome C that led to nuclear DNA degradation.⁴⁵

In ischaemic stroke, these combined events contribute to the death of the cells through necrosis, apoptosis and autophagy. The cells within the ischaemic core tend to undergo the most lethal cell death mechanism which is the necrosis. Necrosis causes the organelles of cells to expand and burst the membrane, excreting the cellular content. This activates the inflammatory responses to clear up the excreted cellular content. Excitotoxicity also contributes to triggering apoptotic processes. The cells that undergo apoptosis tend to display morphological features such as chromosome condensation, nuclear fragmentation and disruption of membrane.⁴⁶

Finally, the cells that undergo autophagy by formation of an autophagosome (a vesicle containing all the excreted damaged organelles and proteins). Subsequently, the autophagosome is then combined with lysosomes which degrade the contents within the vesicle to produce nutrients and metabolites for neighbouring cells, therefore often regarded as a cellular degradation mechanism.^{46,47} In ischaemic stroke it has been linked with the pro-survival inflammatory responses, as part of the recovery of the cells post insult.⁴⁷

1.3.1 Oxidative stress

In the infarct core, damage to the mitochondria initiates oxidative stress mechanisms. Oxidative stress in ischemic stroke is governed by production of free radicals that are extremely reactive moieties with addition of one or more electrons. These include superoxide ($\text{O}_2^{\cdot-}$), hydrogen peroxide (H_2O_2), hydroxyl radicals ($\text{HO}\cdot$) and NO.⁴⁸ These free radicals contribute to the breakdown of the cytoskeleton of cell

membranes. These groups of free radicals are classed as the reactive oxygen species (ROS) and in ischaemic events they are produced during malfunction of the mitochondria during electron transport chain. The radicals can inflict further damage to the cells by initiating other processes such as proteolysis, lipolysis and disintegration of the cell membrane.

Ahmadinejad.F *et al*⁴⁹ showed that scavengers of oxygen and hydroxyl radicals such as edaravone can block the lipid peroxidation and lipogenesis pathways. These oxidations lead to greater tissue damages and also trigger further apoptosis during ischemic stroke. During an ischaemic event, alongside the ionic and pH imbalance, the mitochondrial permeability transition pore (MPTP) causes the mitochondria to become much more permeable, releasing the ROS into the cytoplasm. This causes disruption of the mitochondrial electron transport chain and oxidative phosphorylation which is essential for ATP production.⁵⁰ This in turn also leads to leakage of cytochrome C from the mitochondria that signals the apoptosis and inflammation process that promotes cell death. The reactive nitrogen species (RNS) and ROS both contribute to protein degradation, lipid peroxidation, deactivation of enzymes and damages to the deoxyribonucleic acid (DNA).

1.3.2 Inflammation processes

Within a few hours of infarction onset, the blood brain barrier breakdown occurs and further damage to the surrounding tissue is inflicted through inflammatory responses. There is increased production of adhesion molecules (e.g P-selectin), platelet and leukocyte aggregation that cause BBB breakdown. The disruption of BBB leads to migration of immune cells into the ischaemic region which activates inflammatory mediators such as neutrophils, microglial cells (mononuclear phagocytes) and monocytes. Neutrophil accumulation and activation can worsen the neurological outcome. Hudome *et al*⁵¹ used rats to reduce the amount of neutrophils in their systems with anti-neutrophil serum to demonstrate that a reduced infarct volume can be observed with these animals in stroke. This allows initiation of necrosis that involves neutrophils to release cytokines/chemokines that further activate glial cells and cause breaking down of dead cells.

Microglia cells are responsible for scanning the brain tissue for external pathogens, plaques, damaged neurons and synapses that may cause damage to the CNS.

Microglia cells contribute greatly to inflammation pathways after stroke initiation, both activating and inhibiting inflammatory pathways.⁵² There are two main activation phenotypes of microglia cells; M1 activating inflammatory responses and M2 inhibiting inflammatory responses. M1 have shown to have cell surface marks such as cluster of differentiation 31 (CD31) and iNOS that can increase inflammatory and oxidative stress response due to greater production of NO and ROS.

NO is produced from amino acid *L*-arginine from the NO synthase (NOS) sub-types and can damage tissue under ischemic conditions. The neuronal (nNOS) activation requires calcium/calmodulin and the inducible (iNOS) can be produced through inflammatory cells such as microglia and monocytes. The transcription factors such as tumour necrosis factor- α (TNF- α), cytokines interleukin 1 β (IL1 β) and IL6 are triggered which also initiate inflammatory response through M1 microglia cells. Combined all these contribute to BBB breakdown and activation of matrix metalloproteinase (MMP-9).⁵³

M2 phenotype inhibits-inflammatory pathways by activation of cytokines such as IL4, IL10 and IL13 that promote tissue repair and wound healing. The M2 phenotypes have also been known to initiate transcription factors such as nuclear factor-kB (NF-kB), brain-derived neurotrophic factor (BDNF), neuroprotective chemokine CX3CL1 endothelial growth factors (VEGFs), mainly involving the subtype VEGF-A that can increase angiogenesis in ischemic brain and promote stroke recovery. It is important to note that whilst M2 phenotypes may be activated in the acute ischaemic insult, if the damage is not controlled it can lead to progression toward chronic insult and this results in microglial cells to move towards the destructive phenotype M1.⁵⁴

The chemokine CXC motif ligand 1 (CX3CL1) takes part in the signalling pathway which can be disrupted during stroke resulting in accumulation of microglia at the ischaemic site. Expression of inflammatory cytokines such cyclooxygenase-2 (COX-2) are also elevated. The activation of microglia cells has been shown within the ischaemic core and is initiated through excitotoxicity. In the penumbra regions it has been linked with the activation through damaged associated molecular patterns (DAMPs).⁵⁵

1.3.3 BBB breakdown in ischaemic stroke

The mammalian brain is protected by the arachnoid barrier, choroid plexus and the BBB that is made from the neurovascular unit (NVU) which consists of neurons, endothelial, basal lamina pericyte and astrocyte cells (Figure 1.4). The tight junctions in the BBB are made up of endothelial cell lining which prevents the diffusion of hydrophilic molecules and ions through the BBB. The architecture of these tight junctions are also made up of the proteins claudin and occluding zip proteins and they are connected to the cytoskeleton through accessory proteins such as zona occludens (ZO)-1, ZO-2, 7H6 and cingulin.⁵⁶ The BBB is an exclusive regulatory border that monitors the exchange of molecules, ions and cells between blood and CNS.

There is also a range of transporters located on the endothelial cells within the BBB that are essential for uptake of nutrients such as glucose through the GLUT-3, hormones and other co-factors. They also are responsible for inhibiting xenobiotics from entering the brain through efflux pumps such ATP-binding cassette (ABC) transporters (e.g P-glycoproteins (P-gp, ABCB1), the multidrug resistance family transporters (MRPs) and breast cancer resistance protein (ABCG2), (Figure 1.4, section 3).⁵⁷

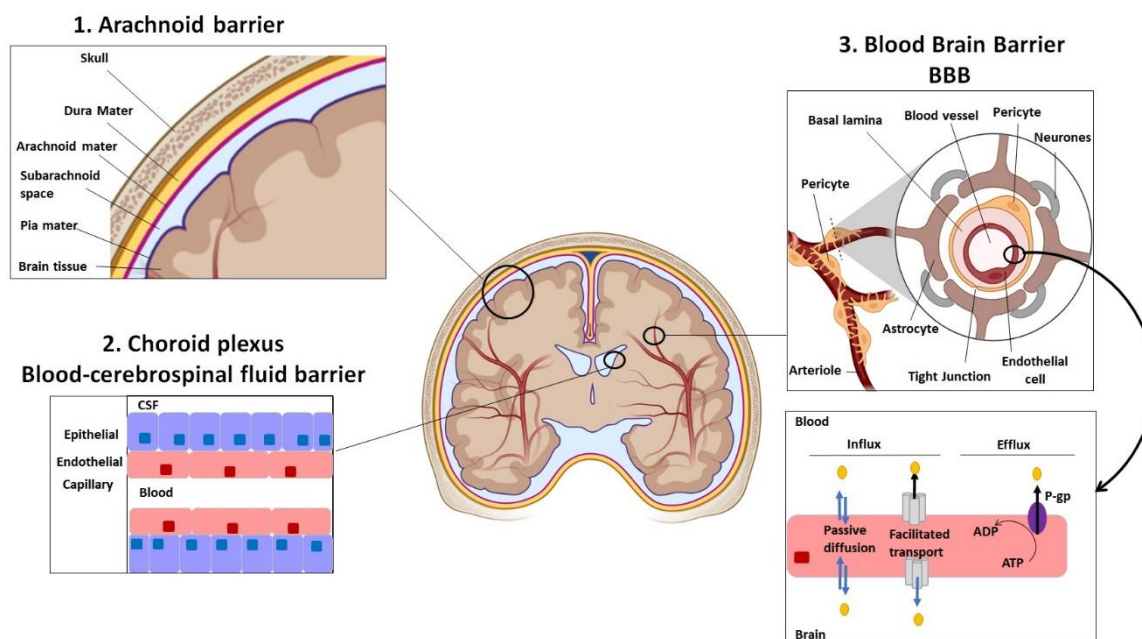


Figure 1. 4 The barriers surrounding the brain.

1) The arachnoid barrier is present around the whole skull and is made out of multiple layers covering the brain tissues. 2) The choroid plexus is made out of epithelial, endothelial and capillary cells. The blood is distributed throughout from the capillary cells. 3) The BBB is made out of the neurovascular unit (neurons, endothelial, pericytes, astrocytes and basal lamina). These cells are arranged around the blood vessel to form tight junctions. There are efflux pumps within the endothelial tissues ensuring no external xenobiotic substances can enter the brain. Adenosine diphosphate (ADP), adenosine triphosphate (ATP). Adapted from www.biorender.com Used with permission under the terms of the creative commons attribution licence (CC-BY).

Within hours of ischemia onset, the BBB breakdown is also initiated through activation of the matrix metalloproteinase 9 (MMP9) causing the extracellular fluid build-up (vasogenic oedema).⁵⁸ The breakdown of BBB is also one of the processes that contributes to further damage to the tissues in ischaemic stroke as discussed above due to neuroinflammation processes (see section 1.3.3) thus allowing immune cells into the brain.

As briefly explained above, ischemic stroke is a complex disease that consists of multiple cellular pathways which both initiate neuroprotection and neurodegeneration. However, the understanding of stroke pathophysiology is much better today and this has allowed for the progress of small molecules and other

modulators to be investigated in clinical settings, which is essential for development of better suited therapeutics.

1.4 Treatments for Ischaemic stroke

To date, the gold standard treatment for ischaemic stroke is the breakdown of the clot that has caused the obstruction of the blood flow (thrombosis) in a procedure referred to as thrombolysis.⁵⁹ Tissue plasminogen activator (tPA) (e.g alteplase, reteplase and tenecteplase) remains the only approved thrombolytic that is used in hospitals. These drugs functions as fibrinolytic, activating plasminogen to produce plasmin that breaks down fibrin and degrades the blood clot allowing restoration of blood flow to the ischaemic site.

However, the major limitation of thrombolysis is that it is most effective when given to patients within approximately 4.5 hours of stroke onset.⁶⁰ This ultimately means that the majority of patients are not suitable candidates as most do not arrive in the hospital early enough to be eligible. The American Stroke Association has reported that only 3-8% of stroke patients receive tPA,⁶¹ There is, therefore, a pressing need for new neuroprotective agents to treat approaches for ischaemic stroke patients.

Another available treatment includes surgically removing the clot (thrombectomy)⁶². Although, this is a complex surgical procedure with great risks such as causing excess bleeding in the brain that can lead to the death of the patient or damaging neighbouring blood vessels. It can also cause infections and some patients might show reactions to anaesthesia used.⁶² However, with timely intervention, the damage inflicted to the penumbra can be reduced significantly by perfusion of the blocked blood vessel. Neuroprotective treatments although still experimental; have tremendous potential as they allow the opportunity to salvage the neurons in the ischemic penumbra and even prevent the rapid damage altogether.⁶³

Preventive treatments for ischaemic stroke include management of the modifiable risk factors. For example, patients with hypertension (>139/85 mmHg systolic blood pressure/diastolic blood pressure) have more than 50% chance of suffering from stroke.⁶⁴ Therefore, use of antihypertensive drugs such as beta-blockers, angiotensin II type 1 receptor blockers (ARB), angiotensin-converting enzyme (ACE) inhibitors and calcium channel blockers are often prescribed for the primary prevention of

stroke patients. The heart outcome prevention evaluation (HOPE) trial demonstrated that the use of ACE inhibitor, ramipril for patients considered high risk of stroke (i.e. >55 year old, existing cardiovascular disease and diabetes) against placebo group of patients reduce the risk of a stroke.⁶⁵

Approximately 26% of ischaemic strokes have been also linked to non-valvular atrial fibrillation which is a form of cardiac arrhythmia. Seiffge *et al* reports that in a randomised controlled trial the anticoagulants such as apixaban, edoxaban, dabigatran and rivaroxaban can be used to reduce the risk of stroke and halves the risk of developing haemorrhagic stroke.⁶⁶ Warfarin (anticoagulant) and aspirin can also be used as an anticoagulant to reduce risk of stroke in patients. Management of the other co-morbidities such as obesity, high cholesterol and lifestyle modifications can really reduce the risk of stroke and aid long-term management of the disease.

1.5 Role of NMDARs in stroke: function, regulation and initiation of excitotoxicity

In the mammalian brain, excitatory synaptic activity is mediated largely by the amino acid *L*-glutamate with half maximal effective concentration (EC_{50} at $2.3 \mu\text{M}$)⁶⁷, which is able to activate two types of glutamate receptors. They are the metabotropic glutamate receptors (mGluR) and ionotropic glutamate receptors (iGluR). The latter group consists of three distinct families. These include α -amino-3-hydroxy-5-methyl-4-isoxazole propionic acid (AMPA receptors) containing GluA1-4, kainite receptors GluK1-5 and the *N*-methyl-*D*-aspartate receptors (NMDARs).^{68,69} The topology of the NMDAR receptor is demonstrated in Figure 1.5a. The architecture of NMDARs consists of an external amino terminal domain (ATD), ligand binding domain (LBD), transmembrane domain (TMD) and carboxyl terminal domain (CTD) which is found in the intracellular segment of the receptor (Figure 1.5b/c).⁷⁰ The CTD engages in the activation of scaffold proteins and intracellular messenger systems of the postsynaptic processes.

NMDAR are heteromeric transmembrane ion channels that are activated by both glycine or *D*-serine and glutamate binding to the GluNR1 and GluNR2 sites, respectively (Figure 1.5b). Both AMPA and kainite receptors can be activated solely by a single *L*-glutamate molecule and form functional homotetrameric channels. NMDAR has been shown to play a crucial role in transmission and plasticity of

excitatory signals of the central nervous system (CNS). NMDARs are mainly expressed in the CNS, however, they have also been observed in external tissues such as the heart,⁷¹ pancreatic islet beta-cells, lymphocytes⁷² and bones.⁷³ Neuronal injury caused by excitotoxicity is due, at least in part, to over stimulation of ionotropic glutamate NMDA type receptors. In 1984, Simon *et al.*⁷⁴ were the first to propose that inhibition of NMDARs can protect neurons from ischaemic insults and it is now emerging that their participation in excitotoxic mechanisms during ischaemia is more important than other processes such as voltage-gated calcium channels or non-NMDA receptors.⁷⁵ This has led to the advancement of the hypothesis that there is a direct pathway to neurotoxicity triggered by NMDARs.

The role of NMDARs in the pathophysiology of stroke has been the focus of considerable research. Extensive clinical data supporting their role in excitotoxic pathways is available. It therefore follows that NMDAR antagonists are predicted to be beneficial in the management of acute ischaemic strokes.⁷⁶

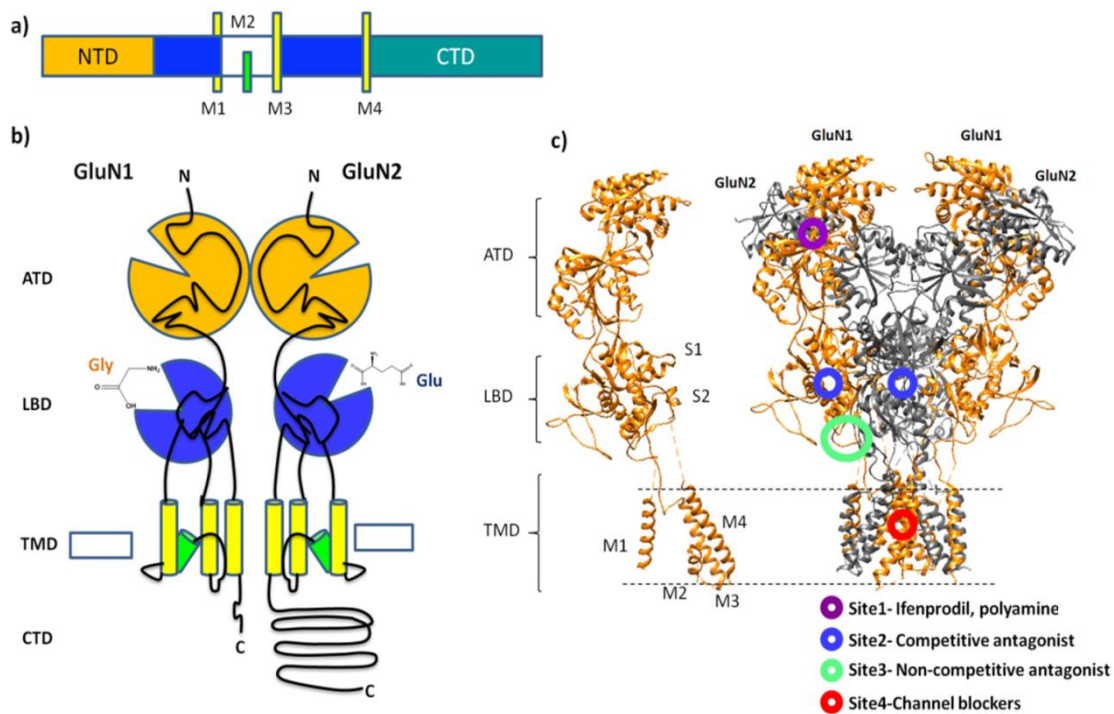


Figure 1.5 Structure of heterotetrameric GluNR1a/GluNR2b NMDA receptor

1.5a) Topology of generic glutamate receptor subunits with amino terminal domain (ATD), the four (M1-4) membrane binding domain (MBD) and carboxyl terminal domain (CTD), **1.5b)** Molecular organisation of homodimers form of GluNR1/NR2 subunits. **1.5c)** protein data bank (PDB) (4PE5) | crystal structure of GluNR1 (in orange) and GluNR2 (in grey), Left-demonstrating the two extracellular clam shell like domains, with amino domain (ATD) and ligand binding (LBD) containing upper S1 and lower S2 linked to the ion pore formed between membrane helices that are connected to the carboxyl terminal domain (CTD). The position of NMDAR antagonists for ischaemic stroke is also presented with coloured circles throughout the receptor.

1.5.1 Pharmacology of NMDAR

In excitatory synapses, NMDARs are found in the postsynaptic membrane, where they are arranged in a multi protein structure referred to as the postsynaptic density (PSD). Like many receptors, the function of NMDARs correlates with its subunit structure and assembly. The most common receptor type located in the forebrain of excitatory neurons is the GluNR1/GluNR2a/GluNR2b subunits. The NMDARs can be found on channel pores which are gated in a voltage dependent and ligand manner. The LBD contains upper S1 and lower S2 regions that are linked to the pores formed in between membrane helices. In healthy cells, NMDAR membrane potential is

brought to a resting state by a single magnesium ion (Mg^{2+}) that binds into the pore of the receptor, thus preventing the flow of positively charged ions (Ca^+ and Na^+) into the cells. This results in a large number of receptor types that show unique function in physiological function in *in vivo* studies.⁷⁷

This function has also been linked with alternative splicing and RNA assembly of iGluR complexes.⁷⁸ NMDARs heterotetramer structures contain two GluNR1 subunits which are mandatory subunits present in all receptors and two variant GluNR2ad and/or GluNR3a,b subunits (Figure 1.6a). In the hippocampus which is a critical part of the brain that deals with memory and cognition, as neurons age the GluNR1/GluNR2b receptors are converted into extra-synaptic receptors, allowing GluNR1/GluNR2a,b to become the main synaptic receptors in the hippocampus and forebrain. The glycine binding subunit GluNR1 exists as 8 spliced variants (GluNR1a-1a/4ay and GluNR1-1b/4b) of a single gene, as coded by the post-transcriptional RNA protein.^{79,80} The presence and absence of a sequence of 21 amino acids, GluNR1:exon5 (Figure 1.6c) in the NTD and the variation in exons 21 and 22 which governs the altered CTD region C1,C2 and C2' (Figure 1.6b).

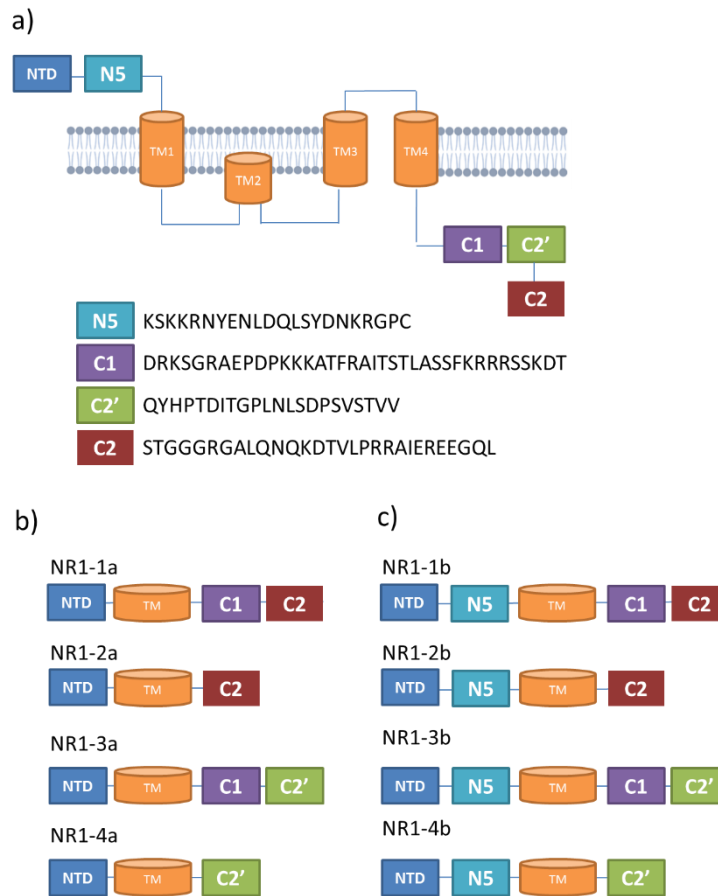


Figure 1. 6 The GluNR1 splicing sites

1.6a) The location of the splice variation in the receptor and the sequence of each exon. **1.6b)** The splice variation of GluNR1-1a-4a are demonstrated and **1.6c)** showing is the GluNR1-1b-4b isoforms. Figure adapted from Flores *et al*⁸¹ used with permission under the terms of the creative commons attribution licence (CC-BY).

The location of NMDAR in the cell membranes are controlled by the exons on the CTD. The exon 21 at C1 has Ser890 that can be phosphorylated using protein kinase C that leads to distribution of GluNR1 subunit and is reversed by dephosphorylation of the same amino acid. Moreover, it is also a site for the interaction with calmodulin kinase which reduces NMDAR activity.⁸² The C2' sequences in the CTD interact with postsynaptic density-95 discs large zonula occludens-1-binding motif (PDZ) that regulates the NMDAR forming clusters on the cell surface. C2 and C2' sites can also influence synaptic activity and result in a link between activity of the receptor and the subunit expression in postsynaptic neurons. Interestingly, the variety seen in C2' and C1 (exon 21) have a greater variability in

different species such as in fish and in birds which suggests that the number of NMDAR on synapses vary considerably in different animals.⁸³ The GluNR2 and GluNR3 subunits are formed as a product of the four genes that govern most of the structural basis for the heterogeneity in NMDARs and a greater number of the native NMDARs are triheteromeric. The GluNR2 subunit has also varied forms within the CNS that can change during development. It has much more complex CTD in comparison to GluNR1 and is also been linked with modulating the receptor's expression on the cell membrane.

The predominant subtypes in the adult brain are the diheteromeric GluNR1/GluNR2a, GluNR1/GluNR2b or triheteromeric GluNR1/GluNR2a/GluNR2b which are located on the cortex and hippocampus. Hansen *et al*⁸⁴ examined the activation of the GluNR1/GluNR2a/GluNR2b using transfected HEK293 cells by using selective GluNR1/GluNR2a antagonist ifenprodil, traxoprodil and TCN-201. The alternative subtypes such as GluNR1/GluNR2c, GluNR1/GluNR2d, GluNR1/GluNR2a/GluNR2c, GluNR1/GluNR2b/GluNR2d and GluNR1/GluNR3a occupy the striatum and cerebellum regions.⁸⁵ Interestingly, the GluNR1/GluNR2c are only expressed late in the development of the neurons.⁸⁶

Despite the diversity observed in NMDAR subunits, currently most investigations heavily rely on antagonists and modulators of GluNR1/GluNR2a or GluNR2b diheteromeric forms. This could be the reason why the exact physiological functions of the triheteromeric subunits are not fully understood. These alternative subtypes of NMDAR can provide the receptor with distinct pharmacological and electrophysical properties.⁸⁶

1.5.2 Dual nature of NMDAR

1.5.2.1 NMDAR promoting neuron survival pathways

In a healthy neuronal cell, neurotransmission mediated by NMDARs is essential for development and normal function of the mammalian brain. They are involved in complex functions of the brain such as learning, problem solving and memory storage.⁸⁷ In addition, due to the intricate nature of the brain and its function, NMDARs are amongst the receptors with central roles in many different cellular

mechanisms,⁸⁸ capable of promoting and preventing cellular survival (Figure 1.7a). Yan *et al.*⁸⁹ first reported the dual nature of NMDARs *in vitro* when they noticed changes in receptor activity when exposed to different antagonists. For example, in neuronal granule cell cultures small doses of *N*-methyl-*D*-Aspartate (NMDA) and amino 5-phosphonovaleric acid both increased neuronal survival, however in the same conditions a higher dose caused the opposite effect, leading to neuronal death.

In vivo studies carried out by numerous laboratories were also consistent with these findings and showed that complete NMDAR inhibition or genetic deletion causes extensive neuropathy in rodents.^{90,91} R.Chittaiallu *et al*⁹² confirmed this by demonstrating NMDARs, depending on its location in the CNS, can take part in both neuroprotective and neuronal injury as discussed in section 1.5.1.

In normal healthy cells the EAAT-2 are responsible for removing excess glutamate released by the postsynaptic neurons and therefore allow control signal conduction. There have been a number of neuronal survival pathways linked with the activation of the NMDAR. For instance, the extracellular signal-regulated kinase 1 and 2 (ERK1/2) or mitogen-activated protein kinase (MAPK) downstream cascade. This process facilitates cell functions such as cell growth, differentiation and adhesion.⁹³ In 1997, English and Sweatt⁹⁴ were first to examine ERK1/2 pathways in rat hippocampal cells and were able to show NMDAR activation was crucial for long term potentiation by increasing the high frequency of active potentials and causing their function in synaptic plasticity. Activation of NMDARs is responsible for promoting the survival pathways for neurons in stroke such as the Akt kinase/phosphoinositide-3-kinase (PI3K).⁹⁵ This process is crucial for functions such as cell growth, movement, differentiation and proliferation.

In addition, Akt also promotes neuron survival through phosphorylation causing inactivation of the glycogen kinase-3- β (GSK3- β). This ensures that the heat shock factor protein 1 (HSF1) can be activated and allow transcription of cytoprotective heat shock proteins (HSP). HSP; forexample HSP70 acts as chaperones to help with regulation, folding and degradation of cellular proteins which are part of cellular recovery process.⁹⁶ Miyawaki *et al*⁹⁷ in 2008 demonstrated that blockade of the PI3K with selective PI3K inhibitor LY294002 can interfere with the downstream

function of Akt phosphorylation, preventing neuroprotection and increases the damage to the neurons in ischaemic conditions, a further summary of this process is shown in Figure 1.7 where the dual nature of NMDAR demonstrates the opposite effects of both a role in neuronal survival and neuronal apoptosis and the pathways involved. Akt causes phosphorylation of different targets such as glycogen synthase kinase 3 β , forkheadbox proteins (FOXO) and Bcl-2 associated agonist of cell death (BAD), shown in Figure 1.7a. This prevents the mitochondrial cytochrome c release and caspase activation. In addition, activation of Akt also prevents the elevations of p53 upregulated modulator of apoptosis (PUMA) and therefore this contributes towards cell survival.⁹⁸ The other pathways that promote survival such as brain-derived neurotrophic factor (BDNF) are initiated by the synaptic NMDARs causing activation of the cyclic adenosine monophosphate response element-binding protein (CREB).⁹⁹

On the other hand, the opposite was observed in the extra-synaptic NMDARs where suppression of BDNF was promoted, leading to mitochondrial dysfunction and increased levels of nitric radicals, causing death of the neurons, demonstrated in Figure 1.7b.¹⁰⁰ In addition, the high concentration glutamate released in the synaptic cleft leads to hypoglycaemia and hypoxia resulting in excessive calcium ions entering the mitochondria and causing the loss of mitochondrial membrane potential (Ψ_m). This in turns lead to initiation of toxic ROS production processes as ATP production is also reduced, causing release of cytochrome c giving rise to apoptotic pathways.¹⁰¹

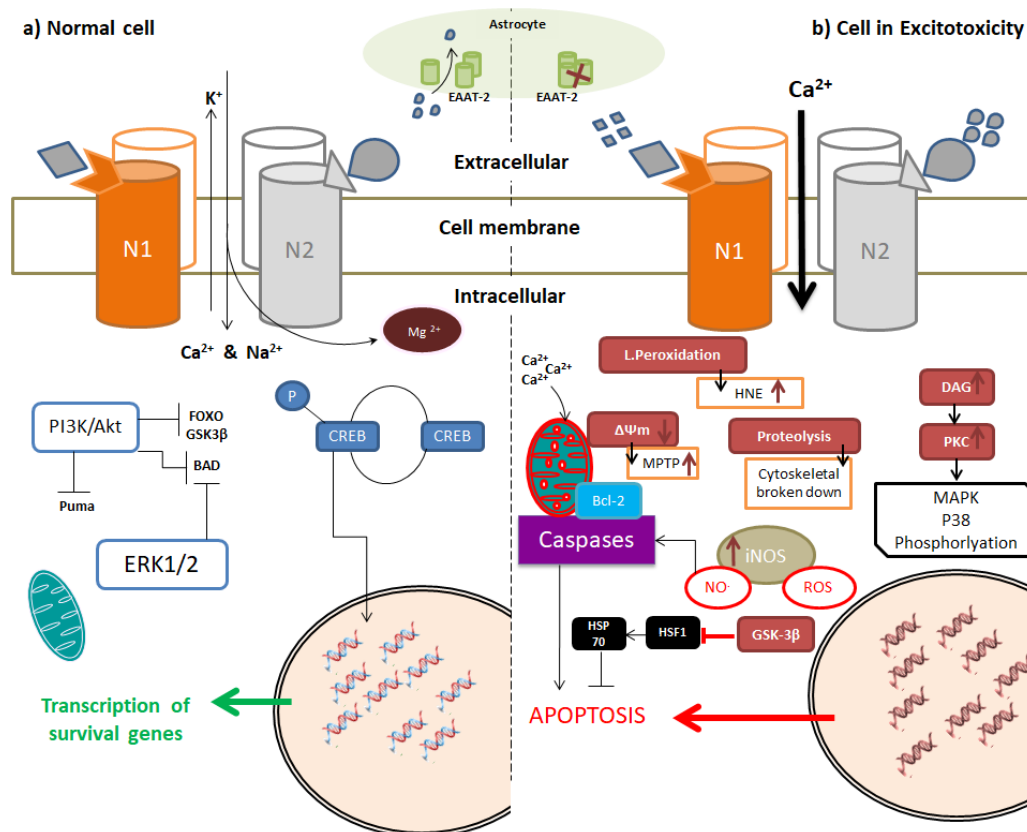


Figure 1. 7 Schematic representation of NMDA receptor function within normal cells and during excitotoxicity.

(1.7a) Stimulation of NMDAR causes the initiation of subsequent pathways that lead to transcription of pro-cell survival genes. When stimulated they allow slow channel opening and influx of cations, (Ca^{2+}) in the intracellular space, that initiates complex biological pathways for higher functions of the CNS. At rest, external magnesium ion (Mg^{2+}) enters through the NMDAR, binding tightly to the pore and preventing further ion permeation. The synaptic NMDAR promotes the activation of the PI3K/Akt. This prevents the activity of GSK-3 β by numerous mechanisms that cause inhibition of the pro survival transcription factors CREB and heat shock protein-1, the neuroprotective chaperon can reduce ischaemia induced apoptosis but also involved in reducing the inflammatory effects produced through the NG-kB. **(1.7b)** Hypoglycemia and hypoxia can lead to energy failure which causes excessive stimulation of the excitatory glutamatergic system. As a result the NMDAR becomes over activated, causing an excess Ca^{2+} influx into the cells and initiating the complex biochemical cascades that ultimately lead to damage to lipids, proteins and DNA. . The extrasynaptic NMDAR causes inhibition of activity from ERK1/2, Jacob and CREB pathways. In turn they promote the FOXO and cause deregulation in the mitochondrial membrane potential (Ψm).¹⁰²

Key:  Glycine,  Glutamate  Mitochondrion,  ROS (reactive oxygen species), EAAT-2 (excitatory amino acid transporter), HNE (4-hydroxynonenal), FOXO (forkhead box transcription factors), BAD (Bcl-2 associated agonist of cell death), PUMA (p53 upregulated modulator of apoptosis), iNOS (induced nitric oxide synthase), Bcl-1 (B-cell leukemia line), PKC (protein kinase C), MAPK (mitogen activated protein kinase), DAG (diacylglycerol), HSF1 (heat shock factor protein 1), HSP (Heat shock protein), GSK-3 β (Glycogen Synthase Kinase 3 β), Ψm (mitochondrial membrane potential).

1.5.2.2 NMDAR promoting neuronal death pathways

In the ischemic brain the GluNR2b-PSD95-nNOS are coupled together initiating multiple apoptosis pathways. For example, this complex can, through nitric oxide synthase (nNOS), initiate the production of damaging radicals such as peroxynitrite that is able to cause severe DNA damage to the cells. nNOS can also stimulate the mitogen-activated protein kinase (MAPK) p38.¹⁰³ The cysteine protease and calpain is Ca^{2+} dependent. The dexamethasone-induced Ras protein has also been shown to interact with nNOS, which can manipulate Dexras1 and cause reduction of downstream iron transport and increase neurotoxicity. The high concentrations of Ca^{2+} through the NMDAR also causes phosphorylation of the death-associated protein kinase 1 (DAPK1).¹⁰⁴ This leads to p53 nuclear translocation to be initiated and causes death of the neuron. Further studies are required to understand the exact mechanism of action of the peptide and its overall influence in excitotoxic pathways. Although, to some extent the NMDAR subtypes can be responsible for the dual nature of the receptor in the CNS and ischemic brain, there are other potential hypotheses to address the questions about the downstream pathways activated by the receptor. Location of the receptor, synaptic or extrasynaptic can also influence function (see above).

Extrasynaptic NMDARs promote cell death pathways. Hardingham *et al*¹⁰⁵ discussed the benefits of weaker GluNR2b selective inhibitors as they were more likely to inhibit the extrasynaptic NMDARs and maintain better safety profiles in clinical trials. It would be interesting to investigate into methods that can enhance the NMDAR-mediated cell survival signalling pathways that would also be beneficial therapeutically as few studies have investigated this alternative approach. This data suggests that complete and permanent inhibition of NMDARs can be harmful for the developing and developed adult brains. This may explain why reversible antagonists (e.g memantine) are clinically more tolerable in neurological disorders such as Alzheimer's disease.¹⁰⁶ Memantine is neuroprotective in stroke and has ability to reduce infarct volume when tested using *in vivo* models. However, clinical studies are needed.

Whether the synaptic and extrasynaptic NMDARS can perform as two functionally distinct receptors is still debatable. Choi¹⁰⁷ suggested that during excitotoxicity, the concentrations of glutamate can be so great (above the approximate levels in the tissue 15mmol/kg) that the majority of Glutamate receptors are activated irrespective of their location. Going forward, greater understanding of the function of synaptic and extrasynaptic NMDAR would allow better design of subunit selective antagonists that may also demonstrate greater differentiation between the cell survival and death pathways.

1.6 Small molecule inhibitors of NDMAR

Due to the pivotal role that NMDARs play in excitotoxic pathways of stroke, there has been much research interest in developing small molecules that can modulate these receptors.¹⁰⁸ Simon *et al*¹⁰⁹, demonstrated that inhibition of the NMDAR with 2-amino-7-phosphonopheptanoic acid (APH) can be neuroprotective in ischemic brain damage *in vivo* by using transient global ischaemia (TGI) model in rats. From these initial studies, much effort has been placed into developing NMDAR antagonists in diverse animal models of ischaemic brain to identify the drugs suitable for humans. From these global efforts it was clear that NMDARs contain multiple binding sites that can be modulated with small molecules and change the receptor activity (Figure 1.8). Ligands were designed for the same site as the neurotransmitters (glycine and glutamate) acting as competitive inhibitors such as gavestinel and selfotel. There were also other known binding sites for example the polyamine site on the GluNR2 that accommodates traxoprodil. The Zinc ion binding site is at the NTD of GluNR1a site. The other binding sites identified included the phencyclidine (PCP), the site that MK801 and memantine bind to and below that region the Mg²⁺ ion binding site that regulates the receptor in a voltage dependent manner.

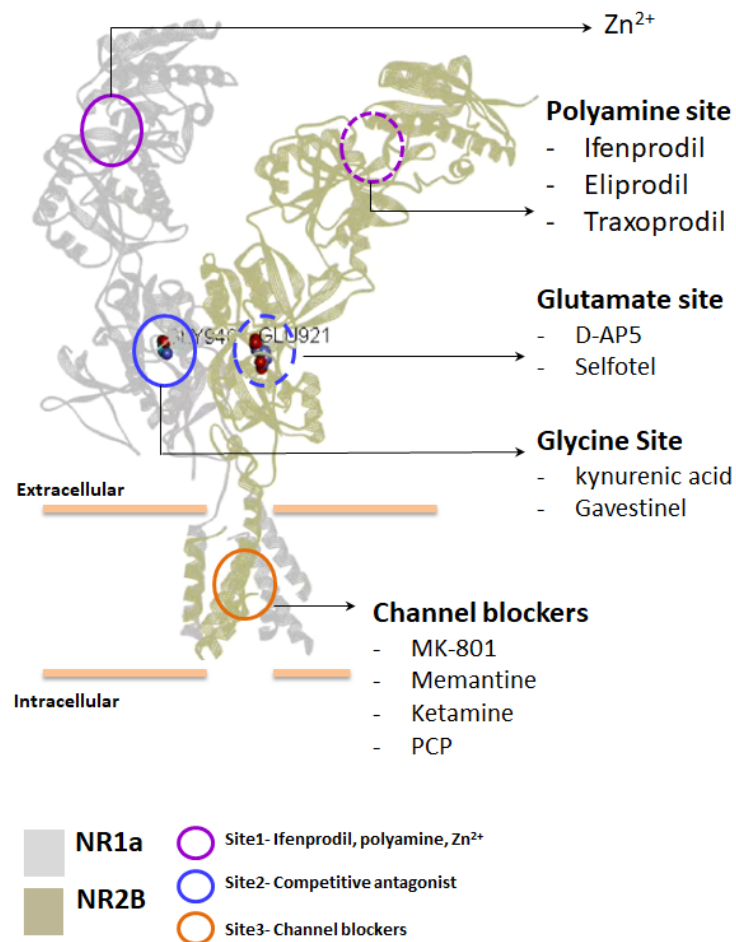


Figure 1. 8 Antagonists developed for the NMDAR

The crystal structure of NMDAR represents the two main subunits GluNR1 (grey) and GluNR2 (flaxen), (PDB:4PE5). The GluNR1 inhibitors have been shown from allosteric site binders at the *N*-terminal domain, Zn²⁺ and competitive antagonists at the LBD such as kynurenic acid and gavestinel. For the GluNR2 inhibitors the allosteric site binders include polyamines and competitive antagonists such as 2R-amino-5-phosphonovaleric acid (D-AP5) and selfotel. The Mg²⁺ is bound at the inner pore of the receptor blocking the entry of Ca²⁺ at the resting state of the receptor. There have also been channel blockers developed for the receptor that can also exhibit their therapeutic effect by binding in the inner pore of the receptor.

MK-801 (dizocilpine), discovered by Merck in 1982 was one of the initial inhibitors for NMDAR. It is a potent channel blocker antagonist of NMDAR with half maximal inhibitory concentration (IC₅₀) of 18 nM and the equilibrium dissociation constant (K_i) of 0.743 μM.¹¹⁰ MK801 was shown to easily cross the BBB and was found to exhibit anti-convulsive and anaesthetic properties as well. However, further research showed that it was also linked with an increase in brain lesions in animal models, as well as adverse effects such as psychotic and cognitive dysfunctions.¹¹¹

As a result, an alternative analogue, ketamine was developed with an IC_{50} of 0.35 μM and K_i 0.25 μM .¹¹² Ketamine acts as a channel blocker, but with a shorter half-life in the human body. In addition, it was much better tolerated and safer in clinical trials showing anesthetic, analgesic and less psychotic effects, therefore approved for surgical procedures.¹¹² The main side effects of ketamine include problems with memory and delusions and neurotoxicity at higher concentrations. Currently, a phase II clinical study is underway. QUEST-KETA investigates the efficacy of ketamine in ischaemic stroke patients to determine if it can lower disability in a randomised trial.¹¹³ However, in the past most clinical trials of NMDAR antagonists (belonging to different compound classes), even at alternative binding sites of the receptor, have ended prematurely due to severe side effects or lack of efficacy in the larger clinical trials. Furthermore, some of the antagonists had displayed unacceptable side effects such as confusion, paranoia, hallucinations and severe motor dysfunction.¹¹⁴ The chemical structures, animal models and stages of clinical trials for some of the significant inhibitors mentioned are summarised in Table 1.1.

For example, aptiganel (CNS1102), is a diarylguanidine that was another channel blocker developed by Cambridge Neuroscience as a potential drug for stroke. Reddy *et al*¹¹⁵ reported the potency of the ligand in an *in vitro* assay using radioligand competitive binding assay with [3H] MK801 on rat and guinea pig brains. In this study they were able to demonstrate the SAR of these analogues, where the unsymmetrical diarylguanidines, specifically substituted with the naphthyl had greater affinity for NMDAR, IC_{50} 36 nM.

In the animal model of temporary focal ischaemia in rats, aptinagel was able to demonstrate protection from ischaemic injury.¹¹⁶ However, despite the promising preclinical results it failed the clinical trials due to lack of efficacy. In addition it also demonstrated side effects such as hallucination and high sedation. The glycine site antagonists gavestinel (kynurenic acid derivative), IC_{50} of 0.038 μM ¹¹⁷ developed by GlaxoSmithKline and licostinel (dihydroquinoxaline), IC_{50} of 5 nM¹¹⁸ developed by Acea pharmaceutical both failed to show efficacy in the larger stroke clinical trials.

119,120

The competitive antagonists at the GluNR2 subunit selfotel (IC_{50} 50 nM) and D-AP5 (IC_{50} 0.46 μ M) demonstrated severe side effects such as psychotomimetic, motoric and cognitive problems. SAR studies had shown that the larger carbon ring structures (e.g eight membered ring) had poor activity. This was also observed for the length of the side chain as larger aliphatic chains resulted in poor NMDAR affinity.¹²¹ In addition, substitution of the electronegative phosphoric acid group with tetrazole or carboxylic acids were shown to not introduce any improvements to the activity of the drug. Selfotel at 40mg/kg was able to reduce the infarct volume in rats by 50%. However, in the phase III clinical trials, the injection of 1.5mg/kg dose failed to improve the outcome for the patients within the six hour onset of stroke. Moreover the trial was terminated due to the high mortality rate observed (22%) in comparison to the placebo group (17%).¹²²

As time progressed, further knowledge about molecular biology and subunit composition of NMDAR was obtained. The GluNR2b subunits were predominantly located in the forebrain in comparison to cerebellum and limbic system. Ifenprodil (IC_{50} 40 nM), a phenylethanolamine was discovered to potently inhibit the GluNR1/GluNR2b subunit by binding to the N-terminal domain of the subunit. Furthermore, it was able to demonstrate neuroprotective effects in animal models of global and focal brain ischaemia. Mott *et al*¹²³ found out that the ifenprodil is more neuroprotective in acidic pH than within a neutral pH (7.4). This was interesting as during an ischaemic event the brain tissue affected would also have lower pH in comparison to healthy tissue of the brain. However, it demonstrated poor solubility which led to synthesis of alternative analogues of the compound such as eliprodil and traxprodil.

Traxprodil (IC_{50} 3.9 nM) was developed by Pfizer and Synthelabo.¹²⁴ Traxprodil was found to be more potent than ifenprodil (~1.7 fold greater). Its structure varies from ifenprodil by containing an additional hydroxyl group thereby increasing its water solubility. In addition, traxprodil was further stabilised in the pocket of NTD binding site with polar interactions such as hydrogen bonding of hydroxylgroup with the Asp236.^{125,126}

Although traxprodil showed much greater potency and solubility it was unfortunately unsuccessful in clinical trials for stroke as it demonstrated abnormal heart rhythms by prolonging the QT electrocardiographic measurements in patients.

A successful small molecule inhibitor of NMDAR is memantine (adamantine derivative) developed by Eli Lilly in 1968. Memantine was approved by FDA in 2003 and is mainly used to alleviate symptoms for patients with moderate to severe Alzheimer's disease, improving their mental cognition.¹²⁷ It functions as an "open channel" blocker, as it can inhibit the NMDAR only when it is activated. Although, similar to ketamine, memantine has not shown any subunit selectivity for NMDAR inhibition, its binding site is known to overlap with the Mg^{2+} .¹²⁸ It is a relatively weaker NMDAR inhibitor with IC_{50} 2.099 μ M, K_i value of 1.14 μ M. In preclinical studies of ischaemic stroke, memantine had demonstrated neuroprotection *in vitro* studies and animal models of stroke, reviewed in detail by Seyedsaadat *et al.*¹²⁹

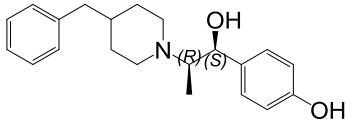
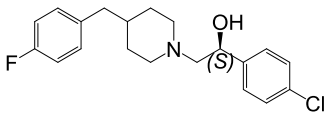
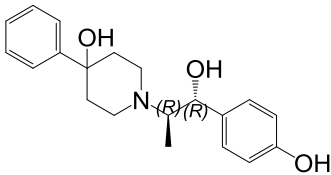
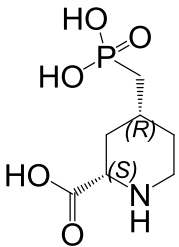
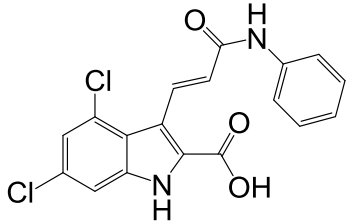
However, the exact molecular mechanism of memantine in ischaemic stroke still needs to be elucidated, Chen *et al.*¹³⁰ had examined if these neuroprotective effects of memantine may be linked to inhibition of calpain-caspase-pathways that cause activation of apoptosis through NMDAR over activation. The authors had demonstrated memantine can decrease ATP depletion by measuring lactate dehydrogenase (LDH) release in primary hippocampal neurons from rats. The lowest dose tested 1 μ M failed to show any neuroprotection, however the higher concentrations 10 μ M and 50 μ M had increased neuronal survival. In addition they also observed 1.5 fold reduction in neuronal death at a dose of 20 mg/kg in middle cerebral artery occlusion (MCAO) model in rats. Currently, there are two ongoing late stage clinical trials evaluating efficacy of memantine in ischaemic stroke patients; evaluation of memantine versus placebo on Ischaemic stroke outcome (EMISO) and memantine for enhanced stroke recovery.^{131,132}

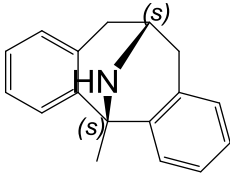
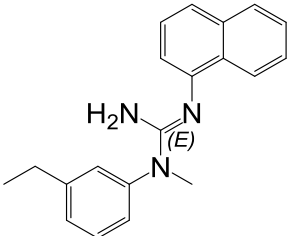
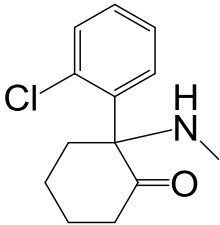
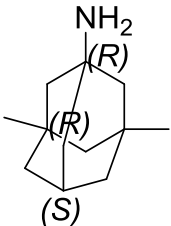
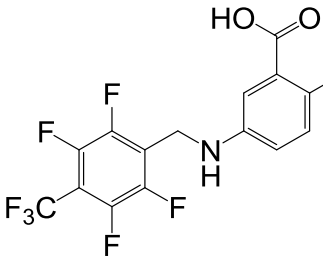
New small molecules that are currently in Phase II clinical trials of ischaemic stroke also include GluNR2b antagonist Neu2000 (Nelonedaz). This drug, identified by South Korean biotech, GNT pharma co, was found to reduce damaging effects of oxidative stress pathways initiated by NMDAR and free radical induced hypoxic cell injury. The compound was a derivative discovered by combining the lead structures aspirin (already used for treatment of ischaemic stroke) and sulfasalazine (anti-

inflammatory drug used for rheumatoid arthritis) to identify the combined 5-aminosalicylic acid with sulfapyridine (i.e Nelonen Daz). The hypothesis behind this was to develop a compound with dual pharmacology to produce neuronal protection after ischaemic brain injury. Nelonen Daz was found to have IC₅₀ of 35.38 µM which was showed the higher affinity of the compound compared to sulfasalazine IC₅₀ of 294 µM.¹³³

Overall, the therapeutic time window to 'save' the penumbra is very short which makes the re-establishment of blood flow (reperfusion) very challenging.¹³⁴ Even with neuroprotection, the narrow therapeutic time window still exists and as time progresses the infarct core expands. The central objective of neuroprotection is to salvage neurons and other cells in ischaemic penumbra by minimising or abolishing secondary damage due to excitotoxicity, oxidative stress and inflammation mechanisms. To achieve, this neuroprotection has to be delivered while there is still a salvageable brain.¹³⁵

Table 1. 1 Historically important NMDAR antagonist for ischaemic stroke

Name	Structure	MOA	AMS	SE	CT	Outcome	Ref
Ifenprodil		NTD-GluNR2b antagonist	Focal ischaemia model in rodents	No severe side effects observed. Failed to show improvement of in morbidity.	/	Not tested in clinical trials for ischaemic stroke.	
Eliprodil		NTD-GluNR2b antagonist	Focal ischaemia model in rodent	No severe side effects observed. Failed to show improvement of in morbidity.	PIII	Failed toxicity tests in human CT. No benefits were observed in time window given 8 hours.	136, 137
Traxoprodil		NTD-GluNR2b antagonist	Focal ischaemia model (MCAO in cats)	-ECG abnormalities	PII	Major side effect, led to termination of the clinical trial.	138
Selfotel		Competitive antagonist at GluNR2	Focal ischaemia model in rodents	- Psychotic behaviour - Neurotoxic Hallucinations	PIII	Failed toxicity tests in human clinical trials	139
Gavestinel		Comparative antagonist at GluNR1	Focal ischaemia model in rodents	No severe side effects observed, Failed to show improvement of in morbidity.	PIII	Not as effective as predicted by animal models	140
Magnesium Sulfate	$Mg^{2+}SO_4^{2-}$	Channel blocker	Focal ischaemia model in rodents Global ischaemia model in rodents	No severe side effects observed, Failed to show improvement of in morbidity.	PIII	Not as effective as predicted by animal models	141

MK801		Channel blocker	Focal ischaemia model in rodents	Drowsy, psychotic behaviour Neurotoxic at high dose	/	Failed to reduce infarct size and severe side effects in in vivo studies	142
Aptiganel		Channel blocker	Focal ischaemia model in rodents	Sedation Hallucinations	PIII	Not as effective as predicted by animal models and undesirable side effects	143
(R,S)-Ketamine		Channel blocker	Focal ischaemia model in rats	Sedation Hallucinations	On going PII	Clinical trial QUEST-KETA	144
Memantine		Channel blocker	MCAO model in rats	Mild sedation Hallucinations	On going PII	Clinical trial -MESR, -EMISO	131, 132
Nelonemdaz		GluNR2b antagonist	Focal ischaemia model in rats	On going Still gathering results	On going PII	Clinical trial -SONIC	145

MOA = Mechanism of action , SE = Side effect, CT = Clinical trials, AMS = Animal models of stroke

N-terminal domain (NTD), Electrocardiography (ECG), Middle cerebral artery occlusion (MCAO), Focal ischaemia model (Permanent MCAO and temporary MCAO), Memantine for enhanced stroke recovery (MESR) NCT02144584, Evaluation of memantine versus placebo on Ischaemic stroke outcome (EMISO) NCT02535611 and Safety and optimal neuroprotection of neu2000 in ischaemic stroke with endovascular recanalization (SONIC).

1.7 The discovery of peptide P8 sequence on NMDAR and its significance as a potential binding site for NMDAR antagonists

Since the discovery of the link between NMDARs to ischaemic excitotoxicity in numerous pre-clinical studies and clinical studies, efforts have focused on subunit selective inhibition of the receptor with the aim of leaving the expression and normal functions intact. Multiple binding sites available on the receptor and other potential binding sites on the transmembrane protein could potentially be exploited for their pharmaceutical properties.¹⁴⁶

The overall aim being the prevention of the NMDAR induced secondary cellular cascades that are detrimental in ischaemic stroke. This project builds on work carried out by Professor Majid's team, where they developed polyclonal antibodies against short peptide segments of the ligand binding site and transmembrane domain of the NMDA GluNR1/GluNR2b receptor (Figure 1.9a).

These sequences were selected specifically, as they do not participate in NMDA encephalitis (autoimmune inflammation of the brain caused by autoantibodies). The selected regions were also predicted to stimulate antibody production as they activate B lymphocytes and not other white blood cell subtypes such as inflammatory T lymphocytes. From the 18 polyclonal antibodies tested (Figure 1.9 a,b), P8 (Val 40, Lys 41, Lys 42, Val 43, Ise 44, Cys 45, Thr 46, Gly 47) showed to be highly protective against ischaemic stroke model of transient middle cerebral artery occlusion (tMCAO) without any observed adverse effects. Epitope mapping studies were also performed to confirm the antigen binding site of the active polyclonal antibody (Figure 1.9c). Interestingly, this effect was only observed at the P8 epitope in comparison to the other segments, suggesting that the safe inhibition of NDMAR can be achieved by targeting P8. The antibodies against P8 were effective in protecting cultured cortical neurons from NMDA induced excitotoxicity in the lactate dehydrogenase (LDH) assay and successfully protected against middle cerebral artery occlusion (MCAO) and transient focal ischaemia. Taken together, these studies suggested that binding to P8 could provide neuroprotection in ischaemic conditions and more importantly, show no sign of adverse effects which is one of the main limitations for first generation and second generation NMDAR antagonists.

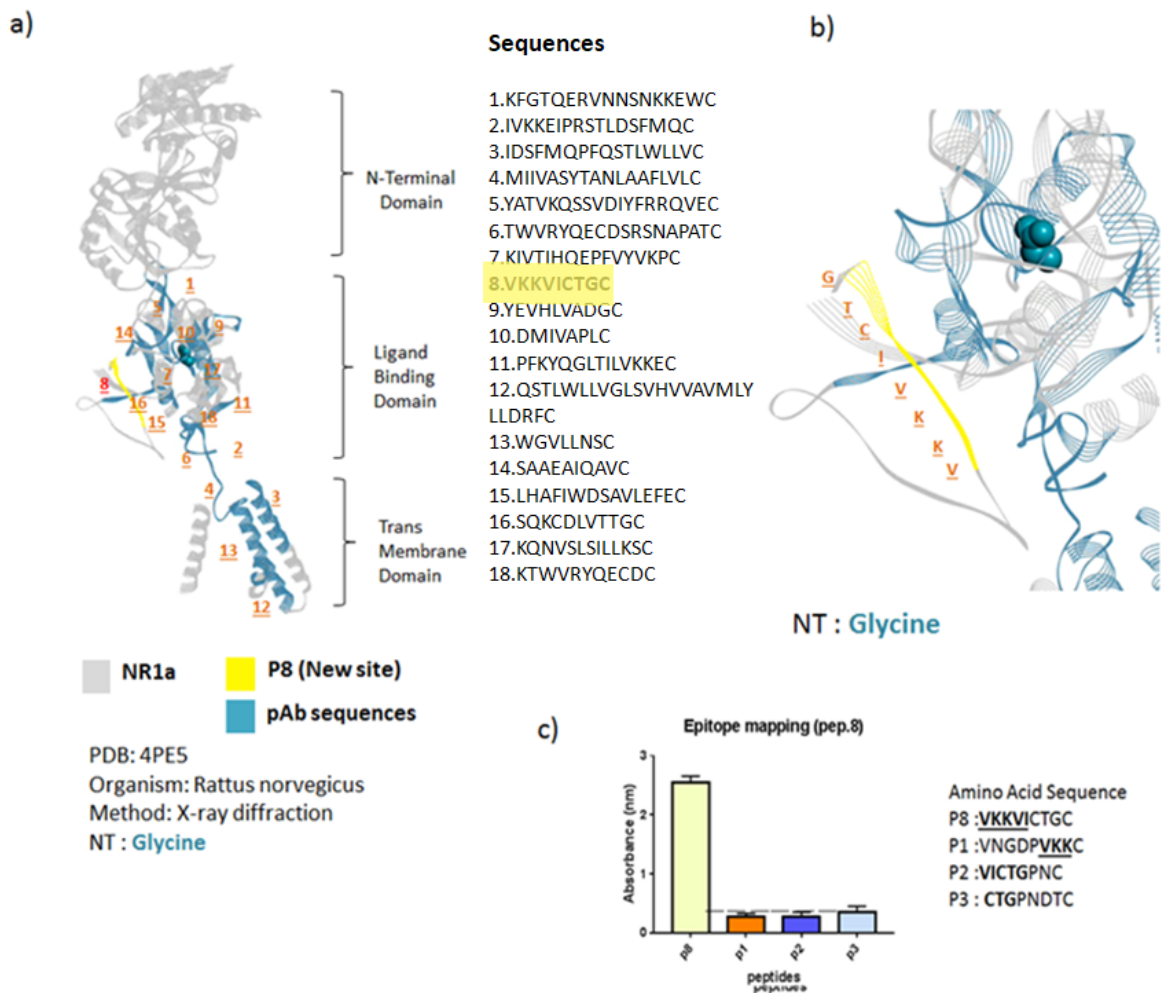


Figure 1. 9 The sequences of the 18 polyclonal antibodies on the human GluNR1 subunit.

1.9a) The GluNR1a subunit from the full crystal structure of rat NMDAR (PDB:4PE5) demonstrated in lined ribbon format, where the regions that antibodies were designed for are demonstrated in blue and the potential neuroprotective sequence (P8), highlighted in yellow. The sequences of each of these segments are shown under sequence numbers. **1.9b)** Showing a close view of the P8 sequence (yellow) and the position of the neurotransmitter glycine (cyan) demonstrated in space filling format. **1.9c)** Epitope mapping experiments on the P8 sequence and demonstrating the key residues, from Dr Jain's work unpublished data.

1.8 Overall aims and objectives of the project

The approach used to identify the P8 region of GluNR1 may be difficult to translate clinically as vaccination carries many risks and development of a vaccine is a lengthy and expensive process. Small molecules have a much more established and clear development plan. Despite the great advances in vaccine development and delivery, it still has major challenges during development.¹⁴⁷ Some of these key issues and possible solutions have been summarised in Table 1.2.

Table 1. 2 Challenges in successful vaccine development.^{147,148}

Challenges	Solutions
<ul style="list-style-type: none">• Uncertainty about the data for the protective immune response.	<ul style="list-style-type: none">• Extensive preclinical data required. More animal models of the disease needed.• Large clinical trials required to assess the safety in healthy volunteers
<ul style="list-style-type: none">• Production and distribution challenges• Manufacturing, formulations and bioprocessing problems.	<ul style="list-style-type: none">• Products must be able to be produced in reasonable time frame and readily available to the needs of the patients.• More stability in the product would help distribution to different populations of patients.
<ul style="list-style-type: none">• Inadequate and lack of financial resources for development leading to early abandonment of projects.• Poor availability for low income countries.	<ul style="list-style-type: none">• Requiring very large investment in vaccine research (\$1-2 billion)• For developing countries produce alternative pricing strategies with the help of their governments.

To further support this approach, a major advantage of a small molecule therapeutic is that by having a more conventional pharmacokinetic profile than antibodies they are often associated with enhanced oral bioavailability, which can be readily upscaled for analysis and production; therefore they are generally more economical than vaccine therapeutics. The majority of antibodies tend to stay within biological systems for extended periods of time (on average 6-12 months).

Furthermore, if there is an unwanted side effect to the treatment such as allergies, the patients may experience these for a long period of time after the initial exposure. In comparison, the routine and daily dosing typically observed with oral small molecules would subsequently be cleared within a number of days and hence the effects of the drug would diminish in a much more predictable and manageable timescale. Administration of the small molecule would also be much more applicable and avoid the complicated procedures required with intravenous infusions. Small

molecules also tend to have improved solubility, permeability and can be optimised to have reduced off target toxicity.

Small molecule therapeutics may be more cost effective and require less production time, but this of course depends on the individual compound and the number of stereocenters within the structure, product yield and stability. In addition, for small molecule therapeutics high affinity to a particular target is crucial to avoid nonspecific binding that may cause unwanted side effects. Likewise, there may be an issue with their corresponding metabolites which may cause toxic side effects as well.

The aims of this project are:

1. Identify small molecules that are predicted to favourably interact with the P8 region of GluNR1, using medicinal chemistry approaches.
 - i) Target protein identification and preparation
 - ii) Build a homology model of the polyclonal antibody (pAb) antigen binding domain and prediction of pAb binding with the GluNR1 P8 region through protein-protein docking
 - iii) Virtual screening campaign and identifying initial *in silico* hits
2. Screen for efficacy and safety of these molecules using *in vitro* and *in vivo* models of excitotoxicity.
 - i) Initial phenotypic screening using mutant SOD1 zebrafish model of neuronal stress.
 - ii) Screen for efficacy and safety against excitotoxicity using primary cortical neuron cultures from mice.
 - iii) Determine efficacy in a mouse model of ischemic stroke

Hypothesis: We hypothesised that small molecule inhibitors will interact with P8 site and will exhibit safety and efficacy in models of excitotoxicity and experimental stroke.

The protein-protein interaction of the active polyclonal antibody with the P8 is of crucial importance for the neuroprotection observed in previous animal studies. It can highlight the key interactions that are required for a small molecule to satisfy similar biological effects using *in vivo* models. Unfortunately, the crystal structure of the polyclonal antibody bound to the target was not available, however, with growing

numbers of crystal structures in the Protein Data Bank (PDB) it was possible to use alternative antibody structures to examine how these proteins interact. All of these points are discussed in Chapter 3: Part One. In addition, using protein-protein docking software ZDOCK it was possible to highlight the hot spot regions on the target protein using already available crystal structures of mouse fragment binding antibodies at very good resolutions. These experiments were also supported by a validation study using published bound and unbound forms of antigen-antibody. The results and potential limitations are discussed in this chapter and in conclusion a comparison of the residues highlighted in the protein-protein docking is performed alongside the small molecules selected from the virtual screening campaign.

To achieve our aim of identifying a small molecule, potential compounds that interact with P8 of GluNR1 subunit of the NMDAR were identified using *in silico* virtual screening to select the most promising hits for biological analysis, explained in Chapter 3: Part Two. In this chapter the drug design and development *in silico* methods are explained in detail, focusing on the current methodology and approaches applied within computational aided drug design (CADD). The results and discussion are provided as well as the validation and supporting studies for the biological target. The 24 identified molecules selected from these studies are discussed and for the food drug administration (FDA) approved drugs their mechanism of actions and their pharmacological properties are also discussed. In conclusion, the selected compounds are finalised for the evaluation of biological activity studies after the performance of *in silico* pharmacokinetic studies (ADMET) for each of the selected compounds.

In Chapter 4, the initial selected compounds were analysed through the ZNStress *in vivo* model applying a high throughput screening protocol to assess the ability of the compounds to modulate neuronal stress in transgenic mutant superoxide dismutase 1 SOD1 (G93R) zebrafish model of amyotrophic lateral sclerosis (ALS). This model was chosen because excitotoxicity is thought to play an important role in the pathological process from SOD1 mutation and is further explained in Chapter 4. In this chapter the *in silico* hits identified in Chapter 4, as well as two positive controls, known NDMAR inhibitors and channel blockers MK801 and memantine were tested in the SOD1 zebrafish model in a phenotypic screening method. The results of the assay and evaluation of the model is discussed in detail in this chapter.

Several compounds were also tested for efficacy and safety profiles using an *in vitro* assay that induces NMDAR excitotoxicity. Cellular injury was measured by lactate dehydrogenase (LDH) release in response to NMDA exposure using mouse primary cortical neurons. In addition, high content imaging analysis system (Columbus) was used to assess cell death and nuclear morphology of the cells when exposed to different concentrations of compounds in presence of NMDA, explained in Chapter 5.

Finally using a mouse model of stroke we determined the *in vivo* efficacy of selective compounds in Chapter 6. Modelling of stroke in mice using the middle cerebral artery occlusion (MCAO) is a well established methodology to re-create the devastating effects of stroke on the brain. In this chapter, the small molecules that showed potential in the *in vitro* assays are examined further in the complex *in vivo* model of stroke. In addition, the solvation and vehicle construction for the insoluble compounds are discussed, along with the challenges for the formulation and solubility of the molecule nitrendipine. Overall, the promising results of the *in vivo* experiments are discussed further in this chapter as well as potential future experiments for the next step with these molecules. The limitations and future studies for this project which looks into a potential binding assay for small molecules binding to the novel site on the GluNR1 of the subunit is also discussed in Chapter 7. Moreover, other potential experimental techniques that can aid in determining the binding affinity of these molecules to the receptor is also looked into.

Chapter 2: Methods

2.1 *In silico* Studies

For our project the 3D structure of the biological active pAb was not available. Therefore, to assess the binding of the pAb to GluNR1 P8 region, the structure of the pAb from the database PDB and The National Centre for Biotechnology Information (NCBI) was used to identify the initial unbound antibody models. The softwares used in Chapter 3: part one are summarised in Table 2.1.

Table 2. 1 The softwares used for P8-Fab docking.

Software Suite	Supplier	Notes
Discovery Studio (DS) 3.5	Dassault Systemes BIOVIA ¹⁴⁹	The protein-protein docking investigation of Fab with GluNR1 protein was with : <ul style="list-style-type: none">• ZDOCK• Homology modelling• MODELER (version 9v10)
The National Centre for Biotechnology Information (NCBI)	US National library of Medicine	The basic local alignment search tool (BLAST) Available at : https://blast.ncbi.nlm.nih.gov/Blast.cgi
Protein data bank (PDB)	World protein Data bank	All crystal structures obtained from PDB Available at : https://www.rcsb.org/
PROCHECK v6.0	The European Bioinformatics Institute (EMBL-EBI)	Validation of homogy model generated Available at : https://servicesn.mbi.ucla.edu/PROCHECK/

2.1.1 Fab model built via homology modelling

Bianchi.M, *et al* ¹⁵⁰ have recently published their work on using electronmicroscopy to investigate pAb responses in HIV immunised rabbits. In this study they were able to produce a distinct class of antibodies with high quality structural data of the immune complex with pAb Fab bound segments. The structural information of the epitope-paratope provided in the model (PDB: 5ACO) was used as the query template for the pAb in this study. Sequence similarity searches were carried out with the BLAST (NCBI) server to identify mouse antibody templates for the homology modelling. The target sequences of mouse equivalent antibodies from the PDB were used to construct the homology model using DS (3.5) as well as predict the protein structure with a model antibody framework protocol that used MODELER ¹⁵¹ to

generate 3D models. This allowed the homology model for a Fab domain to be generated by superimposing the mouse Fab templates for the light and heavy chains onto the query pAb structure to give the relative spatial orientation of the chains. The best matched structures were subsequently superimposed and merged into 20 chimeric models. The best model with the lowest Discrete Optimised Potential Energy (DOPE) score and Physical Density Function (PDF) total energy ¹⁵² were selected for the protein docking studies using ZDOCK. Finally, the model structure was evaluated with Ramachandram Plots. ¹⁵³

2.1.2 ZDOCK for P8-Fab docking

In this work, most of the PP docking was performed with ZDOCK software available in the Discovery Studio (DS) 3.5 ¹⁵⁴, where the generated poses were ranked and clustered into groups based on their scores. The cut-off for the protein complexes generated was set at 2000 complexes to ensure a reasonable computational time.

In this investigation, the residues within the membrane segment of NR1 were removed from the ZDOCK studies as no pAb could interact with those segments. When studying the interaction of P8 with the Fab region, key residues of P8 (V40, K41, K42, V43, I44) were classed as part of the PP binding interface. This was to ensure the removal of conformations that did not include the specific residues in the interface. This was done as well to ensure the binding interface reduced the number of hits obtained after the calculations by implementing the experimental data that was available. The scoring functions used were ZDOCK score and some of the poses were also re-ranked with ZRANK to allow further clarification. The top poses have the highest scores indicating favourable binding.

2.2 *In silico* docking studies

The docking protocol and software used during this project are summarised in Table 2.2. For this investigation, GOLD and DS were used to prepare the proteins and *in silico* ligands prior to the initiation of the VS.

Table 2. 2. List of software used.

Software Suite	Supplier	Notes
		The multi-component software that is built from Pipeline pilot, a dataflow programming for VS and ADMET studies. ^[155]
Discovery Studio (DS)	Dassault Systemes BIOVIA	The docking programs used for small molecule VS were : <ul style="list-style-type: none"> • LibDock, LigFit, CDOCKER.
Genetic Optimised Ligand Docking (GOLD)	Cambridge Crystallographic Data Centre (CCDC)	The protein-protein docking investigation of Fab with GluNR1 protein was with : <ul style="list-style-type: none"> • ZDOCK Used for the VS and the ensemble docking docking studies.
Swissadme	Swiss institute of bioinformatics (SIB)	ADMET paramaters and pharmacokinetic properties Available at : http://www.swissadme.ch/
The National Centre for Biotechnology Information (NCBI)	US National library of Medicine	The basic local alignment search tool (BLAST) available at : https://blast.ncbi.nlm.nih.gov/Blast.cgi ^[156]
PDB sum binding clefts	The European Bioinformatics Institute (EMBL-EBI)	Used to identify pockets available at GluNR1 LBD domain available at : http://www.ebi.ac.uk/thornton-srv/databases/cgi-bin/pdbsum/GetPage.pl?pdbcode=index.html
Universal Protein Resource (Uniport) Align	EMBL-EBI, SIB and Protein Information Rescourse (PIR) ¹⁵⁷	Alignment performed by the Clustal Omega program, Available at: https://www.uniprot.org/align/
Pymol	Schrödinger ¹⁵⁸	Calculating the b-factors of NR1 chain
Heatmapper	GenomeAlbert ¹⁵⁹	The cluster groups. The online software heatmapper http://heatmapper.ca/expression/
XLSTAT	Addinsoft's ¹⁶⁰	To graphically represent the ranking methods, receiver operator characteristic (ROC) curves and histograms were used.
Bio3DWeb	Grant Lab ¹⁶¹	To create the Sequence alignment and sequence identity clustering graphs.

2.2.1 Protein preparation

The crystal structures from the PDB often are incomplete models. Therefore, they must be prepared prior to screening. In addition, the structures often miss information regarding bond orders or atomic charges. The tautomeric and ionisation states are often not assigned. Side chains of residues and large loops may have missing sequences due to low resolution or steric clashes that can occur in protein.¹⁶² Other important molecules that may be present and need to be identified include water molecules, cofactors, buffer solutions, ligands and metal ions.

The protocol “prepare protein” in DS was used to address the above issues and subsequently the proteins demonstrated in Table 2.2 were prepared in the following steps. Initially the proteins were “cleaned” by execution of the following functions; adding missing atoms, adding side chains, sorting structural disorder by calculating pKa of protein residues and correct labelling of residue names. The structure was then protonated at pH 7.4 (physiological pH). Finally, the protein was minimised using CHARMM force field to relieve steric clashes. The above steps insured the docking performance improved by representing a more of a realistic model of the biological target. This protocol was used to create a hydrated model (keeping water molecules in the active site) and a dry model (removing all water molecules from the active site).

2.2.2 Ligand preparation

In an attempt to maximise the number of hits for P8, it was important to build a target orientated library of compounds. Therefore, the compounds needed to satisfy molecular properties required for drug-like compounds that could be CNS permeable.¹⁶³ Initially, the *in silico* preparation was carried out with the “prepare ligands” protocol in DS to get the molecules ready for the docking process. This protocol executes tasks such as removing duplicate molecules, calculating ionisation states at pH 7.4, enumerating isomers and tautomers and generate the correct 3D conformations. It is important to apply this protocol due molecules being able to coexist in tautomeric states which can interact with active site residues of the target in different ways.¹⁶⁴ The compound libraries were then further filtered and characterised according to their molecular properties using Lipinski’s “Rule of Five” (RO5)¹⁶⁵ and Veber’s rule.¹⁶⁶

2.2.3 Similarity Search with DS

In this project, these similarity tools were used after the docking studies to group similar ligand analogues. Subsequently, the ideal binding modes were investigated within the largest clusters, to identify key residue interactions.¹⁶⁷ For the clustering of the compounds the fingerprint properties using a Tanimoto¹⁶⁸ method was applied. Tanimoto similarity operates over bits vectors. Bits vectors consist of the fragmentation of the ligands to their functional groups to generate their unique fingerprints. The domain would be classed as absent or present (0 or 1). Subsequently, the fingerprints are then compared with each other to determine how many functional groups are similar between the reference ligand and the compounds. In this method, similarity search was measured as $SA/(SA+SB+SC)$. Here SA represents the number of and bits (bits present in both ligands and the reference), SB: The number of bits in the ligand but not the reference and SC: where the number of bits in the reference but not in the ligands. This fingerprint module uses predefined functional-class extended-connectivity fingerprint count up to 6 (FCFC_6). The FCFC_6 fingerprint calculates minimum, maximum and the average similarities and measurements of the nearest known reference ligand. Alternatively, the similarity search for the comparison of *in silico* hits with approved drugs was also performed using the online search tool Swiss Similarity.¹⁶⁹

2.2.4 ADMET

To examine if the compounds had acceptable pharmacokinetic properties, the libraries were sent through the DS ADMET protocol to assess their drug-like properties. This protocol allows identification of compounds that were able to exhibit the majority of drug like properties and remove any compounds that may exhibit major toxic side effects from the set of compounds selected for post filtering process. Furthermore, the upper limit for the aqueous solubility, absorption and BBB penetration were calculated to evaluate the compounds during hit selection. Table 2.3 demonstrates the descriptive nodes used within DS and their scoring system.

Table 2. 3 The ADMET descriptors used. ¹⁷⁰⁻¹⁷³

Property	Description	Value	
Intestinal absorption	Predicting the compounds ability to be absorbed through intestine after administered orally. Here the upper limit was calculated based on polar surface area of 2D structure of the compounds.	Scale of 0-3	
		0	Good
		1	Average
		2-3	Poor and very poor
BBB Penetration	This model predicts BBB penetration after administration orally. It is based on a quantitative linear regression model for predicting BBB permeability using confidence ellipse with the ADMET_Alog-98 and ADMET_PSA 2D calculations. For the ADMET plot it shows the most BBB permeable compound to be defined within the range of $0 \leq \log BB < 0.7$.	Scale of 0-4	
		0-1	High permeability
		2	Average
		3	Low permeability
		4	Unknown (Out of range)
CYP2D6 binding	Able to class any compounds that may block the cytochrome P450 2D6 enzyme, that has been reported to be involved for many cases of drug-drug interactions. Here a Bayesian learning tools is applied.	Scale True or False	
		True	Higher value than cut-off bayesian score 0.16
		False	Lower value than cut-off bayesian score 0.16
Hepatotoxicity	This model shows the chances of dose-dependent human hepatotoxicity. Using similar Bayesian learning tool as above and also includes SAR technique.	Scale True or False	
		True	Higher value than cut-off bayesian score - 0.41
		False	Lower value than cut-off bayesian score - 0.41
Plasma Protein Binding	Predicts the chances of the compound binding to carrier proteins in blood. This property can affect the efficiency of drug. This tool also uses the similar Bayesian learning method explained	Scale True or False	
		True	Higher value than cut-off bayesian score -2.2
		False	Lower value than cut-off bayesian score -2.2

2.3 ZNStress Assay: Methods and Materials

The ZNstress assay was performed in collaboration with Dr Tennore Ramesh's team in SITraN (The University of Sheffield). The ZNstress assay was performed with PhD student Olfat Abduljabbar. The compound preparation and data analysis was performed by Arshnous Marandi.

The stock solution of the compounds was made at a concentration of 100 mM concentration in DMSO, before diluting down to 10 mM. After addition of the compounds onto a 384 well LDV plate, 10 μ M (final well concentration achieved). All the commercial reagents and products purchased used in the assay are summarised in Table 2.4 and Table 2.5 unless stated otherwise.

Table 2. 4 The compounds purchased for the screening.

Reagents	Catalogue number	Supplier	Notes
Methocarbamol	PHR1395	Sigma Aldrich	
Morantel tartrate	1446906	Sigma Aldrich	
Droperidol	BP675	Sigma Aldrich	
Bufexamac	B0760	Sigma Aldrich	
Floxuridine	1271008-25	Sigma Aldrich	
Acetyl serotonin	A1824	Sigma Aldrich	
Nitrendipine	N144	Sigma Aldrich	
Salsalate	SML0070	Sigma Aldrich	
Torseמידe	T3202	Sigma Aldrich	
Diprophylline	D2800000	Sigma Aldrich	
Tetracaine	T7383	Sigma Aldrich	
3-indoleglyoxylyl chloride	515205	Sigma Aldrich	
Tetrahydrofuran (THF)	401757	Sigma Aldrich	
Triethylamine	471283	Sigma Aldrich	
Sodium sulfate	204447	Sigma Aldrich	
Ethyl acetate (EtOAc)	270989	Sigma Aldrich	
Petroleum ether	300314	Sigma Aldrich	
Ethanol (EtOH)	443611	Sigma Aldrich	
Dimethyl sulfoxide (DMSO) ACS reagent, >99.9%	472301	Sigma Aldrich	Amount 1 L

Table 2. 5 The reagents and machines used in the ZNstress assay.

Reagents	Catalogue number	Supplier	Notes
Amber vial, screw top	27083	Sigma Aldrich	Volume 2 ml
96 well plate micro clear	655096	Grenier BioOne	
E3 pH 7.2	/	/	1L 50x stock solution 0.25 M NaCl (14.6 g) 8.46 mM KCl (0.63 g) 16.53 mM CaCl ₂ .2H ₂ O (2.43 g) 16.51 mM MgSO ₄ .7H ₂ O (4.07 g)
Tricaine methanesulfate (MS-222)	E10521	Sigma Aldrich	
Gibco™ Phosphate Buffered Saline Tablets	18912014	ThermoFisher Scientific	1X Tablet dissolved in 500 ml dH ₂ O, pH 7.45
V bottom 96 well plates	651101	Grenier, Bio-One	

Machine	Source	Function
Echo 550	Labcyte	Automated drug dispensing
Incell analyser 2000	GE healthcare	High content imaging system
PHERASTAR FSX	BMG Labtech GmbH	Measuring the fluorescence levels emitted

2.3.1 The zebrafish model

The parent and larvae fish were housed in the Biological Service Unit (BSU) in The University of Sheffield, (in compliance with the UK Home Office requirements) and kept at 28.5°C in the required aquariums. The embryos were produced by breeding the G93R line with the wild type zebrafish strain.

2.3.2 ZNstress assay protocol

The *in silico* hit molecules were solubilised in DMSO, placed under an inert argon environment 24hr prior to the experiment and stored at -20 °C. For the screening the stock solution was placed into the compounds in the 384 wells using LDV plates and

then further diluted using the Echo 550 automated drug dispenser to generate the final volume 10 μ M concentration in 200 μ l. All the compounds were loaded onto the plate using Echo 550. The final DMSO concentration in the wells of the embryos was 0.1%, which corresponds to the amount used in the assay as the negative control.

The adult wild type female and mutated male fish were bred, and the embryos were collected the day after. The embryos were then manually dechorionated (removal of outer membrane) the day before the loading of them onto the imaging 96 well plates in 70 μ l of E3 media.

Dechorionation of the embryos were essential as it allowed better observation under the microscope and allowed more precise imaging. The genotype of the embryos prior to the screening was then initiated using Incell analyser 2000 and the embryos with DsRed fluorescence were selected for the next stage of analysis to ensure that only the healthy samples with the fluorescent mutation were taken forward.

At 48 hours post fertilisation (hpf) the embryos were placed in the 96 well plates (1 larvae/well) and incubated in the drug solutions (10 μ M) at 28 °C until 6 dpf. They were checked daily to ensure removal of dead or damaged embryos. On the final day, the embryos were anaesthetised using MS-222 and placed into 50 μ l of PBS in the V-bottom 96 well plates. Subsequently the plates were sonicated for 5 seconds at 25% amplitude and then centrifuged at 3000 rpm for 15 minutes. 20 μ l of the supernatant was loaded onto the 384 well plates and the fluorescence was measured using the OMEGAstar plate reader for emission of the DsRed wavelength at excitation maximum at 558 nm and emission maximum at 583 nm.¹⁷⁴ The experimental protocol is summarised in five steps as shown in Figure 2.1.

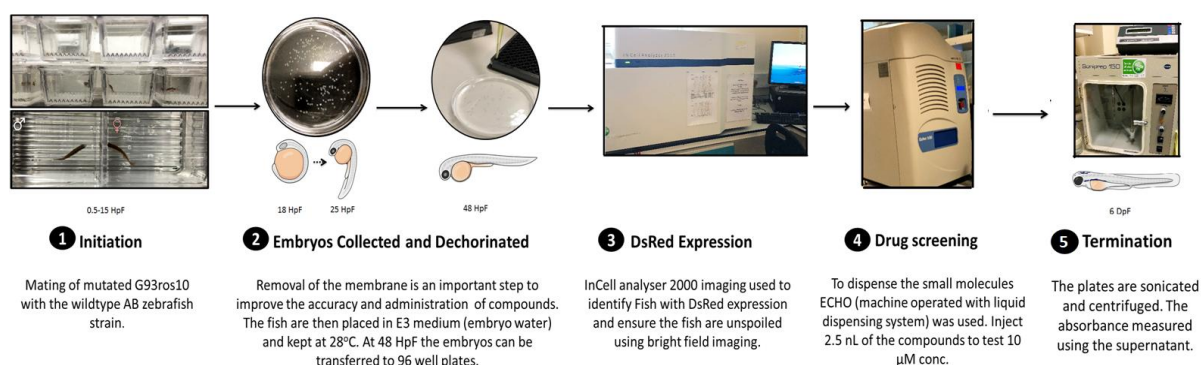


Figure 2. 1. The protocol for the ZNstress assay used for the initial screening of the compounds.

1) The wildtype zebrafish were mated with mutated (G93R) zebrafish. **2)** Embryos were collected dechorinated and plated into 96 well plates. **3)** Zebrafish were confirmed to have the desired mutation using DsRed expression. **4)** Drugs were dispensed using automated liquid handling. The experiment then took an end point absorbance measurement at excitation, maximum 558 nm and emission maximum 583 m after plate sonication and centrifugation.

2.3.3 Data analysis

The statistical analysis of the data was performed using Microsoft Excel to calculate the percentage inhibition. The averages were then further analysed using GraphPad Prism version 9.0 for Windows (Graphpad software, San Diego, California USA). All of the data was demonstrated as a mean and standard deviation (SD) which was also calculated. The statistical analysis used was a One-way ANOVA followed by Dunnetts multiple comparison post hoc tests. Statistical significance was determined when the p-value < 0.05 and was shown as * p<0.05, **p<0.01 and ***p<0.001. Analysis of the data and quality control was assessed using strictly standardised median difference. This statistical testing was applied in Chapter 4,5 and 6 for the analysis of the results.

2.4 *In vitro* assay NMDAR toxicity test: Method and Materials

For the *in vitro* primary culture preparation the dissection equipment, solutions and pipette were autoclaved using Rodwell Autoclave MP25 at 121°C, 15psi for 15 minutes, 24 hour prior to each experiment. All the animal experiments were carried out according to an approved ethical protocol. All buffers and reagents were prepared prior to the experiment. The cell-based experiments and biological samples were used in a class II biological hazard fume cupboard, which was cleaned with

aqueous 70% (v/v) ethanol. All materials in these fume cupboards had been previously autoclaved to ensure a sterile environment. All subsequent drug dilutions were prepared prior to the experiments in the chemistry department in fume cupboards with sufficient air flow. The reagents and materials used in these experiments are summarised in Table 2.6.

Table 2. 6 Reagents and machines used for primary cortical cultures and their suppliers.

Reagents	Catalogue number	Supplier	Notes
Gibco™ Phosphate Buffered Saline Tablets	18912014	ThermoFisher Scientific	1X Tablet dissolved in 500 ml dH ₂ O, pH 7.45
The Hanks Balanced Salt solution (HBSS -/-)	55021C	Sigma Aldrich	Phenol red, no Ca ²⁺ and no Mg ²⁺
The Hanks Balanced Salt solution (HBSS +/-)	H9269	Sigma Aldrich	
Trypsin	15090046	ThermoFisher Scientific	2.5%, No phenol red
Soybean trypsin inhibitor	T9003	Sigma Aldrich	
Deoxyribonuclease I (DNAs I)	D5025	Sigma Aldrich	
Paraformaldehyde	158127	Sigma Aldrich	4% in 1X PBS
Penicillin Streptomycin	17-602E	Lonza	
Albumax	11020021	ThermoFisher Scientific	
Neurobasal medium plus	A3582901	ThermoFisher Scientific	
Glutamax	35050061	ThermoFisher Scientific	
B27- Plus supplement (50x)	A3582801	ThermoFisher Scientific	
Neurobasal medium mixture (NBM)			Neurobasal medium 48 ml Glutamax 0.5 ml Penicillin-streptomycin 0.3 ml B27 plus 1.0 ml
Poly-D-Lysine	P7405	Sigma Aldrich	
PI (Propidium iodide solution) 1 mg/ml	P4864	Sigma Aldrich	1:200 in PBS
Hoechst 33342 solid (50mg)	Cas number 875756-97-1	Tocris	For staining used 10mg/ml (15.77mM, 1:5000) in PBS
N-methyl-D-aspartic acid	M3262	Sigma Aldrich	Aliquot 20 µl and only use 1µl/10 ml (1:10000) for the assay plates
LDH Cytotoxicity Assay Kit	C20300	ThermoFisher Scientific	

Anti-NMDAR1 monoclonal antibody, 1.17.2.6, Rabbit.	#AB9864R	Sigma Aldrich
Anti-Neurofilament H polyclonal antibody, Chicken.	#AB5539	Millipore Sigma
Triton x-100	MFCD00128254	Sigma Aldrich
Goat anti-rabbit IgG H+L (HRP)	Ab6721	Abcam
Goat anti-chicken IgY H+L, alexa fluor 488	A11039	ThermoFisher Scientific
Micro clear 96 well plate, precoated with Poly-D-Lysine, black, F-Bottom	655946	Greiner Bio-One
Cell culture multi well, 24 well plate, sterile and clear	662160	Greiner Bio-One

Machine	Source	Function
Incell analyser 2000	GE healthcare	High content imaging system
PHERASTAR FSX	BMG Labtech GmbH	Measuring the fluorescence levels emitted

2.4.1 Primary mouse cortical neuron culture: tissue preparation

C5BL/6 mice were bred at The University of Sheffield in the Biological Services Unit (BSU). Pregnant female mice (day 14) were sacrificed by cervical dislocation. The primary cortical neurons were obtained from mice embryos (E14). The brain tissue of the pups was isolated and placed in the ice cold HBSS -/- media. Subsequently, the cerebral cortices were prepared by manual removal of the meninges from the tissues, avoiding overexposure of the tissue to the air. The tissues were then washed with 10 ml HBSS -/- media, and then once again suspended in 5 ml HBSS -/- media.

2.4.2 Digestion and resuspension of cells

Trypsin was added to the tissue solution (7 µl trypsin/brain) to obtain the final concentration of 0.025%. The solution containing the brain tissues was incubated for 15 minutes at 37 °C to allow tissue dissociation. At 7.5 minutes the solution was mixed once and placed back into the incubator. 500 µl/brain DNAase solution (10 µg/ml DNAase in HBSSS +/+) was added for 2 minutes and the supernatant was aspirated. 200 µl/brain of triturating solution (1% albumax, 25 mg trypsin inhibitor, 10

µg/ml DNAase) was used to re-suspend the tissue in order to avoid further DNA release. The tissue was triturated through flame polished glass Pasteur pipettes with progressively smaller apertures to obtain a single cell suspension. It was important to ensure that the cells were completely separated. Cells were counted and placed in the wells on prepared 96 or 24 well poly-D-lysine coated plates at a density of 4.5 million/plate in a neuron basal media mixture (NBM) containing B27-supplement. The plates were then maintained at 37 °C, 5% CO₂ incubator. Cell media was changed every 3 days until the experiment.

2.4.3 NMDA induced Cytotoxicity assay

The stock solution of the compounds (10 mM) was prepared. The compound and NMDA concentrations that were used are summarised in Table 2.7 and Table 2.8.

Table 2. 7 The volumes and concentrations

Total within mixture	Volume NBM	Compound Stock Solution	Final Concentration	Dilution Stock	Volume of Drug
1.5 ml		10 mM	1 µM	1:10000	0.15 µl
1.5 ml		10 mM	10 µM	1:1000	1.5 µl
1.5 ml		10 mM	30 µM	1:333	4.5 µl
2.0 ml		10 mM	100 µM	1:100	20 µl

Table 2. 8 The concentration of NMDA from stock solution

Total Volume within NBM mixture	NMDA Stock Solution	Final Concentration	Dilution Stock	Volume of NMDA
15 ml	60 mM	30 µM	1:500	30 µl
1.5 ml	600 mM	300 µM	1:50	30 µl

At day 10 *in vitro*, the NMDAR toxicity assay was performed and after 24 hours the media of the cells was collected for the LDH assay (protocol explained in section 2.4.5) and imaging analysis. Initially the cells were pre-treated with the compounds by removal of 200 µl of media of each well and replaced with 100 µl of the compound media solution for 30 minutes at room temperature (RT). Then 100 µl of toxin NMDA (30 µM) was added to each well and left for 45 minutes at RT. The treatment for the

compound and the toxin was a 1:1 ratio. After the 45 minutes, the wells were washed ($\frac{1}{2}$ and $\frac{1}{2}$) with plain NBM which was replaced with fresh NBM plus supplements mixture. The plates were then subsequently placed at 37 °C, 5% CO₂ incubator overnight.

2.4.4 Lactate dehydrogenase (LDH) assay

The LDH assay was measured using the Pierce cyquant LDH cytotoxicity assay, following the manufacturers instructions.¹⁷⁵ All absorbance were measured at 490 nm and 680 nm using the Pherastar FS microplate reader. The substrate stock solution preparation was done by adding 11.4 ml of ultrapure water to the solids in the substrate mix bottle and mixed to gently dissolve everything. One tube of the assay buffer (0.6 ml) was then combined with the 11.4 ml of substrate thoroughly, avoiding direct light exposure onto the tube. From the 96 well plates, 100 µl was transfer into the 96 clear microplate plate and 50 µl of the prepared reaction mixture was added to each well. The plate was then covered in foil and left at RT for 30 minutes. Next 50 µl of the stop solution was added and mixed by gently tapping the plate. The absorbance was read at 490-680 nm. For the calculation of the % cytotoxicity the formula demonstrated in Equation 2.1 was used ¹⁷⁵:

$$\% \text{ Cytotoxicity} = \frac{\text{Compound treated LDH activity absorbance}}{\frac{\text{Maximum LDH activity}}{300\mu\text{M NMDA average absorbance}}} \times 100$$

Equation 2. 1

The raw absorbance values were normalised to the average of maximum LDH release (300 µM NMDA) for all individual values to obtain the normalised % cytotoxicity of each treatment as a percentage relative to the maximum cell death control.

The propidium iodide (PI) staining was performed on live cells and before cell fixation. The PI and phosphate-buffered saline (PBS) solution (1:200 dilution) was made and 50 µl of this solution was placed on to the cells and allowed to rest at RT for 30 minutes. 50 µl of the media from each well was removed and the cells were fixed using paraformaldehyde (PFA) for 15 minutes to cross-link the cells onto the plates, preserving the soluble proteins in the solution. The plates were then washed

once with 50 μ l PBS. For the Hoechst 33342 staining dilution of 1:10000 PBS solution was used, and the cells were treated with 100 μ l of this solution for another 15 minutes. At the last step the wells were washed three times with 200 μ l of PBS. The plates were then ready for imaging using Incell 2000.

2.4.5 The immunocytochemistry and immunofluorescence protocol for mouse primary cortical neurons

On day 10, the cells were fixed with 4% paraformaldehyde (PFA) solution in PBS and left at RT for 20 minutes. They were then washed with PBS once and three times with the 0.1% Triton-X in PBS. Next the wells were blocked with 3% BSA in the 0.1% Triton-X in PBS solution for 1 hour. The primary antibody (α -chicken neurofilament-H or anti-NMDAR1 rabbit) was added with the dilution of 1:1000, 10 μ l in 10 ml of the blocking solution and left over-night at 4°C. Then the cells were washed with 0.1% Triton-X in PBS once and incubated with 50 μ l of the secondary antibody, the anti-mouse NR1 and anti-chicken NR1 with the dilution of 1:1000, 5 μ l in 5 ml for 1 hour at RT. Finally, the wells were washed three times with 0.1% Triton-X in PBS and left in PBS solution, ready for imaging using Incell 2000.

2.4.6 Synthesis of N-(4-fluorobenzyl)-2-(1H-indole-3-yl)-2-oxoacetamide (3000917)

Additional compound 3000917 was prepared following the protocol from Sridhar *et al*¹⁷⁶ under an inert atmosphere argon gas, of 3-indoleglyoxylyl chloride (0.7 g, 3.4 mmol) was added to a solution of THF (30ml) containing the 4-fluoroaniline (0.32 ml, 3.4 mmol) followed by the addition of dry triethylamine (1.41 ml, 10.1 mmol). The reaction was stirred at RT for 2 hours and the THF was removed in vacuo to give the crude glyoxylamide. The crude material was washed with phase separation using EtOAc 50% and H₂O. The organic layer was dried with Na₂SO₄ and concentrated, giving 1.02 g of crude material. The pure product was obtained from precipitation, using EtOAc/Pet-ether (40% / 60%) to produce (0.83g, 86%) of the compound. Analysed with HPLC, ¹H, ¹³C NMR in DMSO, spectra are provided in Appendix H. ¹H NMR(400 MHz, DMSO) δ 12.34 (1H, brs, NH), 10.76 (1H, s, NH), 8.77 (1H, s, CH), 8.32 – 8.25 (1H, m, CH), 7.96 – 7.84 (2H, m, 2 \times CH), 7.63 – 7.50 (1H, m, CH), 7.33 – 7.27 (2H, m, 2 \times CH), 7.27 – 7.19 (2H, m, 2 \times CH). ¹³CNMR(101 MHz, DMSO) δ 182.3 (C=O), 162.7 (C=O), 159.06 (C, d, J = 241.4 Hz), 139.1 (CH), 136.9

(C), 135.0 (C), 126.7 (C), 124.1 (CH), 123.2 (CH), 122.57 (CH, d,J = 7.9 Hz), 121.7 (CH), 115.84 (CH, d,J = 22.3 Hz), 113.2 (CH), 112.4 (C). Retention time (RT) 16.29, Purity 96.52%.

2.5. *In vivo* Methods and Material

We used transient middle cerebral artery (tMCAO) and permanent MCAO (pMCAO) models to assess the efficacy of the most promising compounds based on the *in vitro* studies. Dr Saurabh Jain performed the testing of nitrendipine in the mouse tMCAO. Dr Milena Defelice tested the diprophylline, methocarbamol, nitrendipine and floxuridine in the pMCAO model.

2.5.1 Mice and anesthesia preparation

Adult C5BL/6 mice (weighing ~25 kg) were used at The University of Sheffield in the Biological Serviced Unit (BSU). All surgical equipment was sterilised using 70% ethanol and H₂O. Isoflurane was used as the anaesthetic for the MCAO and was administered through inhalation. The temperature was regulated using heating pad and heating lamps to ensure normal body temperature is maintained. Full experimental protocol also available at.¹⁷⁷ The reagents and equipment used are summarised in Table 2.9 and Table 2.10.

Table 2. 9 The reagents and suppliers used.

Reagents	Catalogue number	Supplier	Notes
Methocarbamol	PHR1395	Sigma Aldrich	
Floxuridine	1271008-25	Sigma Aldrich	
Nitrendipine	N144	Sigma Aldrich	
Diprophylline	D2800000	Sigma Aldrich	
Tetrahydrofuran (THF)	401757	Sigma Aldrich	
Triethylene glycol (TEG)	T59455	Sigma Aldrich	
Polyethylene glycol 400 (PEG 400)	B21992.30	Alfa Aesar	
Cyclodextrin	C4642	Sigma Aldrich	
Polysorbate 80 (Tween 80)	59924	Sigma Aldrich	
<i>N</i> -methylpyrrolidone (NMP)	PHR1352	Sigma Aldrich	
Ethanol (EtOH)	443611	Sigma Aldrich	
Dimethyl sulfoxide (DMSO) ACS reagent, >99.9%	472301	Sigma Aldrich	Amount 1 L
Isoflurane	ab145581	Abcam	
2,3,5-triphenyltetrazolium	T8877	Sigma Aldrich	

Table 2. 10 The equipments used in the MCAO models and solubility test.

Equipment and reagents	Catalogue number	Supplier	Notes
Bipolar coagulator	966	Codman and shurtelff Inc	
Homeothermic blanket control	PY2 50-7215	Cambridge, MA	
Laser Doppler flow meter		Vasamedics Inc	
Vaporizer anaesthetic solutions		Dragerwerk AG lubeck	
Model 900 small animal stereotaxic instrument	900	Agnthos	
High-speed micro drill	19007-14	Fine science tools	
Surgical equipment			Bipolar forceps, micro scissors for vessels, surgical scissors for animal skin/tissue, micro forceps, needle holder, skin hook to allow skin exposure and small ruler.
OSIRIS 4.19		Geneva	The image analysis software to analyse the brain slices.
Grant Ultrasonic Bath	E8R05651	Findel international	30 °C , Samples left for 30 minutes

2.5.2 Solubility Methods

For the vehicle preparation all glassware and pipettes were sterile, and the chemical solutions were prepared fresh on the day of the MCAO experiments. The excess media formulations were kept at 4 °C and stored for two weeks. The flow chart in Figure 2.2 demonstrates the steps of the solubility tests.

- In step1, for identifying a vehicle solution for nitrendipine, 1mg/ml was prepared and tested in each combination vehicle. If the compound did not dissolve, an alternative vehicle solution containing more of the water miscible organic liquid would be prepared with a fresh sample of nitrendipine (1 mg/ml) to see if the chemical is solubilised.
- In step 2, the solubility of the compounds in each vehicle was determined by initially examining if the compound dissolved at high concentration with the use of a water bath (30°C) and sonicator for 30 minutes. If the chemical did not dissolve, the volume of solvent was increased to reduce the concentration of the compound. The addition of each solution was sequential starting with

the miscible solvents towards the polar solvents (i.e DMSO, PEG400, Tween 80 and H₂O).

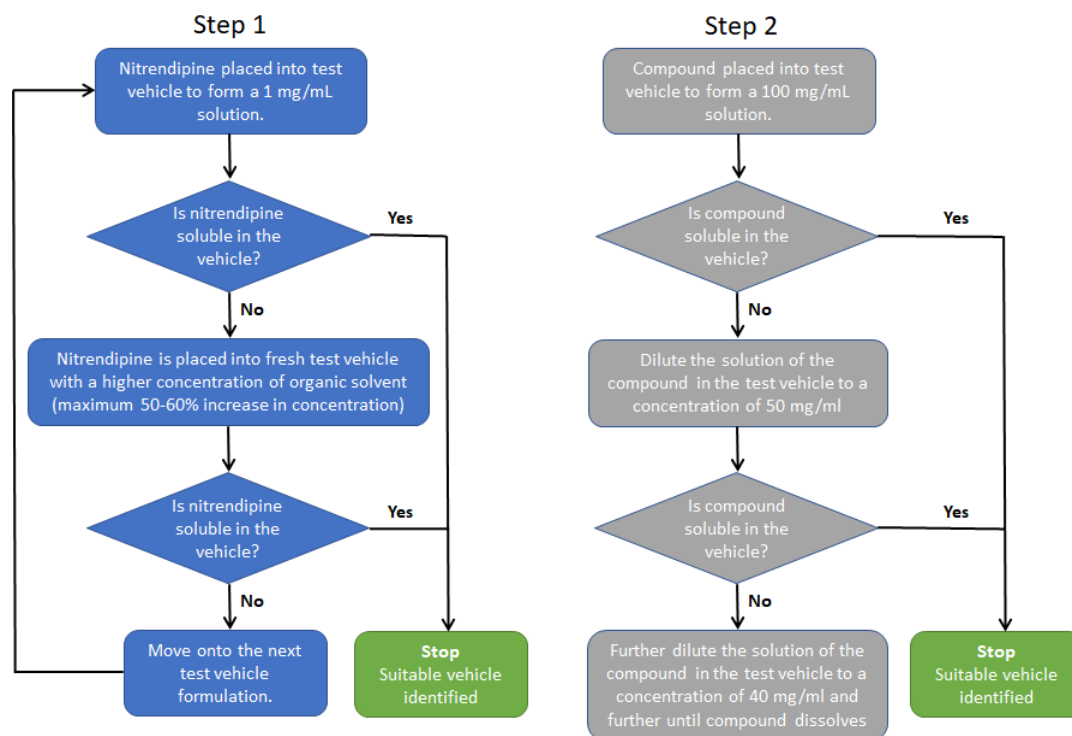


Figure 2. 2 The solubility work flow.

2.5.3 Dosage

To calculate the dose of the compound to be administered to the mouse, the following equation was applied (Equation 2.2): -

$$\frac{\text{Injection } (\mu\text{l/ml}) = \text{Mouse Weight (kg)} \times \text{In vivo Dose (mg/kg)}}{\text{Dose (mg/ml)}}$$

Re-arranging the equation for *In vivo* Dose (mg/kg):

$$\frac{\text{In vivo Dose (mg/kg)} = \text{Injection } (\mu\text{l/ml}) \times \text{Dose (mg/ml)}}{\text{Mouse Weight (kg)}}$$

Equation 2.2

2.5.4 Induction of tMCAO

The mouse was placed under anaesthetic by isoflurane inhalation and inspected under the microscope. The left carotid artery was exposed with an incision. The other branches joining were coagulated along the maxillary artery branches. The internal carotid artery was the only extra-cranial branch that was left open. A 2cm length of 5-0 nylon was placed at the lumen of external carotid artery and moved through to the internal carotid artery. The distance of the bifurcation of common carotid artery was 10-11 mm. (Figure 2.3a) The compounds were then injected (100 μ M) after the obstruction of the artery. Then to achieve reperfusion, the blood flow from the common carotid artery to MCA was allowed. The skin was subsequently stitched up and the mouse was allowed to recover from the anaesthesia in its cage.

2.5.5 Induction of pMCAO

pMCAO was produced by performing a small craniotomy in the skull to gain access to the distal MCA in anaesthetised mice. By applying an electrocoagulator, the MCA was occluded at the bifurcation points as shown in Figure 2.3b (black lines). Occlusion of the MCA was confirmed by measuring blood flow in the region of the ischemic brain using laser Doppler.

In both cases, mice were allowed to recover from the anaesthesia and were then returned to their cages for 48 hours. At that point the mice were sacrificed under deep anaesthesia and the brains were removed cutting into 1 mm slices and infarct volume was quantified using 2,3,5-triphenyltetrazolium chloride (TTC) staining. All of the brain segments were stained with 2% (weight/volume) TTC in PBS at 37°C for 20 minutes (Figure 2.2c). The TTC is a colourless dye that is reduced by mitochondrial enzyme succinate dehydrogenase within living cells, forming formazan which colours healthy tissue deep red. The dead tissue are stained white due to absence of living cells.¹⁷⁸ Then the volume of infarction is calculated through multiplying the distance between each section. Using this stain infarct (stroke) brain appears white whereas normal tissue, appears red. Intravenous injections of the compound occurred straight after the ischaemia.

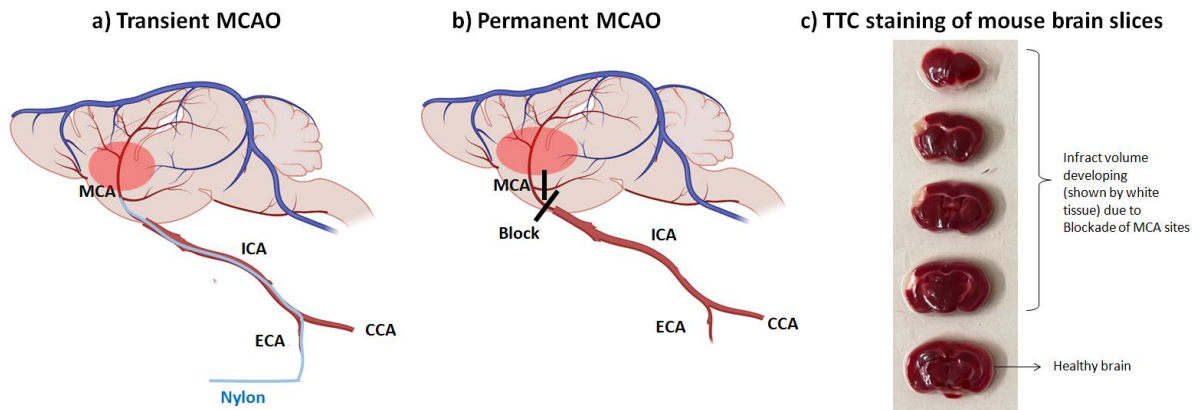


Figure 2. 3 The MCAO models and staining of mouse brain slices from the in vivo experiment.¹⁷⁹

2.3a) tMCAO model the occlusion is formed through the passage of nylon tube through the ECA towards the MCA and then reperfusion is allowed by allowing blood flow to the ischaemic tissue. **2.3b)** pMCAO allows the blockage of the distal MCA arteries in the coronal sections of mice **2.3c)** TTC stain after 48 hour of MCAO. The white segment on the brain slices shows infarcted brain (stroke) and red is the normal tissue. Adapted from www.biorender.com Used with permission under the terms of the creative commons attribution licence (CC-BY). Middle cerebral artery (MCA), (PTE), internal carotid artery (ICA), extra-cranial (ECA) and common carotid artery (CCA).

Chapter 3: Computer aided drug design (CADD) to identify putative bioactive molecules for peptide 8 region of GluNR1

Computer aided drug design (CADD) offers multiple useful tools to understand and guide experimental techniques to accelerate drug design and development pipeline.¹⁸⁰ The two predominant approaches available in CADD are structure based drug design and ligand based drug design.¹⁸¹ There are numerous molecular modelling tools involved in structure based methods that take advantage of the three dimensional (3D) structure of target proteins, such as homology modelling (predicting molecular structure of proteins), molecular docking (predicting ligand-protein binding) and molecular dynamics (predicting movement of protein structures).¹⁸² Homology modelling and molecular docking are discussed in detail in this chapter.

On the other hand, ligand based methods utilise the physiochemical properties and structure activity relationship (SAR) data of known biological active molecules to produce pharmacophore (an ensemble of steric and electronic features that are responsible for the desired biological activities) models, quantitative structure relationships (QSAR) and artificial intelligence (AI) models.^{183,184} Both of these approaches can allow virtual screening (VS) of large compound databases rapidly in drug discovery to identify novel ligands for molecular targets.¹⁸⁵

For this project there was no 3D structure of the antigen-antibody structure complex or 3D structure of the antibody. However, there are x-ray crystallographic structures of NMDAR available in protein data bank (PDB) which allowed a structure based approach of CADD to be applied in order to identify if small molecule modulators for the P8 region of GluNR1, the extracellular portion of NMDAR. The aim of this chapter was to design a small molecule for the P8 region using CADD structure based methodologies. The first objective was to study the antigen (P8)-antibody complex in order to understand how these two molecules can bind with each other so that a potential pharmacophore on P8 can be identified. This work is presented in the Part one of Chapter 3. The second objective was then to conduct a VS campaign

to identify the small molecule that can modulate the P8-antibody binding, which is presented in Part two of Chapter 3.

Part 1:- Predicting the interaction between peptide fragment (P8) on the GluNR1 with its polyclonal antibody via antigen-antibody docking.

3.1 Introduction

The immune system is made of a complex network of cells and its primary function is to defend our body against infection, harmful microbes and other toxins.^{186,187} We usually call these harmful substances, pathogens. Examples of pathogens include viruses, bacterium, fungi, protozoa and other microorganisms which can cause disease in its host. When these pathogens enter our body, they often trigger the body to spontaneously produce a specific family of molecules protecting the body from the damage caused by these pathogens. Peptide fragments or singular shaped protein molecules on the surface of pathogens that are responsible for triggering body's reactions are usually called antigens. The specific protective molecules produced by the body are often called antibodies. The antibodies, also referred to as Igs are produced by B-lymphocytes against specific antigens on a pathogen. They sustain the body from future attacks by the same antigens by marking these pathogens for destruction by cytotoxic lymphocytes killer T cells (e.g CD8+).¹⁸⁸ Therefore, antibodies play a crucial role in the immune system.

Due to their high affinity binding towards specific antigens they are much favoured for therapeutical purposes in diverse diseases. For example, adalimumab (used for treatment of rheumatoid arthritis),¹⁸⁹ trastuzumab (used for treatment of Brest cancer),¹⁹⁰ casirivimab and imdevimab (combination therapy used for treatment of mild to moderate COVID-19 virus).¹⁹¹ In addition, antibodies have been vastly utilised in a variety of medical and life science studies as markers of tissue or cell types, immunoprecipitation techniques, immune binding and many more experimental procedures.¹⁹²

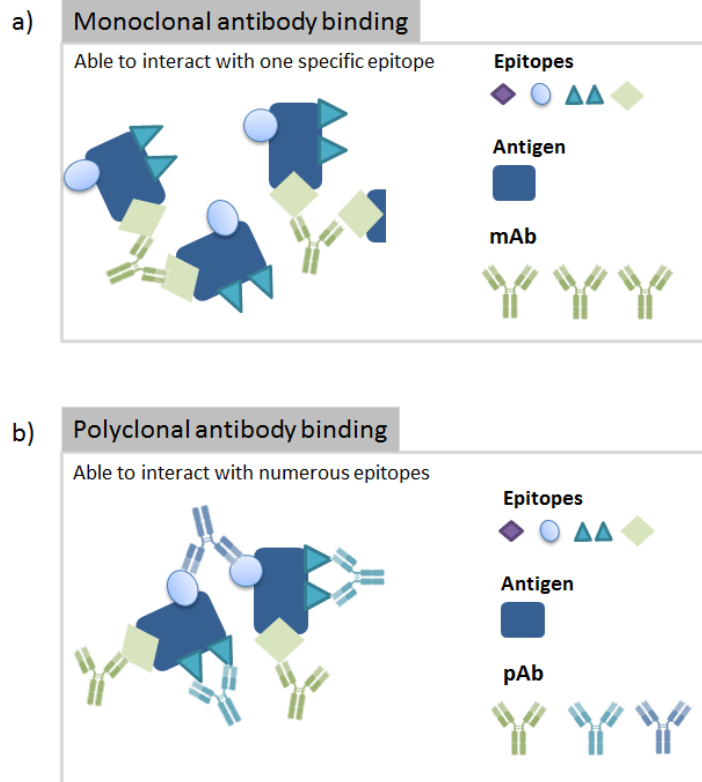


Figure 3. 1 The differences between a monoclonal antibody (mAb) and polyclonal antibody (pAb).

3.1a) The mAb are produced with the same type of immune cells that are all clones of each other and target the same antigen and same epitope. **3.1b)** pAb are produced from several various immune cells. These antibodies will have affinity for identical antigens but different epitopes.

3.1.1 Immunoglobulins (Ig): (monoclonal vs polyclonal antibody)

The antibodies can be divided into two categories based on how they were produced from lymphocytes, these are monoclonal antibody (mAbs) (Figure 3.1a) and polyclonal antibody (pAbs) antibodies (Figure 3.1b).¹⁹³

mAbs have a monovalent affinity, therefore are only able to bind and recognise a distinct epitope of an antigen. They are produced by matching B cells that are cloned from a single parent cell. Most mAbs are produced *in vitro*, using tissue culturing methods, in particular hybridoma procedures.¹⁹³

The technique involves immunisation of an animal to a specific antigen over a period of time. The B-cells are then collected from the animal's spleen and combined with a myeloma cell line, to create immortal B-cancer cell hybridomas. Once the immortal

hybridoma culture has been developed it can be a great source for the high quantity production of mAbs, which can easily be further purified using affinity columns (levels of purity within 98%).¹⁹⁴ However, it should be noted that the production of hybridoma cultures require a high proficiency and expertise that can be laborious (3-6 months) and expensive depending on the antigen that is being investigated. mAbs provide great selectivity in recognition of a desired epitope, which also translates to greater consistency throughout experiments with minimum cross reactivity.¹⁹⁵

In contrast, this high affinity for a particular epitope may be problematic, as in some cases it has failed to reproduce similar activity and neutralisation across different species.¹⁹⁶ The mAbs are most assailable to any alterations of the epitope binding sequence as most often they are produced in a different species than that of the *in vivo* experiment, which can lead to not fully preserving the variable binding region. As a result, this could immensely lower the binding capacity and provide no guarantee to produce a similar biological activity.

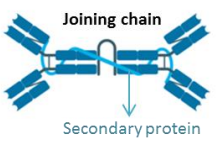
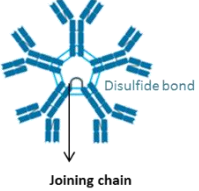
Unlike mAbs, polyclonal antibodies (pAb's) are made up of heterogeneous combinations of antibodies (Figure 3.1b), created by B cell clones.¹⁹⁷ pAbs can identify and bind with numerous epitopes available on a single antigen. Similarly to mAbs, pAb are also produced by the immunisation of animals to provoke a primary immune response, however the overall process is a much shorter period of time (4-8 weeks). pAbs are gathered from the serum, this is the solution component of blood with no proteins or cells. Further purification of specific pAbs or other proteins within the serum can be achieved using specific affinity chromatography columns.¹⁹⁸

3.1.2 Structural and physical features of Igs

The function of an antibody is through its 3D structure. The mammalian Ig have been categorised into five classes based on their heavy chains: IgG, IgA, IgD, IgE and IgM. Their structures are illustrated in Table 3.1.¹⁹⁹

Most antibodies are bivalent and tend to be built from four peptide chains; two heavy chains and two light chains that are connected by two disulfide bonds. The IgG isoform, is the most common type of naturally occurring antibody (~80% present in serum) and is made up of the two identical sets of heavy and light chains combined in a "Y" shape structure.²⁰⁰

Table 3. 1 The different classes of Ig structures details.²⁰¹⁻²⁰³

Classes	IgG	IgA		IgD	IgE	IgM
Structure						
Unit	Monomer	Dimer		Monomer	Monomer	Pentamer
MW (Daltons)	150,000	385,000		180,000	200,000	900,000
Light chain	κ λ	κ	λ	κ λ	κ λ	κ λ
Heavy chain	Human : γ _{1,2,3,4} Mouse: γ _{1,2a,2b,3}	α ₁	α ₂	δ	ε	μ
Subtype	Human: IgG _{1,2,3,4} Mouse: IgG _{1,2a,2b,3}	IgA ₁	IgA ₂	Non available	Non available	Non available
Length of Heavy chain	~450 amino acid	~450 amino acid	~450 amino acid	~ 512 amino acid	~550 amino acid	~550 amino acid
Role in immune system	Antibody in primary and secondary responses. Neutralises toxins and viruses.	Inhibits binding of pathogens to epithelial cells. Found in mucus, tears and saliva.		Important in B-cell activation. Found to also interact with mast cells and basophils to activate these immune cells.	On the basophils and mast cells, responsible for initiation of allergic response and inflammation responses.	Antibody released in primary response.

The light chain contains a single constant segment (CL) with a variable segment (VL). The constant fragments (Fc) are glycosylated, allowing greater stability of the structures and cell to cell adhesion. The structures of the Ig classes are illustrated in Table 3.1. The 3D structure of IgG is provided in Figure 3.2. The heavy and light chains of antibodies are referred to using Greek letters. These letters denote how the chains assemble, specify which group the antibody belongs to and what their specific roles are within the biological immune system.²⁰³

The constant region of the antibody tail also governs its half-life and ensures a greater bioavailability.²⁰³ From the above isotypes IgG and IgA are further divided into subclasses based on differences between the heavy chains.²⁰⁴ The variable region of the antibodies also consists of light chains, denoted as κ (kappa) or λ (lambda) which are common motifs found in all of the classes.²⁰⁵

The specificity of antibodies arises from the unique binding sites available at the tips of the variable domain as there is a pocket-like shape that is formed between the light and heavy chains. The pocket contains different size lengths of amino acid sequences that give rise to numerous loops referred to as complementarity determining region (CDR) loops that form the binding site.

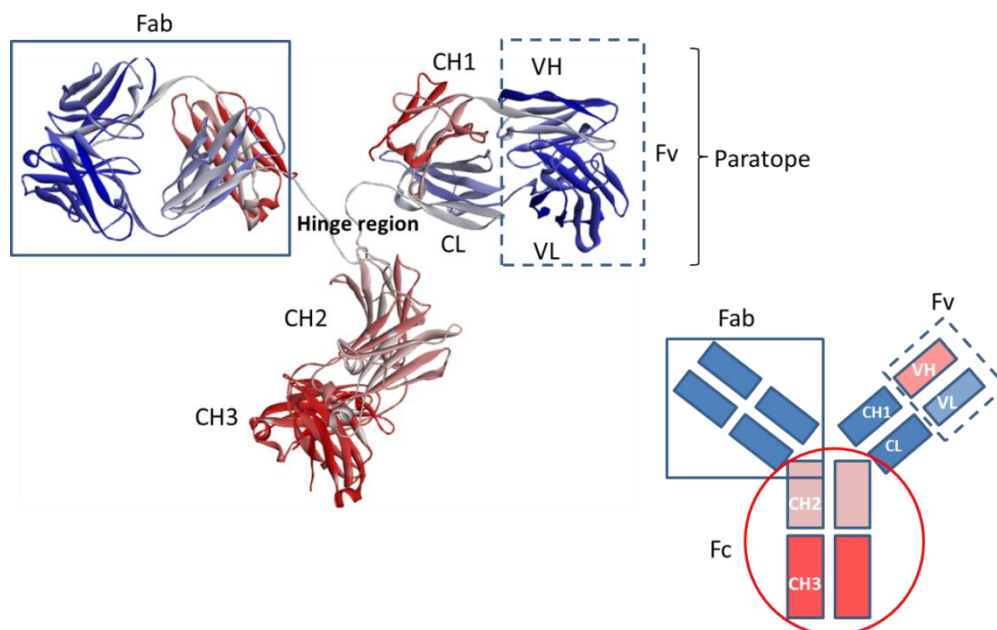


Figure 3. 2 The structure of immunoglobulin, PDB ID | 1IGT

A ribbon representation showing the four chains of IgG2 a monoclonal antibody divided into light chains (L) shown in blue and heavy chain (H) shown in red. The antigen binding site located in the Fab segment of the antibody is shown in blue square. The hinge region is made up of two disulfide bonds that link the variable regions to the constant fragment (Fc) of the antibody.

The hinge region is made up of the two disulfide bonds between the Fab and Fc segment and it allows flexibility at that region. The structure of antibodies can be altered by using enzymes (papain and pepsin) to perform site specific cleavages and

produce Fab fragments. For example, the bivalent $F(ab)_2$ fragment, (made up of two Fab fragments bound by two disulfide bonds) can be produced through pepsin by acid hydrolysis which fragments the Fc region.²⁰⁶

The $F(ab)_2$ region can be used to help trap particular proteins of interest from complex mixtures and even aid precipitation of antigens and co-crystallisation.²⁰⁷ The Fc region is a marker for classifying the antibody classes, and is able to be stabilised onto many innate surfaces in biological systems (e.g. on b-cell surfaces).²⁰⁸

3.1.3 Antigen-binding fragments (Fab)

Antigen-binding fragment (Fab) is referred to as the paratope and it is responsible for the Ig binding to its corresponding antigen using reversible interactions (e.g. hydrogen bonding (HB), van der Waals (VDW), hydrophobic and hydrophilic interactions).²⁰⁹ The structure in Figure 2.3 shows the Fab crystal structures. At the end of each variable domain there are the presence of three CDR loops that combined and are made from ~53 amino acids, (CDR L1-3 and CDR H1-3).²¹⁰ Therefore, in total there are six CDRs located on each variable fragment (FV) in a single antibody that can interact with the antigen of the target protein. This means overall, in an antibody molecule there are twelve CDRs as there are two FVs.

As demonstrated in Figure 3.3 the orientation consists of two closely patched anti parallel β -sheets, one containing four and the other made up of three strands. The whole structure is stabilised together with intra-domain disulfide bonds and weak interactions between the parallel residual side chains.²¹¹ Another significant difference in the structure of variable domains is that they are generally looser and form longer loops to join the individual β -strands.

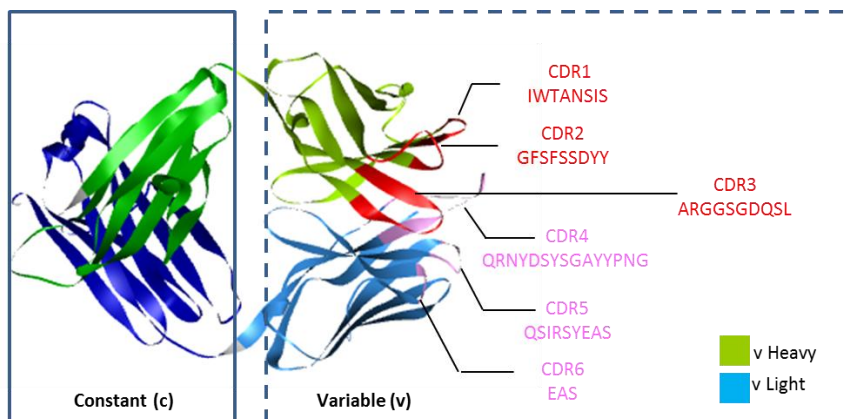


Figure 3. 3 A Fab region of the antibody (10A)

The crystal structure of rabbit mAb (PDB: 6CJK), showing the regions of both heavy (green) and light (blue) chains with their corresponding CDR domains that are illustrated in red and pink.

3.1.4 Fab binding mode hypothesis

The binding of the Fab regions to an antigen causes an alteration in the surface structure complex of both moieties. More specifically, the binding interaction of an antigen and antibody has been shown to be similar to other binding hypotheses, such as lock and key and conformational selection.²¹² The lock and key hypothesis states that two binding proteins can come together in a manner that reduces the change in their surface conformations, whilst maintaining a similar orientation to their unbound states.

Alternatively, another hypothesis proposed by Foote *et al*²¹³ was the conformational selection model which states that the antibody protein can fluctuate between different conformational states before binding to the antigen. The induced fit hypothesis has also been proposed. Here there is a greater flexibility in the Fab, due to conformational changes in the side chains, backbone residues and specifically the CDR to accommodate the binding of the antigen.²¹⁴ Crystallographic studies have also shown that the bound conformation of the CDR and the unbound structure has differences in the H3 loop, which aids antigen binding.²¹⁵

Other investigations experimentally investigate the binding mode of Fab by designing dual-specific antibodies. These antibodies contain dual-action Fab regions for targeting VEGF and HER2 proteins.^{216,217} By using crystallographic and specific mutational studies it was shown that antibody binding surfaces can overlap, thereby

neutralising both VEGF and HER2 cell mediated processes during *in vitro* and *in vivo* tumour progression experiments.

Additionally, this Ig multi-specificity has also been observed when analogous epitopes are presented on more than one antigen. This was reported by Fuh and colleagues²¹⁸ who demonstrated that there was a cross reactivity with antibodies that were binding to orthologous macromolecules in different species. Moreover, the antibodies were able to recognise different targets in the same family. These studies challenge the hypothesis that most mAbs are monospecific, and that they are normally compatible with only a single antigen. This also suggests that the concepts of conformational selection and induced fit may be more suitable for these bindings.

3.1.5 Computational approach for predicting Fab binding to P8 of GluNR1

Computational techniques have greatly contributed in speeding up the development of antibody therapeutics alongside traditional experimental methods.^{219,220} In rational antibody design, specifically methods such as homology modelling,²²¹ protein-protein (PP) docking²²² have greatly contributed to establishing structural features of antigen-antibody complexes.

3.1.5.1 Homology modelling

Homology modelling, is the production of an atomic-resolution model of a query protein (e.g. pAb Fab) from its primary structure (amino acid sequence) and resolved three dimensional (3D) structure of a related homologous protein. Although, there could be multiple known protein structures that can match a particular query sequence, this can help improve the alignment of the amino acid residues between the template sequence and query sequence.²²³ Worldwide, multiple organisations have compiled together their data to unify the published information to help facilitate research projects. Some examples of organisations and databases include The European Bioinformatics Institute (EBI),²²⁴ GenBANK²²⁵ and The International Protein Sequence Database (PIR).²²⁶

Homology modelling has the great advantage of avoiding all the challenges associated with novel protein structure identification and characterisation.²²⁷ For example, structural information from X-ray crystallography and nuclear magnetic resonance (NMR) tends to be very challenging to interpret and these methods are

sometimes not suitable for all protein structures; specifically membrane proteins and multiunit structures.²²⁸ This is mainly due to complexities in purification, the stability of proteins, growing sufficient amount of crystals and the experimental methods used. The more the complex the protein assembly, the more time it would require to resolve its structure with a suitable resolution for further studies.²²⁹

The accuracy of the structures produced through homology modelling relies on the sequence identity between query (target protein) and template sequences. This approach relies on the fact that protein assemblies are reasonably conserved when compared to amino acid sequences between different structures.²³⁰

However in the 30-50% identity range, the errors can be far greater and this is most often observed within the loops of the protein structure. Any identity score <30%, results in serious errors and severe miss predictions for the basic folding of the protein. Lower sequence identity values would lead to poor prediction of the original protein sequence, representing a very different structure from the target protein. Blundell *et al*²³¹, utilised multiple protein references and were able to show that by identifying the regions of molecules that were similar to each other, between different families of the same protein could provide a greater confidence in prediction of a new protein member with greater precision.

Homology modelling has shown to produce much higher quality predictions in protein structure, in comparison to other computational structural methods (e.g. *de novo* modelling). Structures produced through homology method display much lower root mean square deviation (RMSD) values (average distance between atoms of superimposed protein back bone) and better resolution models.²³²

It is also important to mention that new algorithms have been developed that can singularly compete with traditional methods of protein structure predictions. One example is AlphaFold program by Protein Structure Prediction Centre at the University of California.^{233,234} This year, Jumper *et al*²³⁵ reported that AlphaFold software uses a neuronal network to utilise deep learning by selecting patterns in amino acid sequences of proteins from a global database. As it gathers data it can then subsequently identify the structure of a protein within minutes. AlphaFold was originally developed in collaboration with Google and it has shown to be robust in determining the 3D protein structures.²³⁶

2.1.5.2 Antigen-Fab interaction: PP docking

To date, there is an exponential amount of data on the 3D structures of antibodies that has materialised from crystallographic studies. The number of crystal structures of antibodies added in the PDB is about ~2.1%, which include Fabs and single-chain variable fragment (scFvs).²³⁷ These structures also show the number of protein-protein interaction (PPI) of CDR domains with a variety of binding partners (proteins, macromolecules and haptens).

PP docking programs have utilised these data and provide a fast alternative approach to experimentation to characterise these complexes. However, the prediction of antigen-antibody binding still remains challenging due to potential inaccuracies in the models used, complex binding interfaces, variability in the CDR H3 loops/disordered regions when bound/unbound and high flexibility in the docking models creating unlikely induced fit which ultimately produces false predictions.²³⁸⁻²⁴⁰

The PP docking programs produce thousands of potential conformations, which are then subsequently ranked using scoring functions to identify the model that is closest to the native crystal structure. In addition, the identification of residues involved in the CDR domain (paratope region) is accurately predicted when the sequence or 3D model of the antibody is available through computational approaches.²⁴¹

PP docking programs have been developed that incorporate rigid-body docking such as ZDOCK and ClusPro, which excludes conformational changes that may occur during complex formation of antigen-Fab. Alternative methods also apply flexibility within their binding predictions for side chains and back bones such as ATTRACT and HADDOCK.²⁴² However, it should be noted that further flexibility incorporated into these large systems can increase computational time immensely.

In this investigation, to predict the PPI of antigen-Fab, ZDOCK software was used to analyse how the variable region of the Fab would interact with the GluNR1 subunit of the receptor. The ZDOCK protocol initiates the rigid body docking of two proteins²⁴³ The software uses a pairwise shape complementarity (PSC) function which inputs the total number of receptor-ligand atom pairs within a certain distance and subtracts a penalty for clashes. This is an improvement from the previous grid based function that identifies the position of the two complexes by placing a layer of grid points on

the receptor area and matching the grid points to the ligand surface area, and then subtracting any potential clashes. The ZDOCK protocol can be summarised in Equation 3.1.

$$\text{ZDOCK} = \text{PSC} + \text{desolvation} + \text{electrostatics}$$

Equation 3 1 ZDOCK components

ZDOCK is the sum of the PSC, desolvation and electrostatic terms using the Fast Fourier transform algorithm.

The atomic contact energy values were obtained from a training data set of 90 protein-atom-protein contacts from high resolution crystal structures. The PSC function is made out of both a favourable and a penalty term. The favourable term provides the total number of atom pairs between the receptor and the antibody within the distance cut-off. The penalty terms calculates the clashes of core-core, surface-surface and surface-core grid point overlaps. The PSC with desolvation score is combined where a negative score would show more favourable interaction energy.

This project was initiated with the therapeutic effects of an antibody against a sequence of peptide (P8) located on the GluNR1 subunit of the NMDAR. The binding of this antibody with its corresponding antigen would play a crucial role for the observed therapeutic effect.²⁴⁴ However; the molecular mechanism of action of the pAb is not fully understood yet. Therefore, making it much more challenging to elucidate the important residues involved in the binding and more importantly, mimic these interactions with similar molecule binders. In addition, from the large number of antibody sequences released from the NCBI (from mice organisms *Mus musculus*, total 18039 sequences), it is possible to examine if a potential homology model of the Fab region of a pAb could be developed to predict interactions of the Fab region with the GluNR1 subunit.

Zhao *et al*²⁴⁵ had previously reported that by applying homology modelling, molecular docking and molecular dynamics they were able to demonstrate recognition of amyloid- β with Fab homologous antibodies designed for immunotherapy against Alzheimer's disease. In case of crenezumab, there was no 3D crystal structure available. However, the investigators found that crenezumab did

have a high sequence similarity with creneFab (97%), therefore it was possible to produce a template-based homology model of the antibody and examine its interaction with amyloidi- β by PP docking.

3.2 Aims of part one

The specific aim of this part was to understand the pharmacophore involved in P8 GluNR1 through antigen-Fab docking. This understanding will guide the VS of part two. To achieve this aim, the following objectives had to be met:

- i) Building of a homology model of mouse pAb
- ii) Perform supporting studies for the PP docking and examine the validation of the pAb interaction with its corresponding antigen.
- iii) Dock the homology pAb model with the GluNR1 P8 region and understanding the potential PPI between the two molecules

3.4 Results and discussion

3.4.1 Supporting studies for the antigen-Fab docking

To examine how well the experimental docking protocol can predict the native PP interaction of pAb with P8, supporting studies were performed using experimental data which consisted of solved bound and non-bound antigen-mAb structures from the PDB. The antibody structures selected are summarised in Table 3.3. As the active pAb for this investigation was obtained from mice serum, the antibody selected for the docking studies were also from the mouse species.

Table 3. 2 The antibodies selected for initial docking studies

Complex name	mAb PDB	Antigen PDB	Complex PDB	Resolution (Å)	Method	Organism
mAb against chicken egg white lysozyme	1MLC	1LZA	1MLC	2.50	X-ray diffraction	Mus musculus (mAb) Gallus gallus (antigen)

Initially, the crystal structure of unbound antigen (PDB 1LZA) as well as a crystal structure of the mAb-antigen complex (PDB 1MLC) was used to test if the ZDOCK can identify near native structure.

The assessment of the mAb and its corresponding antigen showed the sequence of the CDR segment of the mAb (Figure 3.4a). According to experimental studies from Braden *et al*,²⁴⁶ the antigen binding site consisted of 11 amino acids that interact with the CDR domain from the total of 120 amino acids that made up the lysozyme (Figure 3.4b,c). Subsequently, these sequences were implemented into the protocol to guide the docking studies towards identifying the correct orientation of the two binding partners and reducing the time required to search the conformational space.

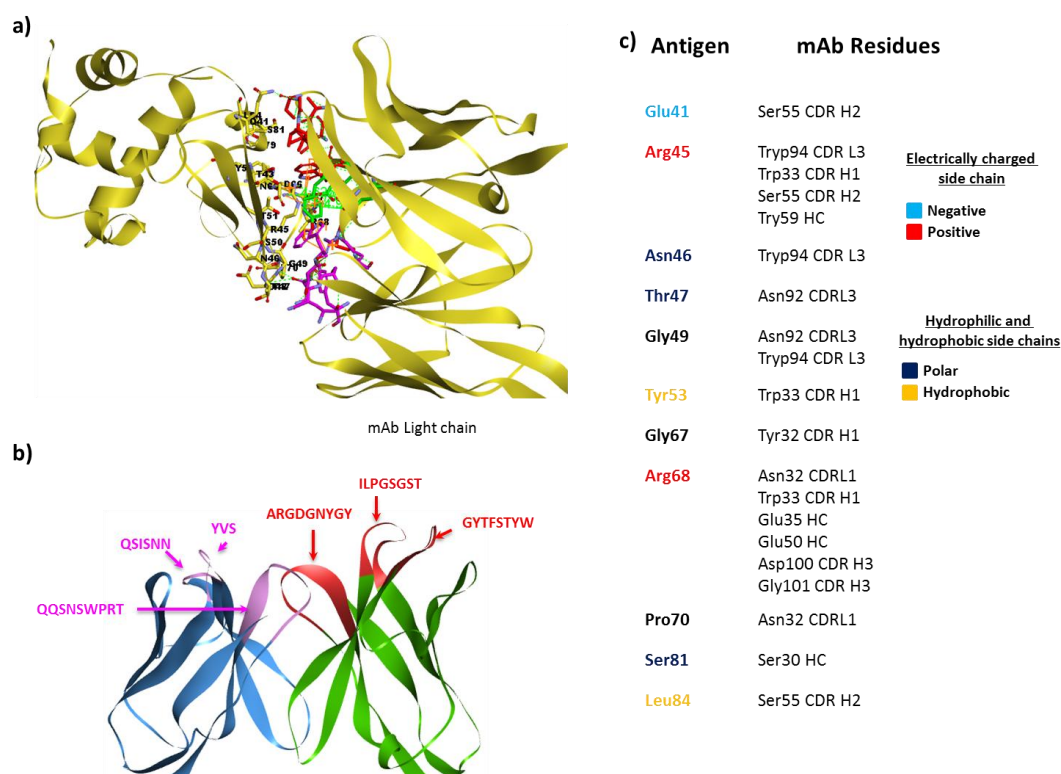


Figure 3. 4 The binding of the mAb against chicken egg white lysozyme.

Fig 3.4a) The lysozyme 11 antigen residues displayed in stick format in yellow and they are in contact with the antibody residues from the CDR domain. **Fig 3.4b)** Better view of the CDR loops in the crystal structure is also demonstrated. **Fig 3.4c)** Illustrating the interacting residues between the antigen and the antibody from the original native complex crystal structure studies.²⁴⁶ There is a total of three salt bridges formed by the antigen Arg68 with mAb Glu40 and Glu55 and antigen Arg45 with Glu55 as well.

Based on the filtering process that excluded the poses which were not able to satisfy the required contact with amino acids in the antigen protein, 168 poses were ranked as the top poses from 2000 poses generated in 86 clusters. There were a total of 16 top poses that were near the native ligand orientation as shown in Table 3.4. The

poses with relatively closer orientation to the crystal conformation were shown to be in cluster 9, which had a total of 45 poses in its set. There was also two poses from cluster 2 and 4 that by visual inspection showed orientation close to the crystal structure. However, the RMSD values for both poses were high, which indicated poor conformation prediction in comparison to crystal structure. In addition, the ZDOCK score and ZRANK for both of these poses was also very low (Table 3.4) indicating unfavourable binding. In pose 89 there is a direct 180° rotation of the Fab binding, placing the CDR domains in wrong 3D orientation in comparison to the crystal structure (Figure 3.5). After investigating all the poses in cluster 9 it revealed that the best pose (pose 1095) had a main chain RMSD of 5.8 Å, with a ZDOCK score of 7.32 kcal/mol and a ZRANK score of 4.90 kcal/mol.

Table 3. 3 RMSD Calculation of Reference 1MLC mAb versus the best docked mAb poses.

Molecule	Cluster	C-Alpha (Å)	Main- chain (Å)	Side- chain (Å)	All Protein (Å)	ZDOCK (kcal/mol)	ZRANK (kcal/mol)
Pose1095	9	5.805	5.803	5.808	5.804	7.32	4.90
Pose1079	9	6.460	6.461	6.480	6.473	6.62	4.60
Pose1027	9	6.552	6.551	6.411	6.486	7.28	2.97
Pose696	9	7.245	7.248	7.203	7.229	6.78	-6.28
Pose1032	9	8.257	8.260	8.280	8.272	6.64	3.16
Pose1202	9	8.843	8.846	8.825	8.838	7.52	7.79
Pose105	9	8.903	8.904	8.860	8.887	7.22	-30.84
Pose708	2	8.903	8.904	8.913	8.912	6.96	-5.81
Pose815	9	9.153	9.150	8.969	9.063	6.84	3.41
Pose977	9	9.804	9.809	9.718	9.768	6.62	1.56
Pose48	9	10.413	10.414	10.388	10.405	7.12	-38.91
Pose1289	9	10.952	10.958	10.931	10.950	6.80	10.0
Pose26	9	13.086	13.090	13.000	13.053	7.02	-43.82
Pose42	9	13.922	13.929	13.838	13.894	6.74	-40.36
Pose30	9	16.273	16.282	16.154	16.232	6.84	-42.80
Pose89	4	29.903	29.878	29.858	29.864	7.04	-32.94

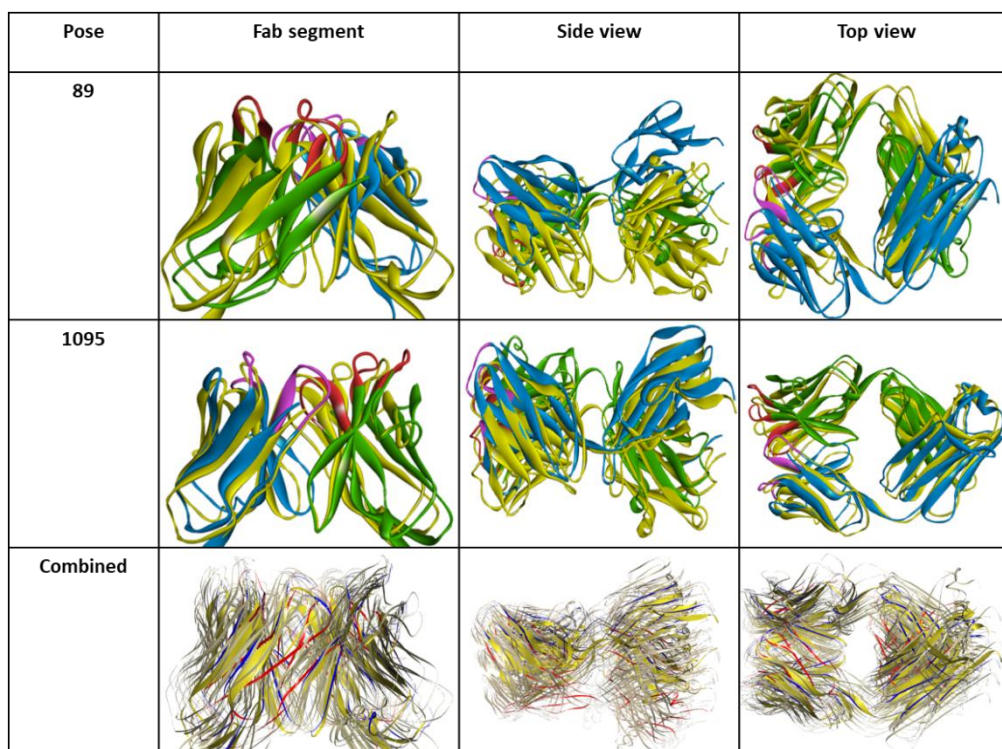


Figure 3. 5 The superimposed poses of docked confirmations with the reference bound mAb crystal structure.

The constant domain of the Fab segment was also elevated above the native conformation (Side view). Pose 1095 was better at mimicking of the native crystal conformation with the correct 3D binding orientation being obtained as well as overlap of some the residues in the constant domain. The combined pose consisted of the 16 docked orientations (shown in the flaxen colour) that were identified that were relatively close to the crystal structure. The best pose 1095 is shown in blue and the worst pose 89 is shown in red.

From the scoring functions, ZRANK was able to identify the unstable contact surfaces and ranked these overall poses with a negative score. In contrast, pose 1095 was able to resemble the native pose with a better quality and overlapping residues of some of the β -pleated sheets of the Fab domain. Of course, the disordered loops within the structure were still not overlapping entirely, and although the CDR binding residues were in the correct orientation their distant positions limited their contact with the antigen molecule. In the light chain residues this led to some of electrostatic interactions between key residues such as Asn32 and Asn92 acting as HBD's.

The heavy chain CDR residues Trp33 and Trp94 contributed to forming the hydrophobic and VDW interactions. HB between Ser55 and Glu41 of the antigen

was also formed. Majority of the residues were shown to have the correct orientation, with the positions of the important heavy atoms matching the native structure. This may have been due to the protocol not allowing any flexibility of the side chain residues as fluctuations at those disordered regions were not permitted.

As this was a rigid body docking, there were not many fluctuations observed when comparing the antigen structure of the unbound conformation from the crystal structure (1LZA_UB_CS) to the antigen bound orientation (1MLC), Table 3.4. The majority of changes in conformation were observed at the residues Arg45 and Pro70 that were involved in the direct binding of the antigen and stabilising the complex. Arg45 was responsible for forming one of the salt bridges with a distance of 4.6 Å in the complex which ensured better stability upon binding. It was also involved in forming two hydrogen bonds with the mAb_B Glu55, with bond distances of 1.8 Å and 2.1 Å, respectively.

Table 3. 4 RMSD Calculation of reference 1MLC_E Antigen in the complex conformation versus the unbound antigen (1LZA) docked and in crystal structure.

Molecule	C-Alpha (Å)	Main-chain (Å)	Side-chain (Å)	All Protein (Å)
1LZA_UB_DP	0.627	0.727	1.693	1.293
1LZA_UB_CS	0.627	0.727	1.750	1.327

Unbound from the docked protocol (UB_DP), Unbound from the crystal conformation (UB_CS)

The RMSD calculations for the antigen in docked pose, unbound and bound showed the side chains were within a 1.75 Å distance meaning that the antigen structure did not drastically change conformation based on the mAb docked pose.

The results demonstrated that it was possible to obtain near native structures in the top ~1100 poses of the antigen-antibody complexes. In the supporting study it was clear that to reduce the number of false positives among the top ranked poses it was important to incorporate as much information available about the binding. Specifically, once the binding site was defined based on the antigen residues within the crystal structure, this helped improve predictions of the mAb binding to its corresponding target. The RMSD distances of the predicted poses of the mAb were also relatively lower when compared to the crystal structure, with the best pose 1095

having a RMSD of 5.81 Å. However, there were no poses that could mimic the correct native conformation entirely or with a RMSD value lower than 2 Å. There were still many poses generated that had a RMSD greater than 10 Å. Although, it was important to note that the RMSD values calculated for these studies were performed on the complete Fab structure instead of just focusing of the CDR segment, which could have explained the large variation in the position of the residues.

3.4.2 Homology model: Alignment and identification of potential Fab templates

The sequence search on the query structure pAb 5ACO was initially carried out to identify mouse derived antibody structures. The binding of the query pAb to its original target BG505 SOSIP²⁴⁷ (PDB 5I8H) is shown in Figure 3.6. The CDR domains calculated are demonstrated in Figure 3.6b and the surface representation is also demonstrated in Figure 3.6c.

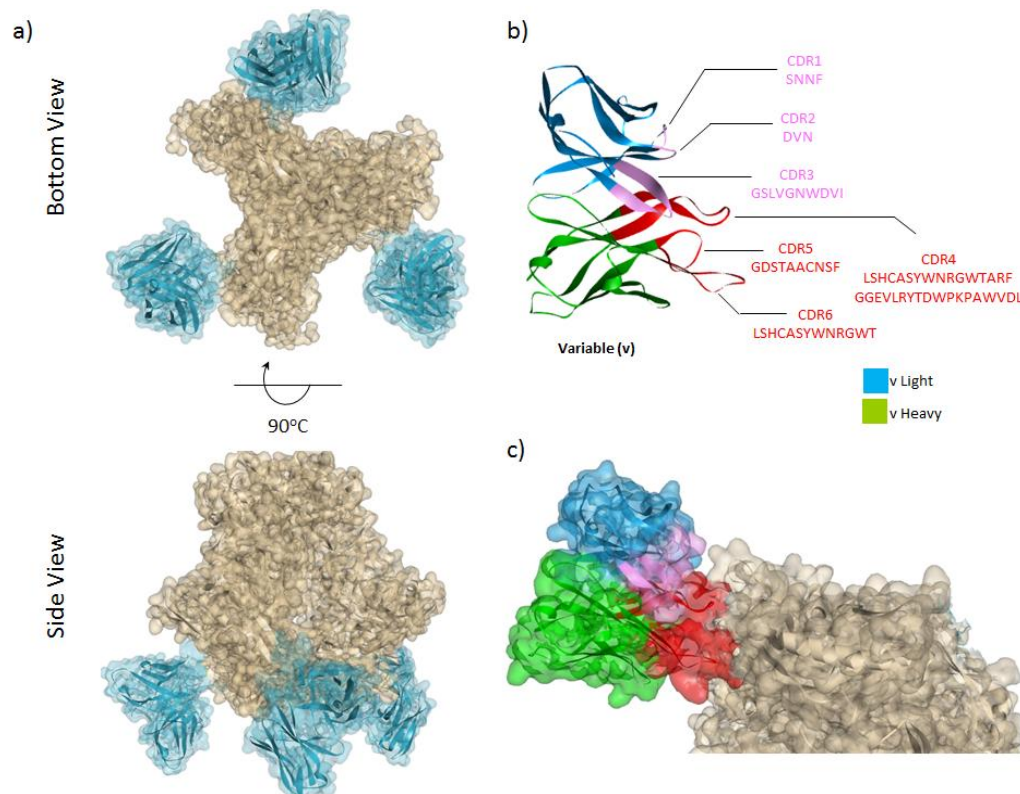


Figure 3. 6 The binding of query pAb with its target protein BG505 SOSIP

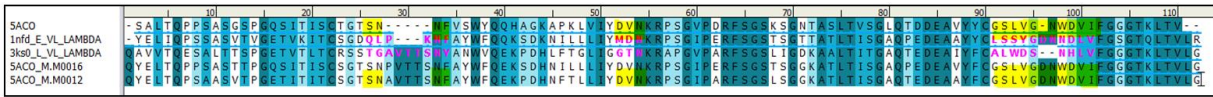
3.6a) The bottom and side view of the immune complexes, BG505 (brown colour) with the pAb Fab region (cyan) that were obtained from rabbit serum. The structure was obtained with cryo-em at a resolution of 4.36 Å shown in surface representation. **3.6b)** The analysis of the pAb binding to the CDRs with sequences. **3.6c)** A surface representation of the epitope-paratope interaction, demonstrating the long pAb, CDR4 and CDR6 are responsible for most of the surface contacts with a lysine rich loop on BG505.

The search showed that there were 37 overall templates identified for the pAb 5ACO, (provided in Appendix B). Table 3.5 demonstrates three of the best matched sequences and their 3D structure resolutions. The templates 3KS0, 1NFD and 3GKZ was used to build the homology model.

a) Original FV region of pAb sequence



b) FV region VL_Lambda



c) FV region VH

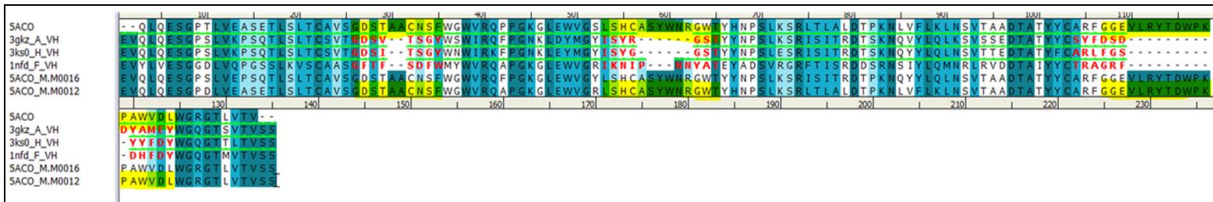


Figure 3. 7 The primary sequence of FV region of pAb query structure, templates and the homology models.

3.7a) The pAb query structure sequence showing the VH chain in green with CDR domain in red and VL region in blue with CDR domains in pink. **3.7b)** The FV region of the query, templates PDB: 3GKZ, 3KSO and 1NFD. The homology models are also shown, 5ACO_M.M0012 and 5ACO_M.M0016. **2.7c)** The primary sequence of VH regions.

The CDR loops in the pAbs were identified and are presented in Figure 3.7a. The next step was to incorporate pAb CDR sequences into the VL and VH chains of mouse antibody crystal structures. The homology model structure produced was built with MODELER (version 9v10) available in DS. The primary sequence overlap is provided in Figure 3.7, showing large regions of overlap between the top models generated 5ACO_M.M0012 and 5ACO_M.M0016 and the crystal structures of the mouse FV segments.

Table 3. 5 The best matched templates identified for the pAb

Top Hit	PDB	Similarity (%)	Identity (%)	Resolution	Organism	Ref
Overall	3KS0	79.8	54.9	2.7	Mus musculus	223
Light Chain	1NFD	76.7	53.7	2.8	Mus musculus	224
Heavy Chain	3GKZ	88.5	64.4	1.9	Mus musculus	225

3.4.3 Homology model: 3D model

The structural features from the template proteins were then used to set spatial restraints which could then be used to produce modelled protein structures using simulated annealing and optimisation procedures. Figure 3.8a shows the templates of mouse crystal structures superimposed over the original crystal structure. Figure 3.8b demonstrated the 20 chimeric templates generated from MODELER. More importantly, it also shows the key CDR domain overlapping sites. By generating multiple models, it gave the opportunity to look into the differences between the structures. The RMSD C- α and the main chain calculation of models generated with the crystal structures was $\sim 2 \text{ \AA}$.

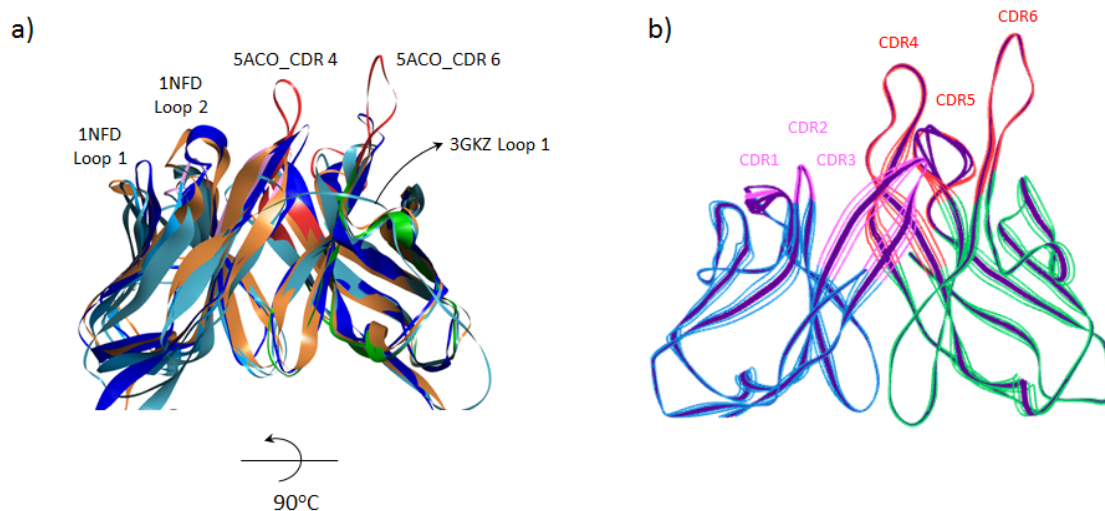


Figure 3. 8 Superimposed structures of query models and homology models

3.8a) The superimposed crystal structures of templates PDB: 3GKZ (cyan), 3KSO (orange) and 1NFD (blue) and the query structure (green). Showing the sites of most variation from the models 3GKZ loop1, 1NFD loop1 and 2. The most distinctive difference between the templates and query structure were also the CDRs 6 and 4 that were larger in comparison.

3.8b) The superimposed structure of the 20 models generated (purple) showing the additional CDR from the query structure into the mouse crystal structures.

The probability density function (PDF) total energy for the homology models were very similar to each other. The DOPE score which is a pairwise atomistic statistical potential was used to examine good models from the bad models. The lower the DOPE score the better and more stable the orientation of the protein structure. Here it was used to compare the homology models that were generated and rank them.

The smallest PDF energy was observed for model 5ACO_M.M0012 which had a total energy of 1633.83 kcal/mol and a DOPE score of -24584.78 kcal/mol. Model 5ACO_M.M0016 had the next smallest energy with a PDF total energy of 1635.27kcal/mol and a DOPE score of -24596.54 kcal/mol. The least stable model was observed for 5ACO_M.M0002 which had a PDF total energy of 1711.7439 kcal/mol and a DOPE score of -24439.9941 kcal/mol. The PDF physical energy of 95.29 kcal/mol for 5ACO_M.M0002 could suggest greater restraints in the folding of the loops making up the Fab segment, causing clashes between the inter-residue bonding.

Table 3. 6 The 20 homology models generated including their PDF and DOPE score values.

Name of Model	PDF Total Energy (kcal/mol)	DOPE Score (kcal/mol)
5ACO_M.M0012	1633.8311	-24584.7852
5ACO_M.M0016	1635.2764	-24596.5371
5ACO_M.M0018	1636.4839	-24570.9492
5ACO_M.M0015	1638.7592	-24541.5332
5ACO_M.M0006	1641.4448	-24516.8594
5ACO_M.M0010	1641.5549	-24506.5625
5ACO_M.M0017	1644.2438	-24516.4629
5ACO_M.M0008	1644.8813	-24462.4922
5ACO_M.M0001	1647.2426	-24500.0605
5ACO_M.M0007	1648.4141	-24490.3672
5ACO_M.M0003	1649.2709	-24492.1738
5ACO_M.M0013	1652.767	-24519.1172
5ACO_M.M0020	1687.1581	-24418.3086
5ACO_M.M0004	1687.3275	-24461.1738
5ACO_M.M0011	1690.1678	-24483.1563
5ACO_M.M0009	1690.1726	-24435.9219
5ACO_M.M0019	1695.5414	-24511.7793
5ACO_M.M0005	1703.0116	-24451.084
5ACO_M.M0014	1706.7236	-24438.2988
5ACO_M.M0002	1711.7439	-24439.9941

The stability observed with the DOPE scores were also shown with Ramchandran charts (Figure 3.9) that confirmed the models had low numbers of residues that cause violation and steric clashes.

In the Ramchandran charts the amino acids are represented as spheres. There were a total of 15 amino acids in the homology model that cause phi (Φ) and psi (Ψ) angles to clash and they were mainly located in the loops of the FV region, not all in the CDR domain. The majority of other amino acids in the largest loops CDR4 and 6 were all shown to occupy the allowed regions of the chart (quadrants I-III).

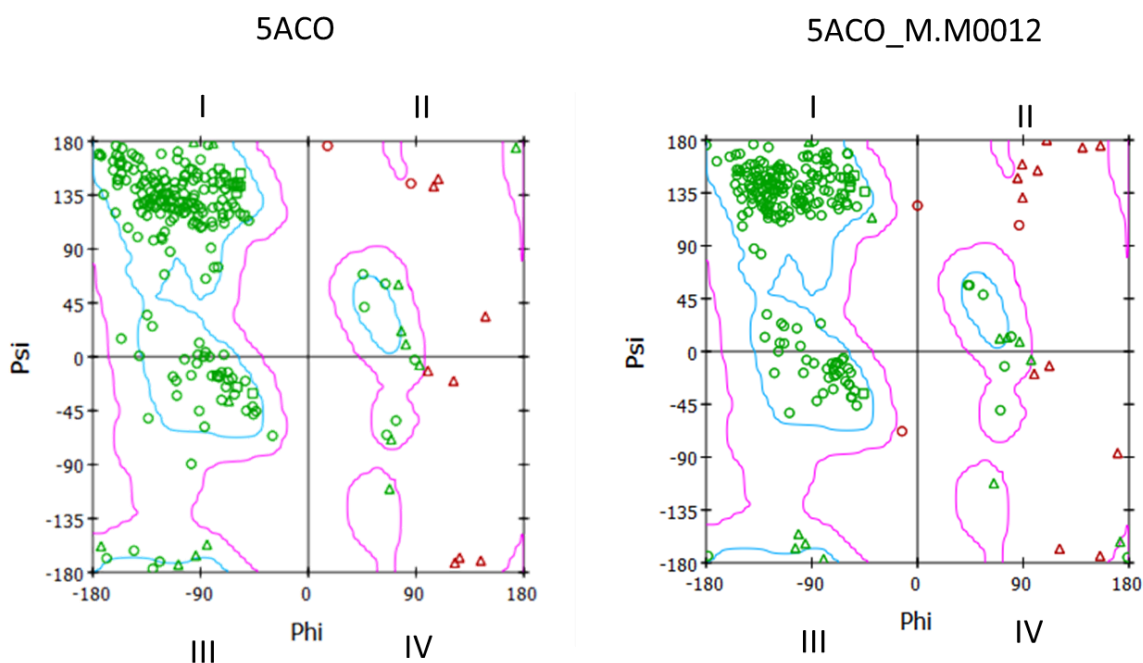


Figure 3. 9 The Ramachandran chart of the query structure 5ACO and homology model.

The charts demonstrate that most amino acids of the query structure and the model tend to occupy the allowed quadrants (I-III). There are few amino acids that are observed in the disallowed region (IV). The amino acids observed for CDR1 (Asn65) and CDR 4 (Asp111) have shown to be in the disallowed region. Overall, the charts demonstrate that the homology model is very similar to the original query structure.

The only amino acids that may be the least stable and have some steric hindrance in the CDR were shown to be in CDR 1 (Asn65) and CDR 4 (Asp111). The other amino acids occupying the white regions of the chart mainly corresponded to glycine residues across the model and these amino acids are the only ones that can occupy these sterically disallowed regions as it does not contain a chiral centre. It is important to note that *L*-amino acids cannot form left handed helices that tend to occupy top right of quadrant (II) of Figure 3.9, however individual amino acids such as Asn28, Asn48 and Asn85 in this model can adopt this position.

To cross validate the quality of the 5ACO_M.M0012 model, a Ramachandran plot was generated using PROCHECK v6.0 (see Appendix C). The homology model 5ACO_M.M0012 showed that 82% of the amino acids of the total residues were in the most favourable regions and only 1.5% of residues were present in the disallowed region. This indicated that 5ACO_M.M0012 was a good quality model.

3.4.4 PP ZDOCK of the Fab model onto GluNR1

To dock the built homology model onto the GluNR1 P8 site, the ZDOCK algorithm was used. The top poses were clustered according to their positions. All of the poses were ranked using the ZDOCK scoring function and re-ranked using ZRANK.

Initially, 5ACO_M.M0012 was docked onto 5H8F_B (LBD) of the GluNR1 subunit. The largest cluster (Cluster 1) contained 45 poses. In the top scoring ranked poses that are presented in Figure 3.10a, it demonstrates the poses are in a tight clustering format in three main sites S1, S2 and S3. The highest scoring poses seem to occupy mainly S1 (ZDOCK 19.84 kcal/mol, ZRANK -86.39 kcal/mol), and S3 (ZDOCK 21.54kcal/mol, ZRANK -29.971 kcal/mol) which are located below and above the LBD segment (Figure 3.10b).

The S1 pose scored fairly well in its corresponding cluster, although by visual inspection the protein complex seemed less stable. Most of the key CDR domains seemed to have less interaction with the receptor and the interactions were mainly with the short looped light chain CDRs. Also, the majority of the residues involved in the interaction were located behind the P8 segment. It's important to mention that the poses generated for S3 could arguably be less likely as the GluNR1 NTD occupies that region, which makes it less likely for the FV to slide in between the two domains.

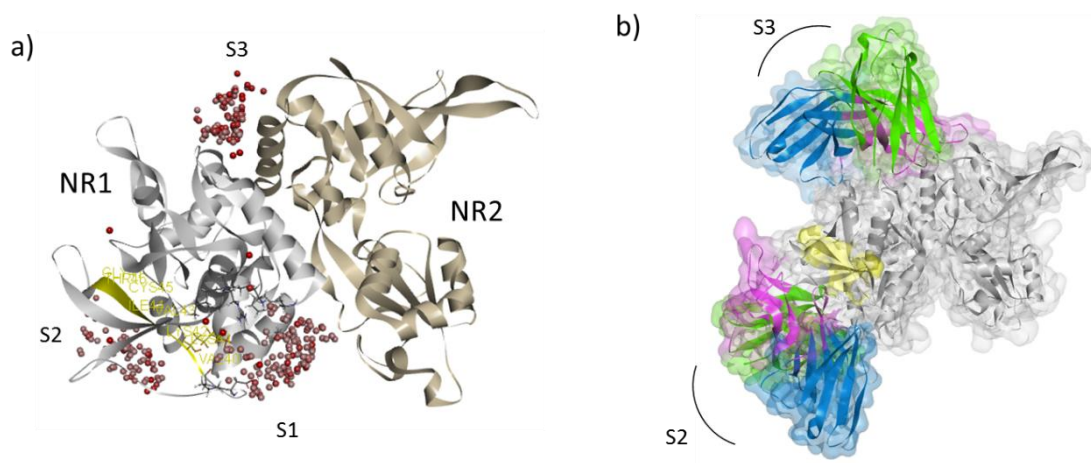


Figure 3. 10 Demonstrating the 3 main clusters generated from ZDOCK.

3.10a) Docking of the 5ACO_M.M0012 (FV) onto the NR1 LBD (PDB: 5H8F) generated in total 478 poses in the 3 best scored clusters. Each sphere represents a binding pose. The best scored poses are indicated by the darker red colour and the pale pink represent lower score poses. **3.10b)** Illustrating the binding orientation of the two molecules at site 2 (S2) and at site 3 (S3), with the surface representation of top FV poses covering large segments of the receptor LBD respectively.

The majority of the binding interfaces for the top scoring poses at S2 did show the involvement of initial amino acids within the P8 sequence, mainly Val40, Lys41 and Lys42. This indicated that even binding from the back of the P8 sequence could cause alternations for these residues to some extent, their involvement in binding through polar interactions. The surface structure of the top scoring poses for the pAb FV region docked onto the S1-3 sites is shown in Figure 3.10b.

Interestingly, none of the poses generated were able to directly cover the full surface of the P8 sequence, which may be due to the flat surface available at that site of the LBD, and therefore the FV segment was unable to be stabilised directly on to the sequence. Given that the full crystal structure of the NMDAR was available, it was possible to examine what poses would be the most stable on the full sequence of GluNR1. The built homology model 5ACO_M.M0012 was docked onto a single GluNR1 subunit (PDB 4PE5_C). Although the resolution of this model may not have been as suitable as the 5H8F_B crystal structure, it was important to examine how

stable the conformations of the Fab segments were when compared to other regions on GluNR1, specifically the NTD and LBD.

In this docking protocol the filter that focuses the binding poses that were close to the P8 sequence were removed and the poses were allowed to be generated from the NTD to the LBD. The only restriction applied was to block docking at the TMD regions as the pAbs would not be able to reach within the membrane of the receptor, and hence would not be suitable to be contained in the docking model. The results demonstrated that the top scoring poses calculated for 4PE5_C were able to cover most of the protein structure from NTD and LBD in comparison to the 5H8F_B protein. The top poses in the larger clusters could be divided into 6 sites onto the protein. The poses predicted for site 3 and 6 could potentially be much less likely to occur due to steric clashes with the GluNR2b chain within the receptor (Figure 3.11). The best docking poses were predicted for site 4 with a ZDOCK score of 26.96kcal/mol, located below the P8 sequence. This was followed by interactions at sites 2, 1 and finally 5. From the docking poses predicted it was clear that the best scoring sites were at a more exposed surface, hence it was easier to accommodate the FV region in a more stable format.

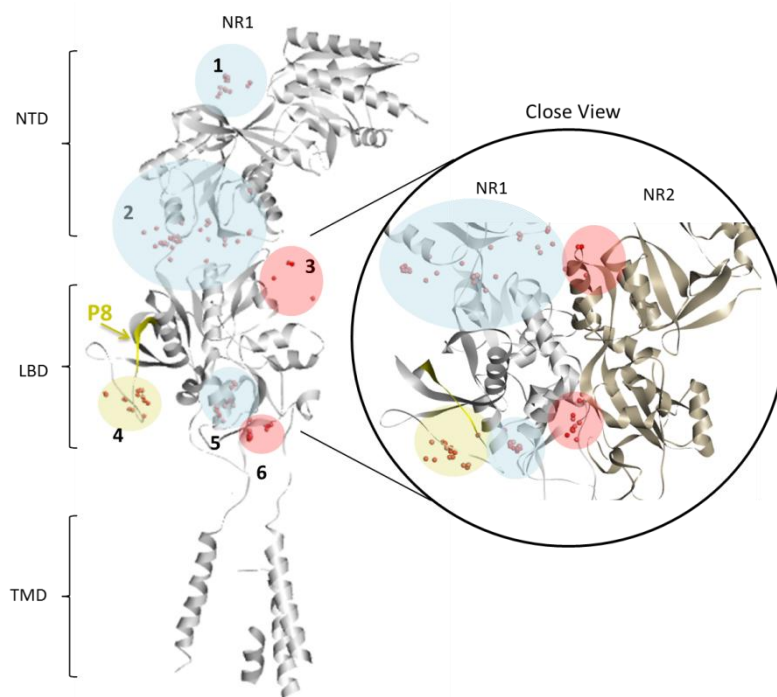


Figure 3. 11 The top poses predicted for docking the 5ACO_M.M0012 binding to NR1 model 4PE5_C.

The top poses in the largest clusters are represented as red dots onto the grey GluNR1 (4PE5_C) chain. A total of 6 sites were calculated, however site 3 and 6 seemed to be in very close contact with the GluNR2 (cream) chain as observed from the crystal structure. As the atomic radii of the amino acid atoms would clash in between the two subunits, it would make the poses invalid. This is because of steric hindrance of the chains within the NMDAR assembly.

The binding scores at other sites illustrated in Table 3.7 suggested that binding of the FV region would be most favoured at site 4 and site 2 which had ZDOCK scores of 26.96 kcal/mol and 18.50 kcal/mol, respectively. This was also supported by the corresponding ZRANK score of -45.69 kcal/mol and -50.56 kcal/mol. This could suggest that the direction of the antibody FV region combining with the GluNR1 segment may not be as vertical as initially assumed, and there may be a higher chance that the antibody is approaching the P8 sequence from below the LBD (Figure 3.12). The other site interactions with the FV region are illustrated in Figure 3.13 with their corresponding docking scores in Table 3.8.

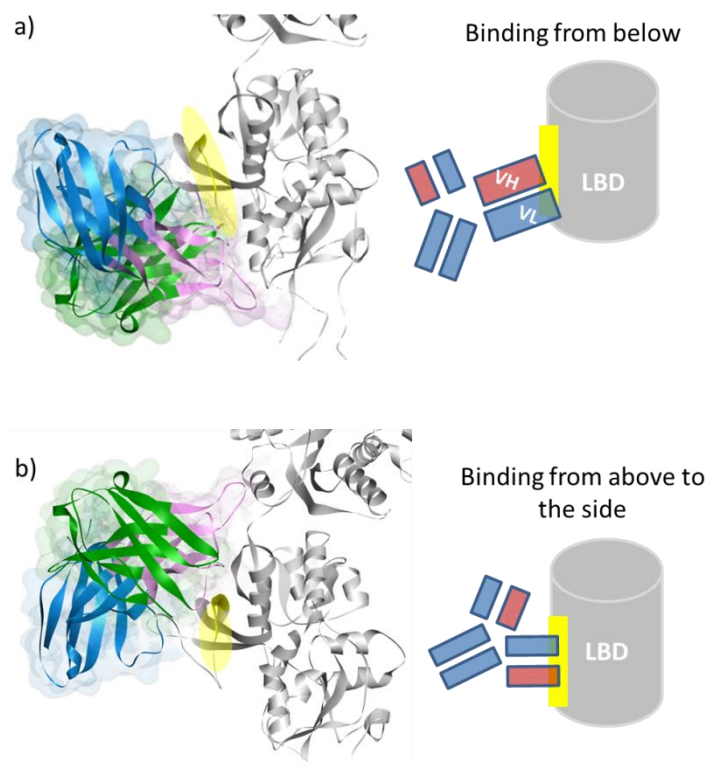


Figure 3. 12 The most stable predicted conformation of binding of FV to the P8 sequence of NR1 is from below.

3.12a) Top pose with ZDOCK score of 26.96 kcal/mole in cluster 4, binding below the P8 sequence illustrated with a schematic diagram showing the most stable orientation. **3.12b)** Pose with ZDOCK score -78.66 kcal/mol from cluster 4 binding above to side of P8 sequence.

Although, all the ZRANK scores for the top poses generated were negative, indicating non favourable interaction. The worst ZRANK score was obtained for the pose at site 5 (-99.88 kcal/mol) and ZDOCK score was 16.96 kcal/mol.

It is also important to note that the loops involved in the binding were the disordered regions which could also contribute to the poor scores observed. The other possible reason could be that the homology pAb docked may have poor affinity for the GluNR1 sites.

Table 3. 7 Docking scores, cluster groups and of the top four models for 5ACO_M.M0012 binding to NR1 model 4PE5_C

Cluster	Cluster Size	ZDOCK score (Kcal/mol)	ZRANK score (Kcal/mol)	ZRANK VDW (Kcal/mol)	ZRANK Electrostatic (Kcal/mol)	ZRANK Solvation (Kcal/mol)
1	27	17.82	-41.592	-122.283	61.206	19.485
2	28	18.50	-50.564	-90.712	40.817	-0.670
4	32	26.96	-45.693	-139.019	91.110	2.216
5	29	16.96	-99.88	-136.734	23.647	13.204

As ZRANK is a linear combination of VDWs attraction and repulsion energies, it may be that for long interactions only fully charged side chains were considered in the calculation. Therefore, the limited number of residues involved could possibly result in these discrepancies observed between the two ranking scores. The poses for FV-GluNR1 complex are also demonstrated in Figure 3.13.

The binding of the FV region to the GluNR1 NTD was predicted to have a ZDOCK score of 17.82 kcal/mol with a ZRANK score of -41.592 kcal/mol. The scores from this model suggest that the binding of the pAb Fv to the NTD of GluNR1 would be less likely at those sites; however it is important to be aware that this was also a potential site that could accommodate antibodies with severe biological effects.

Gleichman *et al*²⁴⁸ previously demonstrated that anti-NMDAR encephalitis (inflammation of the brain) is an autoimmune disorder that is expressed by interaction of antibodies with the NTD of GluNR1, specifically at Asp368 and Gly369 residues. They were also able to demonstrate that these residues, located at the bottom lobe of the GluNR1 domain would solely be responsible for the initiation of the disease, and this process was independent of the other subunits (GluNR2 and GluNR3) variation in the NMDAR tetrameric structure. As a result, this led to direct antagonism of the NMDAR, producing severe side effects such as hallucinations, psychosis, seizures and death.

From the animal studies performed by Dr Jain in Professor Majids group, the pAb investigated in the animal models did not show these side effects and given the location of the antigen it would make it less likely that pAb would interact with the NTD of GluNR1.

The PP interface of FV-NR1 ZDOCK poses and the resulting bonds are summarised in Table 3.9. The top four models from ZDOCK, representative of their corresponding clusters (Figure 3.13) were analysed according to their contact surface areas.

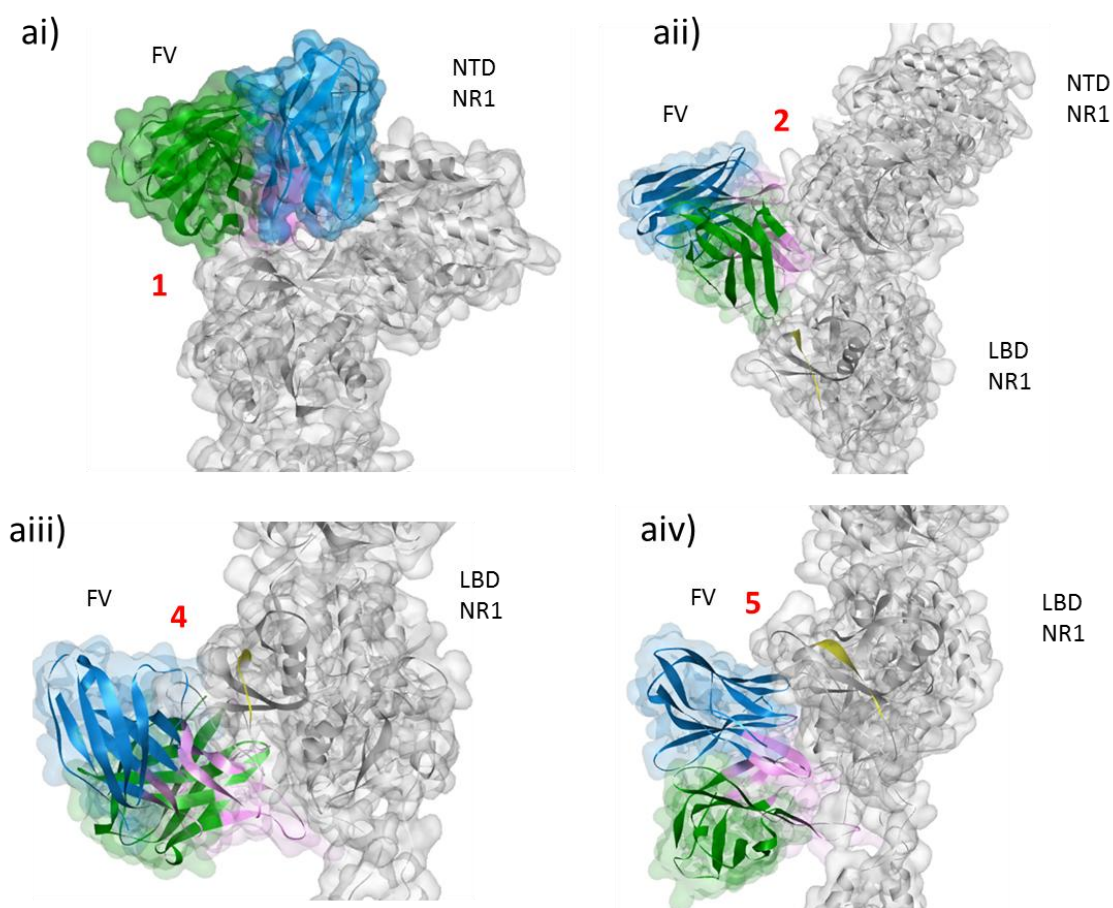


Figure 3. 13 Geometrical characteristics of top poses predicted when docking the 5ACO_M.M0012 binding to NR1 model 4PE5_C

3.13ai) The FV region binding to the N-terminal domain of the NR1 domain (grey), accommodated in the cavity available at the site and stabilised with polar interactions. The volume of the site is $47,364.73 \text{ \AA}^3$. **3.13aii)** FV region binding at site 2, with the volume of site is $48,003.44 \text{ \AA}^3$. **3.13aiii)** Binding at site 4 that has a volume of $59,629.6 \text{ \AA}^3$, **3.13aiv)** Binding at site 5 that has a volume of $42,875.61 \text{ \AA}^3$. The CDR of the FV region are presented in pink.

Table 3. 8 Analysing the protein interface of FV-NR1 ZDOCK poses

Cluster	Total Pi Interactions	Total Hydrogen Bonds	Total Salt Bridges	LCSA (Å ²)	LPCSA (Å ²)	LNCSA (Å ²)	RCSA (Å ²)	RPCSA (Å ²)	RNCSA (Å ²)
1	2	1	0	87.922	26.155	61.767	93.389	26.082	67.307
2	2	1	0	55.004	20.935	34.069	54.979	16.755	38.224
4	2	1	0	74.146	10.163	63.983	81.444	31.864	49.580
5	2	1	0	81.575	25.625	55.951	85.085	17.224	67.861

LCSA : Ligand Contact Surface Area, **LPCSA** : Ligand Polar Contact Surface Area, **LNCSA** : Ligand Nonpolar Contact Surface Area, **RCSA**: Receptor Contact Surface Area, **RPCSA**: Receptor Polar Contact Surface Area, **RNCSA**: Receptor Nonpolar Contact Surface Area

All top poses showed the formation of two pi interactions and one hydrogen bond. There were no salt bridges formed from the docking studies. At cluster 4, the residue that was involved in the hydrogen bonding from the FV region to the receptor were Pro50-Trp118 at a distance of 3.17 Å. There were greater numbers of contact surface areas formed such as LNCSA and RNCSA upon formation of the complex, allowing a hydrophobic interface binding to occur and stabilise the two proteins.

From the docked poses it demonstrated that the interactions between the protein complexes were mainly stabilised through the hydrophilic, and more so the hydrophobic interactions of the surface proteins rather than single amino acids which is expected from PPI. ^{249,250}

3.5 Limitations of antigen-Fab docking predictions and conclusion

The main challenge for this study was the lack of antigen-pAb co-crystallised structure and the high degree of uncertainty about the exact PP interface.²²⁹ Fortunately, antibodies have great similarities between their overall structures and their CDR domains (excluding the variable CDR H3). Therefore, to address the above issue a homology model of the pAb structure was created to understand how the pAb may be interacting with the P8 region of the GluNR1 to offer information regarding the paratope-epitope pairing.

However, there are some important limitations that need to be addressed. Firstly, accurate prediction of antigen-Fab docking may be reduced due to their binding interface representing a less pocket like surface as observed in enzyme-substrate binding. This reduces the surface complementarily area for docking studies and prevents PP docking scoring functions to accurately rank the poses generated, as they are also optimised based on electrostatic interactions.

Secondly, it is also important to mention that although CDR regions are the predominantly site of binding of antigen-pAb, other segments of the antibody may also influence the antigen binding.²⁵¹ The exact residues influencing of antigen binding can be further characterised through structural methods (e.g NMR and X-ray crystallography) or mutagenesis studies. In addition, the constant domains (tail of antibody) may also contribute to the geometry of the variable domain binding to the antigen and how it stabilises onto the receptor.

Overall, the aim of this section was to build a homology model of mouse pAb and subsequently docking the homology model onto GluNR1 P8 to understand the potential PPI between P8 and Fab molecule. This approach was taken due to the 3D structure of P8-Fab segment was not elucidated.

In part one of this Chapter, the PP docking predicted five potential sites available on the GluNR1 subunit that can potentially interact with the pAb. However, the most favourable sites assessed by the scoring functions were site 4 and site 2 onto the GluNR1. Moreover, the P8-Fab docking also demonstrated that the antibody is less likely to interact with other segment of GluNR1 (i.e NTD) as the docked poses showed to be much less energetically favourable. The PP docking studies helped clarify some of the key residues that were involved in the PPI. This could aid identification of the most compatible small molecule compounds at that site. This was investigated in the next stage, part two of this chapter.

Part 2:- SBVS campaign to identify small molecules compatible to the P8 region.

3.6 Introduction

Automated docking studies are applied in many drug design projects, and these computational resources are now routinely used by pharmaceutical companies and academic laboratories in order to assess druggability of novel targets and novel sites where no binders have been identified.²⁵² In addition, the use of computational tools allow a quick analysis of which compounds could progress forward to more extensive tests involving *in vitro* and *in vivo studies*. Finally, the rigorous use of existing data and continuous learning has helped avoid repeating mistakes, pass through to clinical trials and maximise the chances of reaching patients.²⁵³ VS methods consist of two main categories, structure-based virtual screening (SBVS) and ligand-based virtual screening (LBVS).

3.6.1 Structure-based virtual screening (SBVS)

The SBVS methods are based on screening the small molecule libraries directly onto the 3D model of the therapeutical target to identify hit molecules (i.e compound best bound to the target protein).²⁵⁴ The structure of therapeutical target can be obtained from experimental techniques such as X-ray, NMR crystallographic and cryo-em methodologies. However, for novel therapeutics this information may not always be available. SBVS utilises the steric and energetic complementarity of the small molecules and the binding pocket of the target protein to conduct its screening. The molecules can then be ranked based on their compatibility to the receptor using scoring functions. This method allows analysis of molecular interactions in the binding pocket (e.g predicting binding mode of the compound) and the calculation of its binding energies.²⁵⁵

Currently, SBVS methods have been largely been applied in many small molecule discoveries including for treatment of numerous neurological disorders.^{256,257} An example includes Bottegoni *et al*²⁵⁸ conducted a VS to find triazone analogue that was able to modulate both the β -secretase 1 (IC_{50} =18.03 μ M) and GSK-3 β (IC_{50} =14.67 μ M) for potential Alzheimer's disease.

The best scored compound that was able to satisfy the parameters was tested in *in vitro* assay using neuroglioma cells.²⁵⁹

Another method applied in SBVS is ensemble docking. It mainly refers to docking into an “ensemble” multiple active site conformation in structure-based screening.²⁶⁰ This method uses multiple templates of the target that can help to narrow down the ligands that are most tailored for that target in different environments. As crystal structures alone are merely snapshots of complex protein structures in a particular environment, it does not capture all the modes of movement and the energy associated within these structures. However, this approach is able to take advantage of multiple conformations of the therapeutic target or protein rather than only a single model structure. Using the crystal structures of the same therapeutic target with various bound or co-crystallised inhibitors can allow the study of induced fit, and examine the range of flexibility available within the active site. This approach also allows more feasible molecular dynamics to be explored and aids in the identification of the best single protein-ligand docking results.²⁶¹

3.6.2 Ligand-based virtual screening LBVS

The LBVS methods can rapidly screen compound libraries based on the structure of previously known active compounds against a particular target. This approach can be applied in absence of a 3D model of therapeutic target. It takes into account the key functional groups present in the structure of active molecules (e.g 2D finger prints of compounds) that are essential for binding (pharmacophore features) and tries to match compound libraries to these features in order to identify a novel hit compound. LBVS is based on similar property principle²⁶², which hypothesises that similar structure compounds exhibit similar biological activity. However, it is important to note that this concept is an over simplification of potential drug like molecules, as analogues of compounds have displayed unique binding affinities and different mechanism of actions, specifically in case of enantiomer isomers.²⁶³

An example of successful application of LBVS in neurological disorders was reported by Geldenhuys *et al*²⁶⁴, where they used a scaffold hopping method to identify a potent thiazolidinedione analogue, known as rasagiline that functions as a monoamine oxidase (MAO-B) inhibitor ($IC_{50} = 4.43 \text{ nM}$)²⁶⁵ for treatment of symptoms of Parkinson’s disease. Scaffold hopping is an approach used in LBVS

where a novel compound can be produced with similar activity to the reference compound by changing one fragment of the compound to replace it with a bioisostere equivalent.

3.6.3 Combined method: SBVS and LBVS

SBVS and LBVS approaches can be adapted to the purpose of a drug design project with the information available on the biological target and its corresponding active molecules; therefore these methodologies can be applied separately or in combination to reduce the limitation of each individual method.^{267,268} The main objective of these two methods is to narrow down a large set of compound libraries to a small list of molecules that would be most likely to interact and manipulate the activity of the desired biological target.

After the completion of the VS methodologies, the hit molecules are narrowed down further by adopting a consensus approach of each method in post filtering processes and subsequently biological assays are then performed to examine the affinity and efficacy of the *in silico* hit molecules (Figure 3.14).

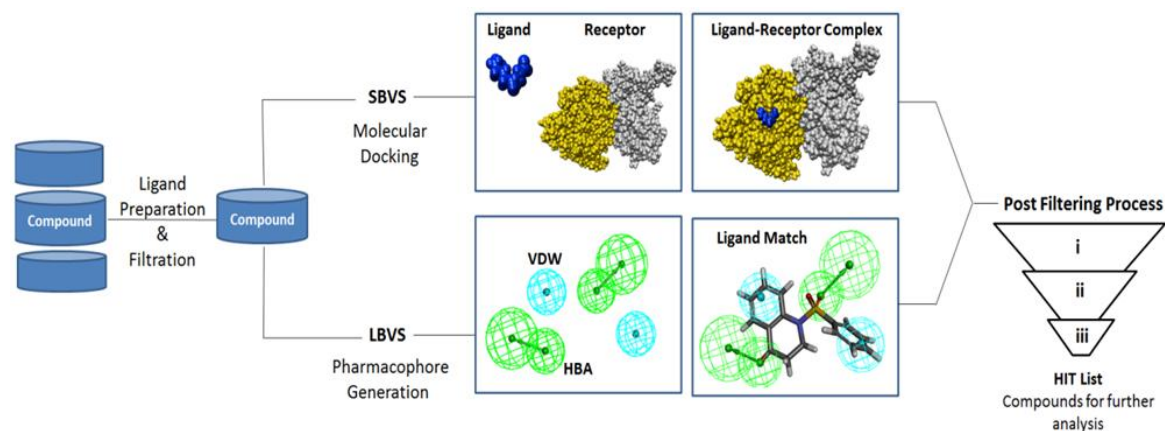


Figure 3. 14 VS methods

The compound libraries obtained undergo preparation and filtration procedures *in silico* prior to the initiation of docking procedures. Post filtering process can be then divided into as many steps required based on the objective of the project in order to select the hit compounds. For SBVS, ligand (Blue), Receptor [PDB: 5H8F_AB (Chain B GluNR1 yellow, Chain A GluNR2 grey)] shown in space filling format. For LBVS, VDW shown in cyan, HBA (hydrogen bond acceptors) shown in green. Ligand in elemental colour in stick format.

Fiorito *et al*²⁶⁹ had successfully applied LBVS and SBVS methods in identifying a dual action compound benzo-1,6-naphthyridine analogue acting as a histamine H3

receptor (H3R) antagonist and 5-hydroxytryptamine receptor (5HT4R) agonist. The compound was shown to have great potencies for both receptors (H3R $K_i=41.6$ nM and 5HT4R $K_i=208$ nM) which could potentially modulate these receptors and prevent neurodegenerative diseases such as Alzheimer's.

Using a pharmacophore approach they built a model based on H3R antagonists and produced a homology model of human H3R. After completing the docking studies into the target protein model, only the compounds that satisfied the pharmacophore features from the model built on known H3R antagonists were selected. This process narrowed down the ~17,194 compounds screened to seven *in silico* hits. Subsequently, experimental testing using Chinese hamster ovary cell H3 (CHO-H3) identified the dual benzo-1,6-naphthyridine to be one of the most potent inhibitors from the hit molecules.

Post filtering processes consists of application of sequential computational methods used to aid the VS in filtering the compounds that display undesirable effects.²⁷⁰ For example, poor compatibility with biological target by using pharmacophore models or clustering and similarity searching techniques based on known active binders to eliminate any compounds that do not match with the desired biological and physicochemical properties.

In addition, compounds that may interfere with biochemical assays due to reactive functional groups can also be removed using pan-assay interference (PAINS) models.²⁷¹ For example, diarylethene and dithienylethene groups can have photochromic properties therefore may interfere with fluorescence and absorption assays.²⁷²

Available pharmacokinetic filters such as AMDET models using quantitative structure activity relationship (QSAR) techniques can also be applied in post filtering processes.²⁷³ This is a model based on structural properties of the compounds and biological activity data available that can aid filtering process to exclude any ligands that do not satisfy drug like properties, display poor absorption and toxicity in animal models.

Armour *et al*,²⁷⁴ demonstrated early drug metabolism predictions for chemokine receptor antagonists can produce quality lead compounds. The initial hits selected

contained the imidazopyridine groups that are known to block the cytochrome p 2D6 (CYP2D6) enzymes. To address the above issue the researchers replaced the functional group with its analogue benzimidazole that produced the lead candidate (UK-374,503), reducing the drug-drug interaction observed previously.

Another example includes pyrazolopyridine glutamate receptor antagonists that demonstrated high clearance and poor ADMET properties.²⁷⁵ By addition of aminosulfonyl group onto the new analogues of the hit molecule resulted in improvement of bioavailability of the initial hit, whilst maintaining its efficacy in the *in vitro* studies.

Overall, most often the post filtering processes are tailored based on the objective of the research project. Combined these models provide further guidance in identifying compounds that are most compatible with the biological target and can maintain the desired drug like properties.

3.7 Docking algorithms

Recently, many existing docking programmes have invested greatly in implementation of upgrades to their algorithms to produce more accurate and high-throughput results. Some examples of well-established docking programs include Genetic Optimised Ligand Docking (GOLD),²⁷⁶ Discovery Studio (DS), AutoDock,²⁷⁷ Internal Coordinate Mechanics Software (ICM),²⁷⁸ FlexX²⁷⁹ and Glide²⁸⁰. All of the above softwares model the interaction of molecules with a binding site by calculating molecular force fields based on molecular conformational terms (e.g. bond stretching, bond angles bending, rotating bonds, non-bonding interactions, electrostatics, and surface effects such as Van der Waals' forces (VDW)). Docking aims to predict a reasonable binding pose of candidate ligands in the active site of a protein by using multiple conformational search techniques that alter the torsional (dihedral) angles and degree of free rotation of the ligand.²⁸¹ Some of the techniques used for conformational search include shape complementarity, systematic and stochastic (random).

Shape matching techniques implement the search for shape complementarities between ligand and the receptor molecule. To predict if the two molecules can bind together it calculates molecular surfaces available in the binding site of the receptor

(as spheres) and then superimposes the spheres onto the ligands. Dock software uses this technique and phase shape has implemented shape based flexible ligand descriptors which has shown to further improve its ligand pose prediction for VS protocols.²⁸²

A systematic search method allows a slight change in the structural parameters of the ligand to promote its rotation in all directions.²⁸³ The algorithm then reviews the energy landscape of the conformational space by conducting multiple evaluation cycles to identify the minimum energy structure. This method is applied in Glide and can successfully explore the conformational space available for a ligand. However, it can be computationally demanding. The number of possible solutions for the ligand can grow exponentially as the degree of movement is increased. This method can also focus on identifying local minimum energy spaces and not be able to detect the global energy minimum, which corresponds to the most stable ligand-protein conformation.²⁸⁴

In comparison, stochastic methods work by randomly modifying the structural parameter or location of the ligand.²⁸⁵ Monte Carlo methods (used in LigFit) and genetic algorithms (used in GOLD) are known to implement this technique, and then evaluate the poses generated using scoring functions.²⁸⁶ Stochastic methods avoid final conformations being trapped at the local energy minimum and increase the probability of locating the global minimum. Due to the broad coverage of energy landscape required this may increase the time of the docking simulation significantly, and enhance computational cost associated with this procedure.

Interestingly, genetic algorithms reduce the computational demand of this method by applying a theory of “natural selection”.²⁸⁷ Initially, hydrogen bond acceptor functional groups and areas for hydrophobic interactions are matched to specific points within the binding site. The algorithm then treats each structural parameter of the ligand as a chromosome, which is represented as a vector.

In the second step, the first chromosome is used in random conformational search and a population of chromosomes is created covering a large energy landscape. Finally, the population is analysed further and the most “adapted chromosome” that has the conformation with the lowest energy score is selected as the model for the next set of ligand conformations. To identify the global local energy minimum the

cycle is then repeated again. The number of cycles repeated depends on ligand size, flexibility and if water molecules are included in the docking protocol. This method significantly reduces the conformational space required to be analysed as the most suitable structural parameters are always passed to the next population.²⁸⁸

GOLD that uses this method was developed in 1995. It was the product of collaboration between The University of Sheffield, Cambridge Crystallographic Data Centre and GlaxoSmithKline plc.²⁸⁹ GOLD software has proven to be efficient in numerous studies and it has constantly been validated and improved using large number of complexes from PDB.²⁹⁰

3.8 Scoring functions

In all computational studies, a major challenge is development of algorithm an energy scoring function that can accurately, and quickly analyse the interactions between bound complexes.²⁹¹ The main objective of using scoring functions in docking studies is to allow the ranking of different ligand poses by predicting and evaluating the binding energy of the ligand with the protein target. For a scoring function to be considered reliable it should demonstrate that it can identify poses that are closest to the experimentally determined binding mode and rank them higher in comparison to compounds that are less likely to bind. This would ensure the correct prediction for the binding mode and allow further efficient ligand selection, modifications in hit identification and lead optimisation.^{291,292}

Scoring functions estimate the binding free energy (ΔG) to predict the binding affinity between the ligand and protein structure.²⁹³ Other scoring functions are trained against a set of data that contains experimental values of binding affinities of ligands with their corresponding protein. Some examples of scoring functions applied in docking studies are demonstrated in Table 3.10. How the scoring functions in each class estimate the strength of binding between the ligand and protein structure is discussed below.

Table 3. 9 Scoring function for small molecule docking²⁹⁴

Classes of scoring functions	Scoring function programs
Force field based	DOCK
	GOLDscore
	Libdock
Empirical	Ludi
	ChemScore
	Flex
Knowledge-based	PMF
	Drugscore
	ASP
Machine Learning	SFCscore
Astex statistical potential (ASP), Scoring function consortium (SFCscore)	

3.8.1 Class 1: Force Field Based

Karplus *et al.*²⁹⁴ introduced the force field scoring function in the 1970s, as a method to estimate affinities by combining the intermolecular VDW and electrostatic energy functions of atoms involved in the binding process. By the end of the 1990s, additional terms had also been taken into account such as hydrogen bonding and solvation energy terms from Generalized Born (GB) or Poisson-Boltzmann models.²⁹⁵ This is shown below in equation 3.2.

$$\Delta G_{\text{Binding}} = \Delta E_{\text{bonded}} + \Delta E_{\text{non bonded (vdw + } \Delta E_{\text{electrostatic)}} + \Delta E_{\text{H-bond}} + \Delta G_{\text{desolvation}}$$

Equation 3. 2

The advantages of force field scoring functions are that they can rapidly generate results and are adaptable to concepts such as solvation models, quantum mechanics and others. In addition, the parameters used in Equation 3.1 are well studied and have a physical basis.²⁹⁶ However, even with incorporating quantum mechanics, force field scoring methods often produce the wrong energies, which contributes to unreliable predictions.²⁹⁷ A possible explanation for this could be the small errors of individual energy terms that tend to be carried forward in force field based methods that are not considered independently. This over estimation can lead

to problems in the ranking of the docking poses. Therefore, as a solution current force field scoring functions tend to use empirical scaling parameters such as linear interaction energy to adjust the final outcome in the experimental binding data.²⁹⁸

The DOCK, GOLDscore and Libdock use force-field based methods allowing hydrogen bonds, entropy and solvation data to be incorporated in their calculations. However, it is important to note that there may be differences in treatment of each of these terms (e.g hydrogen bonds) in the scoring function.²⁹⁹ GOLDscore³⁰⁰ was the original default scoring function in earlier versions of GOLD, it has now been optimised to take into account HB-energy, VDW forces, ligand torsion strains and metal interactions.

3.8.2 Class 2: Empirical

In 1994, Böhm *et al*³⁰¹ published the second class of scoring function referred to as empirical scoring. This method predicts binding energy of a receptor-ligand complex using chemical and physical properties. This class of scoring specifically includes reversible interactions, lipophilic contacts and rotatable bonds present in the ligand.³⁰²

$$\text{ChemScore: } \Delta G_{\text{Binding}} = \text{Score}_{\text{HB}} + \text{Score}_{\text{lipophilic}} + \text{Score}_{\text{metal}} + \text{Penalties}_{\text{strain}} + \text{Penalties}_{\text{clash}} + \text{Penalties}_{\text{covalent}} + \text{Penalties}_{\text{constraint}} + \text{Penalties}_{\text{rotor}}$$

Equation

Equation 3.3

As shown in Equation 3.3, the scoring function is divided into two main terms “Scores” and “Penalties”. The term “Score” represents rewarding scores or favourable interactions such as hydrogen bonding, the term “Penalties” represents the non-favourable interactions in the binding site, for example steric clashes between amino acid residues.³⁰³ The penalties may increase further if many more restraints are introduced in the docking protocol.³⁰⁴ One of the major limitations for empirical scoring functions is their dependence on the training set that is used for their calibration. The data is normally obtained from experimentally determined binding affinities and is used to perform a linear regression analysis to evaluate each term in the equation. Naturally, this works in favour of the empirical scoring function as it is able to produce higher quality results in comparison to different classes of

scoring functions. More importantly, it has a wider range of applications as it can be applied for ligand-binding conformations close to their training set.³⁰⁵

However, it is important to note that experimental binding energies may not be available for all protein targets and most often the data obtained from existing literature is conducted in various experimental conditions. Subsequently, this would affect the accuracy of the result produced. As demonstrated by the equation above, the parameters analysed are the most frequently observed interaction patterns between receptor-ligand complexes. This limits the scoring function to certain parameters as more specific or uncommon interactions, such as water-ligand hydrogen bonds, pi-cation bonding or entropic parameters are not included.³⁰⁶

Finally, there is no penalty term in the equation for poor resolution structures. This may be due to the fact that it is much more difficult to demonstrate a significance of these parameters in regression analysis.

Examples of scoring functions that apply empirical methods include Ludi, ChemScore and Flex. Ludi was first developed by Böhm *et al*³⁰⁷ which takes into account the reversible binding interactions and the number of rotatable bonds of the ligand. Then ChemScore was developed³⁰⁸ used in GOLD software and it contains all the terms used for Ludi, with exception of ionic interactions and having metal-ligand binding function present. Flex scoring function calculates the aromatic interactions. ChemPLP (Pairwise Linear Potentiation)³⁰⁹ a hybrid scoring function and is a more advanced version of ChemScore, taking on board its hydrogen bonding term and adding distance dependent interactions, along with repulsion terms.

3.8.3 Class 3: Knowledge Based

Knowledge based scoring is based on the sum of the statistical potentials of close interactions such as electrostatic, VDW, positive ion- π interaction of atoms in protein-ligand complexes.³¹⁰ This data is derived from large libraries of macromolecular databases (e.g the PDB). These figures help to produce approximations of the potential of mean force (PMF) by assuming that more frequent interactions are much more likely to be favourable and more likely to influence the binding affinity.³¹¹ Equally less frequent interactions are classed as unfavourable contacts. This process is shown in Equation 3.4.

$$A = \sum_i^{ligand} \sum_j^{protein} \omega_{ij}(r)$$

Equation 3. 4

Where, "i" and "j" are the values of the distance potential of atom pairs and the final term " $\omega_{ij}(r)$ " is obtained from the inverse Boltzmann equation.³¹² Knowledge based scoring function are not computationally demanding and do not require specific analysis of the training set data as seen with empirical methods.

In addition, they are able to generalise most of the energetic interactions observed in ligand-protein complex. Knowledge-based potentials have shown to be useful in pose prediction however, not much information regarding binding energy can be obtained as the distance between atoms can also be influenced by surrounding residues and the environmental conditions.³¹³ Scoring functions that allow only structural data to rank different poses in the ligands include PMF, Drugscore and Astex Statistical Potential (ASP)³¹⁴. These scoring functions only differ by their reference state, where the ASP scoring function utilises the environment of atoms of ligand and proteins whereas the others do not include them.

Machine learning technique uses QSAR methods to evaluate binding complexes and analyse the patterns of specific interactions within complexes. Recently published scoring functions that employ this methodology include SFCscore.³¹⁵ The SFCscore utilises both a PDBbind training set data and a random forest regression method to predict binding affinities. These methods can be extremely advantageous as it can allow the design of tailored scoring functions for specific proteins or protein families. Thereby, giving much more robust results; however, this mainly depends on the amount of relevant data available.

3.9 Aims of part two

The specific aims of part two was to identify initial *in silico* hits that are compatible against the pharmacophore of P8 GluNR1 obtained through antigen-Fab docking. This understanding will guide which compounds to screen in the biological assays. To achieve this aim, the following objectives had to be met:

1. NMDAR GluNR1 receptor target selection and preparation.

- i) Prepare the protein (Crystal structure selection and binding site identification)
 - ii) Ligan preparation
 - iii) Supporting studies for validation of the protocol
 - Quality of docked poses
 - Accuracy of scoring function
 - iv) Molecular docking
2. Post filtering process and hit molecule selection
 - i) Ensemble docking
 - ii) Binding energy calculations.
 - iii) Hits identified
 3. Compare the binding of the *in silico* hits with the Fab docking studies.

3.10 Result and discussion

3.10.1 Selecting Crystal structure

The fasta sequence of the NMDAR GluNR1-1a subunit that contained the P8 (VKKVICTG) was used as the query sequence in order to identify matching crystal structures within the PDB database. This was achieved via The National Centre for Biotechnology Information (NCBI) website. Alignment of human (*Homo sapiens*) NMDAR GluNR1 (query sequence) with other species NMDA GluNR1 such as the brown rat (*Rattus norvegicus*), mouse (*Mus musculus*), pika (*Ochotona*), zebra fish (*Danio rerio*) and African clawed frog (*Xenopus laevis*) were performed to record the percentage identity of these sequences and their characteristics in comparison to each other. The percentage identity of 85% or above was considered a good match to the query sequence. Table 3.13 demonstrates degree of sequence alignment varied across the different organisms. The sequence alignments and sequence identity clustering is demonstrated in Figure 3.15.

The rat NMDAR showed the greatest match with the human NMDAR in comparison to the other species. The lowest match was shown to be from zebrafish and African clawed frog, presumably due to the large number of mutations observed within the GluNR1 primary sequence of aquatic vertebrate and amphibians. Hence, the use of crystal structures that were obtained from these animals could lead to alternative models of the target that may not be very close to human receptors.

The alignment of the complete P8 sequence along with the entire NCBI protein reference sequences, and PDB data that contained the sequences from experimentally determined protein structures demonstrated that the complete P8 sequence was observed within NMDAR GluNR1 isoforms.

Another important question that needed answering during the amino acid sequence alignment search was whether the P8 sequence was shared with other known protein targets in humans. Interestingly, the NCBI BLAST search also identified proteins such as capsular polysaccharide (bacterial enzyme), N,N'-diacetylchitobiose phosphorylase (phosphoenol pyruvate enzyme) and RNA lariat debranching enzyme to share the sequence. However, this may be due to the short length of the sequence, as it is only eight amino acids long can be easily shared with other protein families.

Table 3. 10 Pairwise alignment of the human NMDAR GluNR1 with other species GluNR1

Species	% Iden	Identical positions	Note
<i>Homo sapiens</i> vs <i>Rattus norvegicus</i>	99.25	931	Exact match at P8 H : <u>VKKVICTG</u> R : <u>VKKVICTG</u>
<i>Homo sapiens</i> vs <i>Mus musculus</i>	93.02	894	Exact match at P8 H : <u>VKKVICTG</u> M : <u>VKKVICTG</u>
<i>Homo sapiens</i> vs <i>Ochotona</i>	93.01	877	Two a.a mutations close to P8 H: <u>F</u> TVNGDP(P8)PNDTSPG <u>S</u> P: <u>S</u> TVNGDP(P8)PNDTSPG <u>G</u>
<i>Homo sapiens</i> vs <i>Xenopus laevis</i>	88.47	795	Two a.a mutations at P8 H : <u>V</u> KKVIC <u>T</u> G F: <u>I</u> KKVIC <u>N</u> G
<i>Homo sapiens</i> vs <i>Danio rerio</i>	78.76	798	One a.a mutations at P8 H : <u>V</u> KKVICTG Z: <u>I</u> KKVICTG

Alignment performed by the Clustal Omega program, available at <https://www.uniprot.org/align/>, Full sequence and complete percentage identity available in the appendix A. Amino acid (a.a), H (Human), R (Rat), M (Mouse),P (Pika) and Z (Zebra fish). Full sequence alignment available in appendix

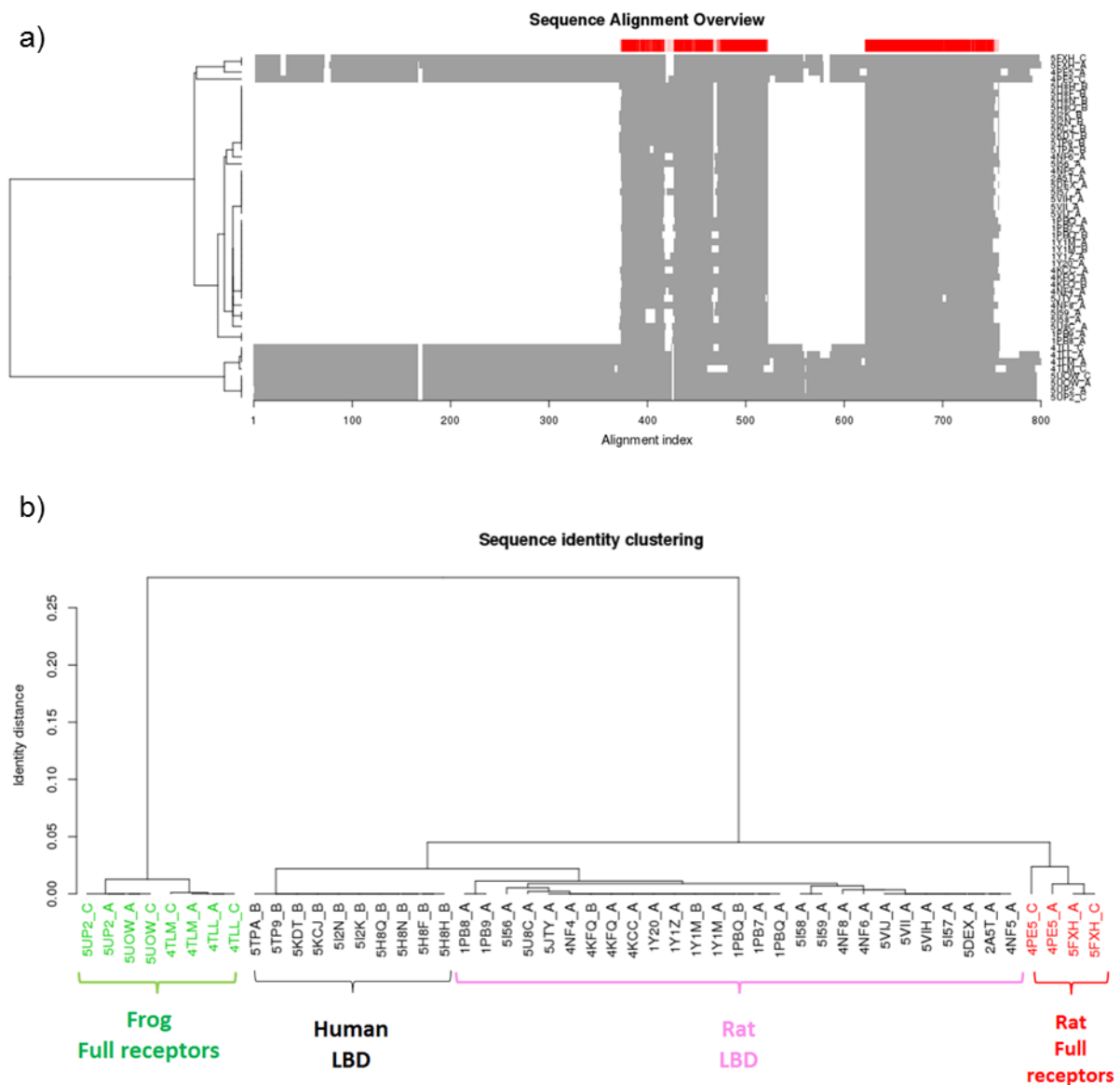


Figure 3. 15 Sequence alignment and sequence identity clustering

3.15a) A schematic overview of multiple sequence alignments of the NMDAR crystal structures available in PDB showing the main three groups in dendrogram format, containing LBD crystal structures and full NMDAR structures. White segments between grey blocks represent gaps within the sequence. The red segments above represents regions shared by all crystal structures. **3.15b)** Shows the sequence identity clustering divided by the species the receptors were obtained from. LBD (ligand binding domain), Full receptor (ATD, LBD and TMD).

To ensure the most accurate model was produced *in silico* for the biological target, the resolution of the structure must be the lowest possible (preferably lower than 2

Å).³¹⁶ The majority of the best resolution crystal structures were segments of the whole receptor as they were less complex and produced much more detailed density maps, from which their 3D conformations were built. Therefore, when selecting crystal structures it was important to calculate how far apart they were in similarity from the complete receptor 3D conformation.

The PDB did not include a complete human NMDAR crystal structure; however, it did contain the full receptor structures obtained from rat. The best resolution structure (PDB code 4PE5)³¹⁷ was used for comparison. To do this the root mean square deviation (RMSD) of the crystal structure was calculated. The RMSD value measures the average distance between two atoms, calculated using the formula shown in Equation 3.7;

$$RMSD(a, b) = \sqrt{\frac{1}{n} \sum_{i=1}^n [(aix - bix)^2 + (aiy - biy)^2 + (aiz - biz)^2]}$$

Equation 3 5

Where, i represents the atoms in molecule a, and b, n refer to the total number of atoms and x,y,z are the 3D coordinates. The lower the value for RMSD, the closer the protein residues are when compared to the native structure.³¹⁸ The human crystal structures of ligand binding domain (LBD) were aligned and superimposed with crystal structures of the full NMDAR obtained from rats in order to calculate RMSD between the amino acid residues of each structure.

As demonstrated in Figure 3.16 the structures were aligned in four different ways. C α , main chain, side chain and all protein. The C α atom stands for one amino acid, so changes in this value means change in a particular amino acid position, whereas, backbone RMSD considers all the atoms over the chain of the protein, not only one particular amino acid. The calculated RMSD values show all are very close to 2 Å. The maximum RMSD values were 2.45 and 2.56 Å for structures 1PBQ and 4NF4 respectively. The minimum value calculated was 0.81 Å for structure 2A5T.

This result indicated close alignment of LBD to the complete crystal structure; therefore this allows the use of the LBD crystal structures with best resolutions for docking as they are very close to full receptor.

RMSD calculated values reference 4PE5 compared the to all the aligned ligand binding domains (LBD).

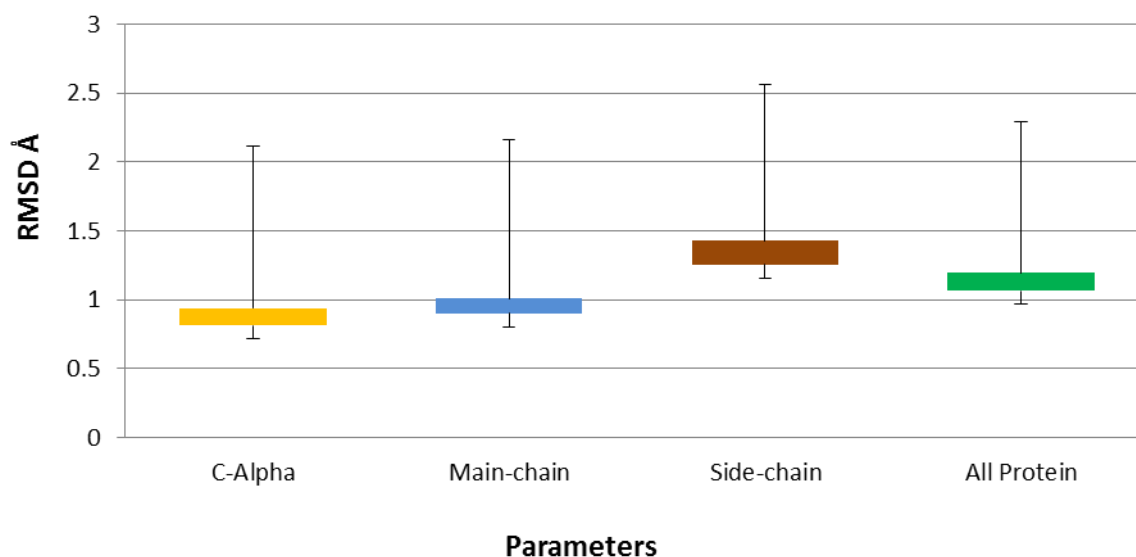


Figure 3. 16 The calculated RMSD values of Human crystal structures LBD with full receptor.

The RMSD represents that no difference was observed from the full crystal structure and the LBD segment crystal structures. The RMSD was calculated from C- α which is measures the distance between the C- α atoms of two amino acids in Å. The main chain takes into account the *N*-terminal and COOH group as well in the calculation. The RMSD of side chain measures the distance of the side chains only and the RMDS of all the protein is a combination of all the methods.

When the structures were superimposed, the majority of the backbone residues of the receptor (Figure 3.17a) was matched well within a close proximity. Flexibility was only observed in the loops of the protein structure. In addition, Ramachandran chart (Figure 3.17b) and B-factor calculations (Figure 3.17c) were performed in order to outline regions of disorder and theoretically unfavourable within the protein structure.

Interestingly, for the LBD structures of NMDAR, the loop was stabilised by addition of a cross linked, L-cysteine bond to enhance thermal stability.³¹⁹ The loops were responsible for the majority of the movement close to the P8 sequence. When the crystal structures of the protein were superimposed, flexibility could be seen for residues Glu32, Phe33, Gly37, Val35, Asn36, Thr 34, Asp 38, Pro 39 and Ser55, Gly54, Pro53, Ser52, Thr51, Asp50, Asn49, Pro48 and Gly47.

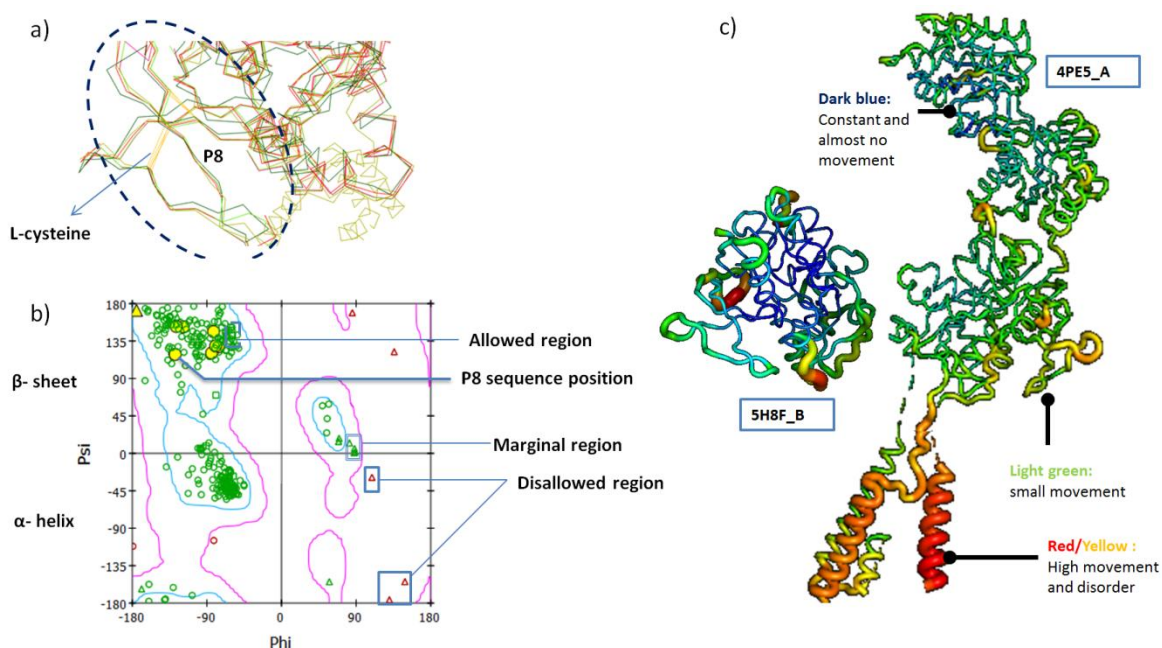


Figure 3.17 Analysis of the crystal structures selected for docking studies

3.17a) Shows a selection of human LBD structures superimposed with full structure obtained from rodent and a snapshot of the P8 sequence. **3.17b)** The Ramachandran chart calculated for human crystal structure 5H8F_B, showing the P8 sequence in yellow dots, occupying the β -sheet segments. **3.17c)** B-factor images calculated in Pymol. Blue (constant region), Green (small movement) and Red/yellow (High disorder).

The Ramachandran chart for the GluNR1 subunit of the NMDAR (5H8F_B) was plotted to examine the phi (ϕ) –psi (ψ) angle constraints of the amino acids in the LBD structure.³²⁰ The majority of the residues were displayed in the allowed regions (91.8%) or marginal regions (7.6%) and only small amount of the residues were present in the disallowed segments (0.6%). This confirmed the correctness of the crystal structure. After the calculation of the B-factor, it was clear that NMDAR GluNR1 subunits were mobile proteins.

In previous studies it was suggested that this flexibility in the structure could allow the NMDAR to bind with ligands in an induced fit manner,³²¹ where it would try to accommodate a compatible ligand. More importantly, the highest disorder was observed for the transmembrane domains. The binding sites of the native neurotransmitters GluNR1 glycine showed to be very stable in comparison to the other parts of the receptor. At this stage, seven crystal structures were taken forward for the docking studies (see Table 3.11) based on their species, resolution and method of crystallography.

Table 3. 11 The seven crystal structures selected for docking studies and full receptor used as a reference.

PDB Code	Species	Domain	Ligand	Resolution (Å)	pH	Method	The % coverage of P8	Ref
5U8C	Rattus Norvegicus	GluNR1 /GluNR 2a LBD	Gly Glu NVP-AAM077	1.60	7.0	X-ray diffraction	100%	322
1PB8	Rattus Norvegicus	GluNR1 LBD	Gly Glu D-serine	1.45	6.0	X-ray diffraction	100%	323
2A5T	Rattus Norvegicus	GluNR1 LBD	Gly Glu	2.00	7.0	X-ray diffraction	100%	324
4KFQ	Rattus Norvegicus	GluNR1 LBD	Sulfate ion Glycerol 4KFQ Ligand	2.20	7.5	X-ray diffraction	100%	325
5H8F	Homo Sapiens	GluNR1 /GluNR 2a LBD	Gly Glu Glycerol	1.81	7.0	X-ray diffraction	100%	326
5H8Q	Homo Sapiens	GluNR1 /GluNR 2a LBD	Gly Glu Acetate ion GNE8324	1.90	7.0	X-ray diffraction	100%	327
5H8H	Homo Sapiens	GluNR1 /GluNR 2a LBD	Gly Glu GNE3419	2.23	7.0	X-ray diffraction	100%	328
4PE5	Homo Sapiens	GluNR1 /GluNR 2b Full NMDAR	Gly Glu	3.96	8.8	X-ray diffraction	100%	329

4KFQ Ligand = 1-sulfanyl(1,2,4)triazolo(4,3,-a) quinoxalin-4(5H)-one, 4PE5 Ligand =4-[(1R,2S)-2-(4-benzylpiperidin-1-yl)-1-hydroxypropyl]phenol

3.11.2 Binding site identification

After preparation of the protein, it was important to map out the binding pocket and clefts on the crystal structure that can be explored by docking studies as demonstrated in Figure 3.17. The spheres location are given by x,y,z coordinates and the radius (r Å) is also calculated (Table 3.15).

The binding sites calculated on the NMDAR LBD include both buried and surface accessible sites, specially, for the sites at the P8 region (Figure 3.18). The surface accessible binding site matches the initial theory of how the antibody paratope was able to interact with the P8 epitope. As antibodies are large macromolecules, they were less likely to interact between the protein subunits due to steric clashes and the flexibility of these binding partners.

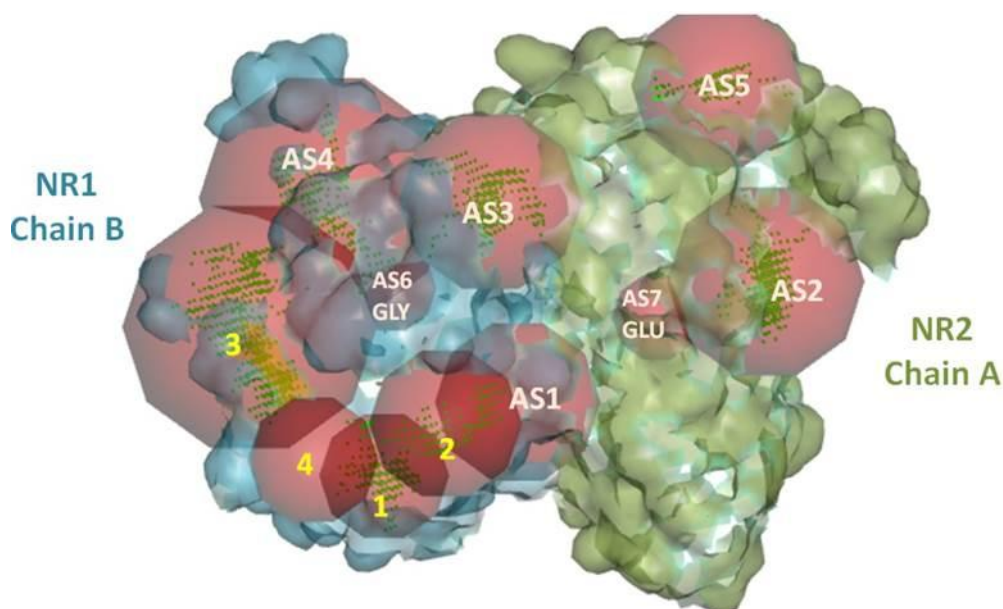


Figure 3. 18 Calculation of the binding sites in the human NMDAR LBD 5H8F.

LBD is divided into 11 sites, the P8 region shows large cavities available at top and bottom of the sequence (1-4), and therefore it was subdivided into 4 smaller volume sites. There was also the presence of 5 alternative binding sites (AS) on the protein, along with the two neurotransmitter binding sites. The protein is represented as a transparent surface where GluNR1 shown in blue and GluNR2 shown in green.

Hence, the main interactions were more likely to occur from the side of the protein. For the design of small molecules; surface accessible binding sites are regarded as much more challenging. They are quite accessible to solvents and often tend to have many water molecules present within them. Water residues can have great influence

in the binding of a small molecule.³³⁰ For ligands to successfully establish binding with P8 they must be able to displace the less stable water molecules.

Table 3. 12 The co-ordinates of binding sites available in human NMDAR LBD (PDB:5H8F_B)

Protein ID (5H8F)	Volume (Å ³)	Surface Area (Å ²)	Radius (Å)	X	Y	Z
BS1	138	411.99	7.30	-0.877	-29.672	-34.488
BS2	113	379.60	8.60	-8.377	-23.542	-23.848
BS3	480	764.73	14.30	-1.712	-10.877	-51.616
BS4	294	2,102.95	10.00	-15.156	-22.752	-36.299
AS1	249	2,320.95	9.30	12.371	-25.194	-27.692
AS2	288	681.53	11.10	26.512	-17.190	-1.017
AS3	242	1,046.35	10.30	5.962	-1.280	-21.377
AS4	298	594.13	14.20	10.270	0.784	-46.120
AS5	115	2,649.70	9.60	31.529	4.806	-5.485
Glu	235	257.616	10.00	19.348	-18.373	-11.666
Gly	118	78.62	10.00	8.335	-10.078	-38.46

Binding site 4 was calculated based on the glycerol molecules (buffer solution molecule).

Alternative site (AS), binding site under investigation close to P8 (BS), glutamate binding site (Glu) and glycine binding site (Gly)

The Site 1 is the smallest binding pocket (radius 7.30 Å). Site 4 was only present in 5H8F_B due to the presence of a buffer molecule, glycerol binding to that region. Crystal structure of 4KFQ_A also confirmed the presence of glycerol molecules at the P8 region. This was interesting to note as it demonstrated the hydrophilic nature of P8 sequence. Therefore, this suggested that ligands may have been more compatible for that site if they contained polar functional groups. In contrast, Site 2 and Site 3 were demonstrated to be cavity like pockets with hydrophobic characteristics that could be explored further (see Figure 3.19).

The binding sites were also cross referenced with binding clefts calculated in the PDBsum³³¹, Figure 3.19a. In all of the cases, the binding sites in 5H8F_B were consistent with the sequence P8 under investigation, as well as the alternative sites on the receptor.

This confirms the presence of the pockets available within the P8 region. Enumeration of the pharmacophore features from the protein active site was performed for each of the binding sites close to the P8 region (Figure 3.19b,c)

building the pharmacophore residues that were able to interaction map. This interaction map consists of hydrogen bond acceptors, hydrogen bond donors and hydrophobic features that are available in the active site sphere. These are represented as a population of clusters in the interaction site. This process is an automated pharmacophore generation technique to help and guide understanding of the most idealised interactions required for ligands to bind in a particular binding site.³³² As antibody mapping studies had already shown the desired activity was observed mainly at the initial sequence of the P8 the (VKKVI) and therefore the docking studies were more focused on binding site 1 and 2. The list of all residues in the binding sites of interest are provided in tables in Appendix D.

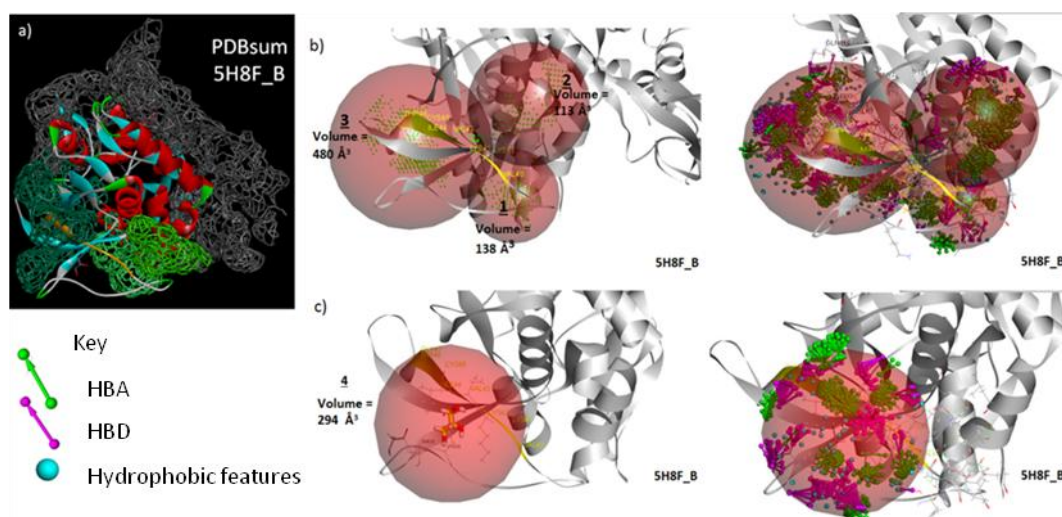


Figure 3.19 Analysis of the binding sites available at P8 GluNR1.

3.19a) PDB sum binding clefts calculated for 5H8F_B, the clefts shown in green are sites on P8. **3.19b)** The three major binding sites close to p8, along with calculated automated pharmacophore based on the structure of the protein. **3.19c)** Site 4, the buffer solution binding site and its corresponding automated pharmacophore analysis demonstrating greater clusters of hydrogen acceptor and hydrogen donor binding points, hence they are more prone to polar interactions.

3.11.3 Ligand library preparation

For selection of database of compounds to be virtually screened in this project there were some key points that needed to be addressed. Firstly, as P8 was a putative binding site that had been identified through antibody binding through protein-protein interaction it suggest that the binding region is fairly large.

As a result there were numerous points of contact that may be observed once a variable fragment binding domain of an antibody interacting with its corresponding antigen site (Chapter 3: part one) Moreover, it was important to note that a small molecule would not be able to interact with the whole P8 regions that the Fab segment may have been interacting with. Therefore, it would be interesting to examine if all of these sites were necessary for the desired biological outcome.

To maximise the chances of success for the screening we took advantage of the data available for known inhibitors of the NMDAR to look into the compound physiochemical properties that most of these ligands shared. For this study, the compound libraries selected contained compounds that were synthetically feasible, readily available and were able to maintain their integrity in activity, storage and handling for future biological assays.

In-house libraries include AFChemPharm compounds and Professor Chen's chemical library from the University of Sheffield. In-house libraries here are defined by the compounds that are synthesised by researchers in Professor Chens group and in AFChemPharm (i.e not commercial bought). The in house libraries were made up of a large collection of novel small molecules including derivatives of acridine, pyridine-2,6-dicarbonitrile, 1,3,5-triazine and phenyl-thiazol-3-ium structures. In addition, there was also a selection of FDA approved drugs available at the Sheffield Institute for Translational Neuroscience (SITraN) that was used for initial screening. Other libraries that were also available included ZINC15 and Sellechem compounds which were also screened. The majority of the compounds purchased for SITraN were from commercial vendors such as the Spectrum (2000 compounds available), Tocris (1120 compounds available) and the Prestwick (1200 available) chemical library.

The compounds were finally categorised into two libraries. To the first library the Lipinski's "Rule of Five" (RO5) and Veber's rule of rotational bonds were applied to maximise the oral bioavailability of compounds. RO5 states molecular weight to be less than 500; the number of hydrogen bond acceptors less than 10; the number of hydrogen bond donors less than 5 and ClogP (octanol water partition coefficient) to be less than 5. Lipophilicity is measured in terms of ClogP. The ligands used in this study and the categories they are in are shown in Figure 3.20.

Veber's rule states for a compound to have good oral bioavailability the number of rotatable bonds has to be less than 10 and the polar surface area (PSA) of the compounds to be less than or equal to 140 \AA^2 , this particular range can increase the probability of the final compounds being cell permeable. The library was of compounds generated mainly designed with the objective to maximise the chances of finding potential hits that may be out of the normal range of CNS compounds, however the molecules could be easily optimised if required. The compounds properties including if they are favourable or unfavourable CNS compounds are further shown in Figure 3.21.

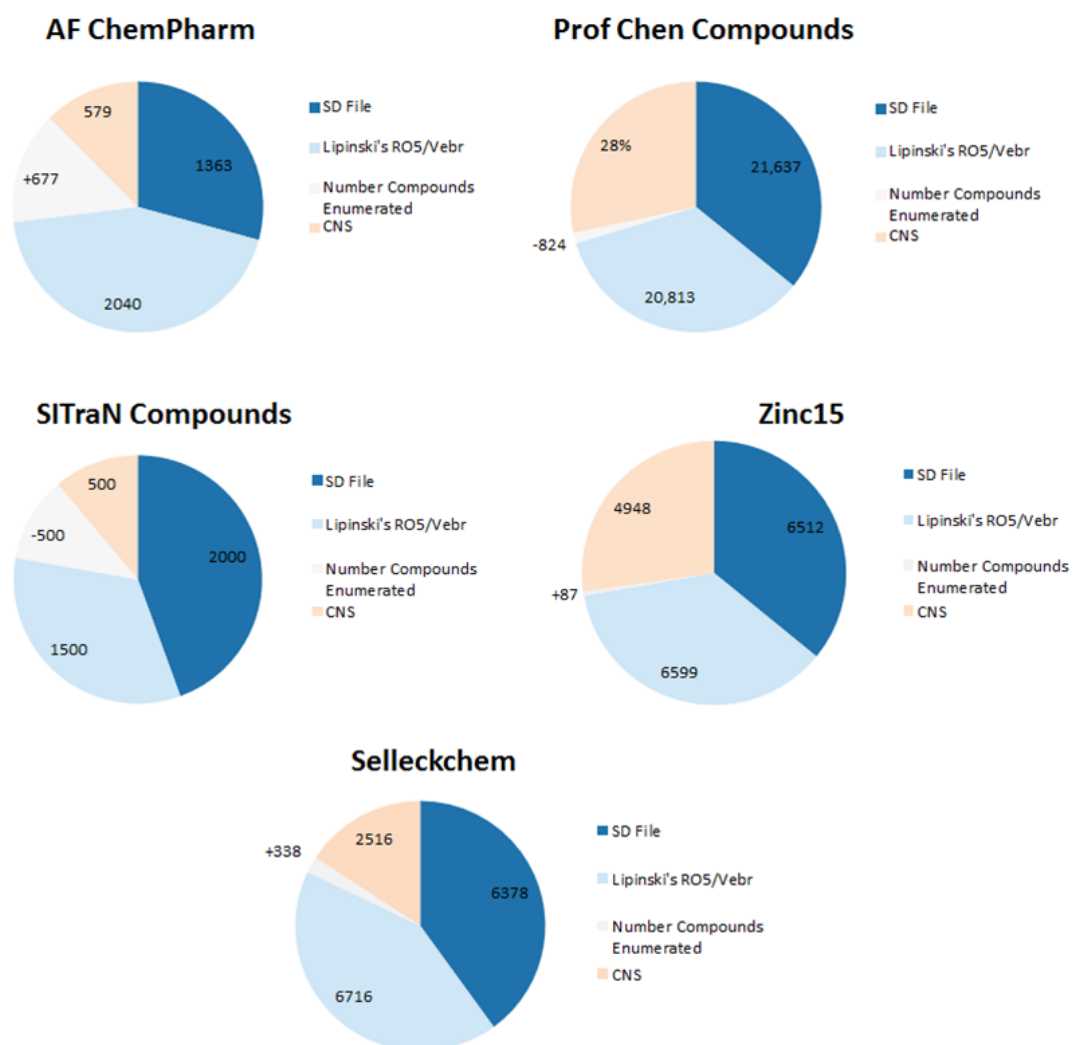


Figure 3. 20 Pie charts representing of the number ligands within the libraries used for VS.

The pie charts are divided into four segments; the number of compounds contained in raw SD file (dark blue), the number of compounds after ligands prepared and RO5 is applied, the number of isomers, tautomers and duplicates removed (grey) and finally the number of compounds within the CNS filtered library (cream).

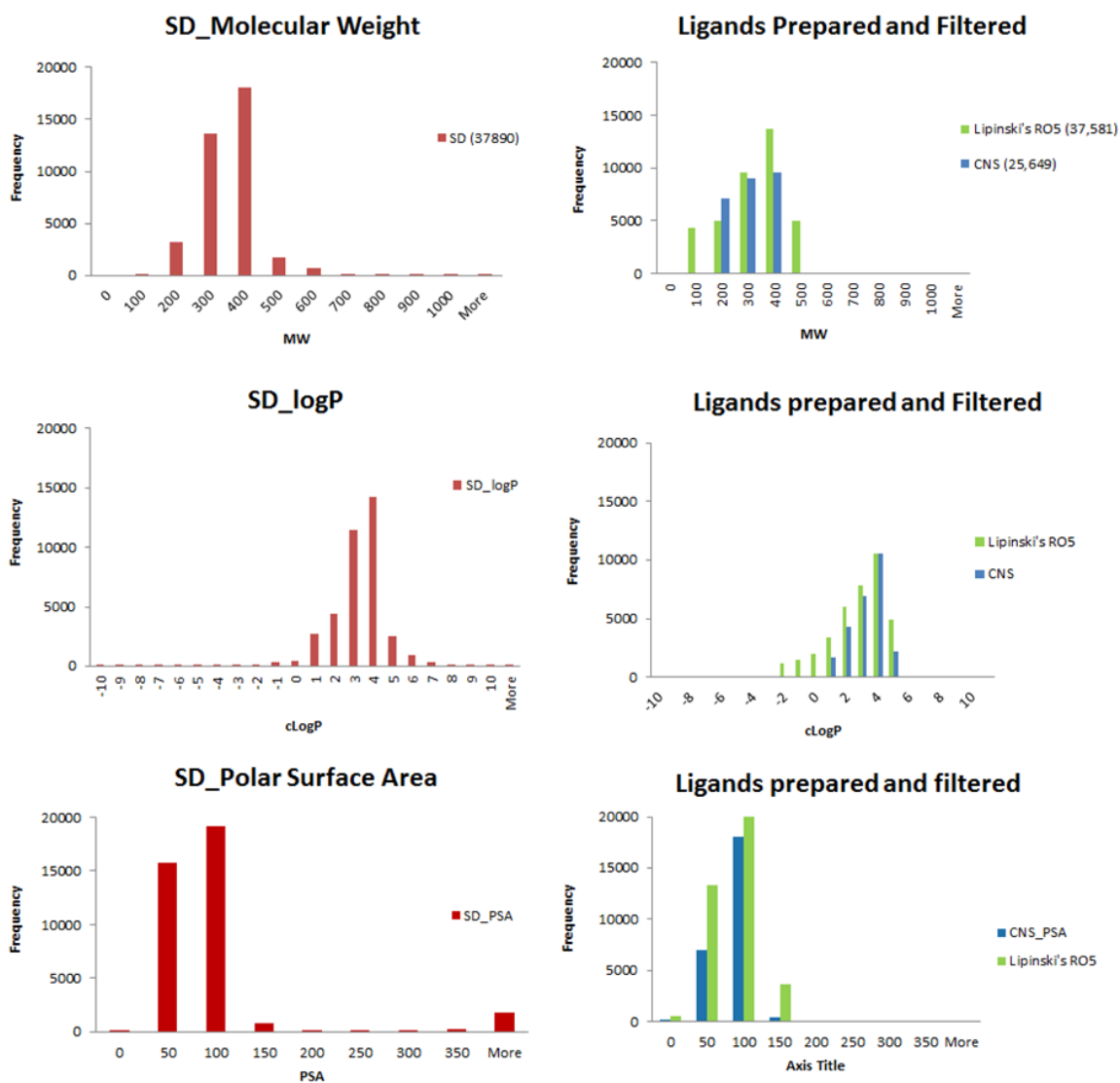


Figure 3. 21 Histogram graphs of molecular properties of the libraries.

On the left hand side are the SD files demonstrating the range of properties in the compound libraries obtained prior to filtration, showing presence of molecules with unfavourable CNS properties. On the right hand side are the properties of the libraries created after filtration using RO5/veber's rule and CNS rule. (Number of ligands in library)

The second library was designed according to physiochemical properties calculated by Travis *et al*³³³, based on a range of CNS drugs (see Table 3.13). In general, the majority of CNS drugs tend to have higher values for lipophilicity greater than 3 and a lower number of rotatable bonds making them much more rigid. The molecular weight also needs to be as low as possible to ensure the compounds can maintain their solubility and reduce off target interactions.

Table 3. 13 Recommended range of molecular properties shown for CNS drugs³³⁴

More desirable range	Less desirable range
MW \leq 360	MW $>$ 400
clogP \leq 3	clogP $>$ 5
HBD \leq 0.5	HBD $>$ 3.5
pka \leq 8	pka $>$ 10
clogD _{7.4} \leq 2	clogD _{7.4} $>$ 4
40 \leq TPSA \leq 90	TPSA \leq 20; TPSA $>$ 120

MW (molecular weight), HBD (hydrogen bond donor), TPSA (total polar surface area)

For NMDAR antagonists a molecular weight of 200-400 is highly desirable. In comparison to non-CNS drugs, the number of hydrogen bond acceptors and donors are lower and the PSA needs to be less than or equal to 90 \AA^2 to ensure penetration through the BBB. The ionisation of molecules also play an important role in route of diffusion of compounds across the BBB. Weak bases and natural compounds have much higher chances of penetrating the BBB when compared to acidic or very basic compounds. Other parameters such as lipophilicity, when increased can aid diffusion of drugs into the brain. However, if this parameter exceeds its optimal value, it can cause binding to plasma proteins and accumulation of the small molecule into fatty tissues, which leads to poor solubility. Solubility can be increased with the addition of the nitrogen and oxygen atoms in the molecule. This results in hydrogen bonding which could stabilise the compounds when they interact with their biological target. For CNS permeable compounds the number of heavy atoms (e.g oxygen and nitrogen) is advised to be kept below 5, to ensure that there is a balance between permeability and solubility for the compound.

3.12 Validation and supporting studies for the docking protocol

Many of the challenges faced in docking experiments are due to the over simplification of complex processes used to achieve a high-throughput speed to assess a large number of ligands. Therefore after the preparation of the ligands and protein models it is important to understand the strengths and weaknesses of the docking experiments.

3.12.1 Quality of the docked poses

The first method was by re-docking the bound co-crystallise ligands, such as glycine into their native proteins (GluNR1 subunit) to confirm whether the bound conformation of the ligand could be reproduced (Figure 3.22). The RMSD of the bound and docked ligands were also calculated along with their corresponding scores and binding energies (Table 3.14 and 3.15). The docking of the glycine molecule demonstrated that there was a rotation of the carboxylic acid and amine group at (180°) during the pose generation. However, the majority of the important interactions with key amino acid residues, Arg132, Ser181 for the carboxylic acid group and Pro125, Thyr127 for amine group were maintained. The interaction with key amino acid residues was also consistent with other GluNR1 binding compounds; both positive and negative allosteric molecules (Table 3.15).

In addition, the hydrogen bonding distance between donor and acceptor groups also matched the active biological conformation. The docking protocol was further optimised in order to ensure that the poses generated were stable and could maintain low RMSD values for the highest scoring poses generated. It was observed that in DS the preparation of the protein can alter the docking scores drastically, hence changing the conformation of the docked poses. The presence of other co-ligands (e.g ions, sugars and buffer residues) can influence the conformation of the protein (Figure 3.23). The simple analysis carried out with re-docking bound co-crystallise ligands, proved that the removal of residues after preparation of the protein even if they are not located close to the binding site tend to give better pose predictions, in comparison to when the co-ligands were included and are kept during the docking process (Figure 3.23b).

The presence or absence of water molecules can influence the docking scores and poses generated. For example, when re-docking a glycine molecules in 5H8Q, the water molecules tend to occupy very close cavities to the glycine and once removed in a “dry model”, docking with Libdock tend to show a greater number of poses that can occupy those cavities (Figure 3.23c). This leads to poorer pose prediction. Conversely, the absence of water molecules does not affect the scores and the quality of poses generated with CDOCKER. In fact it lowers the RMSD of the poses generated even further.

Unfortunately, to what extent co-ligands affect ligand docking at P8 binding sites is still unknown. The only co-ligands found in that region were buffer solution molecules, crystallisation additives and glycerol that had co-crystallised during protein purification and crystallisation.

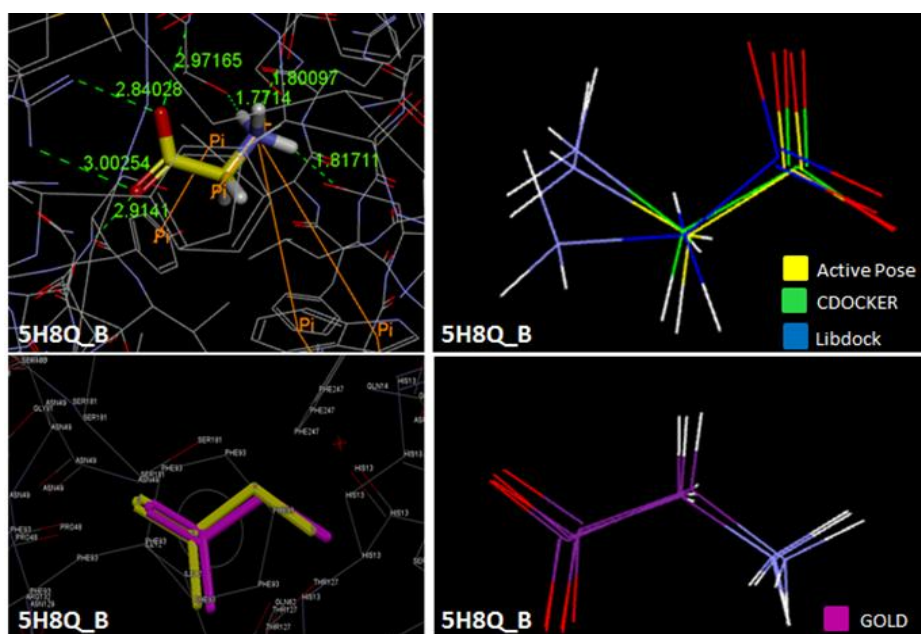


Figure 3. 22 Alignment of the docked glycine ligand with crystallographic ligand

The native neurotransmitter, glycine docked back into its binding site in the GluNR1 subunit. The docking programs used were CDOCKER (green), Libdock (blue) and GOLD (purple). The poses generated show a good match with the crystal conformation (Active pose) shown in yellow. PDB code (5H8Q_B), hydrogen bond distances shown in green and VDW forces are represented in orange.

Table 3. 14 The poses generated and scored in GOLD

Pose	PLP: fitness	Chemscore: fitness	RMSD (Å)
1	77.0275	41.1618	0.3490
2	76.3869	35.6374	0.2968
3	76.336	36.3273	0.2061

Table 3.15 Discovery studio docking software's and binding models for GluNR1 bound ligands.

PDB	Structure	Compound Name	Function	CDOCKER_ score (kcal/mol) Green Pose	Libdock_ score (kcal/mol) Blue Pose	LigScore_ LigFit (kcal/mol) Brown Pose	BE (kcal/mol)	Predicted (Green) vs experimental crystal pose (yellow)	Predicted (Blue) vs experimental crystal pose (yellow)	Predicted (Brown) vs experimental crystal pose (yellow)
5U8C		Glycine	Agonist	56.22	60.61	5.26	-58.98			
5H8F		Glycerol	BS	16.10	50.57	4.23	-134.87			
5ZKX		PAMIS	Agonist	32.79	168.34	5.20	-67.55			
1P88		D-serine	Agonist	39.55	61.15	-63.72	3.33			
1P8Q		DCKA	Antagonist	19.90	73.82	5.17	31.22			
4KFQ		KFQ	Antagonist	1.87	78.41	-75.54	-25.15			

Positive allosteric Modulators (PAMIS)= 2,7-Dimethyl-5H[1,3]thiazolo[3,2-g]pyrimidin-5-one, DCKA = 5,7-Dichloro-4-hydroxyquinoline-2-carboxylic acid, KFQ = 1-sulfany[1,2,4]triazolo-4-quinoxalin-4(5H)-one, Buffer solution (BS)

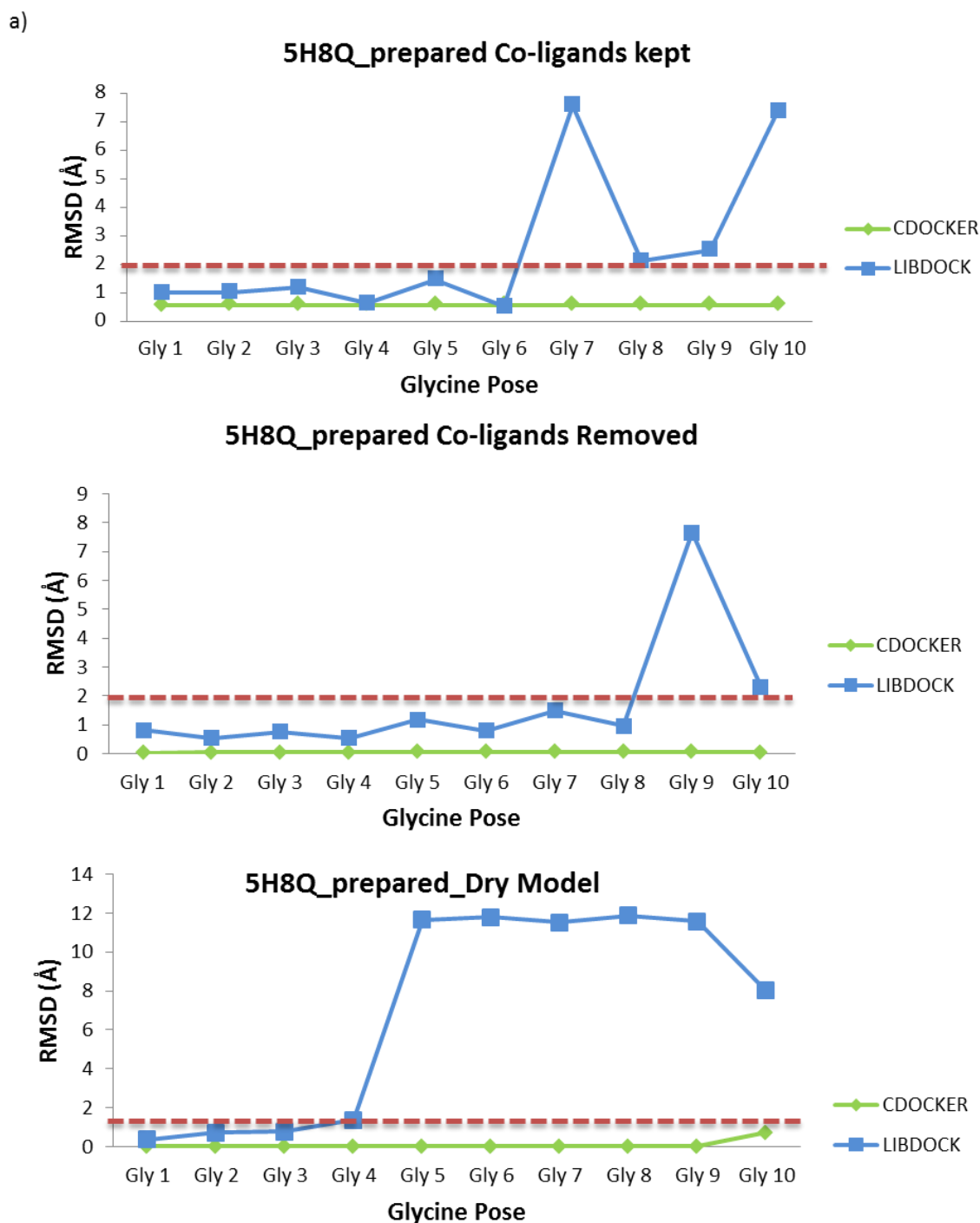


Figure 3. 23 The RMSD values of the top 10 poses generated with Glycine molecule in DS

CDOCKER was able to maintain its stability throughout the poses generated for this molecule; Libdock poses in the top 10 scoring conformations had more outliers in comparison.

----- Desired cut off <2 Å

Depending on the crystallisation protocol buffer molecules are not regarded as being able to form stable ligand-receptor complexes. These molecules are able to move around the protein surface easily and can randomly interact with different regions. However, due to the fact that they bind and interact with the P8 sequence, they do allow the opportunity for exploration of their binding mode. In addition, the presence of glycerol molecules at the P8 segment was also observed in another crystal model (PDB:4KFQ) demonstrated in Figure 3.24a. This could provide a chance to analyse the preferred chemical moieties at that site and investigate how well the docking performs at much more surface exposed binding sites of the protein.

The docking studies demonstrated that the correct crystal conformation can be reproduced. During the visual inspection, the distance of the reversible interactions calculated between the hydroxyl groups and the Asp70 and Pro39 were matched at the correct distances of 1.5-2.6 Å (Figure 3.24b). When the docked pose was superimposed onto the native crystal structure it was clear that the heavy atoms were in the right orientation (Figure 3.24e-h). The best result was obtained from docking with GOLD and was able to show an exact match with the native crystal structure. This was followed very closely with CDOCKER and LigFit. However, using Libdock for this analysis showed a greater value for the RMSD of the docked poses when compared to other programs.

Overall, this analysis docking provided more confidence in producing reliable conformations at the sites close to the P8 region. The re-docking experiments showed they were able to produce reasonable conformations rapidly and also confirmed the quality of the models used. More importantly, scoring analysis of the generated poses was also in sync in the docking experiments. The best poses (lowest RMSD value) have the highest scores and gradually reduce to the worst poses (high RMSD value).

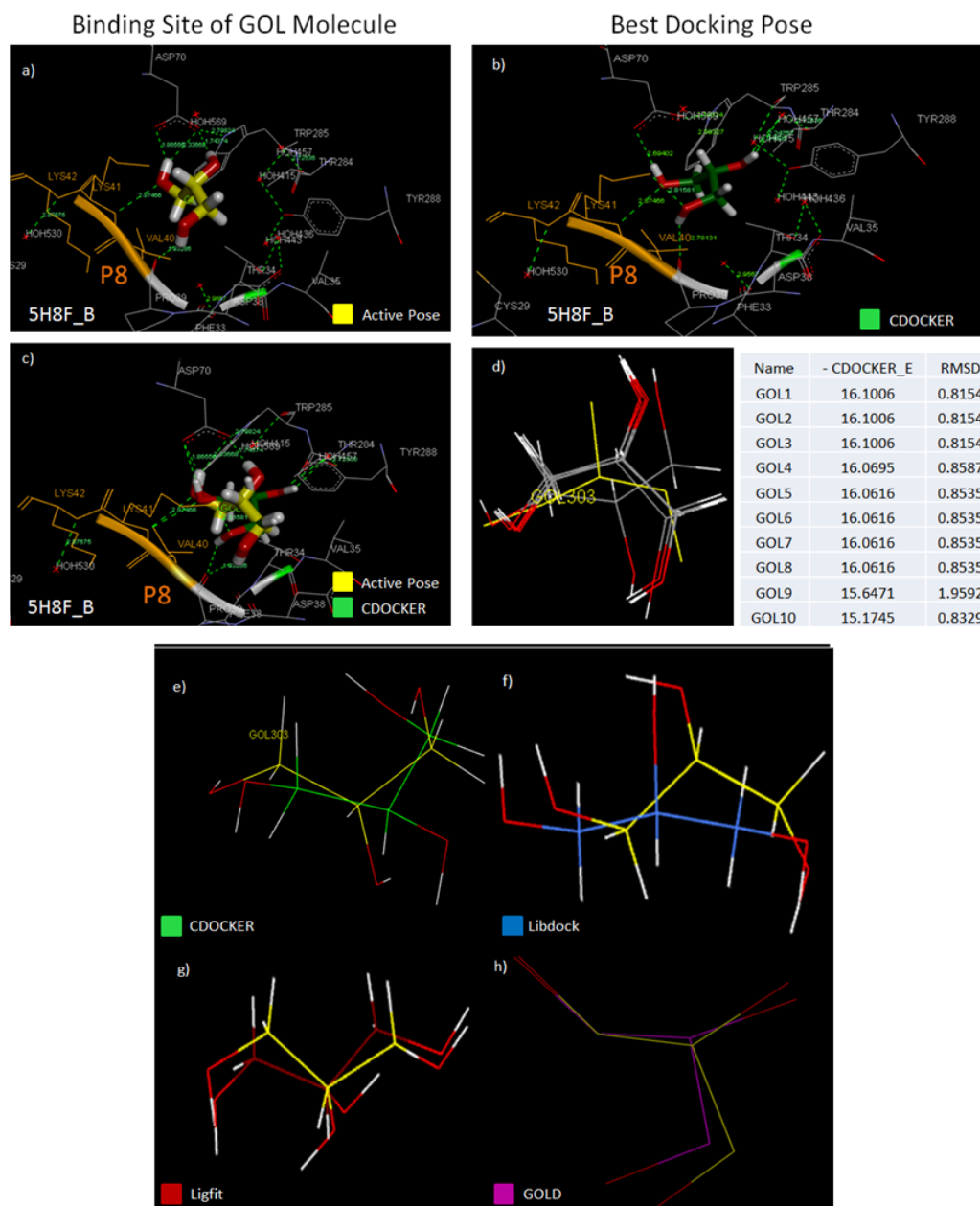


Figure 3. 24 Docking of glycerol molecule into the binding site around P8

3.24a) The glycerol molecule crystal conformation, referred to as “active pose” as it is the stabilised conformation in the bound complex. **3.24b)** The best docking pose generated when docking with CDOCKER. **3.24c)** The best docked pose superimposed onto the crystal structure, able to closely resemble the same conformation. **3.24d)** Top 10 poses generated, along with scores and RMSD values. **3.24e-g)** DS docked poses with active pose, **3.23h)** GOLD top pose for GOL molecule.

3.12.2 Performance of the scoring functions

After establishing the accuracy of the poses generated, it was now necessary to evaluate the performance of the scoring functions in identifying the hit molecules and subsequently their ability in predicting binding energies. It was important to evaluate to what extent are the scoring functions able to discriminate between the active and non-active molecules for the GluNR1 subunit. For this purpose, explicit information obtained from PubChem and the ChEMBL database was used to identify experimental assays performed on the GluNR1. The ligands were generated in their 3D conformation, prepared using the same method as the VS libraries. They were then docked into their native binding site (i.e. as competitive antagonists of GluNR1 subunit, docked into the glycine binding site) and ranked accordingly. If the bioactive conformations of a known inhibitor were available by X-ray crystallographic studies, they were cross referenced with the docked poses, in order to visually inspect differences in the ligand poses.

This approach had two advantages: firstly, it made use of the related experimental data available for a set of compounds in the same experimental conditions, with K_i , IC_{50} values for active and more importantly non active compounds. Programs such as the directory of useful decoys (DUD) can quickly generate large number of random molecule “decoys” based on the structure of an active compound.³²⁶ However, this technique may introduce slight errors into the test, as it is assumed that the random molecules generated are not active for the target protein. In addition, this has not been established experimentally, therefore reduces reliability of the analysis performed.

The active molecules were classed as “true positives” and the non-active molecules as “true negatives”. False negatives compounds represented active molecules that were unidentified by the scoring functions were unable to be identified and were classed in the lower ranks. False positive compounds were non-active molecules; however, it was scored high. The cut-off point for the entire statistical test was similar to the assay data obtained by using and the IC_{50}/k_i values along with the activity observed the compounds into an active set and a non-active set.

The area under the curve (AUC) was calculated to determine the probability of ranking actives rather than non-actives. A higher AUC value means better distinction

is observed.³³⁵ A random ranking method has AUC of 0.5 (50%) where there is no distinction between actives vs non-actives. In this case results would match the equality line where true positive rates are equal to false positive rates. Initially, a small assay sample of eight compounds that were known binders for the glycine site was chosen for analysis (Figure 3.25).

The assay was performed to investigate to what extent the compounds were able to displace the labelled native neurotransmitter [3H] glycine in a radiolabeled ligand binding assay.³³⁶ The docking procedure used was LigFit and the poses were ranked with a range of scoring functions. The study demonstrated that the empirical scoring functions were able to outperform their counterparts (knowledge based, force field-based scoring functions) in identifying the active molecules (see Figure 3.25a-d).

The results generated showed that Ligscore1 and Ligscore 2 were best in terms of ranking the potent compounds (1i-1v) in the top set. From a total 114 poses was generated, 48 poses were active and 66 were non active. In the 50 top ranked poses from Ligscores, 48 were active and 12 were non active. Furthermore, in both scoring functions a small set of non-active analogues were also present and equally scored. This showed that there was a slight overlap in these scoring functions. In the ROC curve analysis Ligscore1 and Ligscore2 were able to demonstrate good discrimination between active compounds to non-active compounds with AUC values of 0.93 and 0.95, respectively, which is most ideal for VS methodologies. The worst performance was observed from the piecewise linear potential (PLP) and PMF scoring functions (Figure 3.26c-d).

The AUC calculated was less than 0.5 which may have been PLP scoring function representing pairwise interaction among selected atom types. Unfortunately this oversimplified the binding process and the top scoring ligands here were the least potent analogues. The other scoring function that miscalculated the poses generated were knowledge based PMF functions. PMF04 score is the upgraded version of the originally introduced PMF score where a large data set was used for equilibration of this scoring function to include additional terms for atomic species such as metal ions and halogen properties.³³⁷

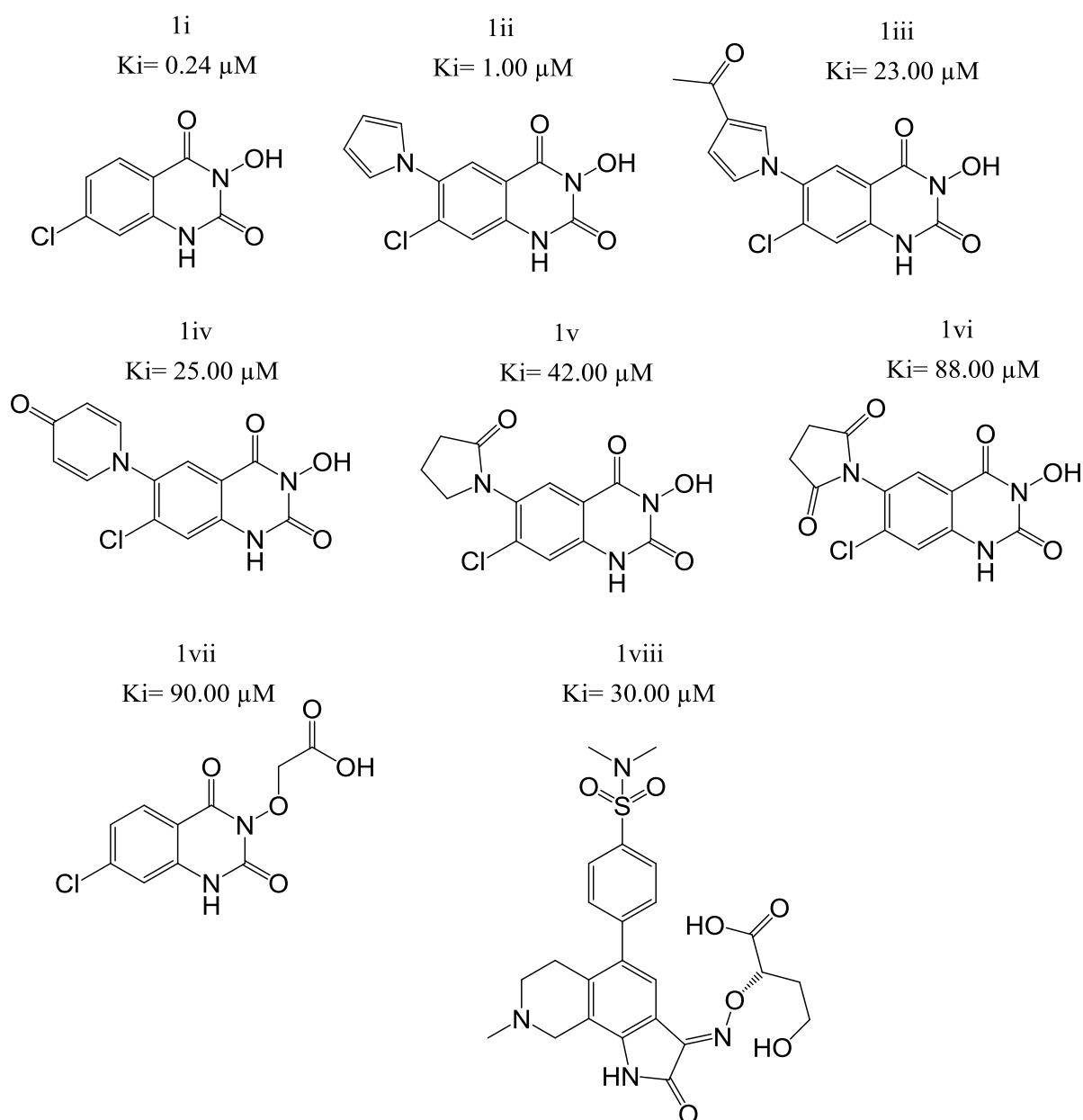


Figure 3. 25 The first set of GluNR1 subunit competitive antagonists

Eight compounds were downloaded and 39 analogues were prepared *in silico* after enumeration of the ligands to create enantiomers and tautomers. 17 were active and 22 were non-active molecules. Structures 1i-1v is the compounds that showed biological activity, the active set and compounds 1vi-1viii were the non-active compounds.

Although, the PMF function was able to distinguish to some extent between active and non-active compounds, in order to predict active compounds in GluNR1, both PMF scores were inverted as the active molecules were given the lowest score, suggesting weak receptor ligand binding affinity.

In the light of these scoring function errors, it was clear that the sampled complex structures failed to be ranked sufficiently with the PMF scoring function. Other scoring functions such as DOCK (force field based) and Jain (empirical) were also equally poor at distinguishing active molecules. There were different possible reasons for this observation. The target protein (GluNR1) might not match with the data set that was used to train these scoring functions or the ligands used may not have matched the parameters used to finalise the ranking system.

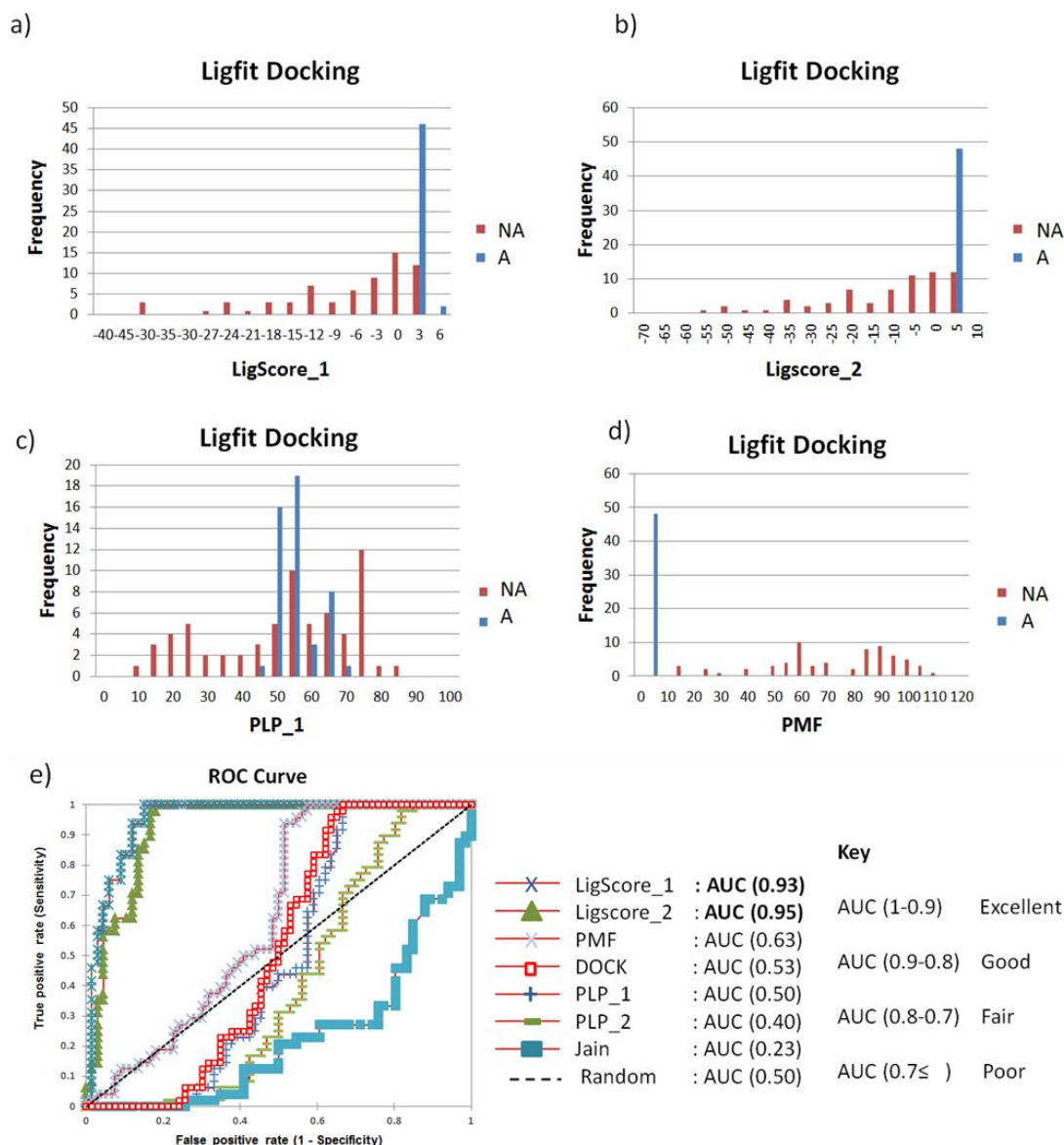


Figure 3. 26 Results obtained from the small screening test with competitive antagonists at GluNR1.

3.26a-d) Histograms showing the scoring of the active compounds in comparison to non-active compounds. **3.26e)** The receiver operator curve (ROC) obtained from the same data set, showing the performance of each scoring function available in LigFit and their corresponding area under curve (AUC) values. Active molecule (A), Non-active molecule (NA).

Figure 3.26 demonstrates the result of the small set of compounds. To confirm these observations other assays were also used with the well-known competitive antagonists of the NMDAR such as kynurenic acid family that were identified as potent and selective antagonists at glycine binding site of NMDAR. ^{338,339}

More importantly, for the potent antagonist 5,7-dichloro-4-hydroxyquinoline-2-carboxylic acid (DCKA) crystallographic conformation was also available in the PDB (PDB:1PBQ). Therefore, the docked poses were compared to the active conformation of the known inhibitor in its bound state. The binding assay data for this study was also obtained by a radioligand binding assay, finally a Ca^{2+} influx assay was performed as a functional assay.

Structures of inhibitors include kynuric acids, dihydroquinoxalinediones and dichlorophenylglycine with potency's ranging from 0.5 μM to >100 μM . Total of 81 compounds were screened in the assay³⁴⁰ and after *in silico* preparation there 133 analogues. Of these analogues, 77 were in the "active set" and the remaining 56 were in the "non-active" group. The active compounds had IC_{50} values less than 10 μM while non-active compounds had IC_{50} values above 10 μM .

In this experiment, the scoring functions of GOLD (Figure 3.27) were superior in identifying the active analogues among the set of decoy molecules. In particular, Chemscore was better, with 70 active compounds identified in the 100 top scoring compounds, leaving only 30 non-active compounds in the same set. GOLD score was able to identify 80 active conformations out of 100 top scoring poses; however, this value was reduced significantly as more overlap was observed in the lower scored poses.

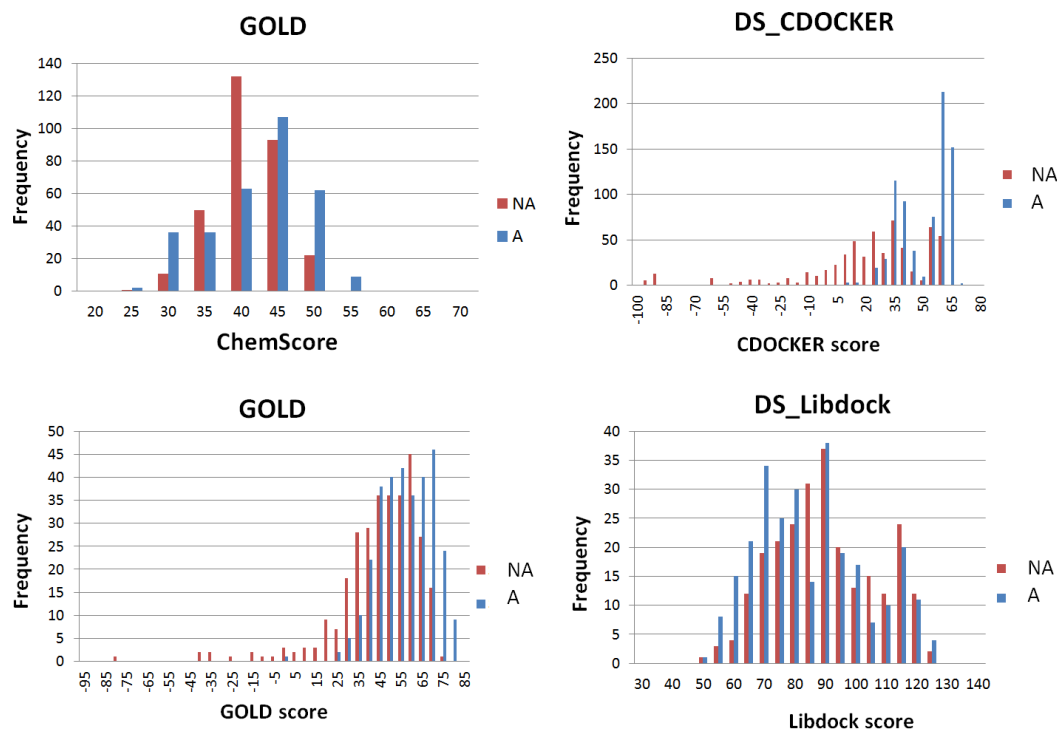


Figure 3.27 Histograms showing the performance of the scoring functions in GOLD and DS on the kynurenic acid compound set

The scoring functions used in GOLD docking studies were able to distinguish between active compounds (A) in comparison to non-active molecules (NA) in the top scoring poses. The scoring functions used in DS for the same assay data. CDOCKER performed much better in comparison to Libdock which failed to show clear separation between the active and non-active molecules.

DS CDOCKER scoring function was able to outperform the DS Libdock scoring function. In CDOCKER, from the top 100 scoring conformations 71 were active and only 21 non active conformation were found from the total 1330 conformations generated. Similar to GOLD score, as the scoring function reduced in value it was less able to distinguish between the active and non-active analogues.

The ROC curves shown in Figure 3.27 illustrate that the scoring functions for this experiment tend to rank the compounds very close to the equality line. The results obtained from LigFit docking once again showed great pose prediction, with the majority of analogues matching the bioactive conformation. The RMSD values of 100 top scoring ligands ranged from 0 to 2.8 Å.

The ROC graphs shown in Figure 3.27, summarise the fact that for all of the scoring functions false positives exist among the top scoring compounds. However, it

appeared that for docking studies into GluNR1, the best performing scoring functions were Ligscore > GOLD score > CDOCKER > PLP1 > ChemScore > Libdock.

In terms of the poses generated during the docking studies, once again all of the software's available were able to match the correct bioactive conformation of the crystal molecule. Libdock poses differed by RMSD of 0 to 5 Å and the majority of poses in CDOCKER, LigFit and GOLD all less than 1.5 Å. This was observed for both active and non-active molecules (Figure 3.28). The intermolecular interactions seen were also compatible with the crystal pose. It was possible that the poses suggested for the less potent inhibitors were probably the most stable conformations of these molecules when forming the ligand-receptor complex; resulting in the molecules being ranked similarly to their more potent analogues.

This efficient pose prediction could suggest why the scoring functions are having difficulty separating potent and non-potent compounds in a given set. This is still an ongoing issue in computational chemistry, as the majority of software are able to reproduce realistic binding poses of ligand-receptor complexes, yet unable to predict affinity of molecules to certain biological targets.³⁴¹ This result suggests that the most stable chemical pose does not necessarily mean greater potency or biological activity, hence experimental assay data is necessary.³⁴²

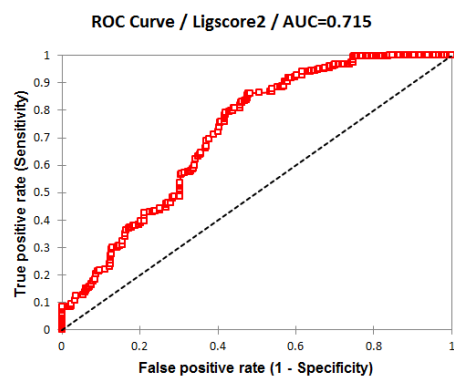
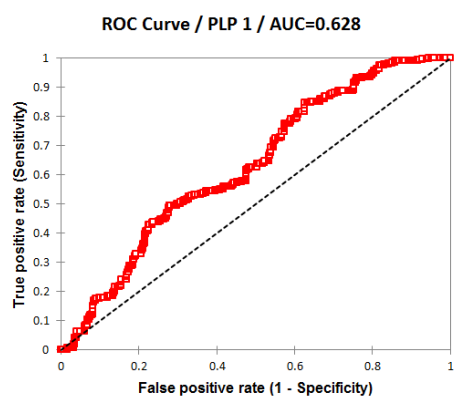
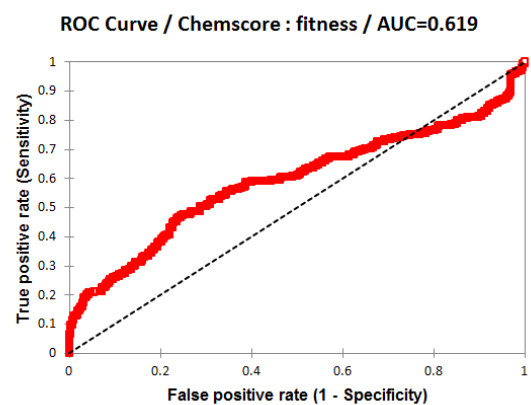
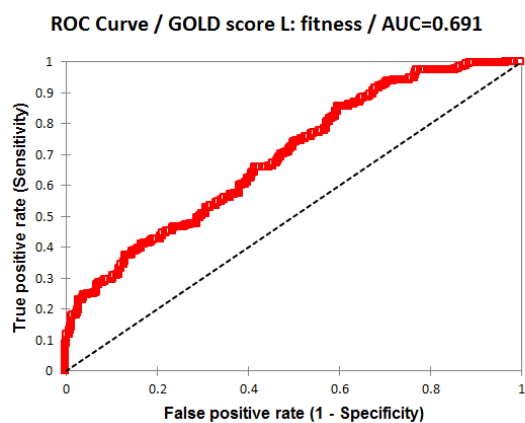
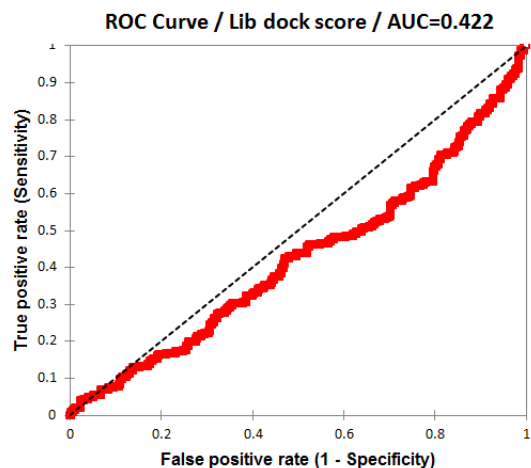
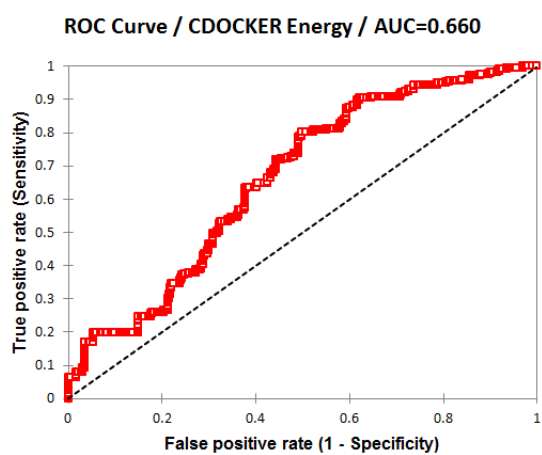


Figure 3. 28 The receiver operator curves generated for the analysis of scoring functions using the kynuric acid inhibitors assay.

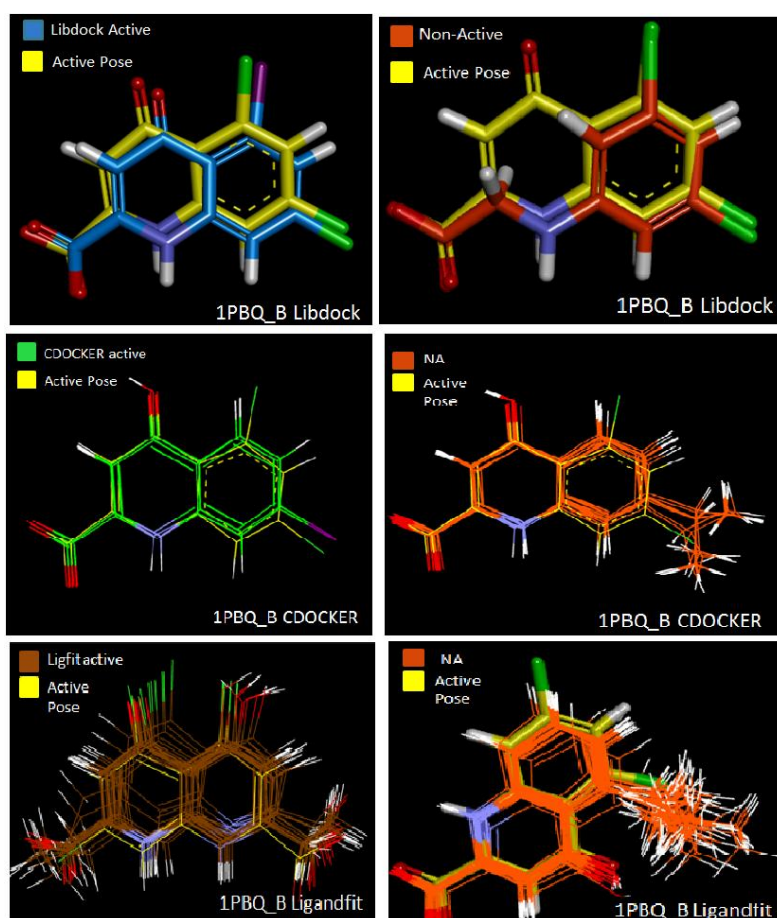


Figure 3. 29 Multiple poses predicted for active and non-active molecules in the docking studies.

All the docked poses were able to mimic the crystal bioactive compound conformation. All the active compounds had an IC_{50} lower than $5 \mu M$, the non-active molecules in Libdock had an IC_{50} value of $49 \mu M$. The non-active molecules for CDOCKER and LigFit had IC_{50} values that were greater than $100 \mu M$.

Overall, the supporting validation studies demonstrated that the scoring functions CDOKCER, Ligscore_2, Chemscore and GOLD score were best in terms of determining active ligands in a mixed ligand library with non active ligands. The RUC curves obtained for GluNR1 kynuric acid antagonists support their selection of active molecules. For the pose prediction majority all of the docking methods were able to match the native crystal structure as demonstrated in Figure 3.29. Therefore for this investigations these were the main scoring functions implemented to identify the small molecule antagonist at P8.

3.13 Initial VS hits selection

Once the validation studies were completed, the docking protocol was ready to be initiated using the prepared biological targets and ligand libraries. The in-house compound libraries were initially screened using DS docking programs CDOCKER and Ligfit against crystal structure 5H8F at the binding sites identified close to P8 (see section 3.11.2). The second set of ligands which used commercial libraries (ZINC15 and Sellechem) of compounds was then screened. The initial virtual screening returned in total 4,027 ranked compounds for binding site 1 (BS1); 4,525 ranked compounds for binding site 2 (BS2), 734 ranked compounds for binding site 3 (BS3) and 714 ranked for binding site 4 (BS4). The compounds that had shown to have top scores both in CDOCKER and Ligfit were then selected for further investigation in the post filtering process illustrated in Figure 3.30.

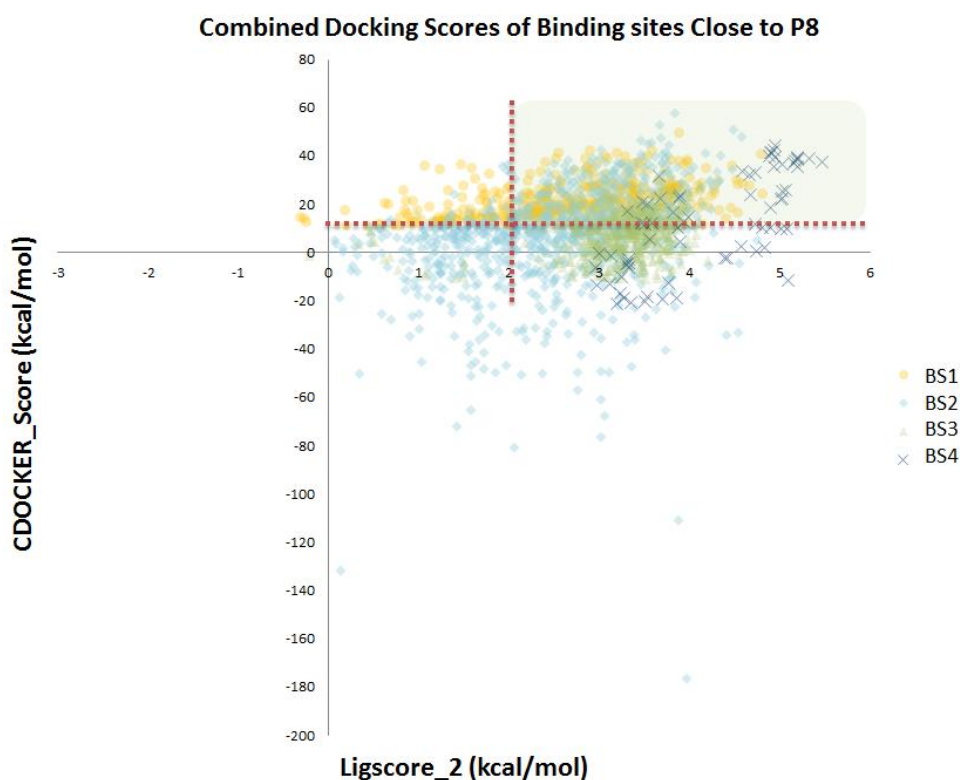


Figure 3. 30 The binding scores of the docked ligands in the four binding sites selected.

The top scoring ligands were selected from the region in the green square where the cut-off of CDOCKER Score >10 kcal/mol and Ligscore2 > 2 kcal/mol. The compounds showed high overlap in their scores.

The compounds with a higher calculated score were ranked the best. Therefore, these compounds had a higher binding affinity/compatibility with the target protein. The top scoring compounds from each binding site totalled to 10,000 compounds. These were then analysed in terms of their 2D structure to examine which features seemed to be more involved in stabilisation of the compound-protein complex. The poses of the top scoring ligands were then clustered based on their chemical structures. Additionally, ligand clustering is a useful model for identifying the common pattern among these top scoring compounds in HTS processes, as it allows the categorisation of small subsets to represent a large data set. In this method all of the molecules that have similar properties are placed in the same cluster. This model uses the RMS difference of descriptor properties such as Tanimoto distance for fingerprints in combination with the feature-class fingerprint of diameter (FCFP6)³⁴³ these were used in the ligand clustering process.

Approximately 10,000 compounds were identified for the binding sites around the P8 sequence, 3,383 compounds were the same across all sites to be ranked in the top set of ligands. These include analogues of 5,6-dihydro-5-fluorouracil, hexahydroquinolin, hexahydroanthracene-9,10-dione, isoindoline and oxa-8-azatricyclopentadecane. 6,617 compounds were found to be more unique to the binding regions in which they were screened. The ligands were then categorised into 20 clusters (Figure 3.31a) to represent the most common features of the top scoring ligands. To do this, agglomerative hierarchical clustering was used to treat each compound in the list as its own cluster. As a measure of similarity the euclidean distance between each cluster was then determined as a measure of similarity between the compounds. This process was repeated until all compounds could be linked into one cluster. To generate the dendrogram in Figure 3.31a, complete linkage clustering was applied, which applies the farthest maximum method. This technique defines the distance between two clusters, as the farthest distance between members from each cluster to yield clusters that are well parted. The structure of each cluster centre is provided (Figure 3.31b).

The heat map (Figure 3.31a) demonstrated the closeness of the ligands in each cluster. From this data set, cluster centre 2 ((2R)-N-(6-methoxy-1,3-benzothiazol-2-yl)-2,3-dihydrobenzothiophene-2-carboxamide) and cluster centre 8 (N2-benzyl-N4,N4-diethyl-6-pyrrolidin-1-yl-1,3,5-triazine-2,4-diamine) had the greatest number

of compounds that matched with them. A sum of 741 compounds for Group 2 and 565 compounds for Group 8. After categorising the structures of the top scoring ligands to the BS at P8, further narrowing down of the compounds was performed. In total 5,124 compounds were taken to the next filtering stage, which was ensemble docking.

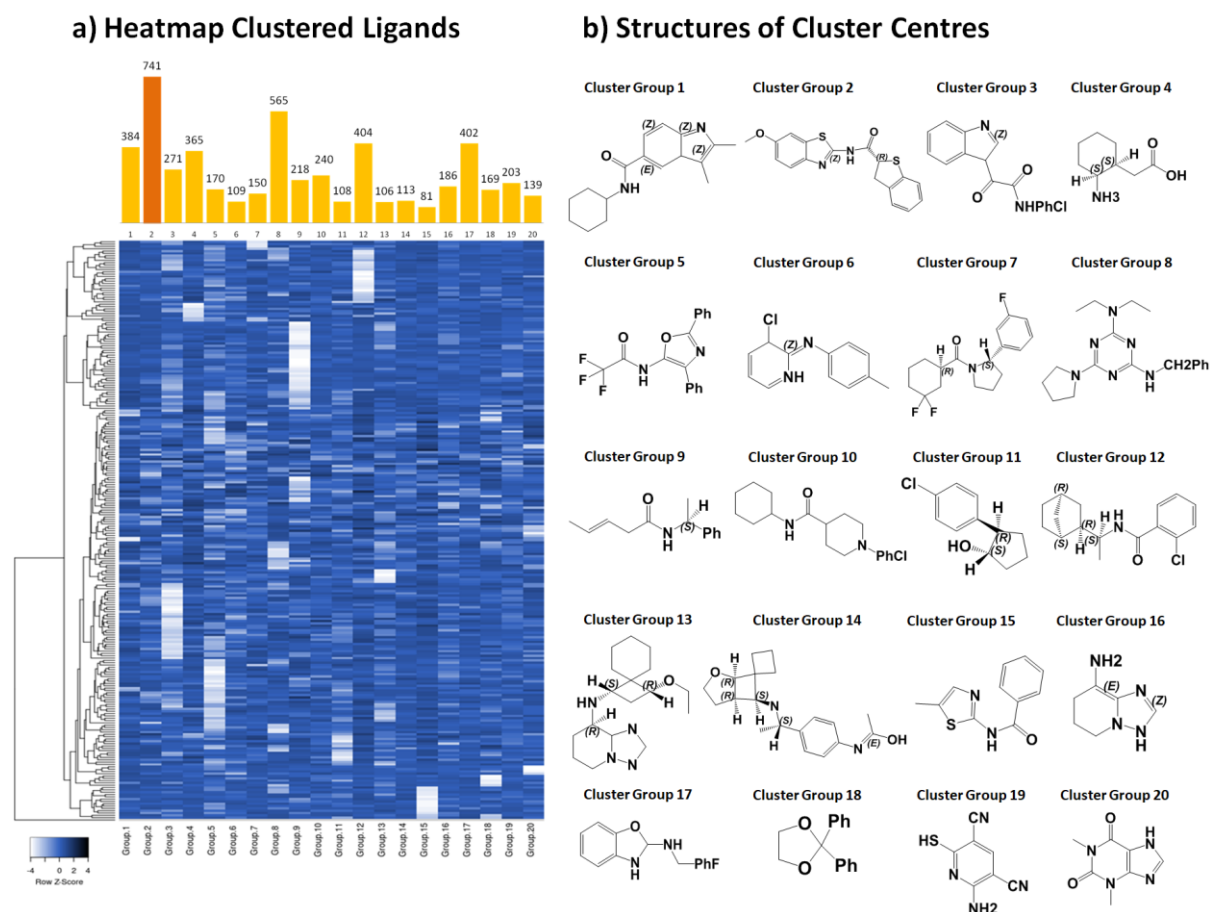


Figure 3.31 Clustering of the top scoring ligands.

3.31a) Heat map and dendrogram generated regarding the cluster groups. The online software heatmapper (<http://heatmapper.ca/expression/>) was used to visualise the data as a heat map. The higher the value to the cluster centre is represented with dark blue and lower the similarity between compounds in clusters represented by lighter blue and no similarity by white. The columns of the heatmap represent each cluster compound, with the sum of total compounds shown in bar charts above each cluster. The rows measure the differences in distance observed in the data. **3.31b)** The structure of each cluster group that was set as the cluster centre.

3.13.1 Ensemble docking

In this study, the ensemble docking was performed with GOLD software using the following crystal structures 5H8F_B (Human), 5H8H (Human), 1PB8 (Rat) and 2A5T(Rat) (Figure 3.32). This protocol was developed by Jones *et al*³⁴⁴ to apply the genetic algorithm for docking onto multiple targets.

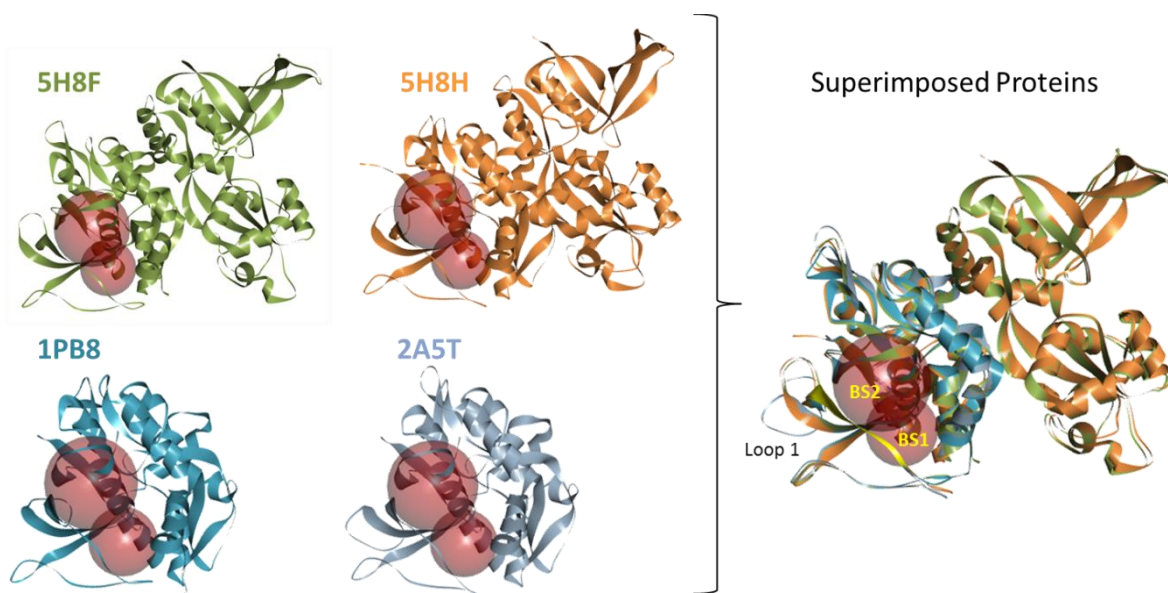


Figure 3. 32 Ensemble Docking procedure, align and superimpose the structures.

The ensemble consists of four models of the GluNR1 LBD, demonstrated in green (5H8F), orange (5H8H), blue (1PB8) and grey (2A5T). The structures were aligned and superimposed. The binding site of interest BS1 and BS2 shown in red spheres.

Table 3. 16 Superimposed RMSD and Number of Overlapped Residues (NRES) with respect to 5H8F used for ensemble docking

Protein	C- α RMSD (Å)	Main-chain RMSD (Å)	NRES
1PB8	0.938	0.968	286
5H8H	0.869	0.883	560
2A5T	2.370	2.393	284

The following protein models had the native neurone transmitters glycine (IC₅₀ 6.2 μM) and glutamate half maximal effective concentration (EC₅₀ 1.8 μM) already bound within the NMDAR ligand binding domain. Structure 5H8H also had the positive allosteric modulator of NR2a containing NMDARs, 7-[[ethyl(phenyl)amino]methyl]-2-methyl-[1,3,4]thiadiazolo[3,2-a]pyrimidin-5-one (EC₅₀ 1.9 μM) and Ca²⁺ ion bound within the structure. 1PB8 structure had the alternative agonist of the GluNR1 subunit, *D*-serine bound (EC₅₀ 7.02 μM).^{345,346}

A common feature within these models is that they all have an active conformation of GluNR1. They have their respected agonists bound. This can be an allosteric binder or native neurotransmitter. The main hypothesis here was to use these models to select compounds that have a greater selectivity for the active conformation of the GluNR1/GluNR2a subunit and therefore improve the chances of inhibiting to inhibit the over active receptors during the excitotoxic events in stroke. Moreover, the majority of antagonists of the GluNR1 LBD are xenobiotic and not present during the initiation of the physiological pathway of NMDAR in stroke.³⁴⁷

Using the superimposed models (Table 3.16) it was demonstrated that although there was a very close overlap of the C-α and the main chain atoms of the structures (RMSD values ≤2 Å), there were distorted residues (Asn48, Asp49, Thr50, Ser51, Pro52, Gly53, Ser54, Pro55, Arg56 and His57) in loop 1. The structure 2A5, clearly showed greater deviation in loop1 when compared to the other structures. However, this distortion did not greatly influence the binding sites close to the P8 region. This was due to the stability of the β-strand being maintained through disulphide bridges from the following residues Cys29, Cys63, Cys45, and Cys64. The superimposition of the molecules allowed a single binding site to be set up across the whole ensemble as most of the structures shared a close geometry.

After setting up binding site one and two, the docking protocol was ready for initiation. The docked solutions were scored using the GOLD score rescored with the ChemPLP scoring function. Comprehensive enumeration of all ensembles was conducted to obtain approximately 100 solutions that were reasonably well bound to the binding sites of interest (Figure 3.33). The highest scoring compound from the ensemble docking was compound 300-1113 which is a synthetic amino acid with a phenylpyrazol side chain, structure demonstrated in Figure 3.33a. It also had the

best score in the 5H8F model in BS2. However, this molecule had a fairly large MW (476.93 g/mol) and was extremely hydrophobic, causing it to have very poor solubility. The other top scoring compounds included droperidol that had better solubility predictions.

These molecules also scored best in binding site 2, where the benzimidazolone structure was able to be stabilised into a pocket binding site which allowed better access to the long chain on the surface of the protein above the P8 sequence. Additionally, as these were larger molecules they demonstrated greater hydrogen contact in the BS1 which was substantially much smaller in size. These close contacts were between the ligand atoms and the amino acids Ser169, Tyr19, and Val34.

It was clear that from both scoring functions there were 4 compounds that showed to be scored lower within both scoring functions ChemPLP and GOLD score fitness. They were amsacrine< trimethoxyisoflavone< ethyl carbamate< trihydroxybenzylidene. The worst poses for both binding sites in this study were generated from amsacrine with a binding score of ChemPLP 12.91 kcal/mol and GOLDScore 10.86 kcal/mol. trimethoxyisoflavone also scored poorly, ChemPLP 15.42 kcal/mol and a GOLDScore 9.88 kcal/mol.

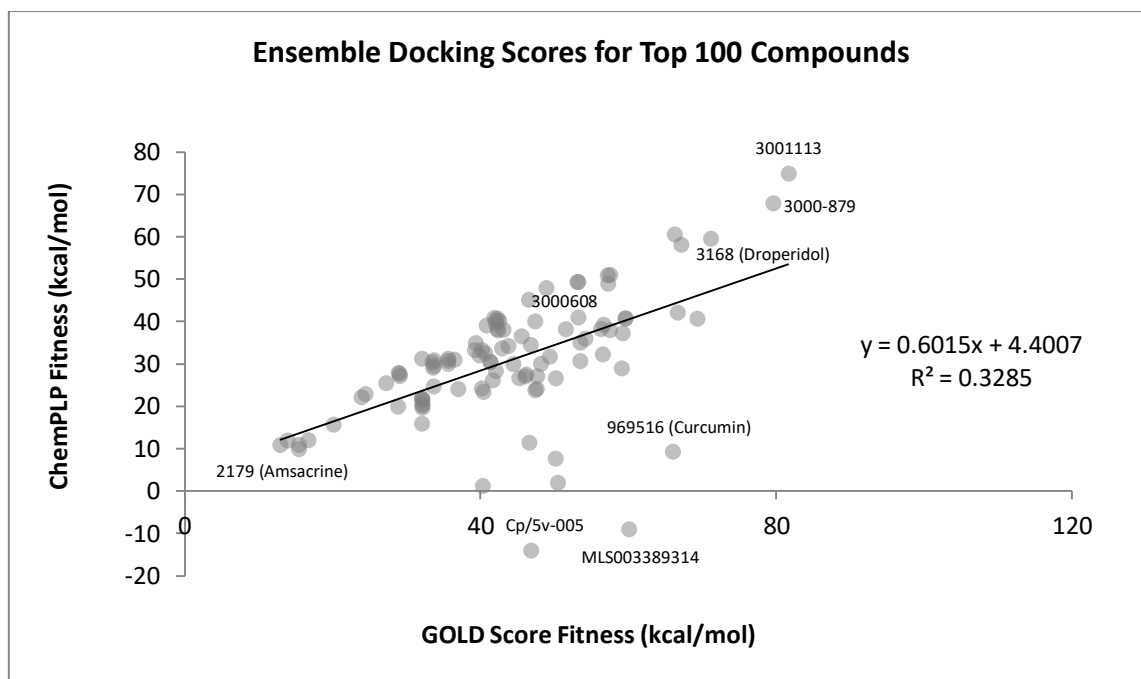


Figure 3. 33 The binding scores obtained after the ensemble docking.

The scatter diagram of the scoring functions demonstrated a partial positive correlation. The best and worst scoring ligands are labelled, with each circle representing one compound. The compounds that demonstrated overlap in their scores are highlighted in darker grey.

Figure 3.34a and 3.34b demonstrates the 3D and 2D interactions of some of the top scoring ligands. It was crucial to search through all the poses generated, in order to prioritise a number of structures for the hits. Interestingly, majority of ligands rejected through the docking process were compounds that caused great electrostatic repulsions (e.g. closer than 3.5 Å for oxygen-oxygen contacts) and were incompatible through 3D shape.

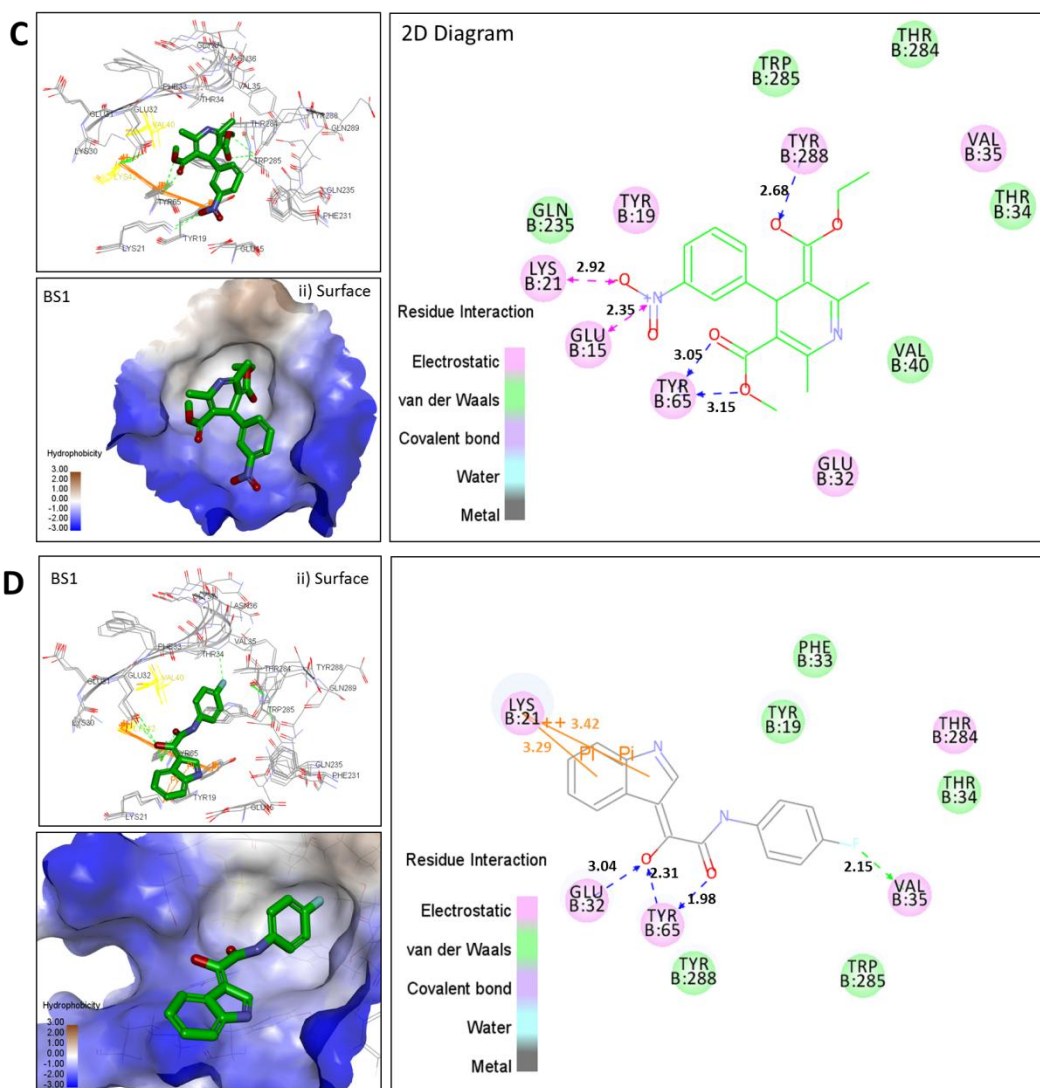


Figure 3. 35 The binding of nitrendipine and 3000917 with GluNR1 P8 sites.

3.35C) Nitrendipine best fitted at BS1, showing a network of hydrogen bonds with the residues Trp288, Lys21, Glu15 and Tyr65. **3.35D)** 3000917 was found to be best stabilised in BS1 with a BE of -2.47 kcal/mol. The diketones in the compound were shown to act as hydrogen bond acceptors with the residues Glu32 and Tyr65. Both ligands demonstrated in their tautomeric forms.

After visual inspection, to aid narrowing down to the most stable ligand poses at the sites of interest, the binding energies of the ligands were calculated. This was done with CHARMM based implicit solvation methods available in DS to estimate the free energies of the bound ligands.³⁴⁸ The implicit solvent generalized Born with molecular volume (GBMV) model was used. It was important to use a solvent model

to predict better binding energies to avoid modeling the system in a vacuum. Binding energies demonstrated in Figure 3.36 and the selection of final *in silico* hit molecules is demonstrated in Table 3.19.

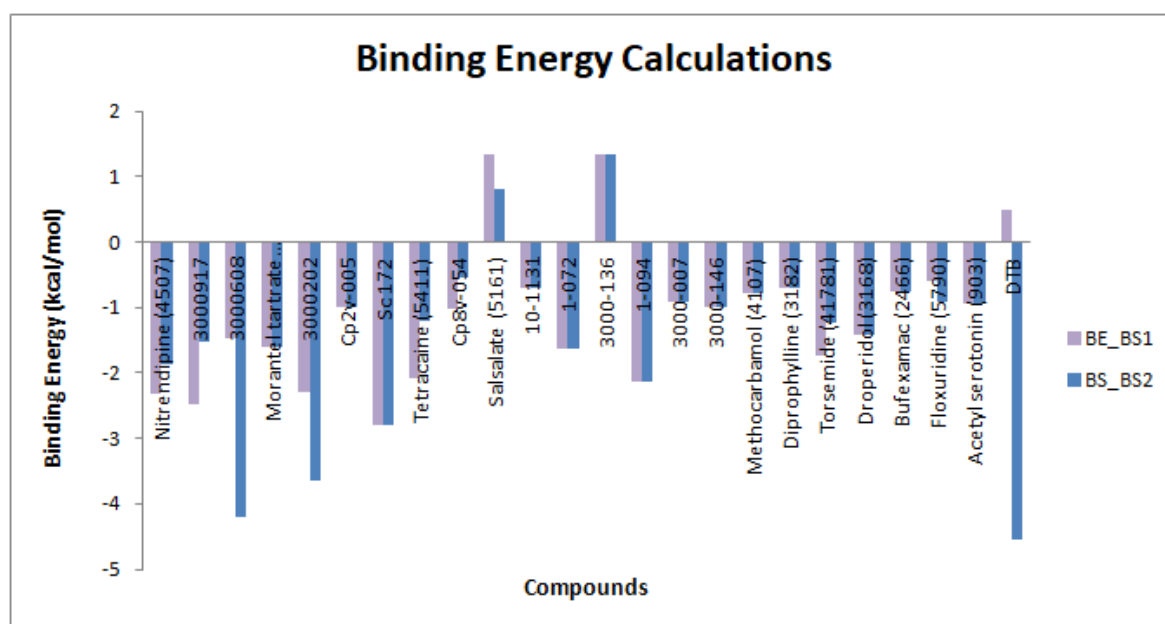


Figure 3. 36 The Binding energies of the top 27 *in silico* hits

The binding energies show that the majority of compounds that were the highest scored had stable binding energies within binding site 1 (BS1) and binding site 2 (BS2). This was with the exception of 5161 (Salsalate), 3000-136, 1-7168 and 3000-879.

BS1 and BS2, with exception of salsalate (BS1 1.35 kcal/mol, BS2 0.81 kcal/mol) and 3000-136 (BS1 1.34 kcal/mol, BS2 1.34 kcal/mol). This may be due to less shape match between these molecules and the binding sites. Particularly in case of 3000-136 where the pyridine-3,5-dicarbonitrile was shown to be fairly rigid in the binding sites, therefore not able to make many interactions with the residues available.

Compound 3000608 and DTB demonstrated to be much more stabilised at BS2 in comparison to BS1, with the BE values of -4.19 kcal/mol and -4.54 kcal/mol, respectively. This may be due to the larger pocket size of the BS2 available in comparison to BS1, therefore able to accommodate these compounds easier at that region.

Although both of these compounds illustrated relatively unstable binding energies, they were still taken forward as potential hits. This was done due to the compounds exhibiting good binding scores with the target protein and demonstrating diversity among the ligands selected. In addition, they could also provide an opportunity to examine if the binding energies calculated by the model were correct in its prediction from the biological assays.

As expected, the majority of ligands rejected through the docking process were compounds that caused great electrostatic repulsions (e.g. closer than 3.5 Å for oxygen-oxygen contacts) and were incompatible through 3D shape.

One of the highest scoring compounds and with most stable binding energy was 3000202 from the Professor Chen library, (demonstrated in Table 3.19). It obtained a ChemPLP score of 48.90kcal/mol, GOLD score 47.90 kcal/mol and lowest binding energy of -3.64kcal/mol at BS2. The amine group was able to hydrogen bond with Lys41 and a pi-pi (π - π) interaction from the benzyl group at 3.18 Å. The morpholine group was able to stack between the Lys44 and Arg77 side chains providing more electrostatic interactions.

Droperidol (Pubchem CDI: 3168) and nitrendipine (Pubchem CDI: 4507) showed to have their lowest binding energies of calculated to be -1.39 kcal/mol at BS1 and -2.30 kcal/mol at BS2, respectively. Droperidol was found to have a ChemPLP binding score of 71.17 kcal/mol. Droperidol is a butyrophenone that is mainly applied as a sedative after surgical procedures. At BS1, hydrogen bonding with Tyr288 (1.53 Å), Glu32 (2.01 Å) and Lys21 (2.33 Å). It was also able to accommodate in the binding pocket formed in the receptor by a number of pi-sigma interactions involving Tyr19, Thr34, Val35, Val40, Thr284 and Trp285.

Interestingly, nitrendipine which had a ChemPLP binding score of 43.09 kcal/mol was the best fit at BS1. This drug was approved by the FDA in 1985 as a potent antihypertensive drug, mainly executes its effect by inhibiting the L-type calcium channels located in the smooth muscle cells of the cardiac muscle. It subsequently reduces the calcium levels in the cell and allows better blood flow through smooth muscle dilation.^{349,350} It has IC₅₀ of 95 nM for L-type calcium channels.³⁵¹

Additionally, this drug consists of one stereo centre which allows it to be sold as a

racemic drug, a mixture of equal amounts of *R* and *S* enantiomers. Although, there are some *in vivo* studies that suggest the *S* enantiomer is the active compound, showing approximately 6 times more potency in comparison to the *R* enantiomer by inhibiting A2 induced coronary vasoconstrictions .^{352,353}

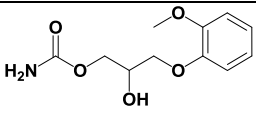
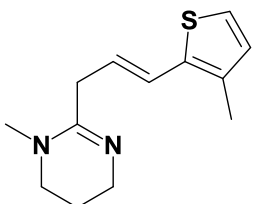
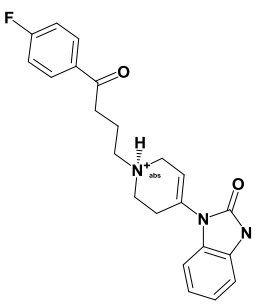
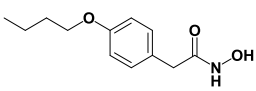
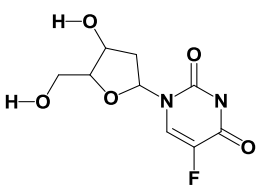
By visual inspection of the molecule, the *S* enantiomer allows the hydrogen on the pyridine ring to act as an HBD Glu32 however the *R* enantiomer cannot find the correct pose in the BS1 binding pocket. The CDOCKER docking studies revealed that the *S* enantiomer of nitrendipine had better scores for both BS1 and BS2, with values -7.88 kcal/mol and -13.20 kcal/mol in comparison to the *R* enantiomer with CDOCKER scores for BS1 -12.82 kcal/mol and for BS2 -13.42 kcal/mol. This could be possible due to the *S* enantiomer being able to stabilise the nitrobenzene in the opening of the pocket and allow it to act as a hydrogen bond donor at that site. Additionally, the binding energies of the two enantiomers confirmed that the most stable conformation of is the *S* enantiomer at BS 1 and for -9.55 kcal/mol and *R* enantiomer at -6.85 kcal/mol. Full table of the BE of the enantiomers demonstrated in Appendix E.

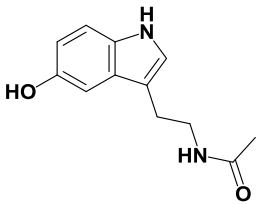
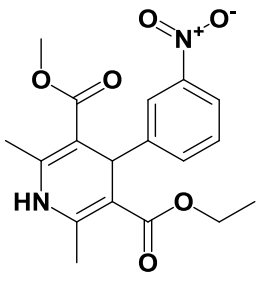
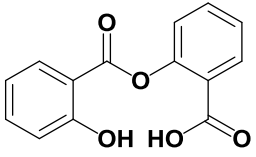
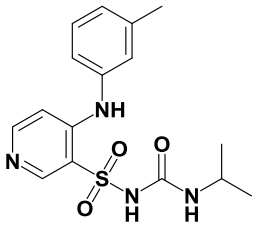
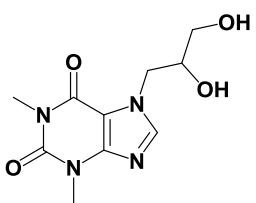
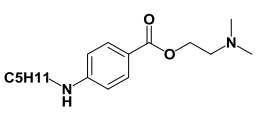
From the in-house library drugs 1-094 and 3000917 ((N-(4-Fluorobenzyl)-2-(1H-indol-3-yl)-2-oxoacetamide) were shown to be best binders. The 3000917 analogues have been known to take part in neurodegenerative disease such as prions disease. Prions is the abnormal aggregation of proteins such as amyloids, which accumulate in infected tissue and are associated with neuro damage and cell death.³⁵⁴

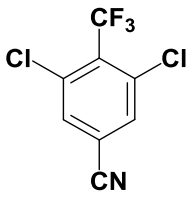
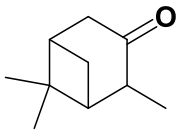
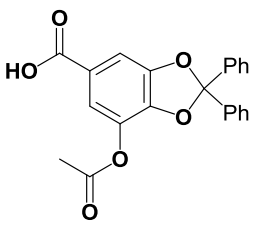
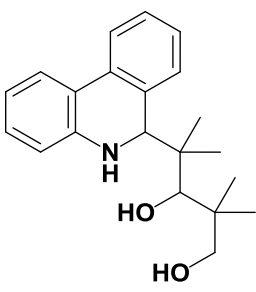
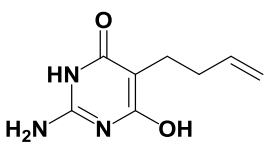
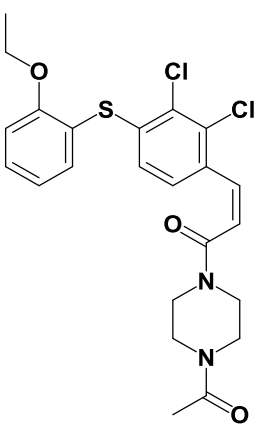
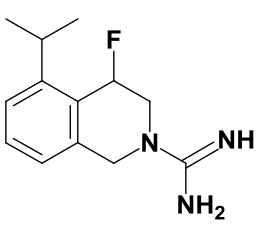
After taking into consideration the ranking scores, the binding energies calculated for each of the docked poses, and visually inspecting each of these compounds *in silico*, the top 24 compounds that showed to maintain their high score throughout the dockings were selected (Table 3.17) and were then analysed by pharmacokinetic ADMET models.

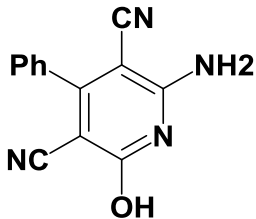
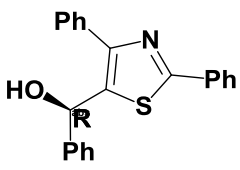
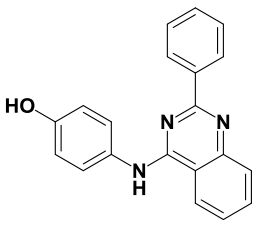
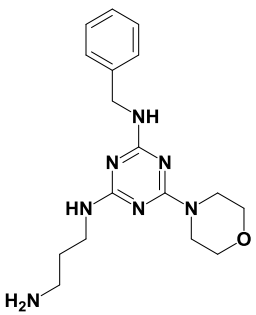
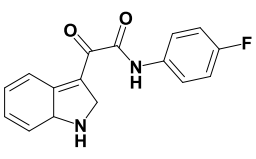
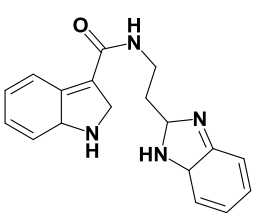
Table 3. 17 The *in silico* hit compounds from the VS campaign.

Starting from the best scored ligands in each library.

No	Ligand	2D Structure	Function
1	4107 (Methocarbamol)		FDA approved drug. Methocarbamol is a guaiacol glyceryl ether used to treat muscle skeletal pain. It provides relief from associated acute pain from muscle injury. ³⁵⁵
2	5702276 (Morantel tartrate)		FDA approved drug. Morantel is mainly used in veterinary medicine as an anthelmintic (antiparasitic) drug, removing worms from live stock. It functions as a non-competitive voltage sensitive open channel blocker of nicotinic acetylcholine receptors. ³⁵⁶
3	3168 (Droperidol)		FDA approved drug. A butyrophenone mainly used as a anti-nausea and sedative drug. The mode of action of droperidol is still unknown, however it has shown to cause D2 receptor antagonism and also blocking the GABAergic interneurons. ³⁵⁷
4	2466 (Bufexamac)		Experimental drug. Bufexamac is used to treat subacute and chronic eczema and other inflammatory dermatoses conditions. The mode of action is still to be elucidated it is thought to block cyclooxygenase. ³⁵⁸ In 2010 it was withdrawn from the market by European medicine agency due to lack of clinical efficacy. ³⁵⁹
5	5790 (Floxuridine)		FDA approved drug. Floxuridine is an anti-cancer drug mainly used for treatment of colon cancer. As an antimetabolite it prevents cell division by inhibiting RNA formation and blocking uracil riboside phosphorylase that stops the translation of uracil in RNA synthesis. It also blocks thymidylate synthase that blocks DNA synthesis. ³⁶⁰

- 6 903
(Acetyl serotonin)
- 
- FDA approved drug. The *N*-acetyl serotonin is the precursor and an intermediate compound in conversion of melatonin from serotonin. It has been known to function as an agonist at the melatonin receptors, TrkB receptors.³⁶¹
- 7 4507
(Nitrendipine)
- 
- FDA approved drug. Nitrendipine, is dihydropyridine analogue that predominantly acts as a calcium channel blocker by inhibiting the L-type calcium channels. It is mainly used as a hypertensive drug as it can block the myocardial smooth muscle cells, leading to vasodilation and allowing better blood flow.³⁶² It has also been known to modulate NMDAR in rodents.³⁶³
- 8 5161
(Salsalate)
- 
- FDA approved drug. Salsalate functions as an anti-inflammatory drug by reducing the synthesis of inflammatory chemical for example TNF-alpha and interleukin-6. It is also known to interact with IκB kinase and reducing the NF-κB genes.³⁶⁴
- 9 41781
(Torsemide)
- 
- FDA approved drug. Torsemide functions as a high ceiling loop diuretic by activating excretion water and salts (sodium or chloride). It can prevent edema caused by heart failure, kidney and liver disease.³⁶⁵
- 10 3182
(Diprophylline)
- 
- FDA approved drug. Diprophylline, contains a theophylline core and can function as a bronchodilator by directly binding to the pulmonary blood vessels. It is used for treatments of asthma, cardiac dyspnea and bronchitis. The mechanism of function is proposed through inhibition of phosphodiesterase PDE3 and 4.³⁶⁶
- 11 5411
(Tetracaine)
- 
- FDA approved drug. Tetracaine is mainly used as an ophthalmic anesthetic. It functions by acting as an allosteric inhibitor of intracellular sodium channels.³⁶⁷

- 12 2,6-Dichloro-4-(trifluoromethyl)benzonitrile (DTB)

- DTB is a compound from the AFchem library in the organic building block. No biological activity was known to date.
- 13 Cp2v-005
2,6,6-trimethylbicyclo[3.1.1]heptan-3-one

- Cp2v-005 is a compound from the AFchem library in the organic building block. No biological activity was known to date.
- 14 SC 172
7-acetoxy-2,2-diphenylbenzo[d][1,3]dioxole-5-carboxylic acid

- 172 is a compound from the AFchem library in the organic building block. No biological activity was known to date.
- 15 Cp 8v-054
4-(5,6-dihydrophenanthridin-6-yl)-2,2,4-trimethylpentane-1,3-diol

- Cp 8v-054 is a compound from the AFchem library in the organic building block. No biological activity was known to date.
- 16 1-072
2-amino-5-(but-3-en-1-yl)-6-hydroxypyrimidin-4(3H)-one

- 1-072 is a compound from the AFchem library in the organic building block. No biological activity was known to date.
- 17 1-094
(2Z)-1-(4-acetylpiperazin-1-yl)-3-(4-((2-ethoxyphenyl)sulfanyl)phenyl)prop-2-en-1-one

- 1-094 is a compound from the AFchem library in the organic building block. No biological activity was known to date.
- 18 10-1131
4-fluoro-5-isopropyl-3,4-dihydroisoquinoline-2(1H)-carboximidamide

- 10-1131 is a compound from the AFchem library in the organic building block. No biological activity was known to date.

- 19 3000-136
2-amino-6-hydroxy-4-phenyl-pyridine-3,5-dicarbonitrile
- 
- 3000-136 is from the University of Sheffield Professor Chen group's chemical library.
- 20 3000-007
(R)-(2,4-diphenylthiazol-5-yl)-phenyl-methanol
- 
- 3000-007 is from the University of Sheffield Professor Chen group's chemical library.
- 21 3000-146
4-[(2-phenylquinazolin-4-yl)amino]phenol
- 
- 3000-007 is from the University of Sheffield Professor Chen group's chemical library.
- 22 3000-202
N2-(3-aminopropyl)-N4-benzyl-6-morpholino-1,3,5-triazine-2,4-diamine
- 
- 3000-202 is from the University of Sheffield Professor Chen group's chemical library.
- 23 3000-917
N-(4-fluorophenyl)-2-(1H-indol-3-yl)-2-oxoacetamide
- 
- 3000-917 is from the University of Sheffield Professor Chen group's chemical library. Previously they have been found to act as potential anti-prion agents. Prion disease (transmissible spongiform encephalopathies) is a neurodegenerative disorder affecting humans and animals.
- 24 3000-608
N-(2-(1H-benzo[d]imidazol-2-yl)ethyl)-2-(1H-indol-2-yl)acetamide
- 
- 3000-608 is from the University of Sheffield Professor Chen group's chemical library.

3.13.2 ADMET of the molecules

The ADMET profile is a vital component of drugs and is widely applied in CADD to reduce undesired adverse effects in the drug discovery process. The method used was optimal predictive space validation (OPS) to analyse how far the compounds fall from the training set.³⁶⁸ The ADMET OPS model for the 24 *in silico* hits is shown in Figure 3.37 with a heat map demonstrating compound predictions in Figure 3.38.

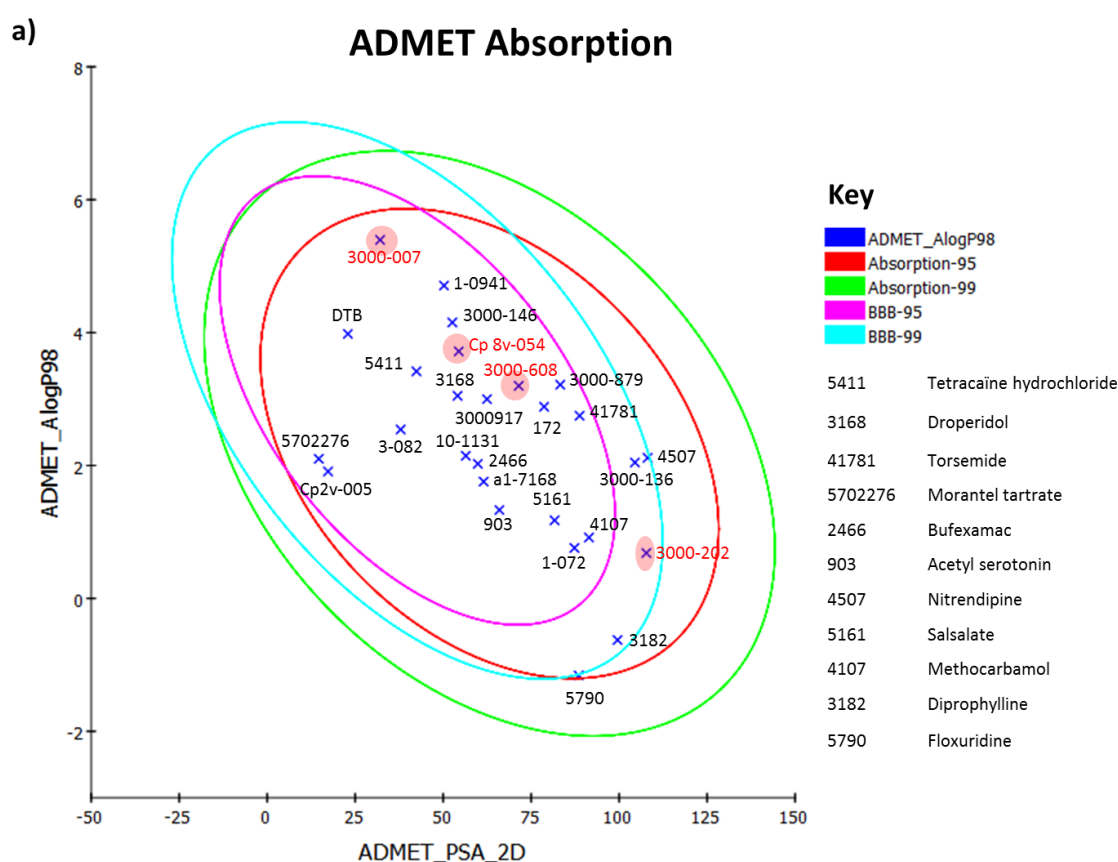


Figure 3. 37 The ADMET absorption model.

The model predicted that most compounds were within 95% of the ellipses which suggest these compounds were well absorbed through the BBB and human intestinal system after oral administration, while for compounds 3000-136, 4507, 3000-202, 3182 and 5790 they would be more poorly absorbed through the BBB. The data was calculated based on the ADMET_Polar Surface Area from the 2D structure and the AlogP98 values of the compounds. Compounds 3000-007, Cp 8v-054, 3000-608 were predicted to be effluxed from the CNS through p-gP.

Heat Map of ADMET Properties

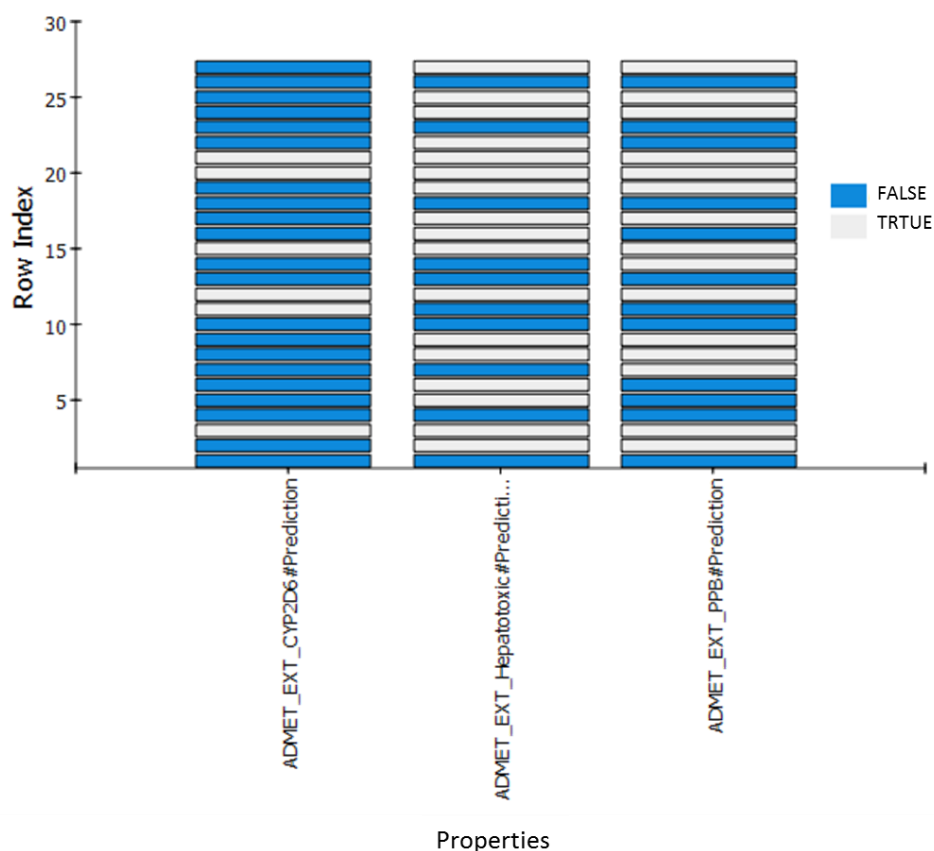


Figure 3. 38 The heat map of the ADMET properties.

The heat map demonstrates the compounds predictions for the three models tested; the cytochrome P450 2D6 (CYP2D6) inhibition using 2D chemical structures, liver toxicity and plasma protein binding in the blood.

The ADMET protocol calculates probable toxicity values for a chemical structure by computing a defined score based on the QSTR model. Bayesian models were used for the classification protocol and the partial least squares (PLS) method was used for the regression techniques. The results demonstrated that the majority of compounds were shown to be less likely to be metabolised by the CYP2D6 with exception for six compounds droperidol, tetracane hydrochloride, DTB, Cp 8v-054, 3000-007 and 3000-146.

There was also large number of compounds that may have caused damage to the liver and potentially be substrates for plasma binding proteins. However, at this stage

of the project it was important to ensure that an initial hit molecule could be identified. Also that most of the compounds were in the agreement of the desired drug-like parameters and in compliance with approved drug physicochemical properties. Further optimisations could be applied if any of these compounds were able to show the desired biological activity in regard to potential lead optimisation procedures.

In an effort to examine the relationship between the properties of the hit molecule with the data already published for pharmaceutically relevant compounds, including known drugs a radar chart was constructed using data available on the ChEMBL website on NMDAR antagonists (Figure 3.39ab). This allowed a direct comparison of the physical chemical properties for the compounds developed for stroke treatments and identify key factors required for the hit selection.

As an example, compound 3000202 (demonstrated in Figure 3.39d), showed a good correlation with the chemical properties of known inhibitor drugs of the NMDAR. The HBA/HBD and logP values were a reasonable match with the known drug memantine, however the molecular weight of the triazine compound (388.5 g/mol) needed to be lower, closer to the range of 200-360 g/mol. Also the polar surface area needed to be increased to within the range of 90 Å³.

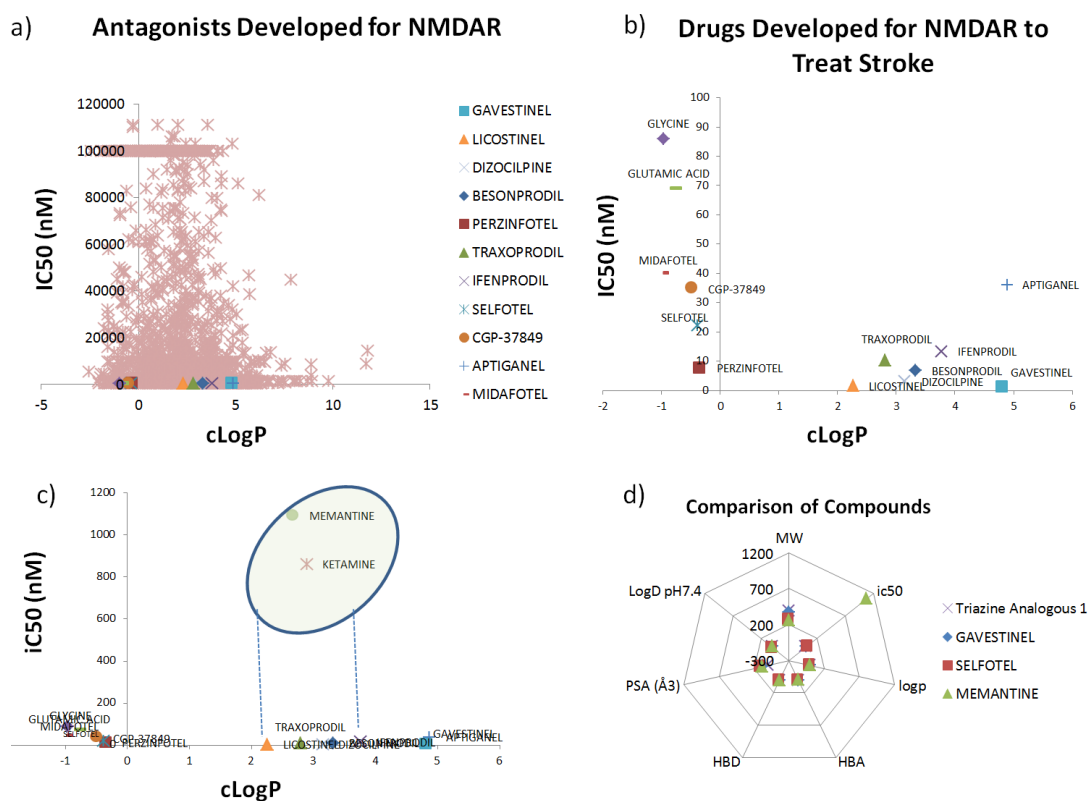


Figure 3.39 Discovery trajectories of NMDAR antagonists.³⁶⁸

3.37a,) NMDAR antagonists and their corresponding logP value ranges, **3.37b)** A sample of already developed NMDAR drugs that were designed for stroke. **3.37c)** Showing the successful drugs, the less potent channel blockers memantine and ketamine. The important region for logP shown in green. **3.37d)** A radar chart demonstrating the parameters of known drugs for NMDAR in comparison to one of initial hit compounds 3000202.

3.13.3 Do Fab binding areas overlap with the binding sites of small molecules?

After the binding regions of the homology model of the FV segment with NR1 was created (Chapter 3. Part one), demonstrated in Figure 3.40a, it was interesting to compare these regions with the binding sites of small molecules selected from in this section. As expected the small molecules could not fully satisfy all the interactions involved in the binding of the FV segment with the NR1 protein. In total, the binding of the homology model to the FV shows 56 amino acids, in close contact.

This number is much larger in comparison to the amino acids involved in the small molecule binding site, ranging from ~7-10 amino acids for BS1 and BS2, while for BS3 the number is ~30 amino acids.

However, the binding sites identified with the small molecules on the target protein do share features with the PP model (Figure 3.40b). As expected the small molecules tend to adopt a specific conformation within the N1 LBD in which a groove is present to allow the small molecule to bind. In comparison, when the FV interacts with NR1 flat contact surface area presented. For binding site 2 (BS2) the compound 3000-608 showed to have van der waals interactions with the amino acids Val431, Lys432, Arg468, Ile 464 and Phe784. This sequence is located close to the antigen site (the P8 sequence).

During the scanning of residues it was shown that some binders do share the same hot spot on the GluN1 subunit. For example in BS1 the binding of 3000- 063, a 2,4-di(1-pyrrolidiny)-1,3,5-triazine analogue shows VDW interactions with amino acids Tyr19, Lys21, Val35, Thr34 , Val40, Thr284, Tyr288, Trp285.

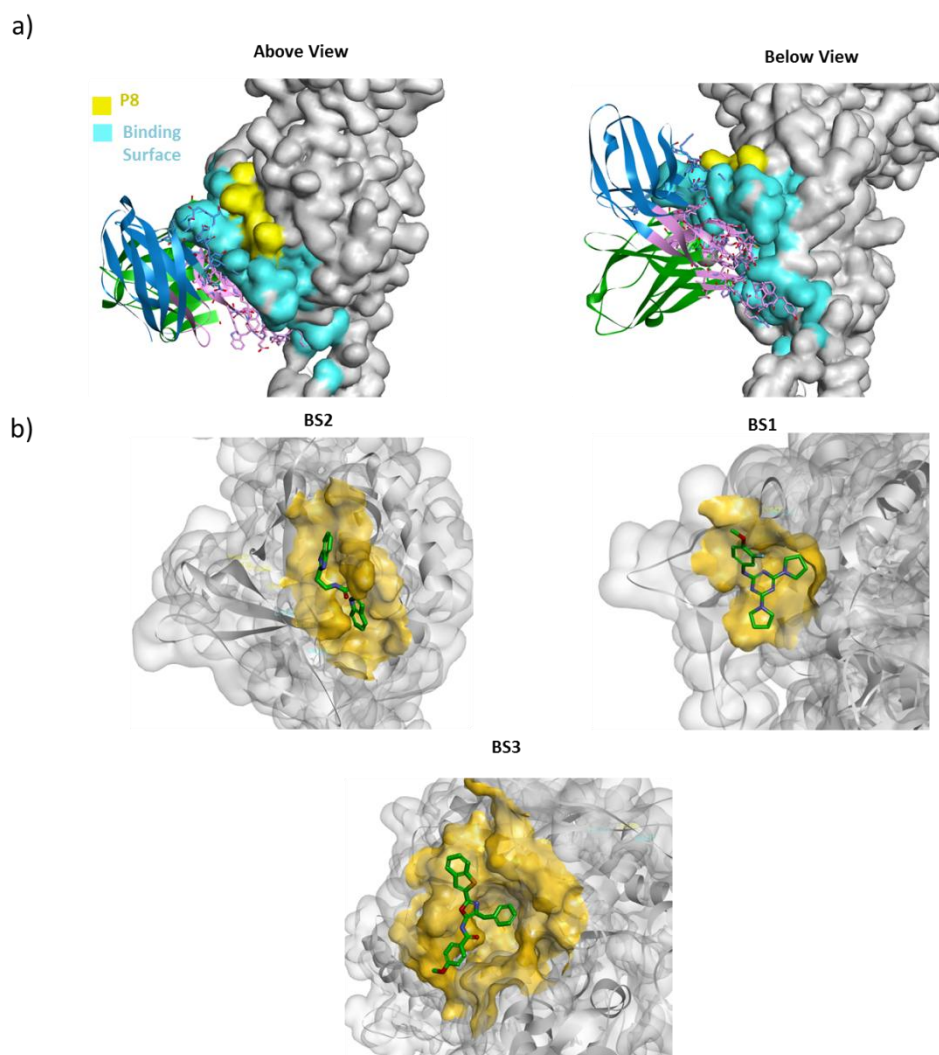


Figure 3. 40 Five comparisons of how the protein interacts with the FV segment and with synthetic small molecules.

Figure 3.38a) The structures of the FV-NR1 complexes predicted are demonstrated. The target protein NR1 (grey) is demonstrated as a filled surface model and the binding of the FV segment is represented as a ribbon diagram, with selected binding amino acids shown as sticks (elemental colour). The best binding mode of the pAb with NR1 highlights the amino acids involved in the binding are shown in cyan. **Figure 3.38b)** The structures of protein-small molecule complexes illustrated in the binding sites BS1 to BS3. Small molecules are illustrated in stick format (green) and their surface of contact is shown in orange. It is clear that the PP region surface is much greater and flatter than the protein-small molecule binding surface area. BS1 shows binding of 3000-063, BS2 shows binding of 3000-608 and BS3 shows the binding of 300-1040.

These studies suggest that the binding surface of GluNR1 was adaptive and was able to accommodate small drug-like compounds that could share some of the main hotspot residues.

Overall, there is high probability that the small molecules may not be an accurate mimic of the FV-NR1 complex. Nonetheless, their ability to modulate the activity of the receptor was still investigated with biochemical assays and cellular *in vitro* models.

3.14 Limitations of the study

The computational methods applied for analysis of the Fab-GluN1 P8 segment have allowed analysis of the binding orientation of these two molecules. However, there are some key limitations to these studies that have to be taken into account.

In Chapter 3: Part one the PP surface interfaces that are displayed by biomolecules, such as mAb and pAb, often produce more complex challenges in that they have less defined groove or concave binding sites when compared to classical enzyme active sites and receptor binding sites.³⁶⁹ Thereby making it much more difficult for small molecules to bind to.

Another characteristic of PP binders is the large size of the surfaces involved in binding. For PP binding it is estimated that an area of 1500-3000 Å²³⁷⁰ is required for sufficient binding, which is much greater when compared to a protein-ligand interface, where the range is from 300-1000 Å².³⁷¹ Furthermore, for our studies the PP interactions between the pAb and the GluNR1 P8 antigen did not have a 3D conformation or a natural small molecule binder, therefore the important binding patterns required had not been elucidated, making these predictions less reliable. More importantly, in PP interactions there are also some residues that may not be in direct contact with protein chains which can influence the stability of these large molecules.

Despite these challenges, there are some inhibitors that are able to obstruct PP binding. For instance, as highlighted by Clarkson and Wells³⁷² there are “hot spot” regions important for inhibitors of PP interactions which indicates that the size of the binding interface may not be the most important factor and does not necessarily disqualify small compounds from binding.

Protein flexibility remains a major problem.³⁷³ It is clear now that protein flexibility remains important for accurate description of the native binding site. However, if flexibility is applied to larger portion of protein chains, it could introduce significant error in the docking protocol, hence reducing accuracy and preventing scoring function to rank poses effectively.³⁷⁴

Although, it is important to note that not all these sites necessarily contribute to protein-ligand complexes and in fact the majority of bound ligands in their native active sites tend to show less number of potential interactions.³⁷⁵

Water molecules present or absent in the active site play a crucial part in the precision of ligand docking results. Unfortunately, most programs even today have difficulty predicting their influence in binding sites.^{376, 377} For our experiments the water molecules were excluded during the docking. This may introduce errors in the experiment and the environment of the protein model.

Another important issue to consider is that nanomolar potent compounds are rarely found by VS strategies,³⁷⁸ and most often further optimisations are required. Nevertheless, advances in VS methods have led to a range of developments in *in silico* medicine and promising results in drug development across many fields.

For the ADMET studies, the general limitation for such models is that they are unable to predict reliable results outside their data set.³⁷⁹ More importantly, these models only provide quantitative endpoints (e.g. carcinogenic or non-carcinogenic) and provide no understanding of the biological pathway of toxicity which the compound is responsible for.³⁸⁰ In early hit identification, the benefits of using *in silico* ADMET models outweigh the limitations as these methods allows an early assessment of the compounds. It further permits elimination of compounds with unfavourable ADMET properties and allows a reasonable evaluation of proposed structural refinements.

3.15 Conclusion

In this chapter, a homology model was created from the cryo-em structure of a pAb and was used to perform PP docking with the target receptor NR1. The homology model was evaluated by corresponding PDF Total Energy and DOPE scores. *In*

silico molecular docking was subsequently used to identify and predict probable poses of interaction for the biologically active pAb. The sites were also explored with small molecules which were used to investigate binding at the same site of the PP interaction. The results demonstrated that there were three possible sites on to the GluNR1 LBD that may be involved in the interaction and were further compatible with small molecule binders.

Overall, this method was directed towards finding small compounds that were most likely to interact with the NMDA GluNR1 subunit at the binding site of interest and able to satisfy electrostatic and shape complementary with the binding region. The post filtering process included stringent filtering steps to identify the most stable compounds at the site, as well as focusing on selecting diverse structures from the compound libraries that had already been synthesised. The over all work flow applied for this project is demonstrated in Figure 3.41. The selected 24 *in silico* hits were taken forward for the biological assays to examine their safety and efficacy *in vitro* and *in vivo* models for stroke.

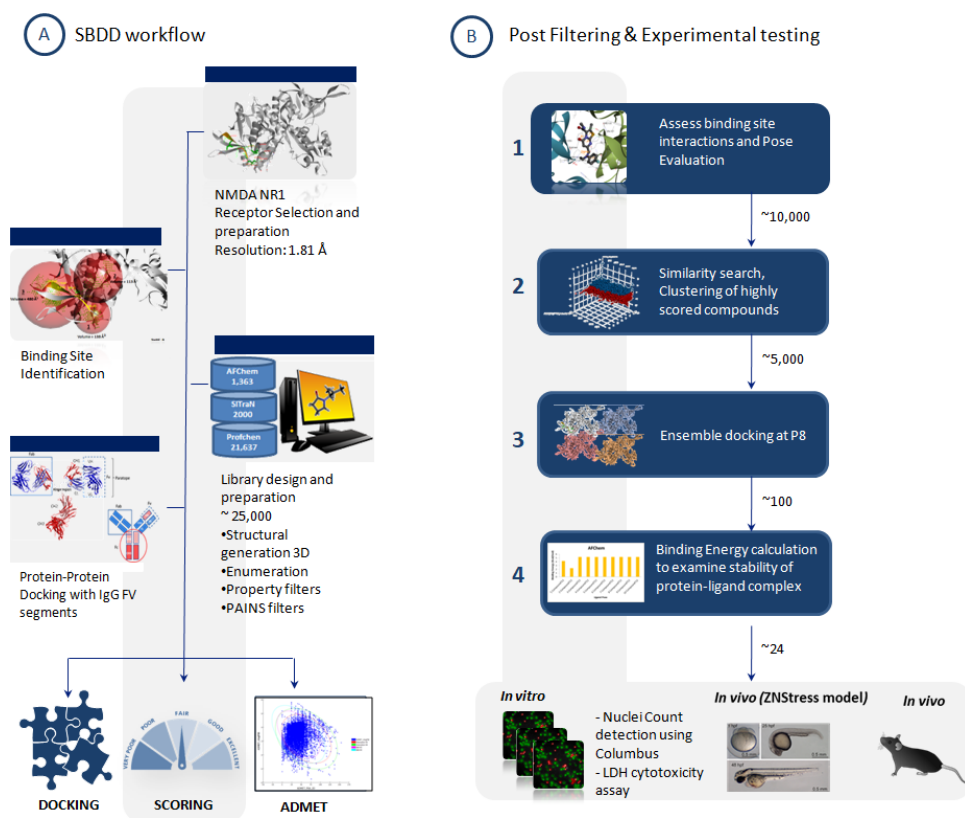


Figure 3. 41 Work flow applied for P8 *in silico* hit identification. VS methods and the biological testing for identification of HIT molecules for P8.

The above workflow was implemented which started off by applying structure based drug discovery methods, in combination with pAb docking to GluNR1 stage to select the ligands most compatible for P8 binding site. The next stage was a post-filtering process, which included four steps pose evaluation, clustering of ligands, ensemble docking and binding energy evaluation where the number of ligands was further narrowed down to give the most stable conformations. Finally, the compounds were selected for the cell based *in vitro* assays using a Lactate dehydrogenase assay and the nuclei count of damaged cells.

Chapter 4. Phenotypic screening *in vivo* using a high throughput zebrafish model

4.1 Introduction: Phenotypic screening

There are two main drug discovery strategies that are commonly employed. Target based screening is hypothesis driven for a specific biological target, while phenotypic screening allows the measurement of a phenotypic response in a disease model. Interestingly, phenotypic screening has proved to be a much more successful approach for identification of a first in class drugs for small molecules³⁸¹ as it provides a more realistic model of the disease and chance to optimise multiple targets through different molecular mechanisms of action.³⁸²

This occurs particularly, in cases of complex neurodegenerative diseases such as stroke where the disease mechanism has shown to trigger multiple downstream pathways leading to irreversible neuronal damage. However, there are still challenges in both screening approaches in the interpretation of the structure activity relationship of small molecules with biological targets³⁸³ As a primary screening assay, phenotypic screening shows great potential to identify hit molecules that can have a direct effect on the outcome of the disease before moving forward towards mechanistic based secondary assays or targeted screening which can demonstrate a clear selectivity and potency for the biological target. This can then be validated in the preclinical animal model for the disease.³⁸³

In the last decade, CNS drug development has been dampened by significant failures, despite the urgent need for neuroprotective drugs for neurodegenerative conditions.³⁸⁴ This is partly due to CNS targeted therapeutics having to overcome a greater challenge due to the physiological structure.³⁸⁵ Moreover, partial understanding of the molecular mechanisms in the development of CNS diseases and very limited utilisation of successful HTS experiments have also contributed to poor clinical results for CNS drug development.

The design and development of animal models of stroke has been vital to the understanding of the pathophysiology and hypothesis testing of potential treatments. While most stroke animal models consist of rodents, there is a renewed interest in

the use of zebrafish (*Danio rerio*) for modelling CNS disease in vertebrates and neuropathology.³⁸⁶

The zebrafish model provides a high degree of evolutionary similarities between itself and human homolog proteins, signalling cascades and brain structure.³⁸⁷ In this chapter the testing of the *in silico* compounds in a phenotypic assay using the mutant superoxide dismutase 1 (SOD1) zebrafish model will be discussed. The toxicity studies are also explained in this chapter, as well as the potential challenges with the interpretation of the results from this assay.

4.1.2 Advantages of using Zebrafish for HTS

Zebrafish are common aquarium fish belonging to the *Cyprinidae* family.³⁸⁸ They are natively found in South Asia and India. These vertebrates are widely utilised in drug research in many different preclinical models as they have many of the same organs found in humans (Figure 4.1). For example, zebrafish are extensively used in research for many diseases such as cancer³⁸⁹, toxicology³⁹⁰ and cardiovascular disease.³⁹¹

An important advantage of using zebrafish for research for their fast development. They reach full adulthood by 90 days post fertilisation (dpf). They can breed easily and produce large numbers of offspring weekly.³⁹² In addition, the offspring would not require external feeding beyond 8dpf, which is extremely useful for HTS applications. During the embryo to larvae stage the developing zebrafish is transparent which makes them ideal for study using imaging techniques. In addition, they are easily used as the larvae are between 3-4 mm and the adult fish are not greater than 3 cm. This makes them more economically feasible and less expensive than mice.³⁹³ Rodent models are highly inbred, which could influence the progression of the disease being investigated. This may lead to greater levels of toxic proteins and distortion of the pathology of the disease compared to humans. More recently, zebrafish have been widely used to investigate neurological disorders.³⁹⁴

The CNS development of these fish is like humans exhibiting the same subdivisions of the brain. In particular they have been shown utilise many NT that are used by humans such as gamma-aminobutyric acid (GABA)³⁹⁵, histamine, acetylcholine,

adrenaline and glutamine that are key targets for pharmacological and toxicological studies.³⁹⁶ These neurotransmitters are important players in neurological function in health and disease and therefore key targets for pharmacological and toxicological studies. Parng *et al*,³⁹⁷ confirmed that neuronal cell death, proliferation and oxidation can be observed very early in zebrafish larvae (3dpf). In addition, they also reported that for compounds such as 6-hydroxydopamine (6-OHDA), ethanol and acrylamide similar toxicity was observed as those seen in mammalian models.

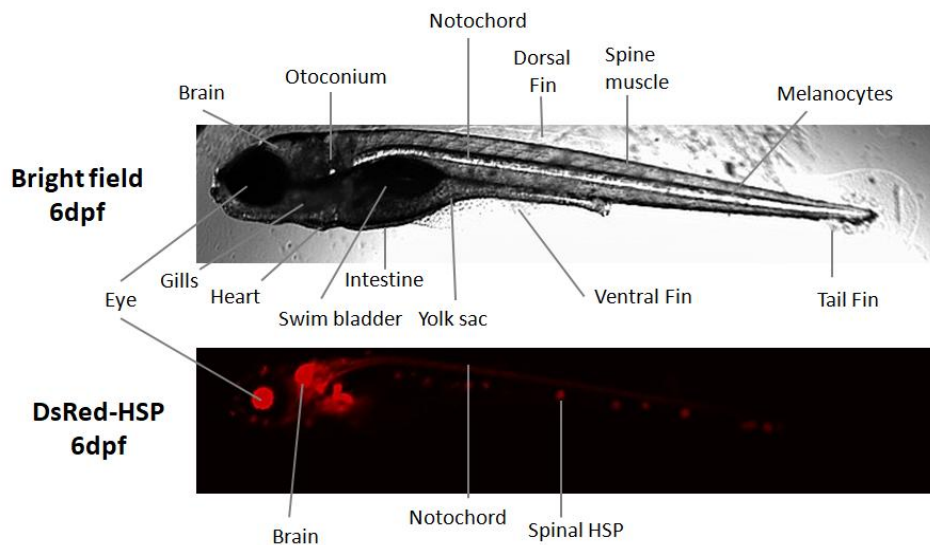


Figure 4. 1 A superoxide dismutase mutant zebrafish larva at 6-day post fertilisation (dpf) after treatment with 0.1% DMSO.

The organs are visible due to transparency of the larvae at this stage and the DsRed-HSP70 imaging is showing the accumulation of the fluorescence tagged heat shock protein (HSP70) within the head region.

The complete zebrafish genome was published in 2013³⁹⁸. Zebrafish genetics can be manipulated with great precision by using genetic tools such as CRISPR/Cas9 to generate models of human disorders.³⁹⁹ For example, Armstrong *et al*⁴⁰⁰ generated a knockin point mutation model for amyotrophic lateral sclerosis (ALS) using CRISPR/Cas9 in zebrafish. They demonstrated the insertion of two SNPs (tradbp A379T and fus R536H gene) in zebrafish can mimic hallmarks of ALS observed in patients with (tradbp A382T and fus R521H gene).

In comparison to other in vivo models such as fruit fly (*Drosophila melanogaster*) and worms (*Caenorhabditis elegans*), the zebrafish has greater genetic similarity to humans.^{401,402} Zebrafish provide the opportunity to study complex physiological and

pathological processes without a long experimental cycle being required as is the case in models involving rodents. For now, experiments performed on the embryos and larvae of the zebrafish (3dpf-5dpf) does not require regulatory approval they have not begun independent feeding. However, these regulations are still controversial and currently under review.⁴⁰³

4.1.3 The challenges of phenotypic screening using zebrafish

Although there are numerous benefits of using zebrafish in drug screening processes as outlined above, the model also has its own limitations in comparison to mammalian models as outlined below. This can limit the translatability of the screening potencies and data from toxicity experiments, leading to false positives and false negatives in the assay. The method of drug administrations in the zebrafish model is often through immersion, which can lead to lipophilic compounds being poorly absorbed.

Extremely non water soluble compounds have previously been injected into zebrafish to achieve sufficient exposure. This can then limit the translatability of the screening potencies and data from toxicity experiments, leading to false positives and negatives in the assay.⁴⁰⁴ Additionally, injecting the compound directly into the zebrafish has its own complications as the fish are small and technically difficult to inject. Direct injections is no longer conducted in HTS due to the time required and the technical difficulty involved.

Another major challenge is that the toxicity observed in water from larval studies is not equivalent to other non-clinical toxicological studies as the upper limit lethal dose measurements, and pharmacokinetic data is often quite different from mammalian models.⁴⁰⁵ Finally, the translation of animal models to clinical data for CNS drug discovery has proven to be very challenging, specifically if the homology of the species is low in comparison to humans. This is true for both the mammalian research (84% homology) and vertebrates research (~70% homology)⁴⁰⁶, due to phylogenetic distance and anatomical differences.

Overall, the benefits of the zebrafish model outweigh its limitations and data obtained from this model can inform the design of further studies (if warranted) in higher

animals such as rodents. Table 4.1, summarises the advantages and disadvantages of using the zebrafish model.

Figure 4. 2 A summary of the key advantages and disadvantages of using zebrafish in drug screening and toxicological studies

Advantages	Disadvantages
Vertebrates species major organs are compatible with humans with 70% genomic homology.	Not all tissues and organs match with mammals. <ul style="list-style-type: none"> - No lungs, prostate and mammary glands - Kidneys only display a single nephron - Heart only displays one atrium/ventricle - Ectothermic
Can reproduce easily (~200 eggs/spawn every week) and a great number of fish can be kept in a small space with low maintenance and expenses.	Not suitable for multiple endpoint assays or pharmacokinetics experiments. Due to small size the number of biological samples is limited.
Less ethical considerations when compared with other animal models such as rodents	
Compounds easily administered. Most often are just added to the water specifically at larvae stage. Absorbed through:- <ul style="list-style-type: none"> - Mouth - Gills - Skin 	The complete mammalian brain is not replicated in this model and some segments may not develop in the same manner.
Rapid development allows in depth analysis in shorter periods of time.	Interference with drug permeability as some compounds may not be very soluble in water, making it difficult to be administered by immersion.
The embryos and larvae are transparent and therefore allow imaging techniques to capture morphological changes after the treatments.	At the embryonic and larvae stage very sensitive to temperature that can greatly influence their development.

4.2 ZNstress assay: Zebrafish SOD1 G93R model

Superoxide dismutase 1 (SOD1) is a free radical neutralising enzyme that can be found in most cells of the body. The key function of the enzyme is to remove toxic radicals such as superoxide radicals by converting them into oxygen and hydrogen peroxide using metals such as copper and zinc ions bound in the enzyme's active site (Figure 4.3).

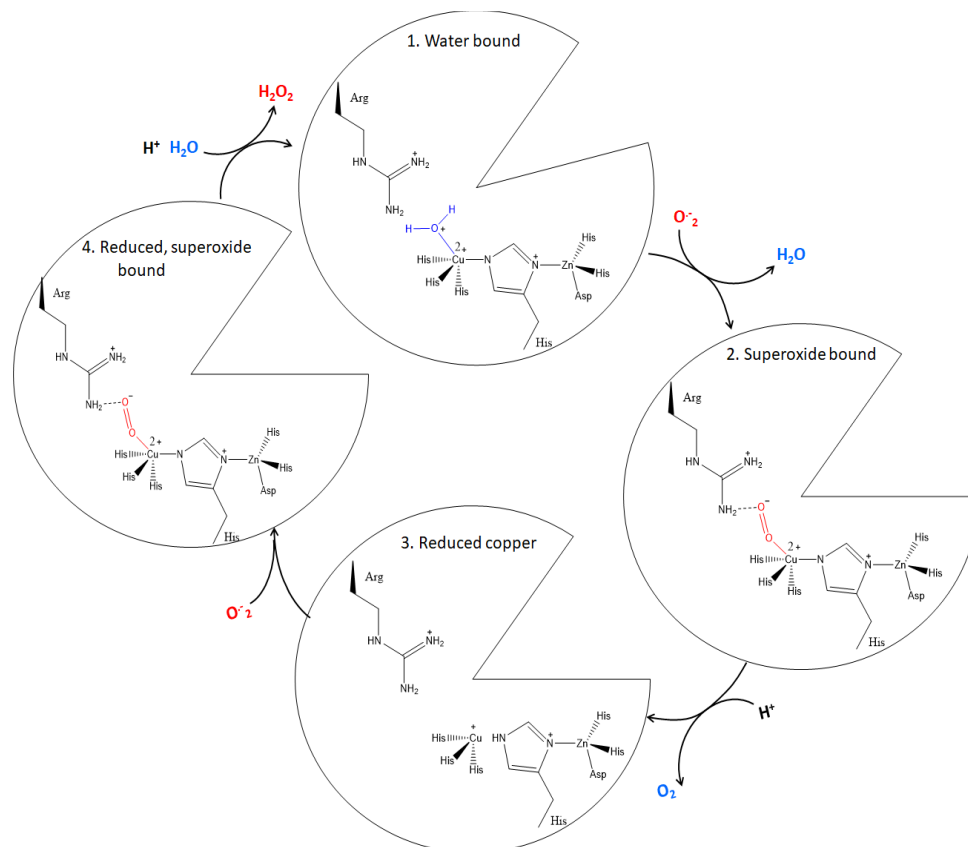


Figure 4. 3 The catalytic mechanism of intracellular Copper, Zinc SOD1 that is present in the cytoplasm of the cells.

The active site reactions are demonstrated. Adapted from ChemLibretex. ⁴⁰⁷

During metabolism, superoxides can be produced and if not removed can bind to the DNA of the cells and trigger apoptosis.⁴⁰⁸ As described in Chapter 1, during ischaemia, there is simultaneous activation of excitotoxic and oxidative stress pathways. This leads to generation of ROS and damaging radicals that cause lipid peroxidation of the cell membrane and significant damage to mitochondrial organelles, which ultimately triggers cell death. Antioxidant enzymes can have a protective effect. Over expression of SOD1 has been shown to be protective in animal models of ischemic stroke and intracerebral haemorrhage.^{409,410}

A mutation of the SOD1 gene (G93R) in zebrafish has been shown to cause amyotrophic lateral sclerosis (ALS), the devastating neurodegenerative disorder that causes death within two to three years of diagnosis. Genetically engineered mutant mice with this mutation have features like human ALS such as reduced muscle strength and loss of motor neurons.⁴¹¹ Mutation of SOD1 results decreased clearance of free radicals which in turn leads to cellular injury as well, therefore contributing to neuronal stress through oxidative stress pathways and causing neuronal stress. This stress causes an upregulation of chaperone proteins such as heat shock proteins (HSPs) to help and reduce the damage caused to the cells.⁴¹²

4.2.1 The role of heat shock proteins (HSPs)

Neurodegenerative diseases like ALS can elevate levels of heat shock proteins (HSPs).⁴¹³ HSPs are a part of the cellular survival mechanism that is initiated during neuronal stress following cellular insults. They influence multiple functions of the cell during stress but particularly have important roles in protein-protein interactions (PPI) such as folding and assisting in the establishment of proper protein conformation and prevention of unwanted and potentially harmful protein aggregation.⁴¹⁴

The HSP are characterised by their molecular weight and functions within cells. An example is HSP 70 kDa heat shock protein (HSP70), located in the nucleus and cytosol.⁴¹⁴ There are a key group of HSPs that are unregulated in neurodegenerative diseases such as stroke (discussed in section 3.3). They function by interaction with miss-folded proteins through their substrate binding domain (SBD) and their NTD, the mechanism of action of HSP70 is shown in Figure 4.4a. The SBD is made up of large region of hydrophobic residues that can target miss-folded peptides and initiate refolding of the peptides back to a quaternary structure without any changes to the protein sequence. The NTD is responsible for interacting with co-chaperone molecule ATP, that accelerates the process causing open state of the HSP and an ADP is bound during closed state.⁴¹⁵ HSP70 is also known to aid with degradation of misfolding peptides (Figure 4.4b) through the ubiquitin-proteasome pathway.⁴¹⁶

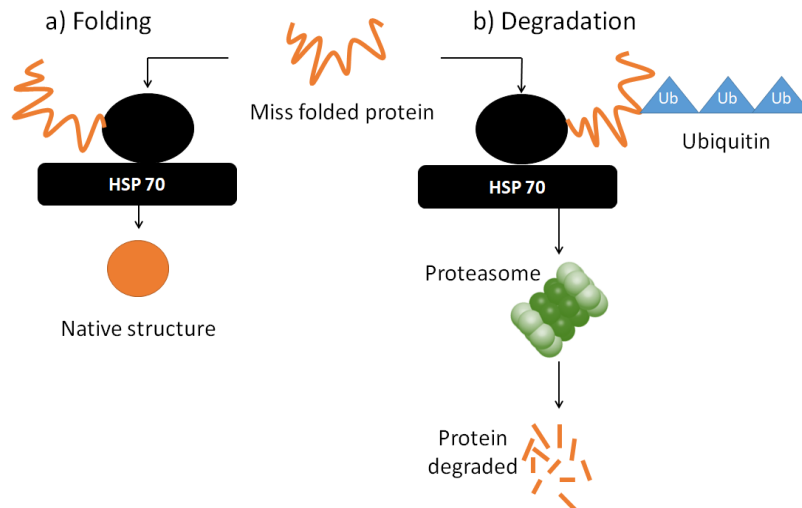


Figure 4. 4 Simple diagram showing the role of HSP70 in protein folding and protein degradation.

4.4a) The misfolded protein generated through autophagy-lysosome processes are then removed by chaperon protein HSP70 by refolding the sequence to native structure. **4.4b)** If the protein cannot be refolded into its native structure it is then tagged with ubiquitin (ub, blue triangle) and moved to degradation by 26S proteasome.^{417,418} Used with permission under the terms of the creative commons attribution licence (CC-BY).

In the ZNstress model, HSP70 is a marker of cellular damage due to the SOD1 mutation, which can be quantified. Ramesh *et al*⁴¹⁹ have demonstrated that using HSP70-DsRed reporter gene they can measure the amount of neuronal stress created through the mutant SOD1 in zebrafish *in vivo*. They also demonstrated that the FDA approved neuroprotective drug riluzole for the management of ALS was able to inhibit neuronal damage and reduce the activation of HSP70. This opened the possibility of using the zebrafish model for a HTS to screen/characterise potential compounds that can modulate HSP70 levels in the in zebrafish. By using automated liquid handling machines and high content live imaging of the larvae, they were also able to investigate both efficacy and safety profiles of large libraries of compounds. The details of the assay are summarised in Figure 4.5.

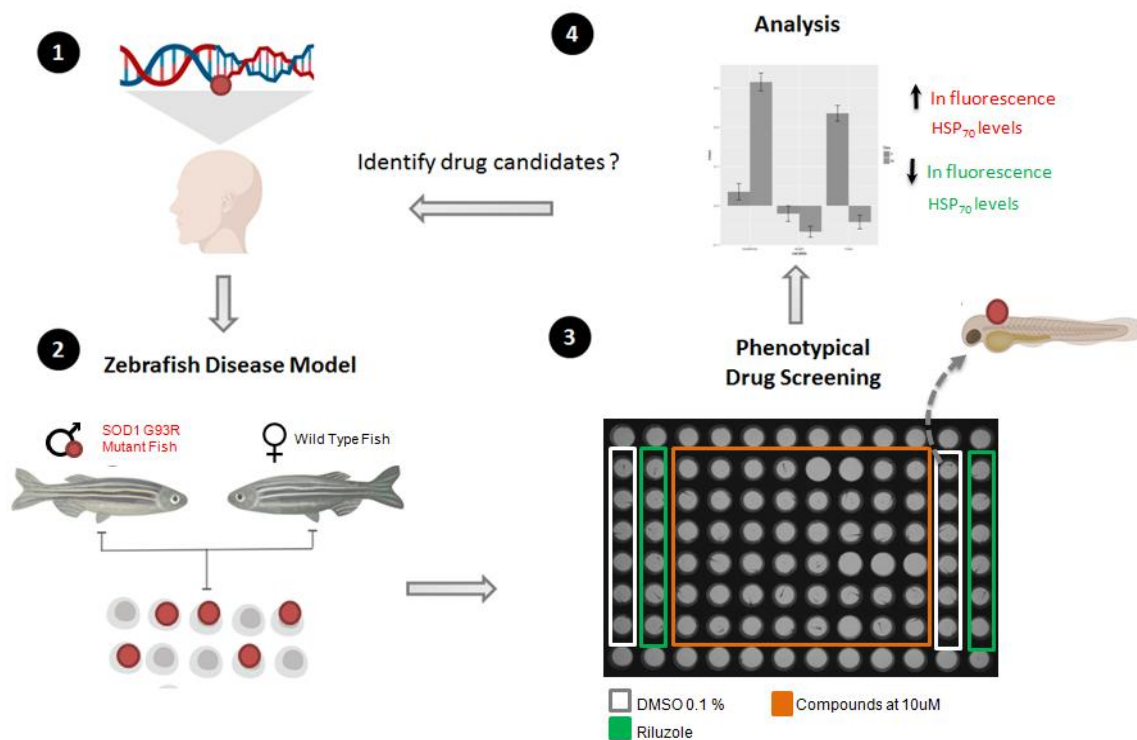


Figure 4. 5 Phenotypic screening using the mutated zebrafish (SOD1 G93R).

1) The SOD1 G93R mutation causes protein misfolding in the CNS that leads to initiation of oxidative stress pathways and neurodegeneration. 2) Zebrafish can be genetically modified to express this specific mutation meaning they are able to exhibit the same phenotypes observed in patients. This allows HTS by identifying and collecting the offspring of the fish that are able to exhibit this mutation. 3) The zebrafish larvae can then be transported into 96 well screening plates and treated with compound libraries to see if neuronal stress can be reduced through the marker protein HSP70-DsRed. 4) The fluorescence emitted from the zebrafish larvae can be quantified and allows identification of compounds that can modulate the release of HSP70 protein from the model.

4.3 HSP70 in ischaemic stroke

As described in Chapter 1, brain ischaemia initiates the activation of numerous genes and proteins that lead to ischemic neuronal damage. Some of these are protective while others are harmful to the cell and lead to ischemic neuronal damage. The HSP70 has been shown to be upregulated in regions of neuronal damage, specifically in the hippocampus and the cortex.⁴²⁰⁻⁴²²

HSP70 acts as a chaperone in the cytosolic and subcellular compartments of cells, modulating protein folding, degradation, assembly and translocation of proteins

within each cell. These functions are essential in the production of new polypeptides. HSP70 levels are initially increased in the penumbra in endothelial, astrocytic and microglial cells after an ischaemic insult, thus can act as a marker of the initial neuronal stress.⁴²³ Yenari *et al*⁴²⁴ demonstrated a direct link of HSP70 overexpression to reduced apoptosis and inflammation in cerebral mouse ischemic stroke models. By overexpressing the HSP70 using a transgenic mouse model, they were able to show protection of both neurons and astrocytes compared to the wild type control mice in experimental stroke. They also observed up regulation of neuroprotective Bcl-2 gene, and a reduction of matrix metalloproteinases. Therefore compounds that could up regulate the HSP response may have a neuroprotective role.

HSP70 has also been shown to be beneficial in preclinical intracerebral haemorrhage models, improving functional recovery through similar pathways. Diazoxide, a benzothiadiazine (non-diuretic drug) that is used for management of hypoglycemia in patients with high levels of insulin, can increase HSP70 and HSP25 in preclinical models of stroke, including haemorrhagic stroke, leading to significant neuroprotection.⁴²⁵

On the other hand, this year, arimoclomol, a small molecule that was shown to increase HSP70 activation and reducing abnormal protein levels failed to exhibit efficacy in phase III ALS clinical trials.⁴²⁶ In development, it showed promising efficacy with favourable safety and pharmacokinetics, and the ability to be distributed well in the CNS.⁴²⁶ Whether it would be effective in AIS remains to be determined.

4.3.1 Screening out *in silico* hits using ZNstress assay

Among the *in silico* hits, there were 13 compounds from the Professor Chen and AFChemPharm libraries that had not been tested in any biological assay. It was important to obtain toxicity information and suitability of these compounds. Although mammals (e.g mouse, rats and rabbits) are regularly used for the assessment of drug safety, they have reduced throughput and are often very expensive.⁴²⁷ In addition, the experiments also require long periods of time due to the physiology of the mice.

By collaborating with Dr Ramesh (University of Sheffield) we were able to take advantage of the ZNstress HTS screening model to examine if any of the *in silico* compounds were neuroprotective in this model.

4.4 Aims and objectives

1. Determine if the *in silico* hit compounds exhibit neuroprotective effects against the mutant SOD1 zebrafish model
2. Determine the effects of *in silico* hit compounds on the zebrafish larvae by examining the cytotoxic side effects of the compounds.

4.5 Results

4.5.1 DsRed SOD1 screen and percentage inhibition of the compounds

The assay has been optimised to demonstrate that the DsRed fluorescence, mainly located within the CNS could be quantified using PHERAstar FSX. DMSO was used for the negative control and the results were normalised to the DMSO (0% inhibition). DMSO was the primary solvent used to dissolve all the compounds within the assay.

The positive control was the drug riluzole that has previously been shown to significantly reduce cellular stress by 65%. The combined results are shown in Figure 4.6a. None of the compounds at 10 μ M were able to reduce neuronal stress in the mutant zebrafish SOD1 model. The compounds 10-1131 (-19% inhibition), methocarbamol (-13% inhibition) and floxuridine (-9% inhibition) showed weak HSP activation although this did not reach statistical significance. Although the main objective of the assay was to select compounds that were able to inhibit or reduce HSP response. There was a total of five compounds that were toxic and caused death of the zebrafish larvae (Figure 4.6b). The most toxic compound was identified to be Sc-172 (diphenyl-1,3-benzodioxole), which killed all the treated fish in the assay (N=3, 6 fish in total). The second most toxic compound was compound 1-094, where in two of the experiments it was shown to be lethal to the fish (N=2, 4 fish in total).

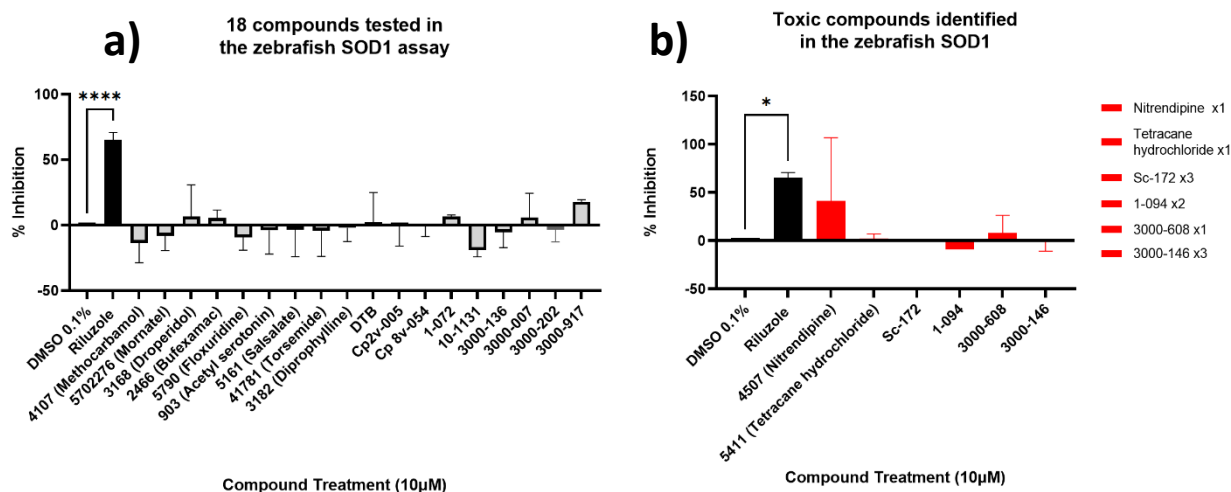


Figure 4. 6 The efficacy of *in silico* hit molecules in the Zebrafish SOD1 Assay.

4.6a) All 18 compounds showed no efficacy in the assay. The compounds at 10 µM were not able to reduce SOD1 stress. Biological repeats N=3, One-way ANOVA, DMSO 0.1% vs riluzole ****p= <0.0001. **4.6b)** Demonstrates the results of six potentially toxic compounds identified to kill the larvae in the assay at 10 µM. The number of biological experiments (N) where the larvae was noted to be dead is presented in the key legend on the graph in 3.5b). The most toxic compound identified was Sc-172 that killed the larvae in all experiments, followed by the 1-094 that was also shown to be toxic. One-way ANOVA, DMSO 0.1% vs riluzole *p= 0.0497. Data shown as Mean ±SD, N=3, For technical repeats the control DMSO 0.1% and riluzole 12 fish/experiment and for the compounds 2 fish/experiment was used.

The high toxicity observed at 10 µM for the compound Sc-172, prompted further investigation into the efficacy/safety of the compound at a lower dose of 1 µM, to examine if the compound was better tolerated. In addition, it could also allow further measurement of the efficacy for this compound as even very potent compounds that can demonstrate toxic effects at higher doses. Unfortunately, as demonstrated in Figure 4.7, even at a lower dose of 1 µM Sc-172 was not able to exhibit efficacy, but was better tolerated by the zebrafish.

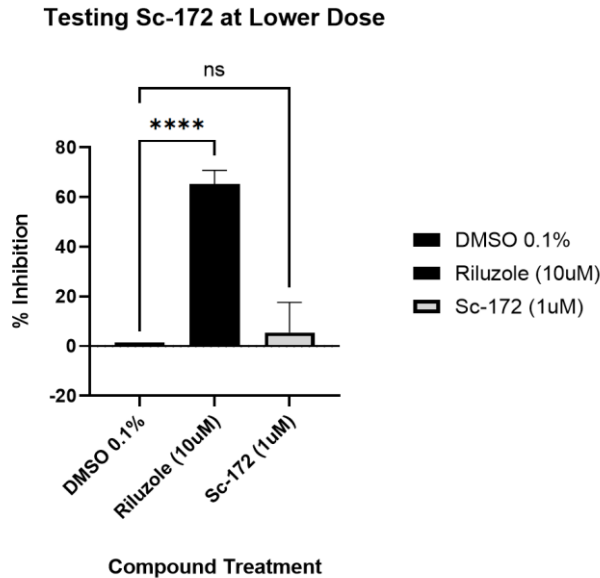


Figure 4. 7 No effect observed with Sc-172 at lower dose 1 μ M

Sc-172 was toxic at 10 μ M. Reducing the concentration to 1 μ M proved to be much better tolerated, however no efficacy was observed for the compound. . One-way ANOVA, DMSO 0.1% vs riluzole **** $p= <0.0001$. Data shown as Mean \pm SD, N=3, For the controls DMSO 0.1% and riluzole 12 fish/experiment and for the Sc-172 N=2, 2 fish/experiment were used.

Riluzole, the positive control was the only compound that reduced SOD1 stress levels, 61% inhibition. How riluzole slows disease progression in this model is still unclear. Previous studies have shown that riluzole inhibits glutamatergic neurotransmission in brain slices and cortical neurons of rodents but other mechanisms may also be involved.⁴²⁷⁻⁴³⁰

Riluzoles known multiple mechanisms of action prompted the question: do other known NMDAR inhibitors and modulators exert any effects in this assay and can they be assessed using the DsRed emission?. To address this, two known NMDA antagonist (MK801 and memantine) and NMDA itself (agonist) were assessed. The results showed that they were also unable to exert any effect in the assay (Figure 4.8).

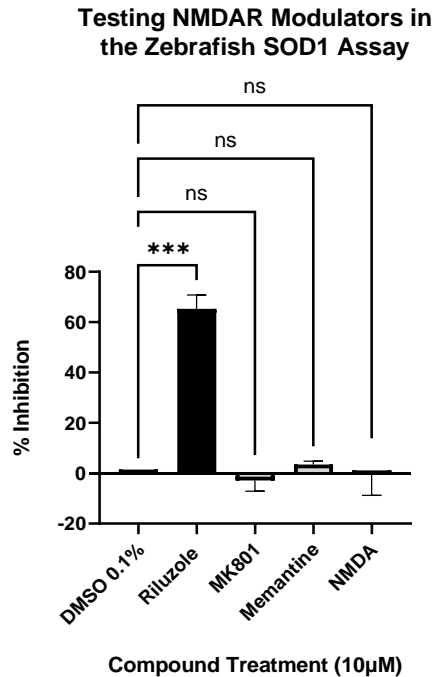


Figure 4. 8 The known NMDAR modulators also failed to show any effect in the SOD1 zebrafish model

NMDAR antagonists MK801 and memantine at 10 µM did not exhibit efficacy. Interestingly, NMDA itself did not demonstrate any changes in the levels of the SOD1 stress response at 10 µM. One-way ANOVA, DMSO 0.1% vs riluzole ***p= 0.0001. Data shown as mean ±SD, N=3, For the controls DMSO 0.1% and riluzole 12 wells/experiment and for the MK801, memantine and NMDA N=2, 2 wells/experiment were used. NS (non significant)

4.5.2 Measurement of toxicity in the ZNstress assay

The images of the zebrafish larvae allowed analysis of the biological effect of the compounds and determine to what extent they were lethal to the fish. One of the challenges in this assay was the analysis of the individual images of the larvae for toxicity effects of the compounds. As the larvae were able to swim from 3dpf, it made it difficult to obtain the correct orientations of the fish when comparing the control groups with the treated fish. Moreover, it also reduced the throughput of this assay as each individual image of each well had to be analysed manually. In this experiment, as the library size was manageable it was possible to perform this task for each individual compound.

The assay demonstrated that 18 of the compounds tested were well tolerated in the zebrafish model. Specifically, the nine compounds that were not FDA approved or had any prior biological assays performed on them. Although, none of the

compounds were able to significantly modulate the regulation of the HSP70, they were shown to be well tolerated at 10 μ M and not interfere with the larvae development. For these 18 compounds, there was no damage to major organs such as the liver and heart. The spinal cord, tail and fin development was also not affected.

The images obtained from the 0.1% DMSO and riluzole control treated fish demonstrate clear reduction in DsRed fluorescence (Figure 4.9a). These controls were compared with two examples of fish that were treated with 4107 (methocarbamol) and compound 3000-202 which also displayed signs of being safe to use in the zebrafish model. It was important to note that although the images of the fish from the third screen suggested a reduction in DsRed fluorescence emission, the combined result for both of these compounds failed to show any significant effect in the assay.

The severe toxicity observed for Sc-172 was also observed in the images as shown in Figure 4.9b. It caused death of the larvae by teratogenic defects such as yolk-sac oedema, pericardial oedema and spinal bent of the larvae. At a lower dose of 1 μ M the toxicity observed for Sc-172 was not reproduced and the larvae seem to develop without any abnormalities. No efficacy was observed at both concentrations. In the case where the larvae were treated with compounds 4507 (nitrendipine), 5411 (tetracane hydrochloride), 1-094 and 300-608 it caused the larvae to die 5dpf. No other morphological abnormalities were observed for those fish.

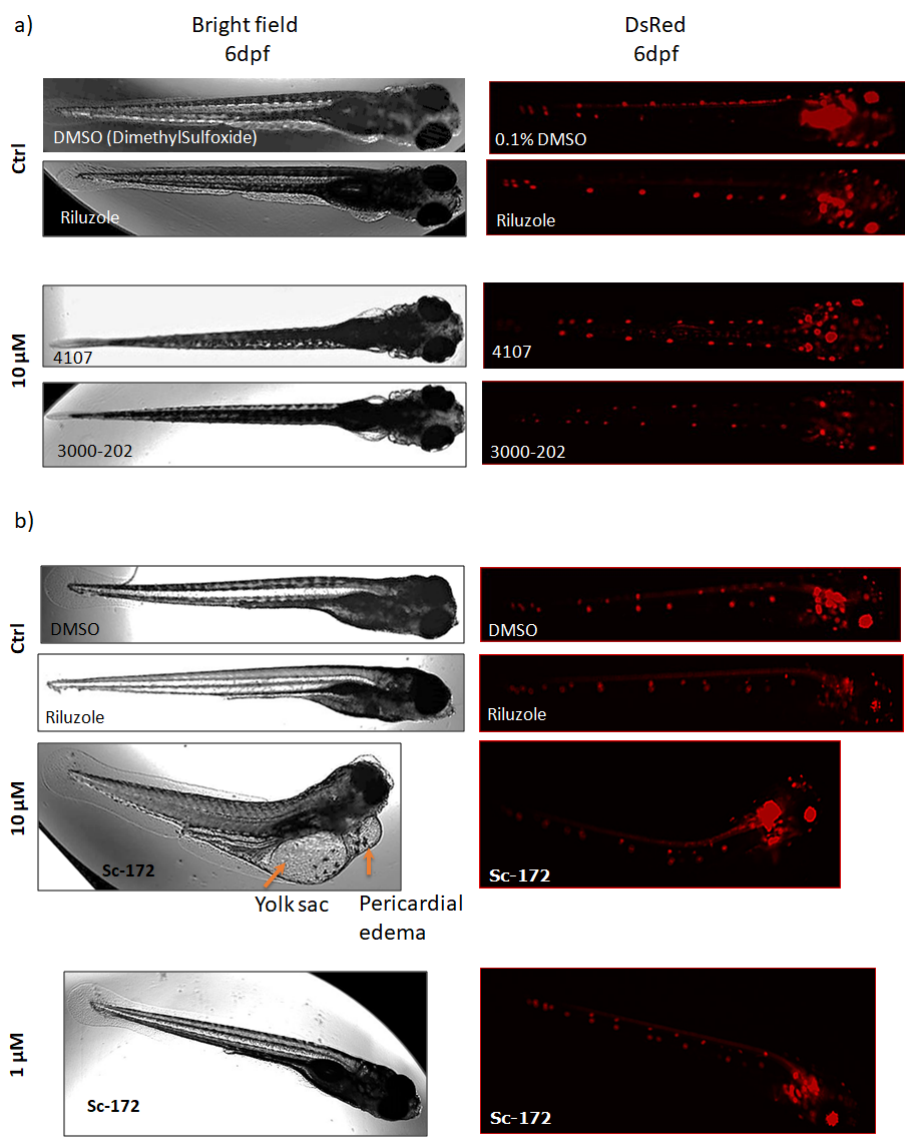


Figure 4. 9 The zebrafish larvae in the ZNstress assay.

4.9a) The top view images, illustrates the reduction of HSP70-DsRed emission in the riluzole treated fish, mainly within the CNS region. The images of two of the fish that were treated with 4107 (methocarbamol) and 3000-202 also displayed. **4.9b)** The side view of the fish of larvae treated with control conditions are displayed. The toxic effect of Sc-172 at 10 µM can be observed clearly in the images obtained from the 3rd screen, showing to have caused severe yolksac and pericardial oedema. Then images of the larvae treated with Sc-172 at 1 µM demonstrate no abnormality development. However, no reduction of DsRed was observed.

Similarly, as demonstrated in Figure 4.10, the fish that were treated with 3000-146 showed development of abnormalities, specifically in the first and third screen. Interestingly, in the second assay the fish that were treated with 3000-146 showed less signs of oedema.

In the first and third screen oedema was observed in the swim bladder and the yolk sac. The head region also appeared more swollen in comparison to the control group fish.

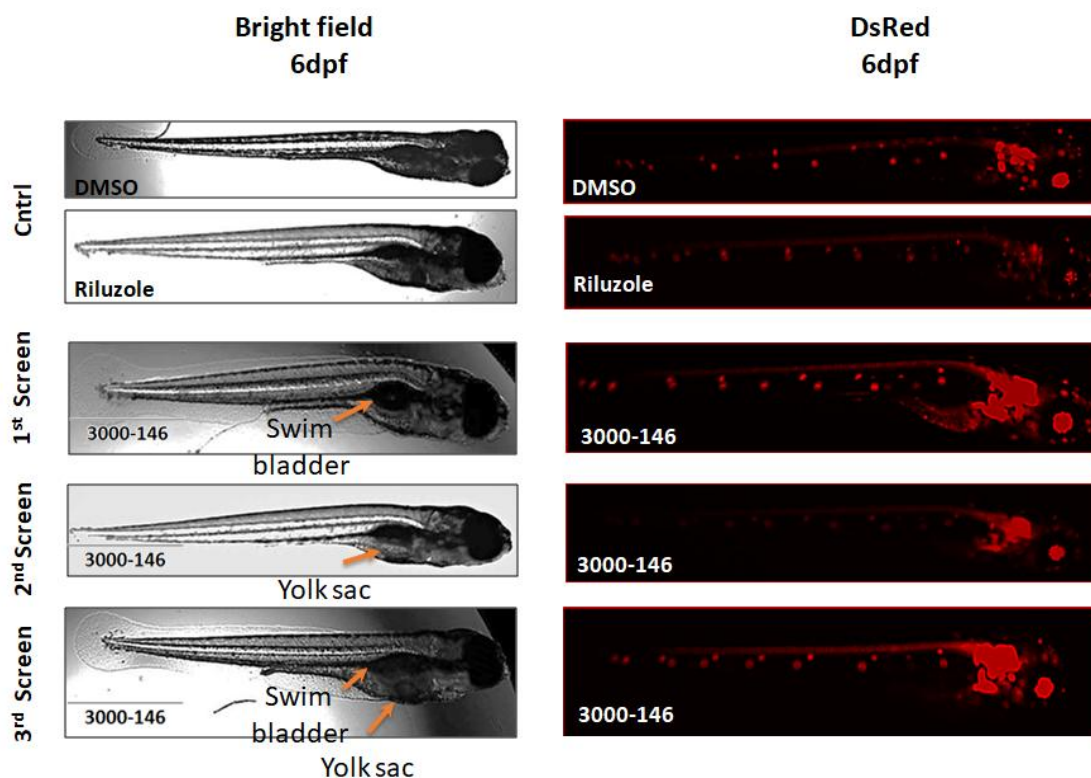


Figure 4. 10 3000-146 causing oedema in the swim bladder and yolk sac.

Images on the left hand side demonstrate the mutated fish in the bright field with a swollen head in the first and third screen images. Images on the right hand side demonstrate the fish in emission of DsRed in the CNS and no reduction of HSP 70 was observed.

4.6 Discussion

The first objective of this project was to examine if any of the compounds selected from the virtual screening against P8 were able to demonstrate neuroprotection in the glutamatergic stress response assay, as observed with excitotoxicity. The initial HTS was implemented for identifying compounds that could reduce the neuronal stress caused by the SOD1 mutation in an *in vivo* model using zebrafish phenotypic screening.

4.6.1 *In silico* compounds and NMDAR antagonists failed to show efficacy in the ZNstress assay.

All the compounds at 10 μM failed to show any significant neuroprotection in the mutated SOD1 zebrafish (Figure 4.6). In this study, known channel NMDA blockers MK801 and memantine at 10 μM did not show any effects in the assay. NMDA, NMDAR agonist despite our initial hypothesis, also did not show any up regulation of the HSP70 protein.

As mentioned above this assay had been optimised to use the HSP70 DsRed gene as marker to measure neuronal stress caused by the SOD1 mutation. As a result, the mutated larvae also showed more activation of the HSP70. This readout is a useful marker of neuronal stress as a result of toxic mutation in the model and therefore activating the protection mechanism using the HSP proteins. However, none of the initial *in silico* hits were able to reduce the HPS70 over expression in the genetically mutated zebrafish model. It is important to note that the genetic transfer of the SOD1 mutation could also limit the translation of this model to ischaemic stroke model, as HSP70 might be overwhelmingly overexpressed in comparison to what happens during an ischaemic event. For the purposes of this study, i.e. to evaluate whether our compounds can modulate NMDAR, the data is of limited value as potent non-competitive inhibitors also did not exhibit neuroprotection, including the FDA approved drug memantine. The use of HSP70 DsRed as a surrogate marker of excitotoxicity is probably an important drawback of this assay as HSP70 DsRed expression in this model may be influenced by many different pathways other than excitotoxicity.

Roh *et al*⁴³¹ had previously reported that 10 μM of MK801 can cause an increase of HSP70 in rat glioma cells, which they quantified by incubation with the anti-HSP70 monoclonal antibody. The explanation for this observation was that this potent channel blocker of the NMDAR could initiate neurotoxicity by also increasing vacuoles in the neuronal cells, observed in the posterior cingulate and retrosplenial cortex of rats.^{432,434} This vacuole formation could cause toxicity and cause denatured proteins which ultimately results in neuronal damage. Therefore HSP70 is expressed higher in the neurons that had vacuoles.

Conversely, Chen *et al*⁴³⁵ had investigated the regulation and expression of the HSP70 gene in neonatal rat models with cerebral hypoxia ischaemia using memantine. They showed that after the treatment with memantine there was a significant decrease in the translation of the HSP gene in the 24-72 hours from the induction of the ischaemia event, as well as a reduction in production of its protein in 48-72 hours. However, as discussed above, in our zebrafish model, memantine also failed to show significant reduction of HSP70 production. This may have been due to the different species used and it is possible that the effect of the drug differs between vertebrates and mammals. Another possible explanation could be that the dose for the memantine might have been too low for the reversible antagonist to demonstrate its neuroprotective effects in the zebrafish model. In addition, a different route of administration in the models may also have influenced the results.

Significant neuroprotection was only observed with the positive control drug, riluzole. However, as mentioned above the mechanism of action of riluzole is not fully understood. The existing literature on the mechanism of action of riluzole fails to resolve the issue of whether it acts directly at the NMDAR receptor and exhibit neuroprotection solely through its interactions with the NMDAR or whether it modulates other targets. Sankaranarayanan *et al*⁴³⁶ have previously shown that riluzole even at 100 μM had failed to demonstrate any inhibition of NMDAR within the radioligand binding assay using rat brain. There are also further studies using cultured hippocampal neurons that showed no inhibition by riluzole at 20 μM for both the non-NMDAR and NMDARs.⁴³⁷ These data suggest riluzole may have effects on excitatory neurons through mechanisms other than interaction with NMDAR as shown in Figure 4.11.

In complex CNS diseases such as stroke where multiple processes are initiated simultaneously, this multiple functionality could be ideal as it can allow targeting of two or more key downstream pathways that contribute to neuronal death. Although there are preclinical models that support riluzoles neuroprotection in global ischaemia and focal MCA ischaemia in rats,^{438,439} there no studis, to date that these data being translated clinic.

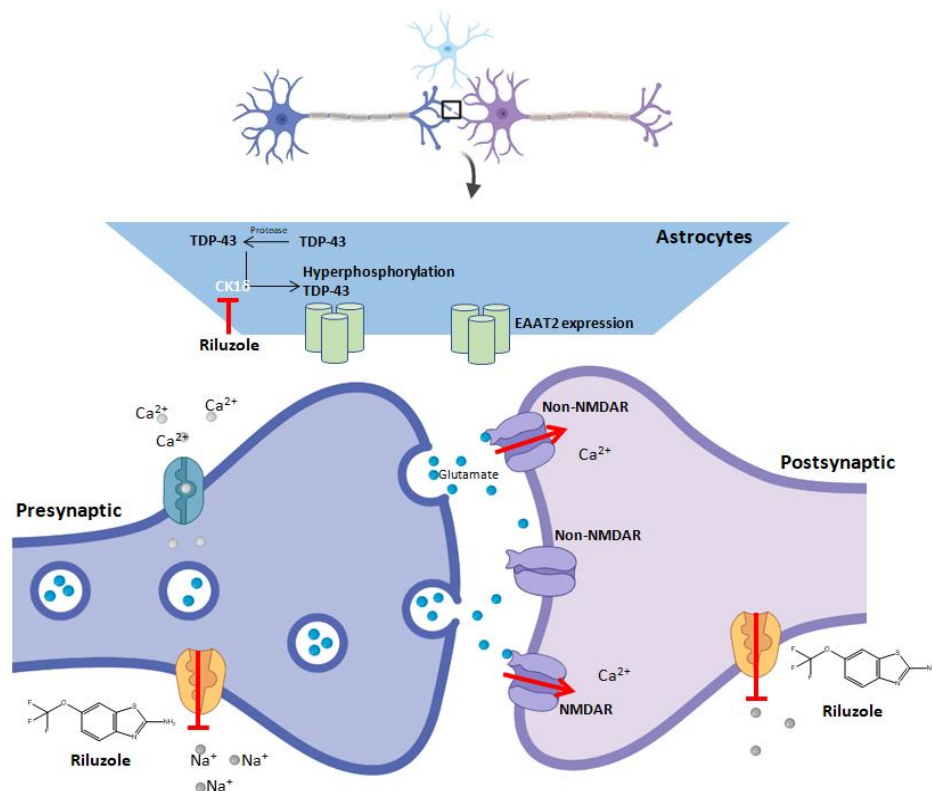


Figure 4. 11 The potential molecular mechanisms of riluzole.

The indirect effect of riluzole on to the excitatory receptors on postsynaptic neurons by inhibition of voltage dependent sodium channels (orange) on both presynaptic and post synaptic neurons is shown. Also demonstrating the new potential route of inhibitions of phosphorylation of the TDP-43 and its product after the reaction with proteasome enzymes. Riluzole can inhibit the hyperphosphorylation step by inhibiting the CK1δ, allowing the translation of the mRNA transcriptions and up regulation and expression of the EAAT2 transporters (green) on the astrocytes. This leads to removal of the secreted glutamate that activates the NMDAR and non-NMDAR (purple) on the postsynaptic receptors. This in turn can reduce the excitotoxic effect observed during neuronal stress. Figure produced using Biorender.

As the known NMDAR modulators (memantine and MK801) also failed to show any effect in this assay, further studies of our *in silico* hits were undertaken *in vitro* assays of primary cortical neurons from mice to evaluate the effect of the compounds on NMDA toxicity directly Chapter 4.

4.6.2 How similar is the zebrafish GluNR1 to human GluNR1?

As mentioned previously in Chapter 3 (section 2.11.1), there is 78% similarity between human GluNR1 and zebrafish GluNR1. In addition, there was a single

amino acid mutation at P8, where the valine residue was displaced with isoleucine in the zebrafish. It could be argued that this reduced similarity could also influence the binding of the selected compounds to the target protein. These mutations within the LBD could cause changes in the overall conformation and assembly of the NMDAR and alter the affinity of potential small molecule binders. Moreover, from the 938 amino acids within the human GluNR1a, 738 amino acids were preserved (78.76 % identity). This number is lower in comparison to the 928 number of amino acids that are identical in the mouse GluNR1a (99.04 % identity), further details are provided in Appendix A.

It is also important to mention that the brain develops with age, allowing more complex tasks and higher brain functions such as memory and learning that NMDARs are directly involved in, these cannot be fully analysed with zebrafish at larvae stage. Miyawaki *et al*⁴⁴⁰ reports that for these functions fish at 90dpf would be required, but at this stage the fish are adults which makes it more difficult to perform HTS. However, for the purposes of this study to initially examine the general functionality of the compounds which have never been tested in biological assays it was extremely useful.

4.6.3 BBB permeability of the compounds in the ZNstress assay

One of the biggest challenges for CNS drug development is obtaining arachnoid barrier, choroid plexus and BBB permeability. In humans, these barriers physically produce a tight junction with capillary endothelial cells and nutrient transporters such as glucose transporters. The barriers also express drug transporters as part of the defence mechanism to prevent the passive diffusion of xenobiotic substances and macromolecules entering the CNS. For example, the adenosine triphosphate binding cassette (ABC) family, multidrug resistance protein 1 (MDR1) and P-glycoproteins all contribute to multidrug resistance in CNS.⁴⁴¹

When comparing the different cellular components in zebrafish and mammalian BBB (human and mouse) Figure 4.12⁴⁴², there are great similarities. In all species the endothelial cells, the glia, pericytes, microglia and neurons contribute to the formation of a complex neurovascular unit. In addition, the functionality of the BBB in both species is similar.

Mammalian brains have an additional level of protection introduced through astrocytes. These are a subtype of glia cells that can also be seen in zebrafish brains. Although, it is not clear how much the glia cells in zebrafish can function in the same manner as astrocytes in the BBB, they are involved in creating an osmotic gradient within the CNS. The glial glutamate transporter EAAT2b also tends to be present within both glia membranes and plays a major role in glutamate clearance.⁴⁴³

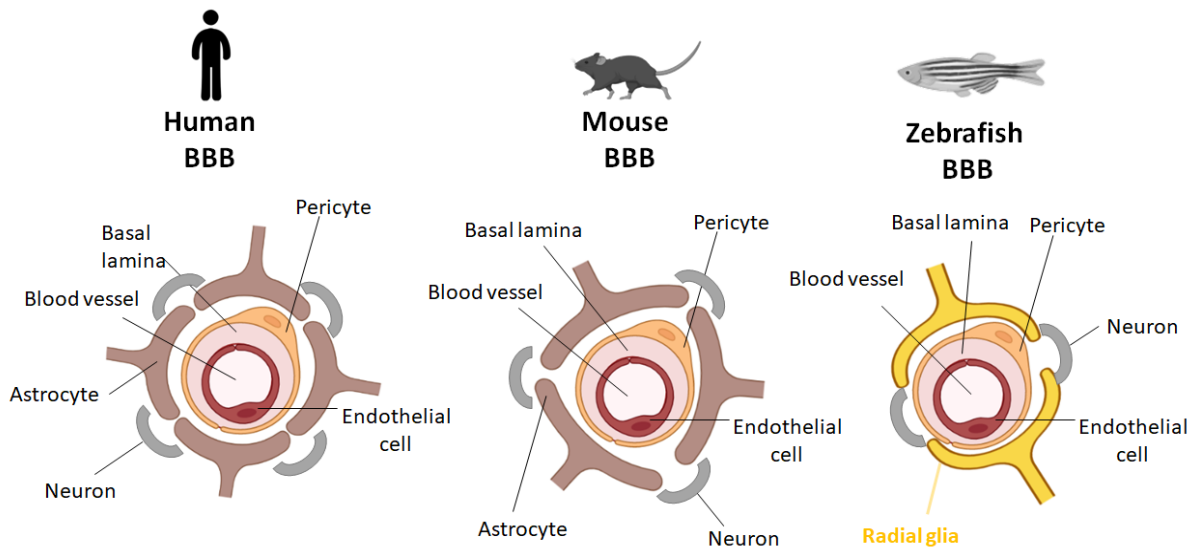


Figure 4. 12 The BBB complex formation in three different species, human, mouse and zebrafish.

The mammalian BBB has similar architecture, structure and function, sharing all the same cells in construction of the neurovascular unit. In zebrafish, the BBB shares the capillary endothelial cells (red) that connect the blood vessels to the pericytes (orange). The zebrafish do not have the typical astrocytes observed in mammals but they do have radial glia in their BBB's. However their complete functions within the zebrafish CNS still needs to be elucidated. The human BBB has also been demonstrated to have more connections to the astrocytes and pericytes in comparison to the mouse and zebrafish model. Figure generated using Biorender and adapted from.⁴⁴³

The BBB in zebrafish is developed by 3dpf and the MDR1 proteins have been shown to be present using immunohistochemical staining at 2dpf. However, according to Fleming *et al*⁴⁴⁴ during the early development stage of the zebrafish larvae, it does not express the ABCD1 gene, but they do express the ABCD4 and ABCD5. They further identified the ABCD1 only at 8dpf using immunohistochemical staining. This

could suggest that none of the compounds are substrates of the ABC proteins and, alternative transporter assay systems might be required.

Xie *et al*⁴⁴⁵ examined the BBB permeability with fluorescent indole compounds using a fluorescence imaging at 3 dpf using immersion and an intracardiac injection route of administration. They concluded that the fluorescent compounds were BBB permeable in both routes of administration. In this study, all of the compounds were administered to the larvae by immersion and it is important to mention that this route of administration is very different to mammals. First, this method favours polar compounds as they are soluble in water, therefore hydrophobic compounds with poor solubility predictions could suffer from insufficient exposure. The lack of exposure can also reduce the correct amount of the drug reaching the target protein and therefore lead to a lack of activity observed. It is worthwhile to mention that for other studies the solution to this issue has been to inject the compound into the fish, however this is technically very challenging and also no longer used in a high throughput manner.⁴⁴⁶ This method of exposing the compound through bathing the larvae in the treatment could also affect the half-life and the secretion of the compounds from the zebrafish, which again could be very varied from animal models.

4.6.4 How relevant is the toxicity reading of the zebrafish to humans?

For the toxicity test in this study, the zebrafish larvae were treated with the compounds during the organogenesis segment of the fish (5dpf). The fish were then observed for any changes in morphological features. Specifically if there were any abnormalities that developed in the shape of the spine, tail, fins, heart, face and organs that were visible microscopically. If the toxicity caused death of the larvae it was noted. Other changes in the features above or development of oedema in any of the major organs was also noted.

Eighteen compounds from the twentyfour tested were shown to be safe in the model, without the compounds affecting the morphological features of the developing fish. However, it is also important to mention that zebrafish have been shown to have a regenerative ability. They can regenerate numerous organs such as the fin, some segments of the brain, retina, heart and the spinal cord.⁴⁴⁷ Usually, there is an initial stage of proliferation and cell migration after the toxicity damage to the cells which

initiates the self-repair process of the damaged tissue. This regeneration process can influence the toxicity data and also the translation of the toxicity of this model to mammalian models.⁴⁴⁸

In this investigation synthetic compounds Sc-172, 1-094, 3000-608 and 3000-146 were identified to be toxic to the zebrafish larvae. The most severe toxicity was observed with the compound Sc-172 at 10 μ M which caused oedema resulting in expansion of the yolk sac and pericardial oedema. Yolk sac oedema might not be as important in elderly humans, but very important in pregnancy.⁴⁴⁹

There is high similarity between the embryonic nutritional mechanism through the yolk sac between humans and zebrafish, even more in comparison to rodents (Figure 4.13). The function of the yolk sac is to allow nutrient and gas exchange between the mother and the embryo.⁴⁵⁰ Most rodent embryos obtain their nutrition from endometrial glands and maternal endometrium by the thin yolk sac of the conceptus.⁴⁵¹ In contrast, human and zebrafish embryos both rely on yolk sacs that have an embedded supply of proteins and lipids to allow better metabolic function and growth until the external feeding period begins. In humans, this is at the end of gestation, where placental fetal development for humans ends and the external feeding begins. In humans, it also serves other important functions such as initial haematopoiesis before liver and bone marrow development. This also includes the umbilical cord development and synthesis of proteins such as albumin and apolipoproteins.

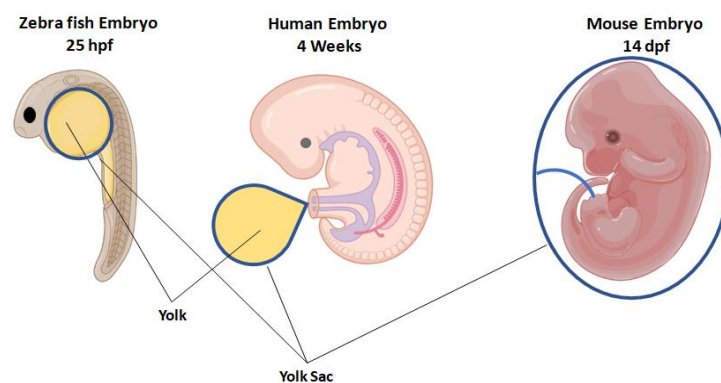


Figure 4. 13 The contrast between anatomical features of embryo development between the three species.

Shown are the embryos of a zebrafish 25hpf, a human embryo at 4 weeks and a mouse embryo at 14 dpf. Adapted from Sant *et al*⁴⁵²

The yolk sac has been shown to be highly lipophilic and therefore it reduces the permeability of water soluble compounds. The lipophilicity and total polar surface area (TPSA²) from the computational studies for Sc-172 were 3.62 logP and 82.06 Å². This could suggest that these lipophilic compounds might accumulate in the yolk sac and cause the toxicity observed. It is also important to mention that compounds such as polycyclic aromatics,⁴⁵³ chlorinated biphenyls,⁴⁵⁴ including some organophosphates⁴⁵⁵ have shown oedema in the yolk sac and causing pericardial oedema in zebrafish models.

Similarly, the FDA approved drugs nitrendipine and tetracaine hydrochloride at 10µM were also shown to be lethal to the fish causing death. Nitrendipine has an oral lethal dose at 50% (LD₅₀) in mice of 2540 mg/kg (1.76 M)⁴⁵⁶ and tetracaine hydrochloride has an LD₅₀ of 2759 mg/kg in mice (2.29 M). A possible explanation for this could be the administration of drugs by immersion causing overexposure to the larvae, as the fish are immersed in the treatment solution which may lead to off target effects. Therefore, this is not comparable to the typical mammalian administration. The pericardial oedema is a broad end point of cardiac toxicity and it does not provide any definitive mechanistic data. Nonetheless, it did provide an opportunity to look into the potential challenges for development and further optimisations required for these compounds.

4.7 Conclusion

The aim of this study was to investigate the efficacy and toxicity of the *in silico* hit molecules in the mutant SOD1 zebrafish model and to examine if any of the compounds were able to reduce the neuronal stress exhibited by these transgenic fish. In this study, at 10 μ M concentration none of the compounds were able to reduce the neuronal stress through reduction of HSP-DsRed protein. However, a majority were well tolerated in the zebrafish, including the novel compounds with no prior testing data such as DTB, Cp 2v-005, Cp 8v-054, 1-072 and 10-1131. Therefore, as a future experiment, potential combination treatments and higher concentration regimes can also be tested to examine if there would be any reduction in the HSP-DsRed protein. An alternative approaches that can also be investigated include into can be increasing the exposure time of the compounds over a longer time rather than just a single time point. The known NMDAR modulators antagonists MK801, memantine and the NMDAR agonist at 10 μ M were also tested in the zebrafish model and did not exhibit efficacy. Consistent with previously published data, riluzole was the only compound to to show significant neuroprotection in this phenotypic screening assay. However, the exact mechanism of action of riluzole in this model is still not fully understood, and it could be that the therapeutic effect observed is a result of riluzole interacting with other targets than the NMDAR or potentially also exhibiting off target activity. It may be binding to multiple targets such as voltage dependent sodium channels and others as discussed in section 4.7.1.

The lack of efficacy of our compounds, memantine and MK801 could be linked to the lack of similarity between the GluNR1 of zebrafish and GluNR1 of humans.

In terms of the toxicological studies, 18 of the compounds were shown to be well tolerated. There were 6 compounds that were toxic in the assay causing death of the larvae. However, the toxicity may have also been as a result of the off target effects or unequal drug distribution during the administration of the compounds. In addition, the results could suggest that the toxicity observed may be structure dependent, as within the literature there have been reports of some compound classes not being tolerated well in zebrafish. These compounds may be safer in mammalian systems.

Overall, this model offers many advantages when compared with other existing non mammalian *in vivo* models, including rapid embryonic development, robust genetic

manipulation and whole animal live imaging during development due to a transparent embryo stage, all of which can provide important information during the drug development. However, the gene similarity, the relative cellular mechanism of the NMDAR induced excitotoxicity and comparable biological tissues were important factors that need to be further considered with these zebrafish studies. Despite all the advantages of using the zebrafish model as an alternative to animal toxicological studies, there were some insufficiencies that limited the model compared to mammalian models and therefore reduced translatability of the toxic potencies on observed tissues. It was important to note that neurotoxicity evaluation by only morphologic analysis did not provide a complete toxicity profile for any compound. Other measurements looking into behaviour and full organ development would be required. In addition, the regenerative capacity of the fish is one of the main factors that could influence the translation of the toxicity endpoint in the model.

Chapter 5. *In Vitro* assay using using primary cortical neurons

5.1 Introduction: *In Vitro* assay

The results obtained from the phenotypic screening for neuronal stress using zebrafish showed no neuroprotection with the *in silico* hits. Importantly, the known NMDAR modulator antagonists, MK801 ($K_i = 0.743 \mu\text{M}$) and memantine ($K_i = 1.14 \mu\text{M}$) and the agonist NMDA EC_{50} at $22.0 \mu\text{M}$ ^{456,457} also did exhibit any activity. Potential reasons for this lack of efficacy/effect have been discussed in Chapter 5.7.1–5.7.3.

An *in vitro* assay using primary cortical neurons was used to directly measure the damage caused by the NMDAR over activation using its potent agonist NMDA and to examine whether our *in silico* hits influence this excitotoxic injury. This assay mimics the actions of *L*-glutamate, which is the endogenous neurotransmitter for the receptor. NMDA was chosen because it has no effect on the other glutamate receptors (AMPA and kainate) and is specific for the NMDAR. Memantine and MK801, non-competitive antagonists were used as positive controls.

For toxicological studies, *in vivo* models are preferred as they more closely represent the complex nature of biological organisms. However, they are more difficult to use and need Home office approval.⁴⁵⁸ In contrast, *in vitro* experiments using assays such as lactate dehydrogenase (LDH) release are less complex and much easier to use. LDH is released from cells when they are injured, and the extent of release correlates with the extent of injury caused to the cell.⁴⁵⁹ LDH release combined with nuclei staining techniques have been used in this study to quantify cell viability before and after treatment with different compounds. These experiments will provide insights into the effectiveness of the compounds against excitotoxicity.⁴⁶⁰ Cell based *in vitro* experiments provide additional data such as incubation times and doses of the compounds required.⁴⁶¹ With a well-designed experiment and appropriate controls in place, *in vitro* assays allow the evaluation of the toxicity of the compounds which can guide further *in vivo* studies.

Most strokes affect the cerebral cortex. The cortex is a structure of the brain that has a significant role in many critical functions, including motor and sensory processing,

language and cognition. Cells from the cerebral cortex are therefore used for these assays to mimic stroke. Excitotoxicity mediated by NMDAR is a key mediator of cell death in the cortex.^{462,463}

The cerebral cortex is composed of diverse cell types that are closely connected. Cells found in the cortex include neurons, astrocytes, oligodendrocytes, endothelial cells and microglia. Neurons in the cortex can primarily be categorised into two groups: the excitatory neurons (~85%) and inhibitory neurons (~15%). Further subcategorization is based on location of the neurons to specific brain areas (Figure 5.1) such as the somatosensory cortex (sensory), motor cortex (motor), visual cortex (light sensing) and auditory cortex (sounds).⁴⁶⁴

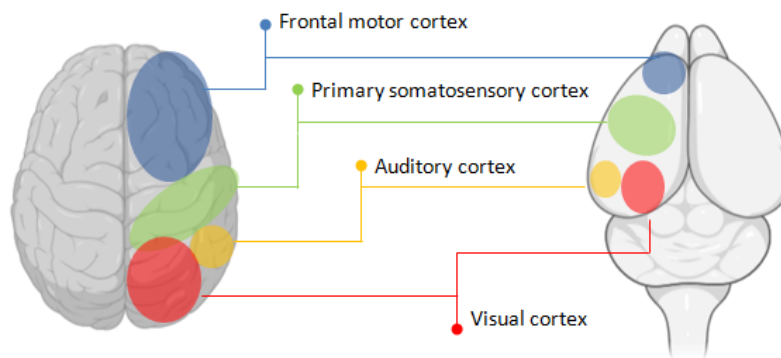


Figure 5. 1 A comparison of the human and mouse cortex areas.

The frontal cortex (blue) is responsible for planning, decision making and movement. The primary somatosensory cortex (green) is responsible for processing sensory input from the body such as limb position, touch, pain and temperature. The auditory cortex (orange) is responsible for processing sound. The visual cortex (red) is located at the posterior end of the brain and it is mainly responsible for processing the visual information from the retinas. Adapted from Fee et al.⁴⁶⁵

5.1.1 Primary cortical neuronal cell cultures

Mouse primary neuronal cells have been utilised in numerous models for investigating mammalian brain development and disease. Primary neuronal and glial cells from the human or animal nervous tissues can be challenging to isolate and maintain *in vitro* but have numerous benefits and uses in neuroscience research.

Primary cells preserve the cell characteristics of the tissue they originated from which avoids genetic alterations that occur in immortal cell lines such as human

teratoma-derived NT2 cell lines or stem cell lines such as induced pluripotent stem cells (iPSC). Hence they are often more biologically and physiologically relevant for CNS drug discovery.

However, there are numerous limitations of *in vitro* primary cellular models of neurological disease including stroke. In general, most studies use pure (or near pure) cultures of one cell type, such as pure neuronal or pure astrocytic cultures. This creates an artificial situation which differs from *in vivo* where multiple cell types are in proximity and have dynamic interaction with each other both physiologically and in disease.⁴⁶⁶ Some groups have tried to address this by using mixed cultures such as mixed neuronal and astrocytic cultures, but these cultures are technically difficult to prepare and can have high variability unless the ratios of each cell type are carefully controlled. More recently, organotypic cultures have received much interest and it is possible that future neuroscience research will involve these types of mixed culture models rather than cultures of one cell type. Nevertheless, pure cultures of one cell type give information on the effect of a drug on that specific cell type which can be obscured when multiple cell types are studied at one time.

Table 5. 1 The advantage and disadvantage of common cell cultures used *in vitro* models for ischaemic stroke.⁴⁶⁷

Cell source	High-throughput	Physiological relevance	Experiments	Notes
Primary cells Organotypic Brain slices	No	High	Useful for excitotoxicity research, oxygen-glucose deprivation models, electrophysiology, immunostaining. Ca ²⁺ imaging, and excitotoxicity models.	Need an animal source for cells. Injury during preparation may increase irregularities in the function of the cells. Most studies use cell type which creates an artificial environment devoid of the influence of other cells.
Immortalised cell lines - NT2 - PC12-rat - SH-SY5Y - HT-22	Yes	Low due to genetic manipulation	These are cell lines widely utilised for excitotoxicity models <i>in vitro</i> .	The cell types can be very HTP for large screening campaigns however their readout should be analysed with caution as they do represent a genetically manipulated cell line.
Stem Cells (iPSC)	Partially	High	Can be used in chemical ischaemia, excitotoxicity and BBB models	Can obtain 100% purity of the neuronal population. Opportunity to study different patient specific cells that may have genetic influence within the disease stroke such as those seen in CADASIL.

Netra D1-NT-2 human tetratocarcinoma (NT2), PC12-rat pheochromocytoma, SK-N-SH neuroblastoma, Hippocampal Tissue-22 immortalised mouse cell line and Cerebral Autosomal Dominant Arteriopathy with subcortical Infracts and Leukoencephalopathy.

A shared limitation of both pure and mixed cultures, including organotypic cultures is that the isolation of the cells and maintenance in cultures may affect the metabolism of the cells. For example, for primary neurons, higher levels of glucose and oxygen are needed to maintain cells in culture.⁴⁶⁸ Table 5.1 demonstrates some of the key cell lines used in ischaemic stroke research along with their advantages and limitations.

Since neurons are the chief cells in the cortex and are primarily affected by excitotoxicity, we focused our studies on pure primary neuronal cultures. Numerous studies have shown neurons in culture express glutamate receptors including

NMDAR.⁴⁶⁹⁻⁴⁷¹ In this study we used primary neuronal cultures to investigate whether our *in silico* hits have their own intrinsic toxicity. We next looked at the extent of cellular injury induced by escalating concentrations of NMDA then investigated whether our compounds could attenuate the extent of injury caused by NMDA.

The *in vitro* experiments performed in this study are also summarised in Figure 5.2, showing the plate preparation from mouse primary cortical neurons and the NMDAR induced cell cytotoxicity assay that was performed.

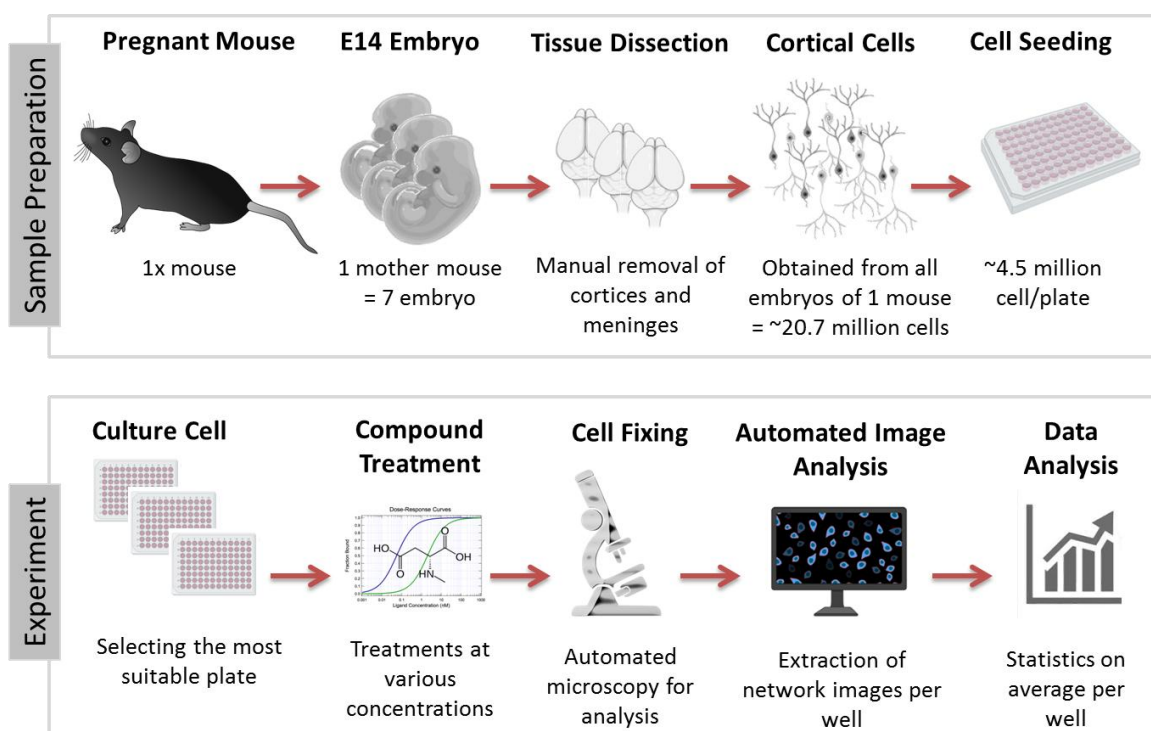


Figure 5. 2 The *In vitro* workflow demonstrates isolation, culture and assay development of cortical neurons.

The primary cortical neurons were obtained from a mouse embryo and were manually isolated and prepared for the cell seeding onto the plates. After 10 days *in vitro*, the culture plates that were axon rich were used for the drug screening experiments. Cells were treated with the compounds under study. Subsequently, the media of the treated cells were collected for the LDH assay and the nuclei of the cells were stained to determine the viability of the cells after the treatments. They were then fixed and imaged with high content imaging instrument Incell 200 and the data was analysed with the image storage and analysis software Columbus. More details about cell count using Columbus are provided in Appendix J.

5.1.2 Measurement of excitotoxicity in mammalian neuronal cells

Cell death occurs by 3 principal pathways, such as autophagy, apoptosis and necrosis. All of these processes have their own distinct features depending on the cell death pathway being activated as explained in Chapter 1: section 1.3.1.

LDH assay uses a colorimetric method to measure the amount of LDH released in the culture medium. LDH is a naturally occurring and stable enzyme in cells that catalyses the oxidation of lactate to pyruvate with the help of the cofactor nicotinamide adenine dinucleotide (NAD⁺) which is converted to its reduced form NADH. The greater the membrane breakdown, the higher the leakage of LDH into the extracellular domain resulting in an increase of NADH.⁴⁷² The concentration of LDH present can then be examined by use of the yellow dye tetrazolium salt (INT). The INT dye is subsequently reduced by the NADH to produce the red fluorescent formazan dye. Enzymes such as glucose-6-phosphate and adenylate kinase can also be used to measure cytotoxicity. However, they are less stable and tend to lose their activity quickly. Figure 5.3 summarises the mechanism of the LDH assay and all reagents used.

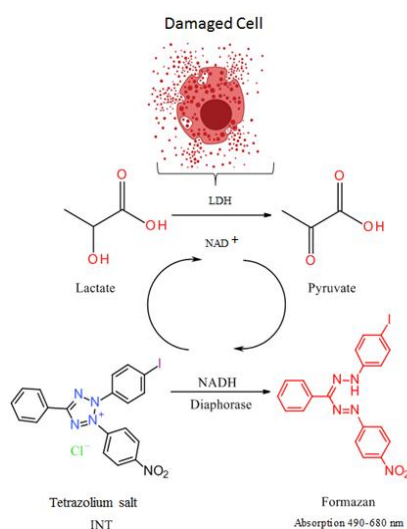


Figure 5. 3 The LDH assay mechanism of detection.

The diaphorase enzyme binds with the reduced substrate NADH formed through the LDH catalysed reaction of lactate to pyruvate. This allows the conversion of the yellow tetrazolium salt into the reduced red formazan.

5.2 Aims and objectives

Investigate the efficacy of the *in silico* hits in primary cortical neuronal cultures by:

1. Determining if any of the compounds alone exhibit any cytotoxic effect.
2. Determining if any of the compounds can reduce excitotoxic damage induced by NMDAR by the percentage of cell death using nuclei staining.

5.3 Results

The global viral outbreak of the acute respiratory syndrome coronavirus disease (COVID 19) impacted this investigation. COVID 19 restrictions caused major delays in the timeline of the project. Due to a national lock down, the University restricted access to laboratories. In addition, delays in reordering supplies, animals and media led to slow progress. Unfortunately, this restriction period resulted in only 8 out of the original 24 compounds being tested in the *in vitro* assay.

5.3.1 Dose response of NMDA induced excitotoxicity

The presence of neurofilaments (confirmation of neuronal cell purity) were initially confirmed using immunocytochemistry and immunofluorescence techniques on the primary mouse cortical neurons (Appendix I). This study verified the purity of the neuronal cultures. Previous work in our lab demonstrated that *N*-methyl-*D*-aspartate (NMDA) could induce cell injury/death in a dose dependent manner using LDH experiments.⁴⁷³ The concentrations tested ranged from 0-1000 μM . Interestingly, the results demonstrated that the cell death plateaued at 60 μM -1000 μM and more importantly there was a sharp increase in cell death at 30 μM in comparison to lower dose treatments of 20 μM , 10 μM and 0 μM . Based on these studies, five concentrations were used to quantify the percentage cytotoxicity of the cells for the experiments performed in this study.

A dose response using NMDA was performed to determine the optimum midpoint concentration required to cause significant cell death, but not causing complete cell death. This midpoint would provide the window for neuroprotective compounds to reduce the extent of cell death caused by NMDA. In addition, the maximum concentration of NMDA required for causing total cell death through excitotoxicity was also identified in the assay (100% or complete cell death).

Initially, the cells were treated with NMDA concentrations (0-300 μM) for 45 minutes and the LDH release was measured after 24 hours. The results illustrate that as NMDA concentration increases, more cell damage is observed (Figure 5.4a). The LDH release in the media was 36.9% for the non-treated cells (0 μl NMDA). This demonstrated that there was baseline cell death in the absence of exposure to exogenous substances. The extent of baseline cellular injury was higher than expected.

However, this may have been influenced by investigator experience and handling primary cortical neurons. There was a non-significant increase in the extent of cytotoxicity when the NMDA treatment concentration was increased from 30 μM (63.07%) to 100 μM (73.93%) cytotoxicity. There was a significant difference observed in the extent of cytotoxicity, when comparing 30 μM NMDA to 300 μM NMDA, the highest concentration $**P= 0.0013$ (Figure 5.4a).

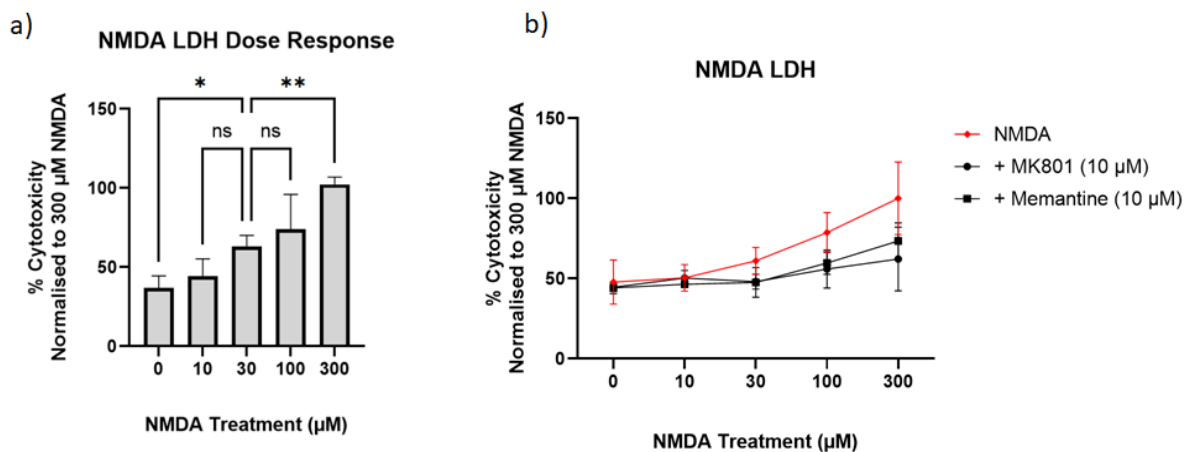


Figure 5. 4 The extent of cytotoxicity induced by NMDA in primary cortical neurons.

5.4a) The LDH release from neurons treated with NMDA (0-300 μM) using 96 well plates. One-way ANOVA $N=4$, 9 wells for 0 and 30 treatments, 3 wells per condition for other treatments. 0 vs 30 ($*p= 0.0262$), 30 vs 300 ($**p= 0.0013$) and non significant (ns) with other treatments vs 30 μM . **5.4b)** A dose response of NMDA, MK801 and memantine. The lowest concentration of NMDA at which neurocytotoxicity was observed was at 30 μM . ($N=3$, 3 wells per condition in each experiment. All data shown as Mean \pm SD).

For positive controls, the NMDA antagonists MK801 and memantine were used. Cell death at 30 μM NMDA was 61.07%, and in the presence of MK801 (48.08%), and with memantine 47.53%. At 100 μM NMDA treatment the extent of cytotoxicity observed for NMDA was at 78.72%. However, in the presence of 10 μM MK801 this was reduced to 55.95% and with 10 μM memantine 59.67%. At 300 μM NMDA exposure (100% cell death), MK801 and memantine were able to reduce cytotoxicity levels to 62.20% and 73.37%, respectively.

The lowest NMDA concentration that exhibited the midpoint for cell death (61.07%) and did not cause severe damage to the majority of the cells was at 30 μM NMDA. Thus, 30 μM NMDA was used for all subsequent experiments.

5.3.2 Cytotoxicity of the compounds tested

The initial experiments investigated whether the test compounds exhibited cytotoxicity. It was important to establish this before evaluation of the test compounds against NMDA cytotoxicity was undertaken. The LDH released for the test compounds is shown in Figure 5.5. The baseline cell death (in the absence of test compounds) was 32.18%. Treatment with solvent (0.1% solution of DMSO) used to dissolve the compounds exhibited 35.21% cytotoxicity (not significant). The majority of the test compounds proved to be well tolerated at the concentrations tested (1 μM and 10 μM) when incubated with the cells for 45 minutes. Moderate cell cytotoxicity for compound Cp 2v-005 (2,6,6-trimethylbicyclo[3.1.1]heptan-3-one) and morantel tartrate was observed at 10 μM , 55.20% and 45.63%, respectively.

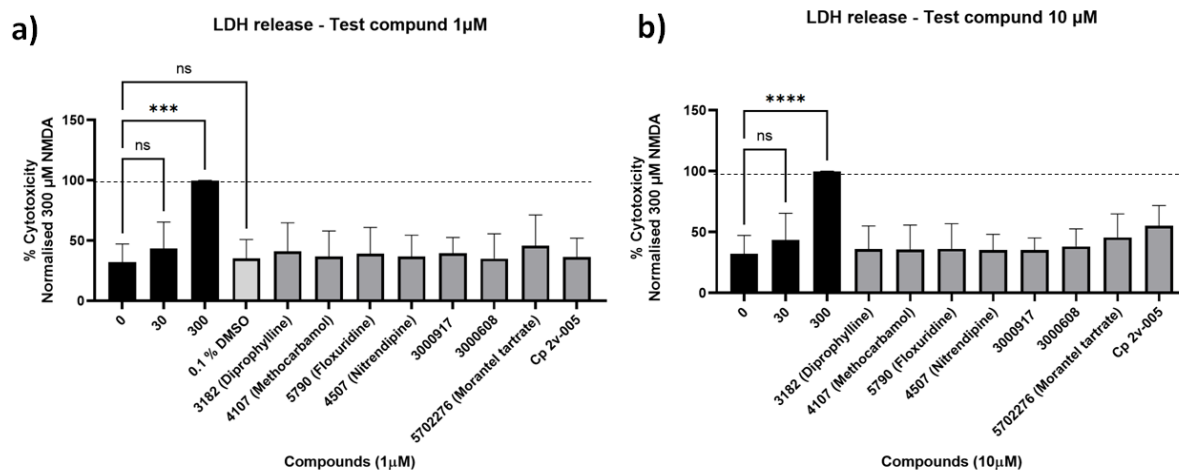


Figure 5.5 Analysis of cytotoxicity of the test compounds in primary cortical neurons.

5.5a) LDH release at 24 hours from neurons treated with 1 μ M of the test compounds. One-way ANOVA, 0 vs 300 (*** $p=0.0001$). **5.5b)** LDH release treated with 10 μ M of the test compounds. One-way ANOVA, 0 vs 300 (**** $p<0.0001$). 0 μ M, 30 μ M, 300 μ M, 0.1% DMSO N=4. (For 0 μ M and 30 μ M 6 wells per condition/experiment). For 300 μ M and 0.1% DMSO treated cells were 3 wells per condition/experiment. For the compounds, N=3 experiments 3 wells per condition/experiment, with exception of 5702276 N=2. All data normalised to 300 μ M NMDA. All data demonstrated as mean \pm SD.

5.3.3 Cell imaging

Nuclei staining with Hoechst 33342 and PI were used to examine cell viability with the test compounds (Figure 5.6a,b). Hoechst 33342 can emit a blue light when bound to the minor groove of the DNA through binding to the nucleic acids adenine and thymine. Hoechst 33342 is highly cell permeable for both live and fixed cells and has an absorption/emission of 350/461 nm (blue).⁴⁷⁴ However, as it is still less permeable for living cells, the images for the cells that have damaged membranes tend to be brighter (Figure 5.6c).

The second counterstain used was PI, which is a red fluorescence nuclear stain that is not membrane permeable, therefore it is extremely useful for identifying and characterising apoptotic and necrotic cells. PI acts as a DNA chelating agent and binds to the nuclei of the cells and which results in an increase in the fluorescence absorption/emission from 493-636 nm to 535-617 nm (red emission).⁴⁷⁵ The Columbus software was trained with 5 of the images obtained from the assays to

perform a batch analysis and count the number of nuclei in each well from the 16 images obtained from each well per condition. The analysis shown in Figure 5.6a, where the nuclei are stained using Hoechst (blue) and PI (red) shown.

During the analysis it was observed that nuclei identification was in some cases difficult to distinguish from overlapped cells. This could potentially introduce greater variability to our analysis. However, filters were applied to exclude the regions that contained clumping of the cells. With both staining techniques, the non-treated cells demonstrated a fairly high level of baseline cell death, with Hoechst (48.33%) and PI (63.69%) (Figure 5.6b,d). This high cell death count could influence the cytotoxicity values obtained from the test compounds. There was in general, greater cell death observed with PI in comparison to Hoechst, by approximately 1.3 fold. In both stains 0.1% DMSO showed non-significant cell death levels when compared to non-treated cells. At 10 μ M, floxuridine demonstrated a significant 81.68% cell death using PI staining compared to non-treated cells, *P=0.04998, (Figure 5.6d,e)

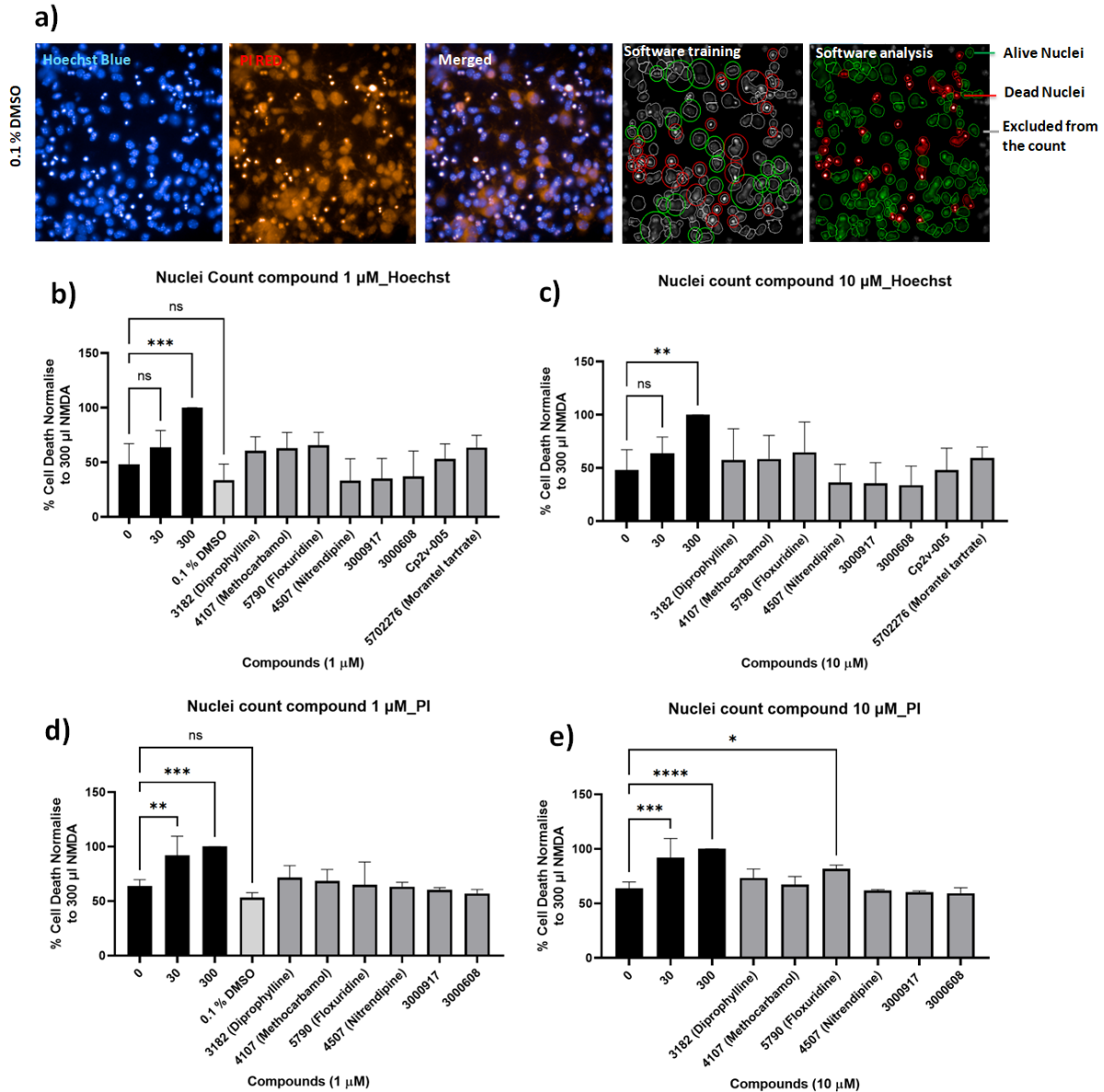


Figure 5. 6 Cell death analysis of cells tested with compounds using nuclei staining with Hoechst and PI staining techniques.

5.6a) Images of cells that were treated with 0.1% DMSO. Hoechst 33342 (blue), propidium iodide PI (red) and a merged image of both stains. Training of the software shown, collapsed nuclei are selected (red circles) and the alive nuclei (green circles). The software uses this training to automatically perform a batch analysis of the images taken from each well. The images obtained from wells treated with 0.1% DMSO, Well C2, Field 1. **5.6b)** 24-hour cell death analysis using Hoechst for cells treated with 1 μM concentration of the compounds. One-way ANOVA, 0 vs 300 (** p = 0.0007). **5.6c)** The 24-hour cell death analysis using Hoechst for cells treated with 10 μM concentration of the compounds. One-way ANOVA, 0 vs 300 (** p = 0.0079). **5.6d)** The 24-hour cell death analysis using PI at 1 μM . One-way

ANOVA, 0 vs 30 (**p= 0.0050), 0 vs 300 (**p=0.0003). **4.6e**) The 24-hour cell death analysis using PI at 10 μ M. One-way ANOVA, 0 vs 30 (**p= 0.0005), 0 vs 300 (***p<0.0001) and 0 vs floxuridine (*p= 0.0498). Same conditions as explained in Figure 5.5a.

5.3.4 Efficacy of the *in silico* hits in NMDA induced cytotoxicity.

5.3.4.1 LDH release

We next evaluated whether the *in silico* hits influenced NMDA induced cytotoxicity in the primary cultured neurons. The excitotoxicity assay was performed on cells in the day 10 *in vitro* (DIV). After exposure to NMDA, LDH release in the incubation medium was analysed 24 hour later. Baseline LDH release from non-treated cells was 32.96%. Cells with 30 μ M NMDA exhibited 45.05% (Figure 5.7a) but this increase did not reach statistical significance. Pre-treatment with the *in silico* hits in presence of NMDA also did not produce significant changes in LDH release. Moreover, the positive controls, MK801 and memantine (10 μ M) also did not exhibit any protection. There was, however, a non-statistically significant trend towards lower LDH release with several compounds including nitrendipine and indole glyoxylamide, 3000917 (Figure 5.7b).

A possible reason for the minimal differences observed in the extent of LDH release may be related to the size of the wells in the 96 well plate. The volumes of media in the 96 well plates are small (volume 0.34 ml and growth area 0.34 cm²) which may introduce technical variation. To address this issue, a 24 well plate was prepared with three of the compounds (Figure 5.7c).

In the 24 well plates, un-treated cells exhibited 29.90% cytotoxicity, and 30 μ M NMDA, 59.92%. The MK801 in the presence of 30 μ M NMDA exhibited 34.59% and memantine exhibited 41.48% cytotoxicity. The lowest cytotoxicity was observed for compound nitrendipine at 42.65%, followed by compound 3000917 at 47.19%.

However, none reached statistical significance when compared to 30 μM NMDA. High variability was also observed which may explain this observation. More biological repeats would be required to reduce the variability amongst the samples.

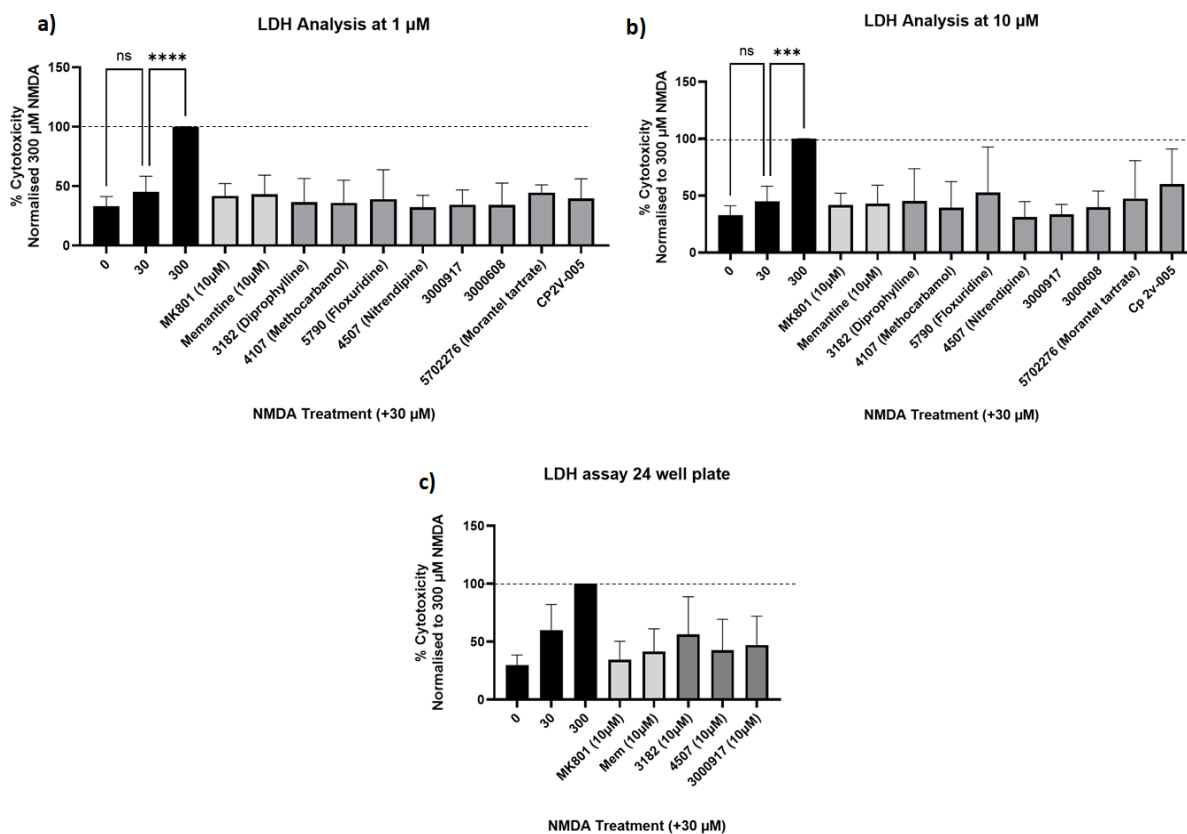


Figure 5.7 Neuroprotective evaluation of *in silico* hits against NMDA induced cytotoxicity.

5.7a) LDH release from the neurons treated with 1 μM compounds. One-way ANOVA, 30 vs 300 (**** $p < 0.0001$). **5.7b)** LDH release from neurons treated with 10 μM compounds. One-way ANOVA, 30 vs 300 (** $p = 0.0005$). All compounds pre-treated for 30 minutes at both concentrations. 0 μM , 30 μM , 300 μM , MK801 (10 μM) and memantine (10 μM) $N = 5$, for the compounds $N = 3$. All data demonstrated as mean \pm SD. **5.7c)** LDH release from the neurons in 24 well plates treated with 10 μM of the compounds. One-way ANOVA, $N = 4$ for all treatments and technical repeats of 3 wells per condition/experiment.

5.3.4.2 Hoechst and PI staining

In the presence of 30 μM NMDA, morantel tartrate and CP2v-005 exhibited the largest cell death at 79.75% and 79.02% at 1 μM and 74.29% and 80.47% at 10 μM , respectively. Diprophylline, methocarbamol and floxuridine did not exhibit decreased cell death. Nitrendipine at 1 μM and 10 μM exhibited 46.06% and 48.81% cell death

respectively by Hoechst staining (Figure 5.8a,b). By PI staining, nitrendipine at 1 μM and 10 μM exhibited 70.85% and 63.27% cell death, respectively (Figure 5.8c,d). However, none of these reached statistical significance.

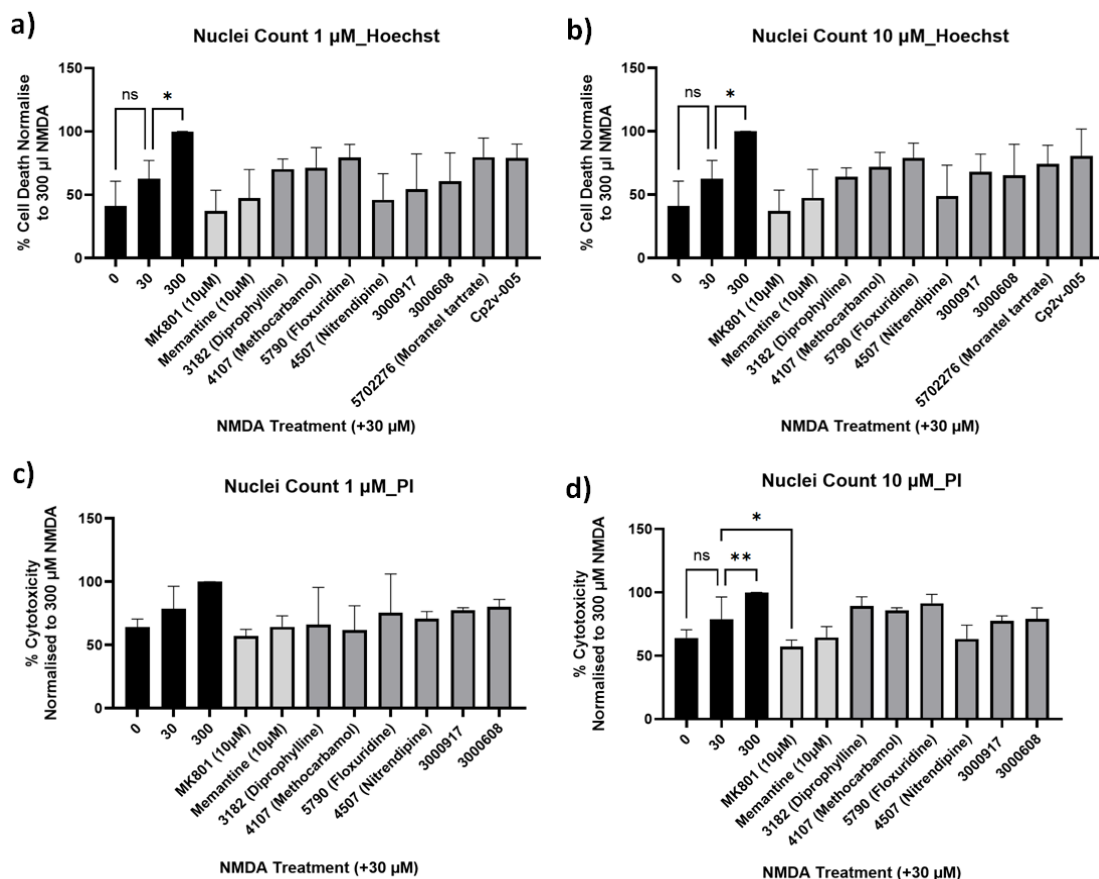


Figure 5. 8 The NMDA induced cytotoxicity assessment using nuclei staining.

5.8a) The Nuclei count using Hoechst for compounds tested at 1 μM . One-way ANOVA, 30 vs 300 (* $p=0.0135$). **5.8b)** The nuclei count using Hoechst for compounds tested at 10 μM . One-way ANOVA, 30 vs 300 (* $p=0.0128$). **5.8c)** The Nuclei count using PI for compounds tested at 1 μM . One-way ANOVA, 30 vs 300 non-significant. **5.8d)** The Nuclei count using Hoechst for compounds tested at 10 μM . One-way ANOVA, 30 vs 300 (** $p=0.0071$) and 0 vs MK801 (* $p=0.0247$). All data demonstrated as mean \pm SD.

5.3.5 The dose response of nitrendipine, 3000917 and 3000608 against NMDA induced cytotoxicity

The compounds nitrendipine, 3000917 and 3000608 exhibited a trend towards lower injury against NMDA induced cytotoxicity. Therefore, to investigate if further neuroprotection could be achieved at higher concentrations, a dose response assay

was conducted using nuclei staining techniques. Compounds 3000917 and 3000608 failed to exhibit any neuroprotection using nuclei staining (Appendix K). Nitrendipine (Figure 5.9) exhibited a trend towards lower cell death at 10 μ M, Hoechst 47.43% and PI 56.32%, however it was not statistically significant. The images of some of the wells in the assay are shown in Figure 5.10.

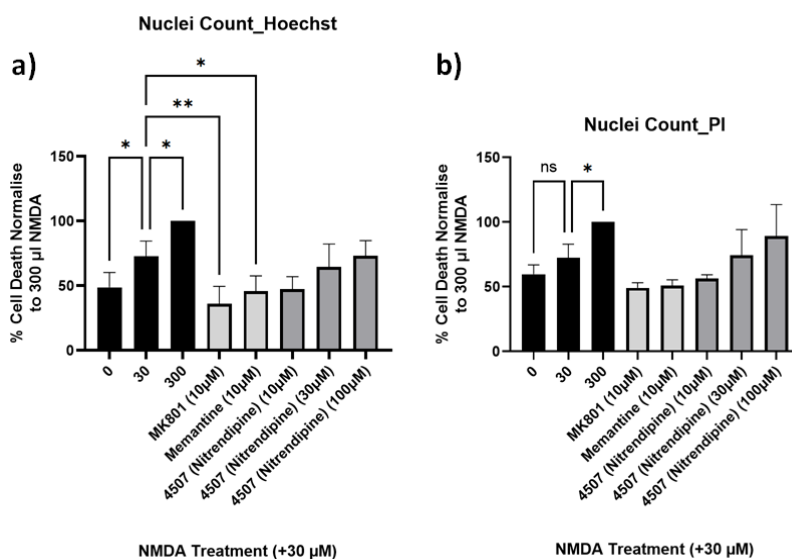


Figure 5. 9 The nuclei count of the dose response with nitrendipine in NMDAR induced cytotoxicity assay.

5.9a) Hoechst staining: nitrendipine 10 μ M in comparison to the higher doses. One-way ANOVA, 0 vs 30 (* $p=0.0470$), 30 vs 300 (* $p=0.0199$), 30 vs. MK801 (** $p=0.0032$) and 30 vs. Memantine (* $p=0.0368$). **5.9b)** PI staining: nitrendipine 10 μ M in comparison to the higher doses. One-way ANOVA, 30 vs 300 * $p=0.0185$. All data demonstrated as mean \pm SD. N=3.

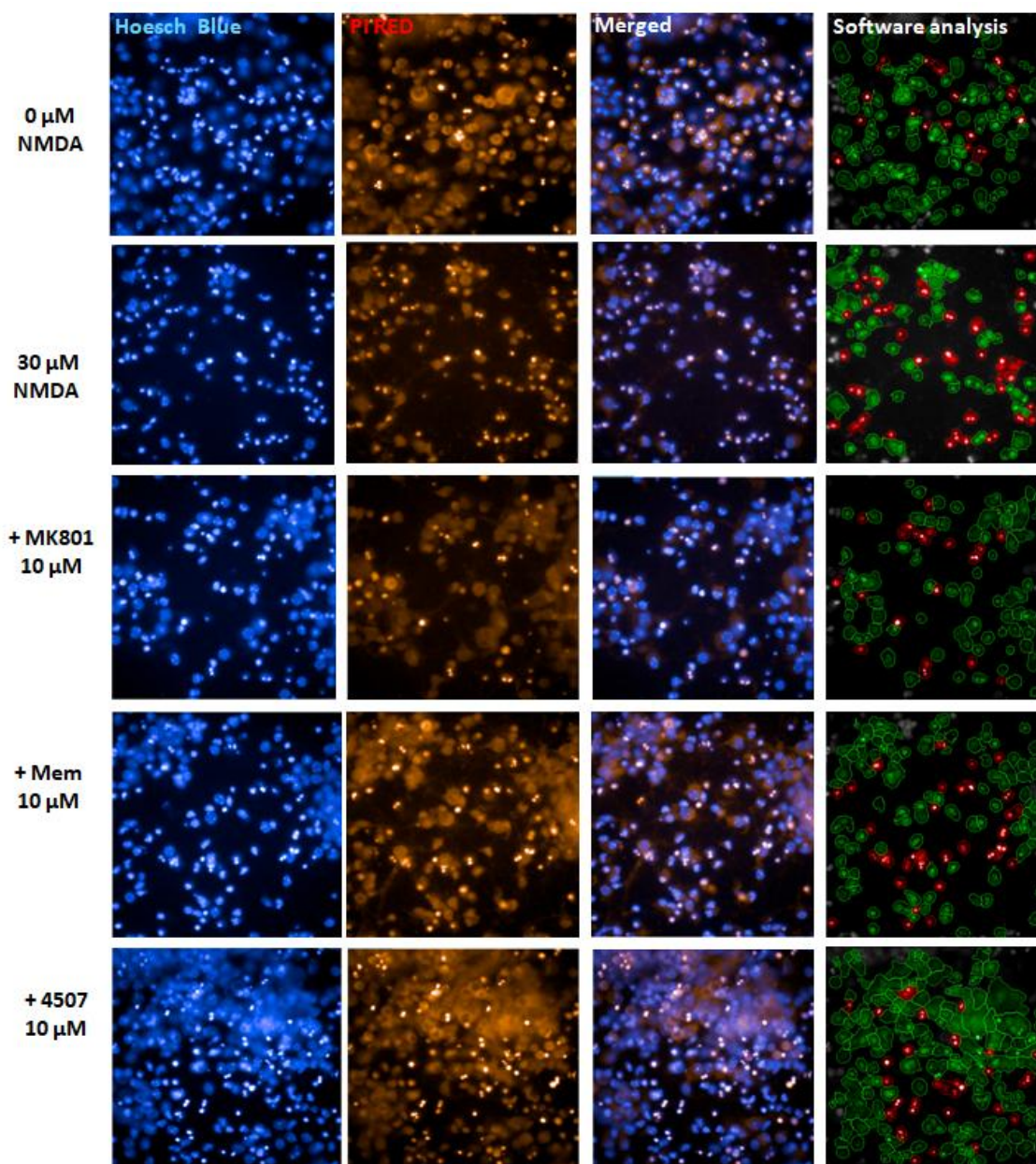


Figure 5. 10 Nuclei count after NMDA induced excitotoxicity. Treatment with positive controls and nitrendipine at 10 μ M.

The cells were initially stained with PI (1:200) and were then fixed with 4% paraformaldehyde. The wells were then co-stained with Hoechst (1:10000). The software analysis of the dead nuclei is also presented, where the dead cells are demonstrated in red and alive nuclei in green.

5.4 Discussion

The second objective of this project was to screen the *in silico* hits for efficacy and safety using *in vitro* and *in vivo* models of excitotoxicity. The research conducted using the *in vitro* model has been presented in this chapter. We used primary cortical neurons to assess safety and efficacy of the *in silico* hits against NMDA toxicity

5.4.1 The neuroprotection observed with nitrendipine

The *in vitro* studies presented above showed that none of our *in silico* hits exhibited significant neuroprotection. Nitrendipine, however, exhibited a trend towards lower toxicity. Nitrendipine is a calcium channel blocker that inhibits the L-type calcium channels ($IC_{50} = 1.57 \text{ nm}$, $ki = 1.39 \text{ nm}$).⁴⁷⁶ One physiological action of nitrendipine is dilation of blood vessels and improving blood circulation⁴⁷⁷ which could also be very beneficial as well as the NMDA cytotoxicity attenuation discussed below.

Nitrendipine was selected from the compounds available in the SITraN library. Interestingly, the influence of nitrendipine on the NMDAR has been previously observed and in 1993 Skeen *et al*⁴⁷⁸ using a radio binding assay showed that nitrendipine had a $IC_{50} = 0.56 \text{ }\mu\text{M}$ and could displace [³H] MK801 in mouse brain slices. These data indicate that there is a reasonable probability that nitrendipine was binding to the channel membrane of the NMDAR and prevented Ca^{2+} influx. This could be the mechanism that mediates the lower trend of cytotoxicity observed with 10 μM of nitrendipine. To examine whether neuroprotection could be further enhanced, higher concentrations of nitrendipine were tested but as shown in Figure (5.9a,b) higher concentrations of nitrendipine at 30 μM and 100 μM failed to exhibit protection.

The approach of using hypertensive drugs for ischaemic stroke has been previously explored. However, those studies were focused on stroke prevention whereas our focus is on acute treatment of stroke. While it is clear that hypertension plays a key role in stroke pathophysiology, the role of antihypertensive agents to save the ischaemic penumbra is less clear and less well tested.

Nimodipine (an analogue of nitrendipine) was studied in ~1,064 patients within the 48 hours from a stroke onset. Unfortunately, no overall benefit was found. However, this may have been impacted by the short therapeutic time window of stroke.

Therefore, a new trial to investigate nimodipine use stroke (VENUS) was carried out where nimodipine was given to patients within 6 hours of stroke onset.⁴⁷⁹ The trial ended early due to lack of benefits observed with nimodipine.

However, in support of nitrendipine, the Syst-Eur study showed that in elderly patients, treatment with nitrendipine (10-40 mg/day) lowered stroke and fatal cardiovascular complications.⁴⁸⁰ The Morbidity and Mortality after Stroke (MOSES) study,⁴⁸¹ randomised patients being treated with eprostatan and nitrendipine for the secondary prevention of stroke. This trial was the first to compare the angiotensin II type 1 receptor antagonist with the calcium ion channel blocker for secondary stroke prevention. In addition, this study mainly focused on high-risk hypertensive stroke patients. The trial ended in 2004 and the combined primary endpoint was shown to be significantly lower in patients treated with eprosartan. However, both these trials focused on the effect of these agents in secondary prevention of stroke, therefore further studies are needed to examine the neuroprotective effect of nitrendipine in acute stroke.

5.4.2 Selection of compounds for in vivo experimental stroke studies in mice

Due to COVID related restrictions on lab access, progress on the *in vitro* studies was delayed and therefore, the *in vitro* studies were still in progress when compounds were selected for mouse experimental stroke studies. Nitrendipine, diprophylline, methocarbamol and floxuridine were selected based on preliminary *in vitro* data, solubility and availability of compounds (Chapter 5).

5.5 Challenges and limitations with NMDA induced cell cytotoxicity analysis

Another important limitation of our study is the relatively small sample size of three biological repeats for most of the *in vitro* assays. This was primarily due to the restricted access to the labs due to COVID. Increasing the number of biological repeats will increase the power of our studies and will reduce type 2 error (false negative). There were several challenges during the optimisation of the assay. For example, the high baseline cell death observed with the un-treated cells and variation in the number of cells in each biological repeat contributed to variability among biological repeats.

As LDH release is an established marker of cell injury and death in cortical neuronal cultures, it was the primary assay used to quantify the cytotoxicity observed by NMDA. This assay has been extensively utilised in neuroscience research for evaluating the safety and efficacy of drugs.⁴⁸² In our hands, the LDH assay showed that on (average ~30%) of cells die in culture without treatment. Primary cortical neurons are extremely sensitive to their environment, specifically changes in temperature, density, and maturity.⁴⁸³ Future refinements in the experimental techniques will likely reduce the extent of baseline cell death.

The extent of cytotoxicity observed using the LDH assay was lower than that observed with nuclei staining (using Hoechst and PI). There could be several reasons for this observation. A large number of cells may have been damaged prior to analysis. The cells may have been damaged at various stages of the preparation including cortical preparation, cell seeding onto the plates and during the cells maturation stages. Therefore, when media was changed during the incubation stage, any LDH released was washed away. However, the injured cells would still stain with Hoechst and PI.

Another possible explanation for the lower observed LDH measured cytotoxicity could be that after exposure of the cells to the compounds for the desired time, the medium was removed from the cells by washing the cells with NBM, prior to the cytotoxicity assay at 24 hours. Hence, this washing step may have removed some of the LDH released from the cells. Furthermore, the use of 96 well plates meant that very small volumes were involved which can introduce inaccuracies due to minor technical errors. To address this 24 well plates were used as shown in Figure 5.7.

The higher cell death observed from the nuclei count may also be due to false positives during analysis with Columbus. If the cells were overlapping or were very closely seeded during plate preparation, the Columbus software would have difficulty distinguishing them from each other and would often count them the same emitted fluorescence intensities of neighbouring nuclei. It is important to mention that there are also other methods for measuring cell viability and cytotoxicity.

For example 3-[4,5-dimethylthiazole-2-yl]-2,5-diphenyltetrazolium bromide (MTT) is another colorimetric assay for quantification of cell damage. In this assay, mitochondrial enzyme succinate dehydrogenase is utilised to measure the MTT-

formazab formed. However, Lobner *et al*⁴⁸⁴ had reported that MTT might not be as sensitive as the LDH assay in quantifying neuroprotective effects.

5.6 Conclusion

In this chapter the *in silico* hits were tested on mouse primary cortical neurons to investigate their potential to modulate NMDA induced cytotoxicity. The methodology and results using traditional toxicity approaches such as LDH release and staining of cell nuclei to identify cell death are presented.

From the initial *in vitro* data none of the *in silico* hits selected was able to significantly reduce cell death in the NMDAR induced cell cytotoxicity. At 1 μ M and 10 μ M the FDA approved diprophylline, methocarbamol, floxuridine and morantel tartrate showed elevated cell death in presence and absence of NMDA. This elevated cell death was mainly observed with cell death was mainly observed with nuclei staining studies in comparison to LDH experiments. From the compounds tested, nitrendipine was the only compound that showed lower number of cell death. However, the combined results for this compound did not reach statistical significance. The synthetic in-house compounds 3000917 and 3000608 were tolerated by the cells, but they also failed to demonstrate any neuroprotection.

It is important to mention that there were many challenges to the *in vitro* cell based studies, specifically during optimisations of the assay. As explained in section 4.7, one of the major challenges for the *in vitro* studies was that the sample size for the assay was limited. Also due to the time required to obtain the cells from animals it also caused restrictions in setting up through-put assay for technical repeats and therefore, unfortunately not all compounds were tested either. Another major issue was the high baseline cell death for the untreated cells which narrowed the gap between the cells that were treated with toxin and the compounds. We believe that a greater numbers biological repeats may have clarified this by reducing variability in the measurements. Combined with the *in silico* data it was suggested that the worst binder of GluNR1 is floxuridine which did demonstrate toxicity at 1 μ M in cortical neurons in our *in vitro* studies.

Chapter 6. Preliminary efficacy evaluation in experimental stroke

6.1 Rodent *in vivo* studies: Experimental Animal models of stroke

6.1.1 Impact of COVID on selection of compounds for *in vivo* testing

Due to COVID, access to the lab was severely curtailed in March 2020 which had a significant impact on the progress of this project. Moreover, supply of chemicals and other consumables was reduced. Therefore, when restrictions were partially eased, a decision was made to run some *in vivo* experiments with the available compounds that were soluble, in parallel to some of the *in vitro* experiments. Although only nitrendipine exhibited efficacy when the *in vitro* studies were completed, all the *in vitro* data were not available, and we proceeded with some *in vivo* experiments based on the availability and acceptable solubility of the compounds.

6.1.2 Blood supply of the brain

The MCA is the main artery that provides oxygenated blood to the brain. It is a branch of internal carotid artery (ICA) and sends branches to the basal ganglia and lateral surfaces of the frontal and temporal lobes which contain the primary motor and sensory cortex. The left and right MCA and the anterior cerebral arteries (ACA), are linked to the posterior circulation (vertebrobasilar arteries) by the posterior communicating arteries (pcomA) to form the Circle of Willis (Figure 6.1). The Circle of Willis provides alternative routes for blood to flow in case compromised in particular blood vessel. This anatomical configuration provides some reserve or compensatory flow of blood during stroke, but it is usually insufficient to prevent stroke if a major vessel like the MCA is occluded.

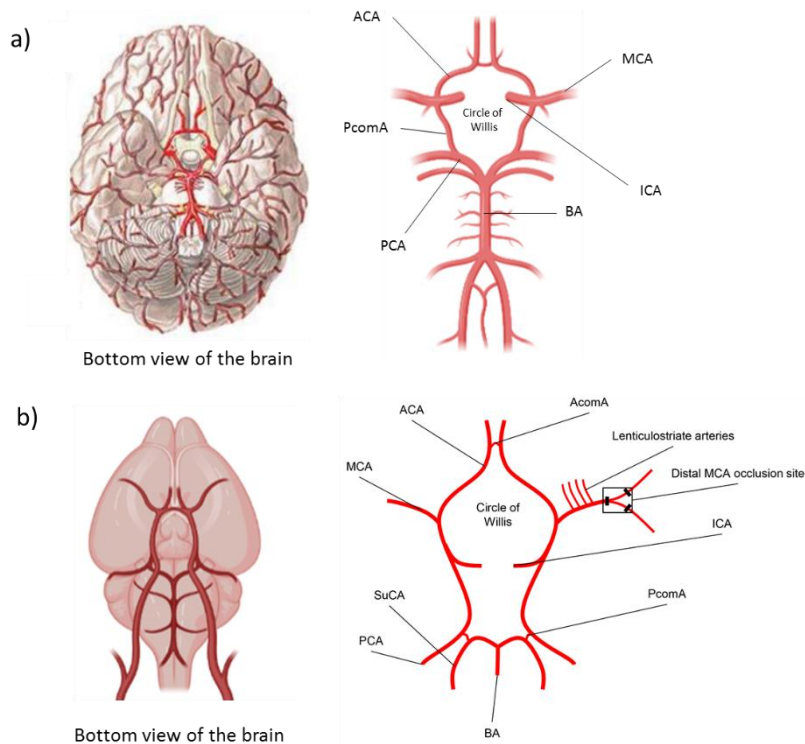


Figure 6. 1 The Circle of Willis in both the human and mouse brain.

6.1a) The human Circle of Willis is a collection of arteries connecting the basilar artery (BA) to the internal carotid arteries (ICA).⁴⁸⁵ **6.1b)** MCAO is achieved by occlusion of the distal MCA. The image of the human brain was obtained from www.neuroems.com⁴⁸⁶ and the mouse circle of Willis in **6.1b** adapted from www.biorender.com. Used with permission under the terms of the creative commons attribution licence (CC-BY).

6.1.3 Middle cerebral occlusion (MCAO) model

Although *in vitro* studies can provide useful indication of efficacy and insights in to potential mechanisms of action, no *in vitro* model can fully mimic the multifaceted processes that involve synaptic, vascular and multi-cellular pathophysiological processes during stroke. Animal models are crucial for preclinical stroke research and for evaluating the effectiveness and safety of new therapeutics before human studies can begin. Moreover, animal studies can provide important vital pharmacokinetic and pharmacodynamic data on which clinical studies can be based.⁴⁸⁷

Our studies using zebrafish, showed that the compounds used do not significantly reduce HSP70 levels and are therefore unable to reduce SOD1 related disease progression in a vertebrate animal model.

However, as explained in Chapter 4.7, the zebrafish model proved to be far more complex than expected and it did not necessarily address the question of whether these compounds could reduce neuronal damage by stroke. Moreover, because NMDAR antagonists like MK801 and Memantine failed to show any effect in the model, it is possible that differences in the structure and function of NMDAR between humans and zebrafish may help to explain the observed results.

An alternative *in vivo* model that mimics stroke in humans is middle cerebral artery occlusion (MCAO) models in mice which was used to examine whether the hits from *in vitro* screening are efficacious in reducing stroke induced brain injury.

The most common location for human ischaemic stroke is in the MCA. Therefore, animal models target this artery.⁴⁸⁸ Two types of models are typically used to mimic the most common types of strokes that are seen in humans, these are transient (tMCAO) and permanent MCAO (pMCAO).⁴⁸⁹ The tMCAO model which involves transient occlusion of the MCA to mimic occlusion and reperfusion (opening) of the blood vessel. This is typically achieved by inserting a filament into the carotid artery and advancing it to the origin of the MCA resulting in blockage of flow in the MCA. Reperfusion is achieved by withdrawing the filament.⁴⁹¹ pMCAO mimics permanent occlusion of the MCA. In the pMCAO model, the distal portion of the MCA is permanently occluded by electrocoagulation and is used as a model for patients that have no vascular recanalisation.^{492,493} There is a difference in the pathological pathways of the tMCAO and the pMCAO. Ford *et al*⁴⁹⁴ performed a gene expression study for the two models and found that the tMCAO model tends to produce inflammation and apoptosis mechanisms where as the pMCAO model induced more excitotoxic pathways due to the presence of genes for ion channels, growth factors and tyrosine kinases. However, further studies are required to elucidate the exact differences between the two models. It is important to mention that potential drug candidates also demonstrate different effects in the two models.⁴⁹⁵⁻⁴⁹⁷ For compounds that are believed to have mechanism of action through radical scavenging and are anti-inflammatory tend to be tested in the tMCAO model whilst glutamate antagonists are most often tested in the pMCAO models.⁴⁹⁸ Although, the mechanisms of injury in the two models are somewhat different in both cases, a stroke that is confined to the neocortex of the brain is achieved.⁴⁹⁹

The most common animals that are used for MCAO models are rodents (mice and rats). Mice and rats have been used extensively for acute ischaemic models as they are “like humans” in both their genetic and molecular composition and exhibit similar injuries.⁵⁰⁰ Rodent stroke models provide great insight into post stroke neurodegeneration and contribute greatly to identify potential medications that are safe and efficacious for translation to human clinical trials.⁵⁰¹

6.1.4 Excitotoxicity and experimental stroke

As discussed in Chapter 1 (Section 1.3.1) numerous studies have shown that excitotoxicity is a critical harmful process that mediates tissue injury and death during stroke. *In vitro* and *in vivo* studies (MCAO models) have shown that NMDA glutamate antagonists are protective in experimental stroke models. However, as discussed elsewhere, clinical translation of the preclinical studies has been unsuccessful. Many reasons for this have been advanced including poor planning of clinical studies and side effects of NMDA antagonists. For example, the therapeutic time window (the time in which the drug must be administered after stroke onset) in the animal studies was very short, typically 3-4 hours, whereas in the clinical studies, the antagonist were administered ~12 hours or longer after stroke onset.⁵⁰²⁻⁵⁰⁵

Lack of selectivity of the antagonists was also a major issue as many NMDA receptor subunits have important physiological functions and it is vital that these are left uninhibited.⁵⁰⁶ We hypothesised that our selective targeting approach would be efficacious in the mouse MCAO model as this is widely used in stroke research and also available in the lab.

6.1.5 Route of delivery, drug solubility and formulation

In stroke, it is highly desirable that the treatment is administered intravenously so that it gains rapid access to the systemic circulation. This is particularly important because stroke has a narrow therapeutic time window. If treatment is delayed or it takes time for the therapeutic agent to reach its target site, for example if administered orally, the ischemic brain will already be irreversibly damaged, and the treatment will not have significant beneficial effects. Extensive progress has been made in the field of small molecule drug delivery that has led to techniques to increase solubility and distribution of compounds; such as the use of lipid based

formulations, microemulsions,⁵⁰⁷ liposomes⁵⁰⁸, amorphous solid dispersions⁵⁰⁰ and nanovesicles.⁵⁰⁹ These options are therefore very useful as it allows solubilisation of a greater number of compounds with direct comparison of efficacy and safety at similar doses. However, whilst these techniques have been employed in clinical studies, their use in early preclinical studies has been restricted. This is mainly due to expense, chemical decomposition and the availability of materials and equipment.⁵¹⁰

6.2 Solubility of our selected compounds

6.2.1 Nitrendipine

Nitrendipine has been reported to be completely soluble in each of the following solvents. Ethanol (2 mg/ml), dimethyl sulfoxide (DMSO) (25 mg/ml) and dimethylformamide (DMF) (30 mg/ml).⁵¹¹ It has been reported that nitrendipine could also be dissolved in 1:4 ratio of DMF:H₂O.⁵¹² However, for animal studies, all these solvents are considered lethal to animals. Therefore, to be able to use them in mice the amount used would need to be reduced significantly and replaced with aqueous solutions. In case of DMF, previous studies had demonstrated that it was an extremely toxic solvent with median lethal dose (LD₅₀) of 6.2 ml/kg and is known to be hepatotoxic to mammals, causing adverse effects such as abdominal pain and vomiting upon exposure.^{513,514} It was not considered any further for these experiments.

6.2.2 Diprophylline

Diprophylline is an antagonist at A₁ (k_i= 810 μM) and A₂ adenosine receptor (k_i= 4 600 μM)⁵¹⁵ and inhibiting the cyclic nucleotide phosphodiesterase (IC₅₀= 200mg/ml).⁵¹⁵ It is a drug often used to treat bronchitis, asthma and chronic emphysema. Diprophylline, as a xanthine with two hydroxyl groups, has shown to be much more soluble in water and DMSO (51 mg/ml)⁵¹⁶ although, much less soluble in alcohol solvent such as ethanol (1 mg/ml).

6.2.3 Methocarbamol

Methocarbamol is a carbamate analogue that is used to reduce musculoskeletal pain and musculoskeletal spasm. The exact mechanism for this effect of methocarbamol

is unknown but there are some studies that have shown it can inhibit the zinc metalloenzyme carbonic anhydrase at much higher affinity ($k_i = 1.4 \times 10^{-2}$) in comparison to its isoform carbonic anhydrase II ($k_i \sim 1 \times 10^{-1}$).⁵¹⁷ Methocarbamol is known to be fairly water soluble (25 mg/ml). It is also soluble in ethanol (14 mg/ml) and (16mg/ml) in DMSO.

6.2.4 Floxuridine

Floxuridine is a pro-drug of 5-fluorouracil demonstrating anti-proliferative activity which can be used as an antitumor drug (IC_{50} 1.1 μ M) in colorectal and lung (IC_{50} 1.7 μ M) cancer.⁵¹⁸ It is soluble in DMSO 50 mg/ml and also the 1 normality (N) of ammonium hydroxide (NH_4OH) 50 mg/ml.⁵¹⁹ The detailed mechanism of these drugs is discussed in section 6.8.2.

6.3 Safety assessment of drug formulations

Another important factor to consider is that the formulation must be tolerated well and not cause unacceptable adverse effects.⁵²⁰ When assessing safety, most laboratory studies using animals assess safety based on the LD50 values from the literature or institutional protocols. This raises many ethical issues and usefulness of the LD50 is debated.^{521,522} In our preliminary experiments, we did not perform LD50 experiments but carried out exploratory evaluations of safety of the solvents and the selected compounds.

For our studies a similar formulation derived from organic solvents which is completely miscible in water was produced to dissolve four of the compounds from the *in silico* hit molecules. These molecules with their corresponding vehicles were then tested in the MCAO model in mice. The compounds tested in this investigation were nitrendipine, diprophylline, methocarbamol, and floxuridine. These compounds were selected for the initial preliminary *in vivo* studies and were also compounds that were simultaneously tested in the *in vitro* experiments (Chapter 5).

6.4 Aims and objectives of in vivo studies in experimental stroke

1. Identify a vehicle suitable to allow solubility of the compounds for injection in the MCAO model.

2. Investigate the efficacy and safety of the *in silico* hits in the tMCAO and pMCAO models.

6.5 Results

6.5.1 Nitrendipine

Of the four compounds tested, the least soluble compound was nitrendipine with a solubility of 1.9-2.1 mg/L, as well as exhibiting a rapid first pass metabolism (concentration of the drug is significantly reduced before reaching blood circulation by the liver) when administered orally.⁵²² Thackaberry *et al*⁵²³ have previously reported that intravenous tolerability of ethanol in mice was 5% (197 mg/kg), DMSO at 30% (1650 mg/kg) and *N*-methyl pyrrolidone (NMP) 10% (514 mg/kg). At higher concentrations of ethanol, they observed that the mice exhibited ataxia, rapid breathing, and rigid torsos after administration. Therefore, it was important to first identify the concentrations of combined solvents needed to dissolve nitrendipine. Table 6.1 summarises the results of the solubility tests performed and amounts of each solvent combination used. Nitrendipine was soluble in three vehicles as listed below.

1. Va = 25% DMSO, 30% PEG 400, 5% Tween 80 and 40% H₂O
2. Vb = 20% EtOH, 30% PEG, 50% H₂O
3. Vc = 20 % NMP, 30% PEG, 50% H₂O

The levels for ethanol and NMP in these solutions exceeded the recommended range for animal studies, therefore prior to the initial pilot safety study of the compounds, these vehicles were injected into healthy mice to determine how well they were tolerated. This work was performed jointly with Dr Saurabh Jain and the results demonstrated that from the above, only Va and Vc were tolerated well in the mice. The mice that were injected with Vb showed signs of vocalisation and signs of struggle during injection. In addition, tremor and a longer recovery time was observed after the administration. Therefore, Va and Vc were chosen as the potential vehicles to be used for the next stage of the study.

Table 6. 1 The solubility of the compounds selected for *in vivo* studies.

Compound	pKa	Solvent	Solubility
Nitrendipine (4507)	5.43 ⁵²⁴	100 % H ₂ O	Insoluble
		50% TEG, 50% H ₂ O	Insoluble
		PEG400 10%, 20%, 30%, 40%, 50% in H ₂ O	Insoluble
		Cyclodextrin 10%, 20%, 30%, 40%, 50% in H ₂ O	Insoluble
		50% TEG, 10% DMSO 40% H ₂ O	Insoluble
		50% Cyclodextrin, 10% DMSO 40% H ₂ O	Insoluble
		15% DMSO, 30% PEG 400, 5% Tween 80 and 50% H ₂ O	Insoluble
		20% DMSO, 30% PEG 400, 5% Tween 80 and 45% H ₂ O	Partially soluble
		25% DMSO, 30% PEG 400, 5% Tween 80 and 40% H₂O	1 mg/ml
		100 % EtOH	Soluble
		15% EtOH, 15% PEG, 70% H ₂ O	Insoluble
		20% EtOH, 15% PEG, 65% H ₂ O	Insoluble
		25% EtOH, 15% PEG, 60% H ₂ O	Partially soluble
		10% EtOH, 30% PEG, 60% H ₂ O	Insoluble
		15% EtOH, 30% PEG, 55% H ₂ O	Partially soluble
		20% EtOH, 30% PEG, 50% H₂O	1 mg/ml
5% NMP, 30% PEG, 65% H ₂ O	Insoluble		
10% NMP, 30% PEG, 60% H ₂ O	Partially soluble		
20% NMP, 30% PEG, 50% H₂O	1 mg/ml		

All samples (1 mg/ml) heated in water bath 30 °C and sonicated for 30 min.

Polyethylene glycol 400 (PEG 400) , Triethylene glycol, polysorbate 80 (Tween 80), Ethanol (EtOH), dimethylsulfoxide (DMSO) and *N*-methylpyrrolidone (NMP)

The lower dose and high dose for nitrendipine that was soluble in both Va and Vc vehicles is given in Table 6.3.

Table 6. 2 Solvents used to dissolve higher dose of nitrendipine

Dose in vehicle (mg/ml)	<i>In vivo</i> Dose (mg/kg)	Vehicle	Solubility
25	100	Va, Vc	Insoluble
20	80	Va, Vc	Insoluble
15 (high dose)	60	Va	Soluble
15	60	Vc	Insoluble
10	40	Vc	Insoluble
9.5	38	Vc	Insoluble
8.5 (high dose)	34	Vc	Soluble
2.5 (low dose)	10	Va, Vc	Soluble

All samples heated in water bath 30 °C and sonicated for 30 min.

Va (25% DMSO, 30% PEG 400, 5% Tween 80 and 40% H₂O) and Vc (20 % NMP, 30% PEG, 50% H₂O)

Nitrendipine at higher doses did not dissolve in the solutions and led to precipitation. Above 15 mg precipitation ensued, even after the solutions were left in the water bath at 30°C for up to 1 hour.

6.5.2 Diprophylline, methocarbamol and floxuridine

Diprophylline, methocarbamol, and floxuridine were much more water soluble. Diprophylline has polar functional groups such as a 1,2-butanediol group and the presence of the carbamate in methocarbamol increases the polarity. The polar segment in floxuridine is the deoxyribose unit which enhances its water solubility. The maximum amounts of compounds dissolved in the Va vehicle is demonstrated in Table 6.5 as well as the negative base10 logarithm of the acid dissociation constant (Ka) of solution (pKa); an increase in quantity of compound resulted in precipitation of the samples in the vehicles due to insolubility.

Table 6. 3 The maximum amount of the compounds dissolved in Va solution.

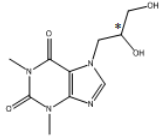
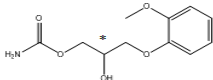
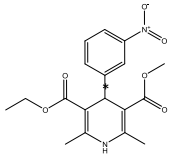
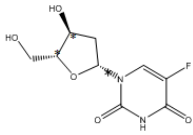
Compound	Predicted Pka ⁵²⁴	Amount (mg/ml)	Solvent	Solubility
3182 (Diprophylline)	13.74 ±0.20	40	Va	Soluble
4107 (Methocarbamol)	13.08±0.20	50	Va	Soluble
5790 (Floxuridine)	7.44	100	Va	Soluble

Va (25% DMSO, 30% PEG 400, 5% Tween 80 and 40% H2O)

6.5.3 Efficacy against tMCAO

The formula was used to convert the dose (mg/ml) to the required *in vivo* dose (mg/kg).⁵²⁵ The doses used for the animal studies are summarised in Table 6.4.

Table 6. 4 Compounds tested against MCAO

Compound	Structure	MW (g/mol)	Injection in 25g mouse	Dose vehicle (mg/ml)	in <i>In vivo</i> Dose (mg/kg)
Diprophylline (3182)		254.24	100 µl	40	160
Methocarbamol (4107)		241.24	100 µl	40 50	160 200
Nitrendipine (4507)		360.36	100 µl	~15	60
Floxuridine (5790)		246.19	100 µl	40 100	160 400

Vehicle 25% DMSO, 30% PEG 400, 5% Tween 80 and 40% H₂O Inject 100µl in 25 g mouse
(-) Stereocenter

Nitrendipine was tested for efficacy in tMCAO using vehicle Vc (20% NMP, 30% PEG, 50% H₂O). The initial pilot study with the vehicles demonstrated that vehicle Vc was tolerated well in healthy mice. Therefore, a low dose of 10 mg/kg and a high dose of 35 mg/kg was prepared and tested for efficacy in the *in vivo* tMCAO model.

In tMCAO, the infarct volume for no vehicle group was 31%, while the treated vehicle Vc group was 19% (Figure 6.4). This large reduction in infarct volume induced by the vehicle made analysis of the effect of nitrendipine difficult for both doses tested. Both the lower and higher doses were able to reduce the infarct volume by ~2.2 fold, 14.5% and 14.3% mean infarct volume respectively. No significant difference between the two doses in terms of their effect on infarct volume was observed. Further biological repeats would be required to confirm the results.

A limiting factor of this study is low sample size for each dose (low dose N=4 and high dose N=3) which led to difficulties in evaluating the effect of these compounds fully. Further studies with larger sample sizes and power are needed.

tMCAO mice C57 (TTC at 48 hrs)
Treatment of nitrendipine administered at ischemia onset

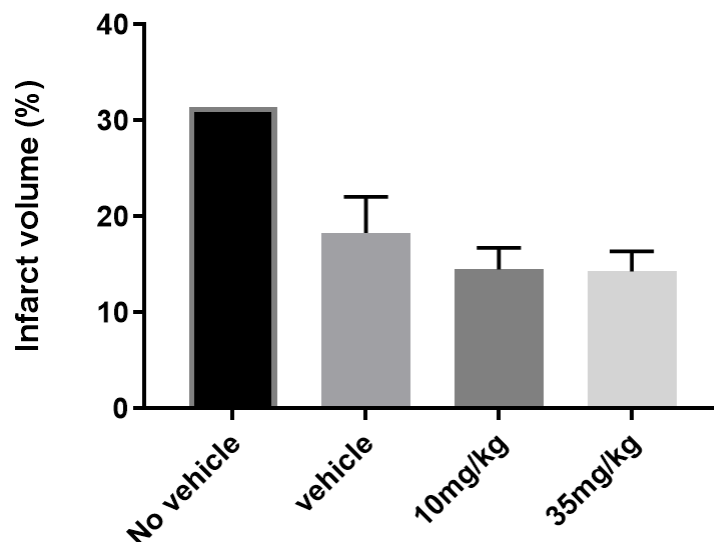


Figure 6. 2 Vehicle (Vc) and using nitrendipine.

Infarct volume for the vehicle Vc and the two doses of nitrendipine tested at 10 mg/kg and 35 mg/kg. Both doses of nitrendipine tested in tMCAO vehicle demonstrated similar infarct volume reduction. One-way ANOVA $p=0.0781$, no vehicle ($n=1$), vehicle ($n=3$), low dose 10 mg/kg ($n=4$) and high dose ($n=3$).

6.5.4 Efficacy against pMCAO

As the Vc vehicle had exhibited some efficacy in the tMCAO studies, the alternative vehicle Va was used to test the compounds in further studies using the pMCAO model. (tMCAO was not available for further studies due to the departure of Dr Jain from the University). The Va vehicle exhibited a slightly higher percentage of infarct volume (13.14%) compared to the pMCAO control mouse (11.3%), Figure 6.4. This finding indicates that the vehicle induced some toxicity and therefore may mask the beneficial effects of the drug being tested.

Nitrendipine 60 mg/kg exhibited a trend towards reduced infarct volume (10.38%, # $p=0.09$) compared to vehicle group, 13.4%.

Diprophylline 160 mg/kg significantly reduced infarct volume (8.24%, $p=0.006$). It was also well tolerated with no signs of ataxia and the mice recovered well after treatments.

Methocarbamol did not exhibit efficacy at low dose (160 mg/kg) and at high dose (200 mg/kg) with percentage infarct at 13.97% and 14.66%, respectively (Figure 6.3). Floxuridine did not exhibit efficacy at both low dose 160 mg/kg (13.02%) and high dose 400 mg/kg (17.00%). Mice treated with floxuridine, 400 mg/kg showed clear signs of toxicity.

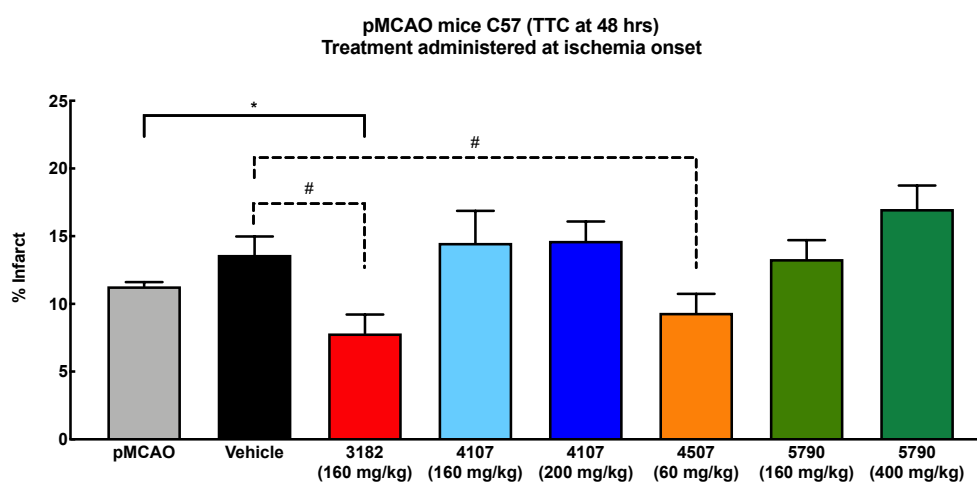


Figure 6. 3 Infarct volumes in the pMCAO model.

Control mice had 11.43% infarct volume. Diprophylline (8.24%, $p= 0.006$). Nitrendipine exhibited a trend towards reduction in infarct (10.38%, # $p= 0.09$). Methocarbamol and floxuridine did not exhibit reductions in infarct volume at both doses tested. $N=8$ mice for all treatments. Experimental results obtained from Dr DeFelice.

6.6 Discussion

An important aim of this project was to screen the *in silico* hits for efficacy and safety using *in vitro* and *in vivo* models of excitotoxicity.

As explained in Chapter 5, there was a trend towards decreased cellular injury with nitrendipine against NMDA induced excitotoxicity. In contrast, diprophylline, methocarbamol and floxuridine did not exhibit significant reductions in excitotoxicity in the *in vitro* model.

Due to COVID, access to the lab was severely curtailed and this had a significant effect on progress of this project. A decision was made to run some *in vivo*

experiments with the available compounds that were soluble, in parallel to some of the *in vitro* experiments. All the *in vitro* data were not available, and we proceeded with some *in vivo* experiments based on the availability and acceptable solubility of the compounds.

For the compounds selected, the VS from computational studies Chapter 3, (Section 2.13.1) demonstrated suggested that BE of nitrendipine was most compatible with the GluNR1 P8 region (BS1 -2.33, BS2 -1.86), followed by methocarbamol (BS1 -0.77,BS2 -0.77), diprophylline (BS1 -0.69 ,BS2 -0.69) and floxuridine (BS1 -0.60,BS2 -0.92).

6.6.1 Efficacy observed with vehicle Vc alone and in combination with nitrendipine.

Initially nitrendipine (the least soluble compound) was tested using vehicle Vc (20% NMP, 30% PEG, 50% H₂O). NMP is utilised in numerous applications such as cosmetics and insecticides.⁵²⁶ In our study, Vc containing 20% NMP was able to reduce the infarct volume in the tMCAO model. Our data show that the mice treated with the Vc vehicle exhibited a mean infarct volume of 18.3%, compared to the control group 31.4% (no vehicle) in mouse tMCAO (Figure 6.3).

This indicates that Vc has itself some neuroprotective properties. This was also a surprising result as previous studies showed that large doses of NMP were associated with an increased mortality.⁵²⁷

Conversely, Walter *et al*⁵²⁸ evaluated the effect of DMSO, PEG40, miglyol and NMP on mouse cortical neurons in controlled cortical impact (CCI) a model for traumatic brain injury. They observed that from the solvent (NMP at 0.5% and 3%) was able to reduce lesion volume 24 hours after the CCI induction as well as significantly reduce brain oedema. The mechanism of action of the solvent could be linked to dampening the inflammation response (post stroke), reducing TNF- α , interleukin 6 (IL6) and cyclo-oxygenase 2 (COX-2) proteins.⁵²⁹ Another potential mechanism of action of NMP could be as a radical scavenger and reduction of the number of biologically damaging radicals such as hydroxyl radicals (OH \cdot) and superoxide ion (O₂ \cdot^-) that are produced in the penumbra regions.⁵³⁰ (Figure 6.4).

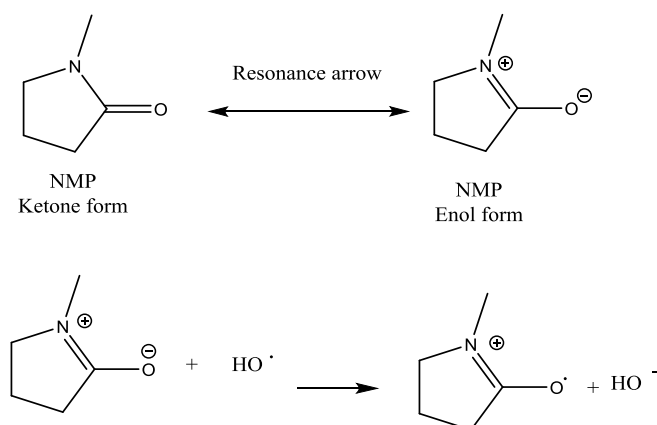


Figure 6. 4 The proposed mechanism of NMP acting as scavenger for hydroxyl radicals

Conversion of ketone form of NMP to the enol form by movement of the electrons from the oxygen in the carbonyl. The enol form can then react with the hydroxyl radicals present and produce hydroxyl ion that can obtain a hydrogen ion and form a water molecule. The enol form of NMP will subsequently be metabolised. Scheme adapted from Hua *et al.*⁵³⁰

The Vc vehicle also consisted of 30% PEG solution which has been previously shown to exhibit neuroprotective properties as well. High molecular weight PEG solutions have also been shown to be neuroprotective preventing the disruption of neuronal membranes. Membrane resealing was also observed for PEG400 in spinal cord injury models and increased the survival of damaged neurons.⁵³¹ When selecting a vehicle that can dissolve lipophilic compounds such as nitrendipine, it is essential to use the optimal ratio of amphiphilic organic solvents to ensure these amounts can be translated into clinical trials. Therefore, further investigations are needed to elucidate the effect of these organic solvents on modulating the secondary brain damage after stroke.

6.7.2 Efficacy observed for compounds tested in vehicle Va

The pMCAO analysis using Va (25% DMSO, 30% PEG 400, 5% Tween 80 and 40% H₂O), proved to be more toxic when compared to the control mice (no vehicle) in Figure 6.4. However, significant neuroprotection was still observed with; diprophylline and a strong trend towards protection with nitrendipine.

6.6.2.1 Nitrendipine

Nitrendipine which is a hypertensive drug that functions through inhibition of *L*-type Ca^{2+} channels exhibited a trend towards neuroprotection in the *in vitro* experiments using primary cortical neurons at 10 μM . Similarly, at 50 mg/kg there was a trend towards reduction in infarct volume in MCAO Figure 6.4 compared to vehicle control, but this did not reach significance $p=0.09$. This could potentially be explained by the toxicity of the vehicle Va. Another more compatible and safer vehicle might help to provide a clearer indication of the extent of neuroprotection.

Another important consideration is that nitrendipine due to poor solubility may precipitate in the blood stream after the injection and therefore not allow the entire provided dose to reach the target site. Further studies are needed to fully explore the best vehicle, dose and therapeutic time window.

6.6.2.2 Diprophylline

Diprophylline is a xanthine analogue that is mainly used for the treatment of respiratory conditions such as asthma and bronchitis.⁵³² Its bronchodilator and vasodilator properties have been highlighted above, and the proposed mechanism of action is competitive inhibition of phosphodiesterase activity which causes elevation of cyclic AMP and relaxation of smooth muscles. It has also been shown to act as an adenosine receptor antagonist.^{533,534} The A_1 subtype adenosine receptor subtype is expressed in the CNS, mainly within the brain cortex, cerebellum and hippocampus.⁵³⁵ There have been reports of A_1 inhibition can modulate the release of glutamate which is the key NT responsible in ischaemic injury pathways.⁵³⁶ Stockwell *et al*⁵³⁷ demonstrated that neuronal death after induced hypoxia in an *in vitro* study using rat hippocampal slices can be increased by selective AR_1 agonist *N*6-cyclopentyladenosine (CPA). In addition, they also demonstrated that using phosphatase inhibitors (okadaic acid 3 nM) can significantly reduce neuronal damage observed following 20 minutes of hypoxia in the hippocampal slices using PI cell death staining techniques.

These data could also explain to some extent the lack of activity observed for diprophylline in the *in vitro* assay. As the *in vivo* model is a much more complex and includes the effect of blood flow and blood vessels, this mechanism of action of

diprophylline, which ultimately may lead to dilation of the blood vessels and allow enhanced blood flow to the damaged region of the brain can take place.

While I am not able to demonstrate that diprophylline has any effect on NMDA toxicity, its overall neuroprotective effect could have clinical applications. Further studies are needed to assess this further including the best solvent, optimal dose and therapeutic time window.

6.6.2.3 Methocarbamol and floxuridine

Methocarbamol and floxuridine were unable to show any improvements and reduction of infarct. Here again, the toxicity may also have contributed due to the vehicle (Va) used to dissolve the drugs. Methocarbamol contains a carbamate and it has shown to have muscle relaxant effects, possibly due to interactions with GABA receptors, however its exact mechanism of action has not been elucidated yet.⁵³⁸

Floxuridine is a pyrimidine analogue that prevents the S-phase cell division which is where DNA in the cells is replicated and is able to selectively inhibit cells that are undergoing division. It is mainly used in the field of oncology as it can be used to treat colorectal, kidney and breast cancer.⁵³⁹ Once floxuridine is in the biological system, it can breakdown to 5-fluorouracil that is able to inhibit DNA synthesis and RNA sequence formation by taking the place of uracil which is one of the four bases in the nucleic acid RNA. Although neurons do not divide in adult mice and most of the cerebral cortical neurons are only generated in the embryonic days E11-17 in mice,⁵⁴⁰ it may be that the toxicity observed for floxuridine is produced through an alternative route. This observation agrees with that of Han *et al*,⁵⁴¹ where they observed that when mice were given 40 mg/kg of the floxuridine it led to greater damage to the myelinated track which caused toxicity in the animals. They observed the damages become progressively worse and therefore the toxicity was not only limited to the dividing cells. Weng *et al*⁵⁴² has argued that the demyelination observed with the chemical reagent Floxuridine may be due to the death of the oligodendrocyte precursor cells.

6.7 Limitation of the study

There are several limitations of this work. The selection of compounds occurred when the full *in vitro* data were not available. Three of the compounds did not exhibit

any *in vitro* effect on NMDA toxicity. However, one of the compounds diprophylline exhibited robust neuroprotection but no protection against NMDA toxicity *in vitro*. It is likely that this drug would not have been selected for *in vivo* testing based on the *in vitro* data alone. This highlights the limitation of the *in vitro* studies which often use models which cannot fully replicate the complex *in vivo* system which involves many different pathways.

Another limitation of our work is that the solvents used had some intrinsic toxic or neuroprotective properties. This has the effect of obscuring the true neuroprotective effect of the selected compounds. Future studies will need to design optimal solvents devoid of intrinsic toxic or protective activity to fully understand the extent of neuroprotection observed.

Another significant limitation is the small sample sizes of the *in vivo* studies. This was partly due to limited access to this model that was available. Further studies will need to be designed with adequate sample sizes and power.

6.8 Conclusion

The modelling of stroke in mice using MCAO models is a well-established methodology used to re-create the devastating effects of stroke on the brain. In this chapter, the compounds nitrendipine, diprophylline, methocarbamol and floxuridine were selected based on *in silico* modelling, availability and solubility. They were then evaluated in the *in vivo* model.

Initially solubility tests were carried out with the least soluble compound, nitrendipine. This was to determine the maximum amount of nitrendipine that could be dissolved in a vehicle formulation which was tolerated in the *in vivo* studies. Nitrendipine showed to be soluble in the three vehicle formulations tested (Va, Vb and Vc). However, only Va and Vc were well tolerated in the mouse as Vb showed signs of distress in the animals such as signs of struggle during injection, tremor and longer recovery time after the administration. In the tMCAO model the Vc formulation had intrinsic neuroprotective properties as explained above and this made it unsuitable to be further used in the animal models to deduce efficacy of the compounds. Therefore, the Va solvent was used for the pMCAO model which also was able to dissolve the other compounds tested at relatively high doses.

In the pMCAO model, although the Va formulation proved to be to some extent toxic to the mice, compound diprophylline was neuroprotective. However, further studies are needed to fully explore the neuroprotective potential of this compound and its mechanism of action as it was not able to produce any neuroprotection in the NMDAR induced neuronal toxicity in the *in vitro* studies. Nitrendipine was also able to exhibit a trend towards reduction of the infarct volume in comparison to the control mice, but this did not reach significance. It may show better efficacy with a better suited vehicle formulation which does not have any toxic effect in the model. Compounds methocarbamol and floxuridine both failed to demonstrate neuroprotection in the doses tested.

Chapter 7. Research limitations and future work.

7.1 Mechanism of action of the drugs and development of a specific binding assay.

This project has shown interesting results regarding identification of potentially neuroprotection small molecules for ischaemic stroke, however there are some areas that are subject to limitations. Diprophylline exhibited significant neuroprotection in the *in vivo* pMCAO demonstrating efficacy in animal models of stroke. However, the mechanism of action of this compound in the model used requires further elucidated as it is not clear if the efficacy observed is related to the P8 region of the GluNR1.

In the case of nitrendipine, there was a non-statistically significant trend towards protection against NMDA toxicity *in vitro*. Similarly, there was a trend towards neuroprotection in the *in vivo* model, but again this did not reach statistical significance ($p=0.09$). Due to decreased lab access, the sample size were smaller than initially planned and future studies with larger sample size may show significance neuroprotection.

Although, there are radioligand binding studies that demonstrate nitrendipine can displace the tagged [3H] MK801 from NMDAR^{543,544} in primary cortical neuron tissues as discussed in Chapter 5.6.2; there have been no studies to investigate whether nitrendipine can also interact with the P8 region. Thus, the mechanism of action in these models still needs to be investigated, as it is still not clear if the trend in neuroprotection is linked with P8 region on the GluNR1 or other potential targets.

In an attempt to address the above issue, one possible option could be to initially isolate the therapeutic antibody from the serum of immunised mice using affinity chromatography techniques⁵⁴⁵ (Figure 7.1a,b). For complex samples, such as plasma containing a mixture of components (e.g abundant proteins/peptides like albumin and antibodies), an initial clean through depletion columns or specific immune precipitation techniques has to be carried out.⁵⁴⁶

The samples obtained will then have a higher concentration of antibodies, however the sample well still be a mixture of multiple antibodies at this stage. Therefore to ensure the correct antibody is interacting with P8 of GluNR1, an affinity column can

be used. Here a recombinant protein of P8 is stabilised onto the agarose beads of the column that contain iodoacetyl groups which can covalently bind to the reduced thiol groups (SH) of cysteine residues in the P8 sequence (VKKVICTG-C), forming a thioether bond that will attach the P8 sequence onto the agarose beads (demonstrated Figure 7.1a).⁵⁴⁷

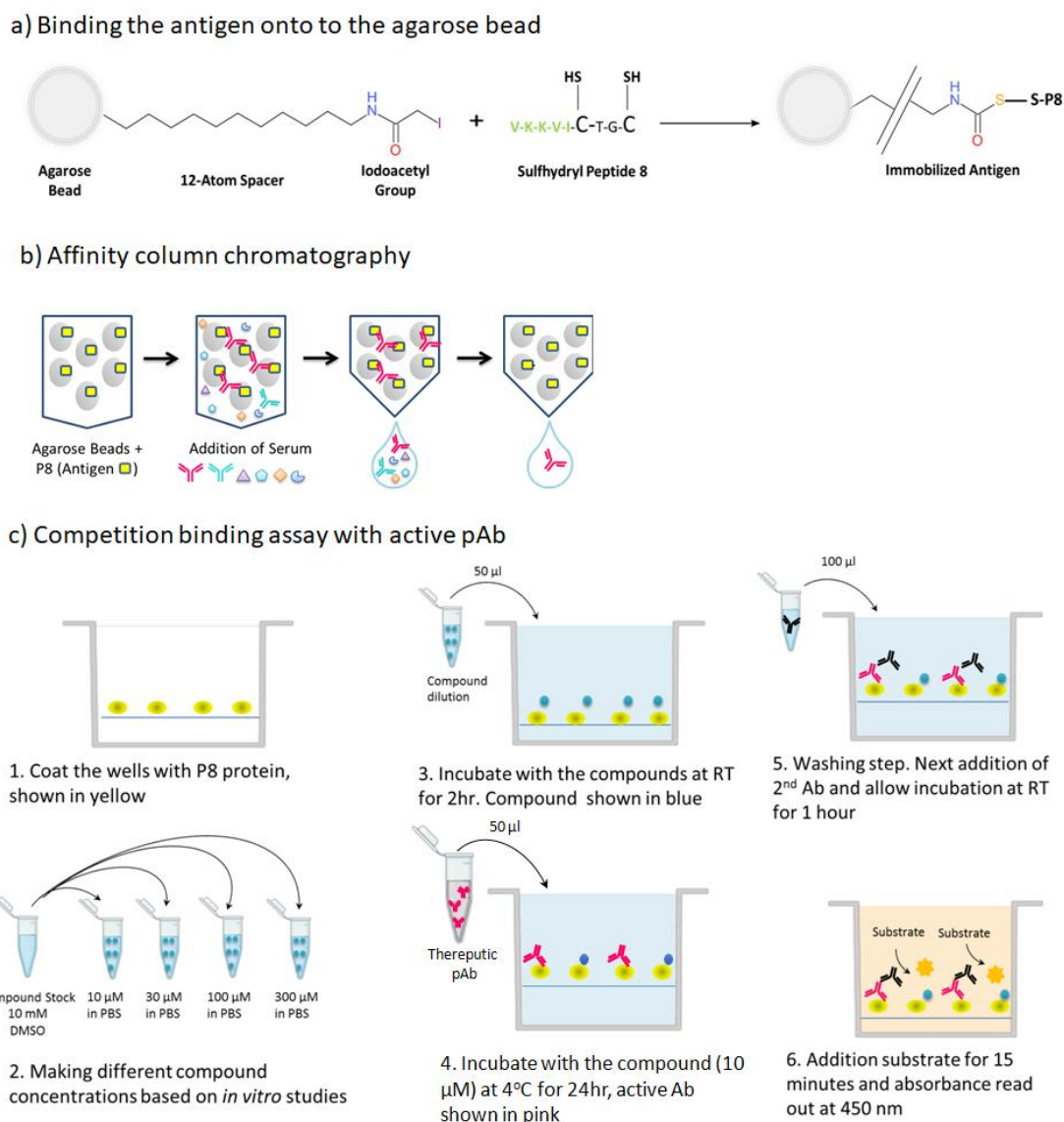


Figure 7.1 Schematic representation of pAb purification from serum and a competitive binding assay using ELISA assay

7.1a) The stabilising of the antigen P8 onto the agarose beads of the affinity column by reacting the reduced thiol groups of the antigen with the iodoacetyl groups present on the beads. **7.1b)** Affinity column chromatography, the serum containing a mixture of proteins and fatty acids passed through the column. The antibodies specific to the antigen would be bound to the agarose beads and the impurities can be washed from the sample. The final step of the column involves dilution of the target antibody from the column. **7.1c)** Demonstrating a sandwich ELISA were the GluNR1 protein containing P8 region is immobilized indirectly. 1) Initially the recombinant GluNR1 is coated onto the surface of the assay plate. 2) The compound concentrations are then prepared in a solvent compatible with the assay. 3) The compounds are pre-incubated with the antigen. 4) The primary antibody is added to the wells. 5) The unbound compounds and primary antibody are washed from the wells. 6) Finally the secondary antibody conjugate is added and it is then allowed to react with the substrate to create a signal which can be quantified.

The depleted plasma solution can then be passed through the affinity column to isolate the specific therapeutic antibody that binds to its corresponding antigen P8, (demonstrated in Figure 7.1b). By selectively isolating the therapeutic pAb a potential competition binding assay can be set up using enzyme linked immunosorbent assay (ELISA).⁵⁴⁸ In this experiment the recombinant GluNR1 protein containing the antigen (P8) can be used to coat the assay plates and subsequently used to be pre-incubated with different concentrations of the compounds. Then the primary antibody that recognises the epitope (P8) on the target antigen can be introduced onto the protein. Next the secondary antibody enzyme conjugate can be added to allow binding to the primary antibody and then using a substrate it can quantify a signal that is detectable using the relevant spectrophotometer (Figure 7.1c). This experiment can also provide further information regarding which compounds can directly interfere with the P8 segment. In addition, if any of the compounds can displace the therapeutic antibody bound to the GluNR1 protein can be determined. This assay is highly selective and specific in terms of studying the compounds that are able to directly interfere with the P8. Moreover, it is also a much cheaper and less complex form of kinetic study in comparison to alternative binding assays that incorporate antibodies and small molecules using multiplex techniques, such as surface plasma resonance (SPR) experiments.⁵⁴⁹

7.2 The limitations of the models used and future experiments to elucidate mechanism of action of the drugs.

In this study, the *in silico* hits were tested in three different models of neurodegradation linked to stroke. Initially they were examined in the HTS with the ZNStress assay and all compounds failed to show any efficacy in the model, as none of the compounds were able to reduce the amount of DsRed HSP. This was also observed with the control compounds, (i.e known NMDAR antagonists) which raised the question to what extent and how translatable the model was for studying NMDAR induced cytotoxicity. Overall, the model lacked a clear molecular pathway link to identify a potential NMDAR induced inhibitor.

Therefore, the compounds were tested in an *in vitro* assay using primary cortical neurons from mice that allowed a direct measurement of NMDAR induced cytotoxicity and identification of small molecules that could inhibit the toxicity. It is

also important to mention that *in vitro* assays have their own limitations in translatability over to *in vivo* models.

As the experiments tend to use much more regulated, for example the cells are grown within high nutrient and glucose rich environments, the results obtained may not be representative of the physiological environment of ischaemic stroke conditions.⁵⁴⁴ However, they do provide a more realistic cellular environment containing a mixture of neurons, astrocytes, other supporting glial cells. More importantly the *in vitro* experiments allowed expression of the NMDAR and throughput analysis for the compounds.

For nitrendipine, there was a trend towards neuroprotection in the *in vitro* assay at 10 μ M. This trend towards efficacy was also observed in the *in vivo* model. Future studies with larger sample size with sufficient statistical power are needed. Diprophylline failed to show any effect in the *in vitro* assay but exhibited a neuroprotective effect in the pMCAO model.

However, the exact mechanism of action of the drug in the model is not known and there may be other targets that diprophylline could be interacting with which could explain the efficacy observed in the MCAO model. Therefore, as well as the potential binding assay explained in this Chapter (segment 7.1), which could examine if the drug is interacting with the P8 sequence, other studies such as patch clamp electrophysiology could be used to understand the mechanism of action for diprophylline by measuring the whole cell currents produced by NMDA to what extent, if any, are reduced by diprophylline in comparison to the control. This technique can also allow the study of an isolated single subtype of the NMDAR such as GluNR1/GluNR2b.⁵⁵⁰ The whole cell clamp analysis thus can quantify the cell excitability and elucidate the mechanism of action of these small molecules and if they are able to modulate the NMDAR.

7.3 Experimental limitations

As with most experimental work, the design of such studies is subject to limitations. The *in vitro* assay using primary cortical neurons was the segment of the study that was greatly influenced by time constraints. Therefore, if further time was available

during the project, it would have allowed testing of the other *in silico* hit compounds in the primary cortical NMDAR induced excitotoxicity assay.

Optimisation of the assay proved to be challenging as the cell cultures used in all some of the biological repeats showed discrepancies. In addition, as primary cortical neurons proved to be extremely sensitive to their environments, many cells died prior to the initiation of the experiments. As explained in Chapter 6.6.1 there was also difficulty in demonstrating clear statistically significant reduction in toxicity. Therefore, although the experiments provided a mechanistic understanding of the effectiveness of the compounds, increasing the biological sample size could have further verified these initial findings.

It is also important to mention that although during ischaemic stroke there is an increase in the permeability of the BBB,⁵⁵¹ the bioavailability of the drugs still need to be elucidated. This is of course essential for development of any therapeutics for ischaemic stroke. The ADMET studies, as explained in Chapter 3.6.8 predicted poor BBB permeability for both nitrendipine and diprophylline within the range of data to allow prediction of P-gp efflux pump activity and plasma protein binding to substrates. However, it was not possible to obtain reasonable predictions for these compounds. Manjunath *et al*⁵⁵² in the past had reported that nitrendipine in a suspension format cannot cross the BBB effectively and was able to demonstrate that the BBB permeability can be improved up to 4.51 folds when administered with solid lipid nanoparticles in biodistribution studies. In the case of the diprophylline, there are no studies that examined its distribution across the BBB.

Therefore, a potential future study could also be to examine how well each compound is able cross the BBB by initially a using less complex model such as a static BBB model (e.g monolayer of endothelial cells) and more efficient triple co-cultured BBB models using a combination of endothelial cells with astrocytes/pericytes.⁵⁵³ Assays such as human P-gp ATPase can also evaluate BBB permeability of diprophylline and nitrendipine. The assay measures if any of the compounds are substrates for the efflux pump P-gp using a cell line tha expresses P-gps or one that can be transfected with Multidrug Resistance mutation 1 (MDR1) gene. The inhibition of the compounds is measured with fluorescence indicator

assays using rhodamine-123 or calcein, where the inhibition/substrates of the efflux pumps would result in accumulation of the dye in the experimental wells.⁵⁵⁴

7.4 Conclusion

The mechanism of ischaemic stroke is complex, triggering multiple processes such as energy failure, dyshomeostasis of ions in the cells leading to excitotoxicity, free radical formations, inflammation processes and the breakdown of the BBB. All of these pathologies are interrelated and contribute to the necrotic cell death in the ischaemic core. However, the penumbra region surrounding the ischaemic core can be salvaged with a timely neuroprotective intervention. This investigation aimed to use rational drug design and SBVS methods to identify small molecules that could target novel site on the NMDAR P8 region. In addition, a study of selected compounds, their safety and efficacy profiles in neuroprotective models both *in vitro* using primary cortical neurons and *in vivo* models using initially ZNStress phenotypic HTS assay and mouse MCAO model of stroke was conducted.

The virtual screening segment of the project was completed by screening over ~25,000 compounds from commercial vendors and in-house libraries. The initial library of compounds was narrowed down to 24 compounds that interacted well with the novel binding site around the P8 region of NMDAR and had reasonable ADMET properties predicted from the computational studies. Although, none of the compounds tested in the *in vitro* assay were able to show significant reduction of NMDAR excitotoxicity; in mouse experimental stroke, nitrendipine exhibited a strong trend towards protection and diprophylline exhibited significant protection. Future studies with larger sample sizes are needed to fully explore safety and efficacy and to elucidate the mechanisms of action of these drugs.

Chapter 8. References

- 1 Reda C, Kaufmann E, Delahaye-Duriez A. Machine learning applications in drug development. *Computational and Structural Biotechnology Journal*. 2020;18:241-52.
- 2 Kiriiri GK, Njogu PM, Mwangi AN. Exploring different approaches to improve the success of drug discovery and development projects: a review. *Future Journal of Pharmaceutical Sciences*. 2020;6(1).
- 3 Hughes JP, Rees S, Kalindjian SB, Philpott KL. Principles of early drug discovery. *British Journal of Pharmacology*. 2011;162(6):1239-49.
- 4 Yang Y, Adelstein SJ, Kassis AI. Target discovery from data mining approaches. *Drug Discovery Today*. 2009;14(3-4):147-54.
- 5 Gashaw I, Ellinghaus P, Sommer A, Asadullah K. What makes a good drug target? *Drug Discovery Today*. 2011;16(23-24):1037-43.
- 6 Brown DG, Bostrom J. Where Do Recent Small Molecule Clinical Development Candidates Come From? *Journal of Medicinal Chemistry*. 2018;61(21):9442-68.
- 7 Simpson.G (2018) CMT Drug Development Process and Therapy Pipeline, Available at: <https://cmtrf.org/research/cmt-research-pipeline/> (Accessed: 9th June 2020).
- 8 Li QX. Application of Fragment-Based Drug Discovery to Versatile Targets. *Frontiers in Molecular Biosciences*. 2020;7.
- 9 Lombardino JG, Lowe JA. The role of the medicinal chemist in drug discovery - Then and now. *Nature Reviews Drug Discovery*. 2004;3(10):853-62.
- 10 Moffat JG, Vincent F, Lee JA, Eder J, Prunotto M. Opportunities and challenges in phenotypic drug discovery: an industry perspective. *Nature Reviews Drug Discovery*. 2017;16(8):531-43.
- 11 Wu LL, Huang CS, Emery B, Sedgwick AC, Bull SD, He XP, et al. Förster resonance energy transfer (FRET)-based small-molecule sensors and imaging agents. *Chemical Society Reviews*. 2020;49(15):5110-39.
- 12 Ou-Yang S-s, Lu J-y, Kong X-q, Liang Z-j, Luo C, Jiang H. Computational drug discovery. *Acta Pharmacologica Sinica*. 2012;33(9):1131-40.
- 13 Eske.J (2020) What is the difference between in vivo and in vitro?, Available at: <https://www.medicalnewstoday.com/articles/in-vivo-vs-in-vitro> (Accessed: 24th August 2021).
- 14 Lombardino JG, Lowe JA. The role of the medicinal chemist in drug discovery - Then and now. *Nature Reviews Drug Discovery*. 2004;3(10):853-62.
- 15 Sartorius (2020) 'The Importance of ADMET in Early Drug Discovery and Development', *The Scientist*, Available at: <https://www.the-scientist.com/the-marketplace/the-importance-of-admet-in-early-drug-discovery-and-development-a-conversation-with-mandy-xu-of-pharmaron-67606>.
- 16 Medicines and Healthcare products Regulatory Agency (11 December 2020) MHRA post-transition period information , Available at: <https://www.gov.uk/government/collections/mhra-post-transition-period-information> (Accessed: 13th December 2020).
- 17 World health organisation (2018) Global Health Estimates 2016, Available at: <http://www.who.int/en/news-room/fact-sheets/detail/the-top-10-causes-of-death> (Accessed: 14th June 2018).

- 18 King D, Wittenberg R, Patel A, Quayyum Z, Berdunov V, Knapp M. The future incidence, prevalence and costs of stroke in the UK. *Age and Ageing*. 2020;49(2):277-82.
- 19 Strong K, Mathers C, Bonita R. Preventing stroke: saving lives around the world. *Lancet Neurology*. 2007;6(2):182-7.
- 20 National Stroke Association (2018) Stroke facts, Available at: <http://www.stroke.org/understand-stroke/what-stroke/stroke-facts> (Accessed: 10th May 2018).
- 21 'Stroke guidelines', Royal College of Physicians. 2016.
- 22 Dirnagl U, Iadecola C, Moskowitz MA. Pathobiology of ischaemic stroke: an integrated view. *Trends in Neurosciences*. 1999;22(9): 391-7
- 23 Woodruff TM, Thundyil J, Tang S-C, Sobey CG, Taylor SM, Arumugam TV. Pathophysiology, treatment, and animal and cellular models of human ischemic stroke. *Molecular Neurodegeneration*. 2011;6.
- 24 Lo EH. A new penumbra: transitioning from injury into repair after stroke. *Nature Medicine*. 2008;14(5):497-500.
- 25 Lee JM, Zipfel GJ, Choi DW. The changing landscape of ischaemic brain injury mechanisms. *Nature*. 1999;399(6738):A7-A14.
- 26 Hossmann KA. The two pathophysiologies of focal brain ischemia: implications for translational stroke research. *Journal of Cerebral Blood Flow and Metabolism*. 2012;32(7):1310-6.
- 27 Dirnagl U. Inflammation in stroke: The good, the bad, and the unknown. *Neuroinflammation in Stroke*. 2004;47:87-99.
- 28 Intercollegiate Stroke Working Party. National clinical guideline for stroke. 2016; 5th edn, London: Royal College of Physicians.
- 29 Nedeltchev K, der Maur TA, Georgiadis D, Arnold M, Caso V, Mattle HP, et al. Ischaemic stroke in young adults: predictors of outcome and recurrence. *Journal of Neurology Neurosurgery and Psychiatry*. 2005;76(2):191-5.
- 30 Benjamin. Heart Disease and Stroke Statistics-2017 Update: A Report From the American Heart Association (vol 135, pg e146, 2017). *Circulation*. 2017;135(10):E646-E.
- 31 Wolters FJ, Paul NLM, Li L, Rothwell PM, Oxford Vasc S. Sustained impact of UK FAST-test public education on response to stroke: a population-based time-series study. *International Journal of Stroke*. 2015;10(7):1108-14.
- 32 Simard JM, Chen M, Tarasov KV, Bhatta S, Ivanova S, Melnitchenko L, et al. Newly expressed SUR1-regulated NCCa-ATP channel mediates cerebral edema after ischemic stroke. *Nature Medicine*. 2006;12(4):433-40.
- 33 Dirnagl U. Inflammation in stroke: The good, the bad, and the unknown. *Neuroinflammation in Stroke*. 2004;47:87-99.
- 34 Allen CL, Bayraktutan U. Oxidative stress and its role in the pathogenesis of ischaemic stroke. *International Journal of Stroke*. 2009;4(6):461-70.
- 35 Strandgaard S, Paulson OB. CEREBRAL BLOOD-FLOW AND ITS PATHOPHYSIOLOGY IN HYPERTENSION. *American Journal of Hypertension*. 1989;2(6):486-92.
- 36 Janardhan V, Qureshi AI. Mechanisms of ischemic brain injury. *Current cardiology reports*. 2004;6(2):117-23.
- 37 Chamorro A, Dirnagl U, Urra X, Planas AM. Neuroprotection in acute stroke:

- targeting excitotoxicity, oxidative and nitrosative stress, and inflammation. *Lancet Neurology*. 2016;15(8):869-81.
- 38 Neuhaus AA, Couch Y, Hadley G, Buchan AM. Neuroprotection in stroke: the importance of collaboration and reproducibility. *Brain*. 2017;140:2079-92.
- 39 Zhou X, Hollern D, Liao J, Andrechek E, Wang H. NMDA receptor-mediated excitotoxicity depends on the coactivation of synaptic and extrasynaptic receptors. *Cell Death & Disease*. 2013;4.
- 40 Inagaki N, Kuromi H, Gono T, Okamoto Y, Ishida H, Seino Y, et al. Expression and role of ionotropic glutamate receptors in pancreatic-islet cells. *FASEB Journal*. 1995;9(8):686-91.
- 41 Kalia LV, Kalia SK, Salter MW. NMDA receptors in clinical neurology: excitatory times ahead. *Lancet Neurology*. 2008;7(8):742-55.
- 42 Villanueva C, Kross RD, Perez-Astudillo L. Free Radicals and Neuronal Recovery from an Ischaemic Penumbra: A Review. *Free Radicals and Diseases*. 2016:299-314.
- 43 Weber JT. Altered calcium signaling following traumatic brain injury. *Frontiers in Pharmacology*. 2012;3.
- 44 Szydłowska K, Tymianski M. Calcium, ischemia and excitotoxicity. *Cell Calcium*. 2010;47(2):122-9.
- 45 Choi WS, Lee EH, Chung CW, Jung YK, Jin BK, Kim SU, et al. Cleavage of Bax is mediated by caspase-dependent or -independent calpain activation in dopaminergic neuronal cells: protective role of Bcl-2. *Journal of Neurochemistry*. 2001;77(6):1531-41.
- 46 Chen Q, Kang J, Fu C. The independence of and associations among apoptosis, autophagy, and necrosis. *Signal Transduction and Targeted Therapy*. 2018;3.
- 47 Rothman S. Synaptic release of excitatory amino-acid neurotransmitter mediates anoxic neuronal death. *Journal of Neuroscience*. 1984;4(7):1884-91
- 48 Manzanero S, Santro T, Arumugam TV. Neuronal oxidative stress in acute ischemic stroke: Sources and contribution to cell injury. *Neurochemistry International*. 2013;62(5):712-8.
- 49 Ahmadinejad F, Moller SG, Hashemzadeh-Chaleshtori M, Bidkhorri G, Jami M-S. Molecular Mechanisms behind Free Radical Scavengers Function against Oxidative Stress. *Antioxidants*. 2017;6(3).
- 50 Li Y, Sun J, Wu R, Bai J, Hou Y, Zeng Y, et al. Mitochondrial MPTP: A Novel Target of Ethnomedicine for Stroke Treatment by Apoptosis Inhibition. *Frontiers in Pharmacology*. 2020;11.
- 51 Hudome S, Palmer C, Roberts RL, Mauger D, Housman C, Towfighi J. The role of neutrophils in the production of hypoxic-ischemic brain injury in the neonatal rat. *Pediatric Research*. 1997;41(5):607-16.
- 52 Dong R, Huang R, Wang J, Liu H, Xu Z. Effects of Microglial Activation and Polarization on Brain Injury After Stroke. *Frontiers in Neurology*. 2021;12.
- 53 Pawluk H, Wozniak A, Grzesk G, Kolodziejska R, Kozakiewicz M, Kopkowska E, et al. The Role of Selected Pro-Inflammatory Cytokines in Pathogenesis of Ischemic Stroke. *Clinical Interventions in Aging*. 2020;15:469-84.
- 54 Patel AR, Ritzel R, McCullough LD, Liu F. Microglia and ischemic stroke: a double-edged sword. *International journal of physiology, pathophysiology and*

- pharmacology. 2013;5(2):73-90.
- 55 Guruswamy R, ElAli A. Complex Roles of Microglial Cells in Ischemic Stroke Pathobiology: New Insights and Future Directions. *International Journal of Molecular Sciences*. 2017;18(3).
- 56 Yang C, Hawkins KE, Dore S, Candelario-Jalil E. Neuroinflammatory mechanisms of blood-brain barrier damage in ischemic stroke. *American Journal of Physiology-Cell Physiology*. 2019;316(2):C135-C53.
- 57 Barar J, Rafi MA, Pourseif MM, Omid Y. Blood-brain barrier transport machineries and targeted therapy of brain diseases. *Bioimpacts*. 2016;6(4):225-48.
- 58 Woodruff TM, Thundyil J, Tang S-C, Sobey CG, Taylor SM, Arumugam TV. Pathophysiology, treatment, and animal and cellular models of human ischemic stroke. *Molecular Neurodegeneration*. 2011;6.
- 59 El Tawil S, Muir KW. Thrombolysis and thrombectomy for acute ischaemic stroke. *Clinical Medicine*. 2017;17(2):161-5.
- 60 Yaghi S, Eisenberger A, Willey JZ. Symptomatic Intracerebral Hemorrhage in Acute Ischemic Stroke After Thrombolysis With Intravenous Recombinant Tissue Plasminogen Activator A Review of Natural History and Treatment. *Jama Neurology*. 2014;71(9):1181-5.
- 61 Powers WJ, Rabinstein AA, Ackerson T, Adeoye OM, Bambakidis NC, Becker K, et al. 2018 Guidelines for the Early Management of Patients With Acute Ischemic Stroke: A Guideline for Healthcare Professionals From the American Heart Association/American Stroke Association. *Stroke*. 2018;49(3):E46-E110.
- 62 Bracard S, Ducrocq X, Guillemin F, Moulin T, Mas JL. Mechanical thrombectomy after intravenous thrombolysis for acute ischaemic stroke Reply. *Lancet Neurology*. 2017;16(2):104-.
- 63 Unal-Cevik I, Kilinc M, Can A, Gursoy-Ozdemir Y, Dalkara T. Apoptotic and necrotic death mechanisms are concomitantly activated in the same cell after cerebral ischemia. *Stroke*. 2004;35(9):2189-94.
- 64 Li CR, Engstrom G, Hedblad B, Berglund G, Janzon L. Risk factors for stroke in subjects with normal blood pressure - A prospective cohort study. *Stroke*. 2005;36(2):234-8.
- 65 Sleight P. The HOPE Study (Heart Outcomes Prevention Evaluation). *Journal of the renin-angiotensin-aldosterone system: JRAAS*. 2000;1(1):18-20.
- 66 Seiffge DJ, Werring DJ, Paciaroni M, Dawson J, Warach S, Milling TJ, et al. Timing of anticoagulation after recent ischaemic stroke in patients with atrial fibrillation. *Lancet Neurology*. 2019;18(1):117-26.
- 67 Verdoorn TA, Dingleline R. EXCITATORY AMINO-ACID RECEPTORS EXPRESSED IN XENOPUS OOCYTES - AGONIST PHARMACOLOGY. *Molecular Pharmacology*. 1988;34(3):298-307.
- 68 Mayer ML. Glutamate receptor ion channels. *Current Opinion in Neurobiology*. 2005;15(3):282-8.
- 69 Bernabeu R, Sharp FR. NMDA and AMPA/kainate glutamate receptors modulate dentate neurogenesis and CA3 synapsin-I in normal and ischemic hippocampus. *Journal of Cerebral Blood Flow and Metabolism*. 2000;20(12):1669-80.
- 70 Regan MC, Rornero-Hernandez A, Furukawa H. A structural biology

- perspective on NMDA receptor pharmacology and function. *Current Opinion in Structural Biology*. 2015;33:68-75.
- 71 Seeber S, Becker K, Rau T, Eschenhagen T, Becker CM, Herkert M. Transient expression of NMDA receptor subunit NR2B in the developing rat heart. *Journal of Neurochemistry*. 2000;75(6):2472-7.
- 72 Inagaki N, Kuromi H, Gonoi T, Okamoto Y, Ishida H, Seino Y, et al. Expression and role of ionotropic glutamate receptors in pancreatic-islet cells. *Faseb Journal*. 1995;9(8):686-91.
- 73 Laketic-Ljubojevic I, Suva LJ, Maathuis FJM, Sanders D, Skerry TM. Functional characterization of N-methyl-D-aspartic acid-gated channels in bone cells. *Bone*. 1999;25(6):631-7.
- 74 Simon RP, Swan JH, Griffiths T, Meldrum BS. Blockade of N-methyl-D-aspartate receptor may protect against ischaemic damage in the brain. *Science*. 1984;226(4676):850-2.
- 75 Ghosh A, Greenberg ME. Calcium signalling in neurons-Molecular mechanisms and cellular consequences. *Science*. 1995;268(5208):239-47.
- 76 Lai TW, Zhang S, Wang YT. Excitotoxicity and stroke: Identifying novel targets for neuroprotection. *Progress in Neurobiology*. 2014;115:157-88.
- 77 Mayer ML. Glutamate receptor ion channels. *Current Opinion in Neurobiology*. 2005;15(3):282-8.
- 78 Traynelis SF, Wollmuth LP, McBain CJ, Menniti FS, Vance KM, Ogden KK, et al. Glutamate Receptor Ion Channels: Structure, Regulation, and Function. *Pharmacological Reviews*. 2010;62(3):405-96.
- 79 Soriano FX, Hardingham GE. Compartmentalized NMDA receptor signalling to survival and death. *Journal of Physiology-London*. 2007;584(2):381-7.
- 80 Regan MC, Rornero-Hernandez A, Furukawa H. A structural biology perspective on NMDA receptor pharmacology and function. *Current Opinion in Structural Biology*. 2015;33:68-75.
- 81 Flores-Soto ME, Chaparro-Huerta V, Escoto-Delgadillo M, Vazquez-Valls E, Gonzalez-Castaneda RE, Beas-Zarate C. Structure and function of NMDA-type glutamate receptor subunits. *Neurologia*. 2012;27(5):301-10.
- 82 Tingley WG, Ehlers MD, Kameyama K, Doherty C, Ptak JB, Riley CT, et al. Characterization of protein kinase A and protein kinase C phosphorylation of the N-methyl-D-aspartate receptor NR1 subunit using phosphorylation site-specific antibodies. *Journal of Biological Chemistry*. 1997;272(8):5157-66.
- 83 Traynelis SF, Hartley M, Heinemann SF. Control of proton sensitivity of the NMDA receptor by RNA splicing and polyamines. *Science*. 1995;268(5212):873-6.
- 84 Hansen KB, Ogden KK, Yuan H, Traynelis SF. Distinct Functional and Pharmacological Properties of Triheteromeric GluN1/GluN2A/GluN2B NMDA Receptors. *Neuron*. 2014;81(5):1084-96.
- 85 Paoletti P, Bellone C, Zhou Q. NMDA receptor subunit diversity: impact on receptor properties, synaptic plasticity and disease. *Nature Reviews Neuroscience*. 2013;14(6):383-400.
- 86 Monyer H, Burnashev N, Laurie DJ, Sakmann B, Seeburg PH. Developmental and regional expression in the rat-brain and functional-properties of four NMDA receptors. *Neuron*. 1994;12(3):529-40.

- 87 Davis S, Butcher SP, Morris RGM. The NMDA receptor antagonist D-2-Amino-5Phosphonpentanoate (D-AP5) impairs spatial-learning and LTP in vivo at interacerbral concentrations comparable to those that block LTP in vitro. *Journal of Neuroscience*. 1992;12(1):21-34.
- 88 Luo T, Wu W-H, Chen B-S. NMDA receptor signaling: death or survival? *Frontiers in biology*. 2011;6(6):468-76.
- 89 Yan GM, Ni BH, Weller M, Wood KA, Paul SM. Depolarization or glutamate-receptor activation blocks apoptotic cell death of cultured cerebellar granule neurones. *Brain Research*. 1994;656(1):43-51.
- 90 Zhou Q, Sheng M. NMDA receptors in nervous system diseases. *Neuropharmacology*. 2013;74:69-75.
- 91 Dobrek L, Thor P. Glutamate NMDA receptors in pathophysiology and pharmacotherapy of selected nervous system diseases. *Postepy Higieny I Medycyny Doswiadczalnej*. 2011;65:338-46.
- 92 Chittajallu R, Wester JC, Craig MT, Barksdale E, Yuan XQ, Akgul G, et al. Afferent specific role of NMDA receptors for the circuit integration of hippocampal neurogliaform cells. *Nature Communications*. 2017;8:13.
- 93 Sun J, Nan G. The extracellular signal-regulated kinase 1/2 pathway in neurological diseases: A potential therapeutic target. *International Journal of Molecular Medicine*. 2017;39(6):1338-46.
- 94 English JD, Sweatt JD. A requirement for the mitogen-activated protein kinase cascade in hippocampal long term potentiation. *Journal of Biological Chemistry*. 1997;272(31):19103-6.
- 95 Zhao H, Sapolsky RM, Steinberg GK. Phosphoinositide-3-kinase/Akt survival signal pathways are implicated in neuronal survival after stroke. *Molecular Neurobiology*. 2006;34(3):249-69.
- 96 Xavier IJ, Mercier PA, McLoughlin CM, Ali A, Woodgett JR, Ovsenek N. Glycogen synthase kinase 3 beta negatively regulates both DNA-binding and transcriptional activities of heat shock factor 1. *Journal of Biological Chemistry*. 2000;275(37):29147-52.
- 97 Miyawaki T, Mashiko T, Ofengeim D, Flannery RJ, Noh K-M, Fujisawa S, et al. Ischemic preconditioning blocks BAD translocation, Bcl-x(L) cleavage, and large channel activity in mitochondria of postischemic hippocampal neurons. *Proceedings of the National Academy of Sciences of the United States of America*. 2008;105(12):4892-7.
- 98 Zhang Y-X, Liu X-M, Wang J, Li J, Liu Y, Zhang H, et al. Inhibition of AKT/FoxO3a signaling induced PUMA expression in response to p53-independent cytotoxic effects of H1: A derivative of tetrandrine. *Cancer Biology & Therapy*. 2015;16(6):965-75.
- 99 Hardingham GE, Fukunaga Y, Bading H. Extrasynaptic NMDARs oppose synaptic NMDARs by triggering CREB shut-off and cell death pathways. *Nature Neuroscience*. 2002;5(5):405-14.
- 100 Zhou XJ, Chen ZY, Yun WW, Wang HB. NMDA receptor activity determines neuronal fate: location or number? *Reviews in the Neurosciences*. 2015;26(1):39-47.
- 101 Papadia S, Hardingham GE. The dichotomy of NMDA receptor signaling. *Neuroscientist*. 2007;13(6):572-9.

- 102 Vyklicky V, Korinek M, Smejkalova T, Balik A, Krausova B, Kaniakova M, et al. Structure, Function, and Pharmacology of NMDA Receptor Channels. *Physiological Research*. 2014;63:S191-S203.
- 103 Lipton SA, Choi YB, Pan ZH, Lei SZZ, Chen HSV, Sucher NJ, et al. A redox-based mechanism for the neuroprotective and neurodestructive effects of nitric-oxide and related nitroso-compounds. *Nature*. 1993;364(6438):626-32.
- 104 Fan X, Jin WY, Lu J, Wang J, Wang YT. Rapid and reversible knockdown of endogenous proteins by peptide-directed lysosomal degradation. *Nature Neuroscience*. 2014;17(3):471-80.
- 105 Hardingham GE, Bading H. Synaptic versus extrasynaptic NMDA receptor signalling: implications for neurodegenerative disorders. *Nature Reviews Neuroscience*. 2010;11(10):682-96.
- 106 Sinis N, Birbaumer N, Gustin S, Schwarz A, Bredanger S, Becker ST, et al. Memantine treatment of complex regional pain syndrome - A preliminary report of six cases. *Clinical Journal of Pain*. 2007;23(3):237-43.
- 107 Choi DW. Excitotoxicity: Still Hammering the Ischemic Brain in 2020. *Frontiers in Neuroscience*. 2020;14.
- 108 Lapchak PA, Boitano PD. Reflections on Neuroprotection Research and the Path Toward Clinical Success. In: Lapchak PA, Zhang JH, editors. *Neuroprotective Therapy for Stroke and Ischemic Disease*. Springer Series in Translational Stroke Research. Cham: Springer International Publishing Ag; 2017. p. 3-71.
- 109 Simon RP, Swan JH, Griffiths T, Meldrum BS. Blockade of N-methyl-D-aspartate receptors may protect against ischemic damage in the brain. *Science*. 1984;226(4676):850-2.
- 110 Song X, Jensen MO, Jogini V, Stein RA, Lee C-H, McHaourab HS, et al. Mechanism of NMDA receptor channel block by MK-801 and memantine. *Nature*. 2018;556(7702):515-+.
- 111 Ellison G. The N-methyl-D-aspartate antagonist's phencyclidine, ketamine and dizocilpine as both behavioural and anatomical models of the dementias. *Brain Research Reviews*. 1995;20(2):250-67.
- 112 Morris PJ, Moaddel R, Zanos P, Moore CE, Gould T, Zarate CA, Jr., et al. Synthesis and N-Methyl-D-aspartate (NMDA) Receptor Activity of Ketamine Metabolites. *Organic Letters*. 2017;19(17):4572-5.
- 113 Aggarwal.S (2019) Quelling of Excitotoxicity in Acute Stroke With Ketamine (QUEST-KETA), Available at: <https://clinicaltrials.gov/ct2/show/NCT03223220> (Accessed: 1st of September 2021).
- 114 Hoyte L, Barber PA, Buchan AM, Hill MD. The rise and fall of NMDA antagonists for ischemic. stroke. *Current Molecular Medicine*. 2004;4(2):131-6.
- 115 Reddy NL, Hu LY, Cotter RE, Fischer JB, Wong WJ, McBurney RN, et al. Synthesis and structure-activity studies of N,N'-diarylguanidine derivatives-N-(1-naphthyl)-N'-(3-ethylphenyl)-N'-methylguanidine- a new, selective non-competitive NMDA receptor antagonist. *Journal of Medicinal Chemistry*. 1994;37(2):260-7.
- 116 Schabitz WR, Li FH, Fisher M. The N-methyl-D-aspartate antagonist CNS 1102 protects cerebral gray and white matter from ischemic injury following temporary focal ischemia in rats. *Stroke*. 2000;31(7):1709-13

- 117 Leeson PD, Iversen LL. The glycine site on the NMDA receptor- structure-activity-relationship and therapeutic potential. *Journal of Medicinal Chemistry*. 1994;37(24):4053-67.
- 118 Di Fabio R, Tranquillini E, Bertani B, Alvaro G, Micheli F, Sabbatini F, et al. Enantiomerically pure tetrahydroquinoline derivatives as in vivo potent antagonists of the glycine binding site associated to the NMDA receptor. *Bioorganic & Medicinal Chemistry Letters*. 2003;13(21):3863-6.
- 119 Honer M, Benke D, Laube B, Kuhse J, Heckendorf R, Allgeier H, et al. Differentiation of glycine antagonist sites of N-methyl-D-aspartate receptor subtypes - Preferential interaction of CGP 61594 with NR1/2B receptors. *Journal of Biological Chemistry*. 1998;273(18):11158-63.
- 120 Woodward RM, Huettner JE, Guastella J, Keana JFW, Weber E. In vitro pharmacology of ACEA-1021 and ACEA-1031 systemically active quinoxalinediones with high affinity and selectivity for n-methyl-D-aspartate receptor glycine sites. *Molecular Pharmacology*. 1995;47(3):568-81.
- 121 Design and Synthesis of [2-(8,9-Dioxo-2,6-diazabicyclo[5.2.0]non-1(7)-en-2-yl)-ethyl]phosphonic Acid (EAA-090), a Potent N-Methyl-D-aspartate Antagonist, via the Use of 3-Cyclobutene-1,2-dione as an Achiral α -Amino Acid Bioisostere
- 122 Ogden KK, Traynelis SF. New advances in NMDA receptor pharmacology. *Trends in Pharmacological Sciences*. 2011;32(12):726-33.
- 123 Mott DD, Doherty JJ, Zhang SN, Washburn MS, Fendley MJ, Lyuboslavsky P, et al. Phenylethanolamines inhibit NMDA receptors by enhancing proton inhibition. *Nature Neuroscience*. 1998;1(8):659-67.
- 124 Chazot PL. CP-101606 Pfizer Inc. Current opinion in investigational drugs (London, England : 2000). 2000;1(3):370-4.
- 125 Ruppia.B et al. (2012). Chapter Seven - NMDA Antagonists of GluN2B Subtype and Modulators of GluN2A, GluN2C, and GluN2D Subtypes—Recent Results and Developments. In: Manoj C. Desai Annual Reports in Medicinal Chemistry. USA: NeurOp. 89-103.
- 126 Perin-Dureau F, Rachline J, Neyton J, Paoletti P. Mapping the binding site of the neuroprotectant ifenprodil on NMDA receptors. *Journal of Neuroscience*. 2002;22(14):5955-65.
- 127 Robinson DM, Keating GM. Memantine - A review of its use in Alzheimer's disease. *Drugs*. 2006;66(11):1515-34.
- 128 Kotermanski SE, Johnson JW. Mg²⁺ Imparts NMDA Receptor Subtype Selectivity to the Alzheimer's Drug Memantine. *Journal of Neuroscience*. 2009;29(9):2774-9.
- 129 Seyedsaadat SM, Kallmes DF. Memantine for the treatment of ischemic stroke: experimental benefits and clinical lack of studies. *Reviews in the Neurosciences*. 2019;30(2):203-20.
- 130 Chen B, Wang G, Li W, Liu W, Lin R, Tao J, et al. Memantine attenuates cell apoptosis by suppressing the calpain-caspase-3 pathway in an experimental model of ischemic stroke. *Experimental Cell Research*. 2017;351(2):163-72.
- 131 Clinical trials uk (2021) Memantine for Enhanced Stroke Recovery, Available at: <https://clinicaltrials.gov/ct2/show/NCT02144584?term=memantine&draw=3&rank=46> (Accessed: 3th of September 2021)
- 132 Clinical trials uk (2021) Evaluation of Memantine Versus Placebo on Ischemic

- Stroke Outcome (EMISO), Available at:
<https://clinicaltrials.gov/ct2/show/NCT02535611> (Accessed: 3th of September 2021).
- 133 Gwag BJ, Lee YA, Ko SY, Lee MJ, Im DS, Yun BS, et al. Marked prevention of ischemic brain injury by Neu2000, an NMDA antagonist and antioxidant derived from aspirin and sulfasalazine. *Journal of Cerebral Blood Flow and Metabolism*. 2007;27(6):1142-51.
- 134 Lee JM, Grabb MC, Zipfel GJ, Choi DW. Brain tissue responses to ischemia. *Journal of Clinical Investigation*. 2000;106(6):723-31.
- 135 Grade S, Gotz M. Neuronal replacement therapy: previous achievements and challenges ahead. *Npj Regenerative Medicine*. 2017;2.
- 136 Emerich DF. Clinical trials with neuroprotective drugs in acute ischaemic stroke: are we doing the right thing? *Trends in Neurosciences*. 2000;23(6):245-6.
- 137 Gogas KR. Glutamate-based therapeutic approaches: NR2B receptor antagonists. *Current Opinion in Pharmacology*. 2006;6(1):68-74.
- 138 Li V, Wang YT. Molecular mechanisms of NMDA receptor-mediated excitotoxicity: implications for neuroprotective therapeutics for stroke. *Neural Regeneration Research*. 2016;11(11):1752-3.
- 139 Perez-Pinzon MA, Steinberg GK. CGS 19755 (Selfotel): A Novel Neuroprotective Agent Against CNS Injury. *CNS drug reviews*. 1996;2(3):257-68.
- 140 Warach S, Kaufman D, Chiu D, Devlin T, Luby M, Rashid A, et al. Effect of the glycine antagonist gavestinel on cerebral infarcts in acute stroke patients, a randomized placebo-controlled trial: The GAIN MRI substudy. *Cerebrovascular Diseases*. 2006;21(1-2):106-11.
- 141 Shkirkova K, Starkman S, Sanossian N, Eckstein M, Stratton S, Pratt F, et al. Paramedic Initiation of Neuroprotective Agent Infusions Successful Achievement of Target Blood Levels and Attained Level Effect on Clinical Outcomes in the FAST-MAG Pivotal Trial (Field Administration of Stroke Therapy - Magnesium). *Stroke*. 2017;48(7):1901-7.
- 142 Memezawa H, Zhao Q, Smith ML, Siesjo BK. Hyperthermia nullifies the ameliorating effect of dizocilpne maleate (MK-801) in focal cerebral-ischemia. *Brain Research*. 1995;670(1):48-52.
- 143 Boast CA, Gerhardt SC, Pastor G, Lehmann J, Etienne PE, Liebman JM. The N-methyl-D-aspartate antagonists CGS-19755 and CPP reduce ischaemic brain damage in gerbils. *Brain Research*. 1988;442(2):345-8.
- 144 *clinicaltrials*. (2019). Quelling of Excitotoxicity in Acute Stroke With Ketamine (QUEST-KETA). Available:
<https://clinicaltrials.gov/ct2/show/results/NCT03223220>. Last accessed 28th September 2021.
- 145 *clinicaltrials*. (2017). Safety and Optimal Neuroprotection of neu2000 in Ischemic Stroke With Endovascular reCanalization (SONIC) (SONIC). Available:
<https://clinicaltrials.gov/ct2/show/NCT02831088>. Last accessed 28th September 2021
- 146 Ghanizadeh A. Targeting of Glycine Site on NMDA Receptor as a Possible New Strategy for Autism Treatment. *Neurochemical Research*. 2011;36(5):922-3.
- 147 Oyston P, Robinson K. The current challenges for vaccine development.

- Journal of Medical Microbiology. 2012;61(7):889-94
- 148 Heaton PM. Challenges of Developing Novel Vaccines With Particular Global Health Importance. *Frontiers in Immunology*. 2020;11.
- 149 Accelrys (2018) Discovery studio science portfolio, Available at: <http://accelrys.com/products/datasheets/discovery-studio-overview.pdf> (Accessed: 6th July 2018).
- 150 Bianchi.M, Turner.H.L , Nogal.B et al (2018) 'Electron-Microscopy-Based Epitope Mapping Defines Specificities of Polyclonal Antibodies Elicited During HIV-1 BG505 Envelope Trimer Immunization ', *Immunity*, 49(2), pp. 288-300.
- 151 Shen MY, Sali A. Statistical potential for assessment and prediction of protein structures. *Protein Science*. 2006;15(11):2507-24.
- 152 Xiang ZX. Advances in homology protein structure modeling. *Current Protein & Peptide Science*. 2006;7(3):217-27
- 153 Lovell SC, Davis IW, Adrendall WB, de Bakker PIW, Word JM, Prisant MG, et al. Structure validation by C alpha geometry: phi,psi and C beta deviation. *Proteins-Structure Function and Genetics*. 2003;50(3):437-50.
- 154 Maynard AJ, Ehlers T, Koska J. Docking and scoring in Discovery Studio. *Abstracts of Papers of the American Chemical Society*. 2011;241.
- 155 Justiz Vaillant AA, Jamal Z, Ramphul K. Immunoglobulin. [Updated 2020 Aug 23]. In: StatPearls [Internet]. Treasure Island (FL): StatPearls Publishing; 2020 Jan-. Available from: <https://www.ncbi.nlm.nih.gov/books/NBK513460/>
- 156 Davies DR, Padlan EA. Structural immunology twisting into shape. *Current Biology*. 1992;2(5):254-6.
- 157 Uniport (2018) uniprot-align, Available at: <https://www.uniprot.org/> (Accessed: 17 July 2018).
- 158 Schrodinger,L.(2010) The PyMoL Molecular Graphics System, Version 1.3r1.
- 159 Babicki S, Arndt D, Marcu A, Liang YJ, Grant JR, Maciejewski A, et al. Heatmapper: web-enabled heat mapping for all. *Nucleic Acids Research*. 2016;44(W1):W147-W53.
- 160 XLSTAT. (2020). Statistical Software for Excel. Available: <https://www.xlstat.com/en/papers>. Last accessed 28th September 2021.
- 161 Bio3DWeb (2018) *Online analysis of user defined protein structure ensembles*, Available at: http://bio3d.ucsd.edu/pca-app/?SSUID=2018-07-16_6835fb1e887 (Accessed: 17 July 2018).
- 162 Sastry GM, Adzhigirey M, Day T, Annabhimoju R, Sherman W. Protein and ligand preparation: parameters, protocols, and influence on virtual screening enrichments. *Journal of Computer-Aided Molecular Design*. 2013;27(3):221-34.
- 163 Banks WA, Greig NH. Small molecules as central nervous system therapeutics: old challenges, new directions, and a philosophic divide. *Future Medicinal Chemistry*. 2019;11(6):489-93.
- 164 Issa NT, Badiavas EV, Schurer S. Research Techniques Made Simple: Molecular Docking in Dermatology - A Foray into In Silico Drug Discovery. *Journal of Investigative Dermatology*. 2019;139(12):2400-+.
- 165 Lipinski CA, Lombardo F, Dominy BW, Feeney PJ. Experimental and computational approaches to estimate solubility and permeability in drug discovery and development settings. *Advanced Drug Delivery Reviews*. 2012;64:4-17.

- 166 Veber DF, Johnson SR, Cheng HY, Smith BR, Ward KW, Kopple KD. Molecular properties that influence the oral bioavailability of drug candidates. *Journal of Medicinal Chemistry*. 2002;45(12):2615-23
- 167 Comeau SR, Gatchell DW, Vajda S, Camacho CJ. ClusPro: An automated docking and discrimination method for the prediction of protein complexes. *Bioinformatics*. 2004;20(1):45-50.
- 168 Racz A, Bajusz D, Heberger K. Life beyond the Tanimoto coefficient: similarity measures for interaction fingerprints. *Journal of Cheminformatics*. 2018;10.
- 169 Zoete V, Daina A, Bovigny C, Michielin O. SwissSimilarity: A Web Tool for Low to Ultra High Throughput Ligand-Based Virtual Screening. *Journal of Chemical Information and Modeling*. 2016;56(8):1399-404.
- 170 Prediction of drug absorption using multivariate statistics. *Journal of Medicinal Chemistry*. 2000;43(21):3867-77
- 171 Egan WJ, Lauri G. Prediction of intestinal permeability. *Advanced Drug Delivery Reviews*. 2002;54(3):273-89.
- 172 Egan WJ, Lauri G. Prediction of intestinal permeability. *Advanced Drug Delivery Reviews*. 2002;54(3):273-89.
- 173 Cheng A, Dixon SL. In silico models for the prediction of dose-dependent human hepatotoxicity. *Journal of Computer-Aided Molecular Design*. 2003;17(12):811-23.
- 174 Remington SJ. Negotiating the speed bumps to fluorescence. *Nature Biotechnology*. 2002;20(1):28-9.
- 175 Thermo Fisher Scientific Inc (2021) CyQUANT™ LDH Cytotoxicity Assay, Available at:
<https://www.thermofisher.com/order/catalog/product/C20300#/C20300>
(Accessed: 28th June 2021).
- 176 Sridhar SNC, Palawat S, Paul AT. Design, synthesis, biological evaluation and molecular modelling studies of indole glyoxylamides as a new class of potential pancreatic lipase inhibitors. *Bioorganic Chemistry*. 2019;85:373-81.
- 177 Chen.J, Xu.Z and Zhang. H.J. (2009). *Animal Models of Acute Neurological Injuries*. New York: Totowa. 130-140.
- 178 Bederson JB, Pitts LH, Germano SM, Nishimura MC, Davis RL, Bartkowski HM. Evaluation of 2,3,5-triphenyltetrazolium chloride as a stain for detection and quantification of experimental cerebral infarction in rats. *Stroke*. 1986;17(6):1304-8.
- 179 Noor.K. (2020). Hyperglycemia and ischaemic stroke. Available:
https://www.gla.ac.uk/media/Media_426952_smxx.pdf. Last accessed 12th September 2021.
- 180 Gomeni R, Bani M, D'Angeli C, Corsi M, Bye A. Computer-assisted drug development (CADD): an emerging technology for designing first-time-in-man and proof-of-concept studies from preclinical experiments. *European Journal of Pharmaceutical Sciences*. 2001;13(3):261-70.
- 181 Yu WB, MacKerell AD. Computer-Aided Drug Design Methods. *Antibiotics: Methods and Protocols*. 2017;1520:85-106.
- 182 Zhang SX. Computer-Aided Drug Discovery and Development. *Drug Design and Discovery: Methods and Protocols*. 2011;716:23-38.
- 183 Gurung AB, Ali MA, Lee J, Abul Farah M, Al-Anazi KM. An Updated Review of

- Computer-Aided Drug Design and Its Application to COVID-19. *Biomed Research International*. 2021;2021.
- 184 Duch W, Swaminathan K, Meller J. Artificial intelligence approaches for rational drug design and discovery. *Current Pharmaceutical Design*. 2007;13(14):1497-508.
- 185 Lyne PD. Structure-based virtual screening: an overview. *Drug Discovery Today*. 2002;7(20):1047-55.
- 186 Janeway CA Jr, Travers P, Walport M, et al (2001). The components of the immune system. In: Immunobiology: The Immune System in Health and Disease. 5th ed. New York: Garland Science. Available at : <https://www.ncbi.nlm.nih.gov/books/NBK27092/>
- 187 Alberts.B, Johnson.A, Lewis.J, Raff.M, Roberts.K, and Walter.P. (2002) 'B Cells and Antibodies', in Alberts.B, Johnson.A, et al (ed.) Molecular Biology of the Cell. New York: Garland Science, pp. Available from: <https://www.ncbi.nlm.nih.gov/books/NBK26884/>.
- 188 Alberts B, Johnson A, Lewis J, et al.. (2001). B Cells and Antibodies. In: Molecular Biology of the Cell.. 4th ed. New York: Garland Science. Available at : <https://www.ncbi.nlm.nih.gov/books/NBK26884/>.
- 189 Vena GA, Cassano N. Drug focus: adalimumab in the treatment of moderate to severe psoriasis. *Biologics : targets & therapy*. 2007;1(2):93-103
- 190 Cho HS, Mason K, Ramyar KX, Stanley AM, Gabelli SB, Denney DW, et al. Structure of the extracellular region of HER2 alone and in complex with the Herceptin Fab. *Nature*. 2003;421(6924):756-60.
- 191 Coronavirus (COVID-19), (2020). Update: FDA Authorizes Monoclonal Antibodies for Treatment of COVID-19. Available: <https://www.fda.gov/news-events/press-announcements/coronavirus-covid-19-update-fda-authorizes-monoclonal-antibodies-treatment-covid-19>. Last accessed 16th Sep 2021.
- 192 Pedotti M, Simonelli L, Livoti E, Varani L. Computational Docking of Antibody-Antigen Complexes, Opportunities and Pitfalls Illustrated by Influenza Hemagglutinin. *International Journal of Molecular Sciences*. 2011;12(1):226-51.
- 193 Creative Diagnostics (2020) *Polyclonal vs. Monoclonal Antibodies*, Available at: <https://www.creative-diagnostics.com/polyclonal-vs-monoclonal-antibodies.htm> (Accessed: 22nd December 2020).
- 194 Liu HF, Ma J, Winter C, Bayer R. Recovery and purification process development for monoclonal antibody production. *Mabs*. 2010;2(5):480-99.
- 195 Frank SA. (2002). Chapter 4 Specificity and Cross-Reactivity. In: Immunology and Evolution of Infectious Disease.. Princeton (NJ): Princeton University Press. Available at : <https://www.ncbi.nlm.nih.gov/books/NBK2394/>
- 196 Pelegrin M, Naranjo-Gomez M, Piechaczyk M. Antiviral Monoclonal Antibodies: Can They Be More Than Simple Neutralizing Agents? *Trends in Microbiology*. 2015;23(10):653-65.
- 197 Nasiri H, Valedkarimi Z, Aghebati-Maleki L, Abdolalizadeh J, Kazemi T, Esparvarinha M, et al. Production and purification of polyclonal antibody against F(ab')₂ fragment of human immunoglobulin G. *Veterinary Research Forum*. 2017;8(4):307-12.
- 198 Leenaars M, Hendriksen CFM. Critical steps in the production of polyclonal and monoclonal antibodies evaluation and recommendations. *Iilar Journal*.

- 2005;46(3):269-79.
- 199 Schroeder HW, Cavacini L. Structure and function of immunoglobulins. *Journal of Allergy and Clinical Immunology*. 2010;125(2):S41-S52.
- 200 Janeway Jr, C. A., Travers, P., et al. (2001). The structure of a typical antibody molecule. In *Immunobiology: The Immune System in Health and Disease*. Garland Science.
- 201 Schroeder HW, Cavacini L. Structure and function of immunoglobulins. *Journal of Allergy and Clinical Immunology*. 2010;125(2):S41-S52.
- 202 Justiz Vaillant AA, Jamal Z, Ramphul K. Immunoglobulin. [Updated 2020 Aug 23]. In: StatPearls [Internet]. Treasure Island (FL): StatPearls Publishing; 2020 Jan-. Available from: <https://www.ncbi.nlm.nih.gov/books/NBK513460/>
- 203 Takahashi N, Tetaert D, Debuire B, Lin LC, Putnam FW. Complete amino-acid-sequence of the delta-heavy chain of human immunoglobulin-D. *Proceedings of the National Academy of Sciences of the United States of America-Biological Sciences*. 1982;79(9):2850-4.
- 204 Goulet DR, Atkins WM. Considerations for the Design of Antibody-Based Therapeutics. *Journal of Pharmaceutical Sciences*. 2020;109(1):74-103.
- 205 Takahashi N, Tetaert D, Debuire B, Lin LC, Putnam FW. Complete amino-acid-sequence of the delta-heavy chain of human immunoglobulin-D. *Proceedings of the National Academy of Sciences of the United States of America-Biological Sciences*. 1982;79(9):2850-4.
- 206 Popov AV, Zou XG, Xian J, NProtein motion and lock and key complementarity in antigen-antibody reactions icholson IC, Bruggemann M. A human immunoglobulin lambda locus is similarly well expressed in mice and humans. *Journal of Experimental Medicine*. 1999;189(10):1611-9.
- 207 Chen R, Li L, Weng ZP. ZDOCK: An initial-stage protein-docking algorithm. *Proteins-Structure Function and Bioinformatics*. 2003;52(1):80-7.
- 208 Vassilev LT, Vu BT, Graves B, Carvajal D, Podlaski F, Filipovic Z, et al. In vivo activation of the p53 pathway by small-molecule antagonists of MDM2. *Science*. 2004;303(5659):844-8.
- 209 Keskin O. Binding induced conformational changes of proteins correlate with their intrinsic fluctuations: a case study of antibodies. *Bmc Structural Biology*. 2007;7.
- 210 Absolom DR, Vanoss CJ. The nature of the antigen- antibody body and the factors affecting its association and dissociation. *Crc Critical Reviews in Immunology*. 1986;6(1):1-46.
- 211 Wong WK, Leem J, Deane CM. Comparative Analysis of the CDR Loops of Antigen Receptors. *Frontiers in Immunology*. 2019;10.
- 212 Martin ACR, Thornton JM. Structural families in loops of homologous proteins: Automatic classification, modelling and application to antibodies. *Journal of Molecular Biology*. 1996;263(5):800-15.
- 213 Braden BC, Dall'Acqua W, Eisenstein E, Fields BA, Goldbaum FA, Malchiodi EL, et al. Protein motion and lock and key complementarity in antigen-antibody reactions. *Pharmaceutica acta Helvetiae*. 1995;69(4):225-30.
- 214 Foote J, Milstein C. Conformational isomerism and the diversity of antibodies. *Proceedings of the National Academy of Sciences of the United States of America*. 1994;91(22):10370-4.

- 215 Davies DR, Padlan EA. Structural immunology twisting into shape. *Current Biology*. 1992;2(5):254-6.
- 216 Guest JD, Vreven T, Zhou J, Moal I, Jeliazkov JR, Gray JJ, et al. An expanded benchmark for antibody-antigen docking and affinity prediction reveals insights into antibody recognition determinants. *Structure (London, England : 1993)*. 2021.
- 217 Bostrom J, Lee CV, Haber L, Fuh G. Improving Antibody Binding Affinity and Specificity for Therapeutic Development. *Methods in Molecular Biology*. 2009;525:353-76.
- 218 Bostrom J, Yu SF, Kan D, Appleton BA, Lee CV, Billeci K, et al. Variants of the Antibody Herceptin That Interact with HER2 and VEGF at the Antigen Binding Site. *Science*. 2009;323(5921):1610-4.
- 219 Lee CV, Hymowitz SG, Wallweber HJ, Gordon NC, Billeci KL, Tsai S-P, et al. Synthetic anti-BR3 antibodies that mimic BAFF binding and target both human and murine B cells. *Blood*. 2006;108(9):3103-11.
- 220 Krawczyk K, Dunbar J, Deane CM. Computational Tools for Aiding Rational Antibody Design. *Computational Protein Design*. 2017;1529:399-416.
- 221 Norman RA, Ambrosetti F, Bonvin AMJJ, Colwell LJ, Kelm S, Kumar S, et al. Computational approaches to therapeutic antibody design: established methods and emerging trends. *Briefings in Bioinformatics*. 2020;21(5):1549-67.
- 222 Fiser A, Sali A. MODELLER: Generation and refinement of homology-based protein structure models. *Macromolecular Crystallography, Pt D*. 2003;374:461-91.
- 223 Brenke R, Hall DR, Chuang G-Y, Comeau SR, Bohnuud T, Beglov D, et al. Application of asymmetric statistical potentials to antibody-protein docking. *Bioinformatics*. 2012;28(20):2608-14.
- 224 Vyas VK, Ukawala RD, Ghate M, Chintha C. Homology Modeling a Fast Tool for Drug Discovery: Current Perspectives. *Indian Journal of Pharmaceutical Sciences*. 2012;74(1):1-17.
- 225 Wellcome Genome Campus (2020) *EMBI The home for big data in biology*, Available at: <https://www.ebi.ac.uk/> (Accessed: 21st December 2020).
- 226 Sayers EW, Cavanaugh M, Clark K, Ostell J, Pruitt KD, Karsch-Mizrachi I. GenBank. *Nucleic Acids Research*. 2020;48(D1):D84-D6.
- 227 Barker WC, Garavelli JS, McGarvey PB, Marzec CR, Orcutt BC, Srinivasarao GY, et al. The PIR-International Protein Sequence Database. *Nucleic Acids Research*. 1999;27(1):39-43.
- 228 Zhao J, Nussinov R, Ma B. Mechanisms of recognition of amyloid-beta (A beta) monomer, oligomer, and fibril by homologous antibodies. *Journal of Biological Chemistry*. 2017;292(44):18325-43.
- 229 Schwede T. Protein Modeling: What Happened to the "Protein Structure Gap"? *Structure*. 2013;21(9):1531-40.
- 230 Baker D, Sali A. Protein structure prediction and structural genomics. *Science*. 2001;294(5540):93-6.
- 231 Blundell TL, Johnson MS, Overington JP, Sali A. Knowledge-Based Protein Modeling and the Design of Novel Molecules. *Protein Design and the Development of New Therapeutics and Vaccines*. 1990:209-27.
- 232 Alexander N, Bortolus M, Al-Mestarihi A, McHaourab H, Meilerl J. De novo

- high-resolution protein structure determination from sparse spin-labeling EPR data. *Structure*. 2008;16(2):181-95.
- 233 Winter.L (2020) 'DeepMind AI Speeds Up the Time to Determine Proteins' Structures', *The Scientist*, 2nd December, Available at:<https://www.the-scientist.com/news-opinion/deepmind-ai-speeds-up-the-time-to-determine-proteins-structures-68221>.
- 234 Schmidt T, Bergner A, Schwede T. Modelling three-dimensional protein structures for applications in drug design. *Drug Discovery Today*. 2014;19(7):890-7.
- 235 Jumper J, Evans R, Pritzel A, Green T, Figurnov M, Ronneberger O, et al. Highly accurate protein structure prediction with AlphaFold. *Nature*. 2021;596(7873):583-+.
- 236 Callaway E. 'It will change everything': DeepMind's AI makes gigantic leap in solving protein structures. *Nature*. 2020;588(7837):203-4.
- 237 Ferdous S, Martin ACR. AbDb: antibody structure database-a database of PDB-derived antibody structures. *Database-the Journal of Biological Databases and Curation*. 2018.
- 238 Keskin O. Binding induced conformational changes of proteins correlate with their intrinsic fluctuations: a case study of antibodies. *Bmc Structural Biology*. 2007;7.
- 239 Krawczyk K, Baker T, Shi J, Deane CM. Antibody i-Patch prediction of the antibody binding site improves rigid local antibodyantigen docking. *Protein Engineering Design & Selection*. 2013;26(10):621-9.
- 240 Kunik V, Ashkenazi S, Ofra Y. Paratome: an online tool for systematic identification of antigen-binding regions in antibodies based on sequence or structure. *Nucleic Acids Research*. 2012;40(W1):W521-W4.
- 241 Burley SK, Berman HM, Bhikadiya C, Bi C, Chen L, Di Costanzo L, et al. Protein Data Bank: the single global archive for 3D macromolecular structure data. *Nucleic Acids Research*. 2019;47(D1):D520-D8.
- 242 Liu HF, Ma J, Winter C, Bayer R. Recovery and purification process development for monoclonal antibody production. *Mabs*. 2010;2(5):480-99.
- 243 Chen R, Weng ZP. Docking unbound proteins using shape complementarity, desolvation, and electrostatics. *Proteins-Structure Function and Bioinformatics*. 2002;47(3):281-94.
- 244 Al Qaraghuli MM, Kubiak-Ossowska K, Ferro VA, Mulheran PA. Antibody-protein binding and conformational changes: identifying allosteric signalling pathways to engineer a better effector response. *Scientific Reports*. 2020;10(1).
- 245 Zhao J, Nussinov R, Ma B. Mechanisms of recognition of amyloid-beta (A beta) monomer, oligomer, and fibril by homologous antibodies. *Journal of Biological Chemistry*. 2017;292(44):18325-43.
- 246 Braden BC, Souchon H, Eisele JL, Bentley GA, Bhat TN, Navaza J, et al. 3-Dimensional Structures of the free and the antigen-complexed Fab from monoclonal antilysozyme antibody-D44.1. *Journal of Molecular Biology*. 1994;243(4):767-81.
- 247 Kong R, Xu K, Zhou T, Acharya P, Lemmin T, Liu K, et al. Fusion peptide of HIV-1 as a site of vulnerability to neutralizing antibody. *Science*. 2016;352(6287):828-33.

- 248 Gleichman AJ, Spruce LA, Dalmau J, Seeholzer SH, Lynch DR. Anti-NMDA Receptor Encephalitis Antibody Binding Is Dependent on Amino Acid Identity of a Small Region within the GluN1 Amino Terminal Domain. *Journal of Neuroscience*. 2012;32(32):11082-94.
- 249 Martinez CR, Iverson BL. Rethinking the term "pi-stacking". *Chemical Science*. 2012;3(7):2191-201.
- 250 Ozbabacan SEA, Engin HB, Gursoy A, Keskin O. Transient proteinprotein interactions. *Protein Engineering Design & Selection*. 2011;24(9):635-48.
- 251 Sircar A, Gray JJ. SnugDock: Paratope Structural Optimization during Antibody-Antigen Docking Compensates for Errors in Antibody Homology Models. Figshare. 2010.
- 252 Stahura FL, Bajorath J. Virtual screening methods that complement HTS. *Combinatorial Chemistry & High Throughput Screening*. 2004;7(4):259-69.
- 253 Peck RW. Driving earlier clinical attrition: if you want to find the needle, burn down the haystack. Considerations for biomarker development. *Drug Discovery Today*. 2007;12(7-8):289-94.
- 254 Wang Z, Sun H, Shen C, Hu X, Gao J, Li D, et al. Combined strategies in structure-based virtual screening. *Physical Chemistry Chemical Physics*. 2020;22(6):3149-59.
- 255 Mobley DL, Dill KA. Binding of Small-Molecule Ligands to Proteins: "What You See" Is Not Always "What You Get". *Structure*. 2009;17(4):489-98.
- 256 Nikolic K, Mavridis L, Djikic T, Vucicevic J, Agbaba D, Yelekci K, et al. Drug Design for CNS Diseases: Polypharmacological Profiling of Compounds Using Cheminformatic, 3D-QSAR and Virtual Screening Methodologies. *Frontiers in Neuroscience*. 2016;10.
- 257 Daidone F, Montioli R, Paiardini A, Cellini B, Macchiarulo A, Giardina G, et al. Identification by Virtual Screening and In Vitro Testing of Human DOPA Decarboxylase Inhibitors. *Plos One*. 2012;7(2).
- 258 Bottegoni G, Veronesi M, Bisignano P, Kacker P, Favia AD, Cavalli A. Development and Application of a Virtual Screening Protocol for the Identification of Multitarget Fragments. *Chemmedchem*. 2016;11(12):1259-63.
- 259 Prati F, De Simone A, Bisignano P, Armirotti A, Summa M, Pizzirani D, et al. Multitarget Drug Discovery for Alzheimer's Disease: Triazinones as BACE-1 and GSK-3 beta Inhibitors. *Angewandte Chemie-International Edition*. 2015;54(5):1578-82.
- 260 Amaro RE, Baudry J, Chodera J, Demir O, McCammon JA, Miao Y, et al. Ensemble Docking in Drug Discovery. *Biophysical Journal*. 2018;114(10):2271-8.
- 261 Hendrickson JB. Concepts and applications of molecular similarity- Johnson, Ma Maggiora GM. *Science*. 1991;252(5009):1189-.
- 262 Nguyen LA, He H, Pham-Huy C. Chiral drugs: an overview. *International journal of biomedical science : IJBS*. 2006;2(2):85-100.
- 263 Geldenhuys WJ, Funk MO, Van der Schyf CJ, Carroll RT. A scaffold hopping approach to identify novel monoamine oxidase B inhibitors. *Bioorganic & Medicinal Chemistry Letters*. 2012;22(3):1380-3.
- 264 Youdim MBH, Gross A, Finberg JPM. Rasagiline N-propargyl-1R(+)-aminoindan , a selective and potent inhibitor of mitochondrial monoamine oxidase B. *British*

- Journal of Pharmacology*. 2001;132(2):500-6.
- 265 Miteva M. Hierarchical structure-based virtual screening for drug design. *Biotechnology & Biotechnological Equipment*. 2008;22(1):634-8.
- 266 Nikolic K, Mavridis L, Djikic T, Vucicevic J, Agbaba D, Yelekci K, et al. Drug Design for CNS Diseases: Polypharmacological Profiling of Compounds Using Cheminformatic, 3D-QSAR and Virtual Screening Methodologies. *Frontiers in Neuroscience*. 2016;10.
- 267 Fiorito J, Vendome J, Saeed F, Staniszewski A, Zhang H, Yan SJ, et al. Identification of a Novel 1,2,3,4-Tetrahydrobenzo b 1,6 naphthyridine Analogue as a Potent Phosphodiesterase 5 Inhibitor with Improved Aqueous Solubility for the Treatment of Alzheimer's Disease. *Journal of Medicinal Chemistry*. 2017;60(21):8858-75.
- 268 Gimeno A, Jose Ojeda-Montes M, Tomas-Hernandez S, Cereto-Massague A, Beltran-Debon R, Mulero M, et al. The Light and Dark Sides of Virtual Screening: What Is There to Know? *International Journal of Molecular Sciences*. 2019;20(6).
- 269 Baell J, Walters MA. Chemical con artists foil drug discovery. *Nature*. 2014;513(7519):481-3.
- 270 Konze KD, Bos PH, Dahlgren MK, Leswing K, Tubert-Brohman I, Bortolato A, et al. Reaction-Based Enumeration, Active Learning, and Free Energy Calculations To Rapidly Explore Synthetically Tractable Chemical Space and Optimize Potency of Cyclin-Dependent Kinase 2 Inhibitors. *Journal of Chemical Information and Modeling*. 2019;59(9):3782-93.
- 271 Baell JB, Nissink JWM. Seven Year Itch: Pan-Assay Interference Compounds (PAINS) in 2017-Utility and Limitations. *Acs Chemical Biology*. 2018;13(1):36-44.
- 272 Ferreira LLG, Andricopulo AD. ADMET modeling approaches in drug discovery. *Drug Discovery Today*. 2019;24(5):1157-65.
- 273 Silva MP, Saraiva L, Pinto M, Sousa ME. Boronic Acids and Their Derivatives in Medicinal Chemistry: Synthesis and Biological Applications. *Molecules*. 2020;25(18).
- 274 Armour D, de Groot MJ, Edwards M, Perros M, Price DA, Stammen BL, et al. The discovery of CCR5 receptor antagonists for the treatment of HIV infection: Hit-to-lead studies. *Chemmedchem*. 2006;1(7):706-+.
- 275 Sun H, Scott DO. Structure-based Drug Metabolism Predictions for Drug Design. *Chemical Biology & Drug Design*. 2010;75(1):3-17.
- 276 Jones G, Willett P, Glen RC, Leach AR, Taylor R. Development and validation of a genetic algorithm for flexible ligand docking. *Abstracts of Papers of the American Chemical Society*. 1997;214:154-COMP.
- 277 Trott O, Olson AJ. Software News and Update AutoDock Vina: Improving the Speed and Accuracy of Docking with a New Scoring Function, Efficient Optimization, and Multithreading. *Journal of Computational Chemistry*. 2010;31(2):455-61.
- 278 Schapira M, Abagyan R, Totrov M. Nuclear hormone receptor targeted virtual screening. *Journal of Medicinal Chemistry*. 2003;46(14):3045-59.
- 279 Rarey M, Kramer B, Lengauer T, Klebe G. A fast flexible docking method using an incremental construction algorithm. *Journal of Molecular Biology*.

- 1996;261(3):470-89.
- 280 Friesner RA, Banks JL, Murphy RB, Halgren TA, Klicic JJ, Mainz DT, et al. Glide: A new approach for rapid, accurate docking and scoring. 1. Method and assessment of docking accuracy. *Journal of Medicinal Chemistry*. 2004;47(7):1739-49.
- 281 Sastry GM, Dixon SL, Sherman W. Rapid Shape-Based Ligand Alignment and Virtual Screening Method Based on Atom/Feature-Pair Similarities and Volume Overlap Scoring. *Journal of Chemical Information and Modeling*. 2011;51(10):2455-66.
- 282 Agrafiotis DK, Gibbs AC, Zhu F, Izrailev S, Martin E. Conformational sampling of bioactive molecules: A comparative study. *Journal of Chemical Information and Modeling*. 2007;47(3):1067-86.
- 283 Gorelik B, Goldblum A. High quality binding modes in docking ligands to proteins. *Proteins-Structure Function and Bioinformatics*. 2008;71(3):1373-86.
- 284 Leach AR. Ligand docking to proteins with discrete side chain flexibility. *Journal of Molecular Biology*. 1994;235(1):345-56.
- 285 Ordog R, Grolmusz V. Evaluating genetic algorithms in protein-ligand docking. *Bioinformatics Research and Applications*. 2008;4983:402-+.
- 286 The Cambridge Crystallographic Data Centre (2011) *GOLD Protein-Ligand Docking*, Available at: <https://cds.dl.ac.uk/cds/datasets/crys/csd/superstar/gold.html> (Accessed: 17th July 2018).
- 287 Pagadala.N.S (2017) 'Software for molecular docking: a review', *Biophys Rev*, 9(2),91–102.
- 288 Brooijmans N, Kuntz ID. Molecular recognition and docking algorithms. *Annual Review of Biophysics and Biomolecular Structure*. 2003;32:335-73.
- 289 Englebienne P, Moitessier N. Docking Ligands into Flexible and Solvated Macromolecules. 5. Force-Field-Based Prediction of Binding Affinities of Ligands to Proteins. *Journal of Chemical Information and Modeling*. 2009;49(11):2564-71.
- 290 Hughes JP, Rees S, Kalindjian SB, Philpott KL. Principles of early drug discovery. *British Journal of Pharmacology*. 2011;162(6):1239-49.
- 291 Andricopulo AD, Salum LB, Abraham DJ. Structure-Based Drug Design Strategies in Medicinal Chemistry. *Current Topics in Medicinal Chemistry*. 2009;9(9):771-90.
- 292 Peppoloni S, Pericolini E, Colombari B, Pinetti D, Cermelli C, Fini F, et al. The beta-Lactamase Inhibitor Boronic Acid Derivative SM23 as a New Anti-Pseudomonas aeruginosa Biofilm. *Frontiers in Microbiology*. 2020;11.
- 293 Konze KD, Bos PH, Dahlgren MK, Leswing K, Tubert-Brohman I, Bortolato A, et al. Reaction-Based Enumeration, Active Learning, and Free Energy Calculations To Rapidly Explore Synthetically Tractable Chemical Space and Optimize Potency of Cyclin-Dependent Kinase 2 Inhibitors. *Journal of Chemical Information and Modeling*. 2019;59(9):3782-93.
- 294 Karplus M, Weaver DL. Protein-Folding dynamics. *Nature*. 1976;260(5550):404-6.
- 295 Zou XQ, Sun YX, Kuntz ID. Inclusion of solvation in ligand binding free energy calculations using the generalized-born model. *Journal of the American*

- Chemical Society*. 1999;121(35):8033-43.
- 296 Friesner R. Calculation of protein-ligand binding affinities via free energy perturbation methods. *Abstracts of Papers of the American Chemical Society*. 2016;251.
- 297 Khoruzhii O, Donchev AG, Galkin N, Illarionov A, Olevanov M, Ozrin V, et al. Application of a polarizable force field to calculations of relative protein-ligand binding affinities. *Proceedings of the National Academy of Sciences of the United States of America*. 2008;105(30):10378-83.
- 298 Michel J, Verdonk ML, Essex JW. Protein-ligand binding affinity predictions by implicit solvent simulations: A tool for lead optimization? *Journal of Medicinal Chemistry*. 2006;49(25):7427-39.
- 299 Kollman P. Free-energy calculations applications to chemical and biochemical phenomena. *Chemical Reviews*. 1993;93(7):2395-417.
- 300 Hartshorn MJ, Verdonk ML, Chessari G, Brewerton SC, Mooij WTM, Mortenson PN, et al. Diverse, high-quality test set for the validation of protein-ligand docking performance. *Journal of Medicinal Chemistry*. 2007;50(4):726-41.
- 301 Bohm HJ. The development of a simple empirical scoring function to estimate the binding constant for a protein ligand complex of known 3-dimensional structure. *Journal of Computer-Aided Molecular Design*. 1994;8(3):243-56
- 302 Verkhivker G, Appelt K, Freer ST, Villafranca JE. Empirical free energy calculations of ligand protein crystallographic complexes. 1. Knowledge-based ligand protein interaction potentials applied to the potentials applied to the applied to the prediction of human immunodeficiency virus 1 protease binding affinity. *Protein Engineering*. 1995;8(7):677-91.
- 303 Li Y, Liu Z, Li J, Han L, Liu J, Zhao Z, et al. Comparative Assessment of Scoring Functions on an Updated Benchmark: 1. Compilation of the Test Set. *Journal of Chemical Information and Modeling*. 2014;54(6):1700-16.
- 304 Cheng T, Li X, Li Y, Liu Z, Wang R. Comparative Assessment of Scoring Functions on a Diverse Test Set. *Journal of Chemical Information and Modeling*. 2009;49(4):1079-93.
- 305 Verdonk ML, Cole JC, Hartshorn MJ, Murray CW, Taylor RD. Improved protein-ligand docking using GOLD. *Proteins-Structure Function and Genetics*. 2003;52(4):609-23.
- 306 Korb O, Stutzle T, Exner TE. Empirical Scoring Functions for Advanced Protein-Ligand Docking with PLANTS. *Journal of Chemical Information and Modeling*. 2009;49(1):84-96.
- 307 Bohm HJ. The development of a simple empirical scoring function to estimate the binding constant for a protein ligand complex of known 3-dimensional structure. *Journal of Computer-Aided Molecular Design*. 1994;8(3):243-56.
- 308 Eldridge MD, Murray CW, Auton TR, Paolini GV, Mee RP. Empirical scoring functions .1. The development of a fast empirical scoring function to estimate the binding affinity of ligands in receptor complexes. *Journal of Computer-Aided Molecular Design*. 1997;11(5):425-45.
- 309 Nissink JWM, Murray C, Hartshorn M, Verdonk ML, Cole JC, Taylor R. A new test set for validating predictions of protein-ligand interaction. *Proteins-Structure Function and Genetics*. 2002;49(4):457-71.
- 310 Grzybowski BA, Ishchenko AV, Shimada J, Shakhnovich EI. From knowledge-

- based potentials to combinatorial lead design in silico. *Accounts of Chemical Research*. 2002;35(5):261-9.
- 311 Muegge I, Martin YC. A general and fast scoring function for protein-ligand interactions: A simplified potential approach. *Journal of Medicinal Chemistry*. 1999;42(5):791-804.
- 312 Kirtay CK, Mitchell JBO, Lumley JA. Knowledge based potentials: the reverse Boltzmann methodology, virtual screening and molecular weight dependence. *Qsar & Combinatorial Science*. 2005;24(4):527-36.
- 313 Zheng Z, Ucisik MN, Merz KM. The Movable Type Method Applied to Protein-Ligand Binding. *Journal of Chemical Theory and Computation*. 2013;9(12):5526-38.
- 314 Mooij WTM, Verdonk ML. General and targeted statistical potentials for protein-ligand interactions. *Proteins-Structure Function and Bioinformatics*. 2005;61(2):272-87.
- 315 Zilian D, Sottriffer CA. SFCscoreRF: A Random Forest-Based Scoring Function for Improved Affinity Prediction of Protein-Ligand Complexes. *Figshare*. 2016.
- 316 Uniport (2018) *uniprot-align*, Available at: <https://www.uniprot.org/> (Accessed: 17 July 2018).
- 317 Karakas E, Furukawa H. Crystal Structure of GluN1a/GluN2B NMDA Receptor Ion Channel. Worldwide Protein Data Bank. 2014.
- 318 Willmott CJ, Matsuura K. On the use of dimensioned measures of error to evaluate the performance of spatial interpolators. *International Journal of Geographical Information Science*. 2006;20(1):89-102
- 319 Liu T, Wang Y, Luo X, Li J, Reed SA, Xiao H, et al. Enhancing protein stability with extended disulfide bonds. *Proceedings of the National Academy of Sciences of the United States of America*. 2016;113(21):5910-5.
- 320 Ramachandran GN, Ramakrishnan C, Sasisekharan V. Stereochemistry of polypeptide chain configurations. *Journal of Molecular Biology*. 1963;7(1):95-&.
- 321 Leong MK, Syu R-G, Ding Y-L, Weng C-F. Prediction of N-Methyl-D-Aspartate Receptor GluN1-Ligand Binding Affinity by a Novel SVM-Pose/SVM-Score Combinatorial Ensemble Docking Scheme. *Scientific Reports*. 2017;7.
- 322 Romero-Hernandez A, Furukawa H. Novel Mode of Antagonist Binding in NMDA Receptors Revealed by the Crystal Structure of the GluN1-GluN2A Ligand-Binding Domain Complexed to NVP-AAM077. *Molecular Pharmacology*. 2017;92(1):22-9.
- 323 Furukawa H, Gouaux E. Mechanisms of activation, inhibition and specificity: crystal structures of the NMDA receptor NR1 ligand-binding core. *Embo Journal*. 2003;22(12):2873-85.
- 324 Furukawa H, Singh SK, Mancusso R, Gouaux E. Subunit arrangement and function in NMDA receptors. *Nature*. 2005;438(7065):185-92.
- 325 Kvist T, Steffensen TB, Greenwood JR, Mehrzad Tabrizi F, Hansen KB, Gajhede M, et al. Crystal Structure and Pharmacological Characterization of a Novel N-Methyl-D-aspartate (NMDA) Receptor Antagonist at the GluN1 Glycine Binding Site. *Journal of Biological Chemistry*. 2013;288(46):33124-35.
- 326 Hackos DH, Lupardus PJ, Grand T, Chen Y, Wang T-M, Reynen P, et al. Positive Allosteric Modulators of GluN2A-Containing NMDARs with Distinct Modes of Action and Impacts on Circuit Function. *Neuron*. 2016;89(5):983-99.

- 327 Hackos DH, Lupardus PJ, Grand T, Chen Y, Wang T-M, Reynen P, et al. Positive Allosteric Modulators of GluN2A-Containing NMDARs with Distinct Modes of Action and Impacts on Circuit Function. *Neuron*. 2016;89(5):983-99.
- 328 Hackos DH, Lupardus PJ, Grand T, Chen Y, Wang TM, Reynen P, et al. 5H8H: Structure of the human GluN1/GluN2A LBD in complex with GNE3419. *Worldwide Protein Data Bank*. 2016.
- 329 Karakas E, Furukawa H. Crystal structure of a heterotetrameric NMDA receptor ion channel. *Science*. 2014;344(6187):992-7.
- 330 Ladbury JE. Just add water! The effect of water on the specificity of protein-ligand binding sites and its potential application to drug design. *Chemistry & Biology*. 1996;3(12):973-80.
- 331 PDBsum (2013) *Pictorial database of 3D structures in the Protein Data Bank*, Available at: <http://www.ebi.ac.uk/thornton-srv/databases/cgi-bin/pdbsum/GetPage.pl?pdbcode=index.html> (Accessed: 17 July 2018).
- 332 Saeed M, Saeed A, Alam MJ, Alreshidi M. Receptor-Based Pharmacophore Modeling in the Search for Natural Products for COVID-19 M-pro. *Molecules*. 2021;26(6).
- 333 Travis T. Wager; Ramalakshmi Y. Chandrasekaran; Xinjun Hou; Matthew D. Troutman; Patrick R. Verhoest; Anabella Villalobos; Yvonne Will ACS Chem. *Neuroscience*.2010, 1, 420-434
- 334 Travis T. Wager; Xinjun Hou; Patrick R. Verhoest; Anabella Villalobos ACS Chem. *Neurosci*.2010, 1, 435-449.
- 335 Yoshimori A, Hu HB, Bajorath J. Adapting the DeepSARM approach for dual-target ligand design. *Journal of Computer-Aided Molecular Design*. 2021;35(5):587-600.
- 336 ChEMBL (2018) *Apparent dissociation constant of [3H]glycine from N-methyl-D-aspartate glutamate receptor in rat cortical slice preparation*, Available at: <https://pubchem.ncbi.nlm.nih.gov/bioassay/272849#section=Data-Table> (Accessed: 17th July 2018).
- 337 Muegge I. PMF scoring revisited. *Journal of Medicinal Chemistry*. 2006;49(20):5895-902.
- 338 Hackos DH, Lupardus PJ, Grand T, Chen Y, Wang T-M, Reynen P, et al. Positive Allosteric Modulators of GluN2A-Containing NMDARs with Distinct Modes of Action and Impacts on Circuit Function. *Neuron*. 2016;89(5):983-99.
- 339 McNamara D, Smith ECR, Calligaro DO, Omalley PJ, McQuaid LA, Dingledine R. 5,7-Dichlorokynurenic acid, a potent and selective competitive antagonist of the glycine site on NMDA receptors. *Neuroscience Letters*. 1990;120(1):17-20.
- 340 Leeson.P.D, Baker.R et al (1991) 'Kynurenic Acid Derivatives. Structure-Activity Relationships for Excitatory Amino Acid Antagonism and Identification of Potent and Selective Antagonists at the Glycine Site on the N-Methyl-D-aspartate Receptor', *J. Med. Chem.*, 34(1), pp. 1243-1252.
- 341 Pantsar T, Poso A. Binding Affinity via Docking: Fact and Fiction. *Molecules*. 2018;23(8).
- 342 Li Y, Han L, Liu Z, Wang R. Comparative Assessment of Scoring Functions on an Updated Benchmark: 2. Evaluation Methods and General Results. *Journal of*

- Chemical Information and Modeling. 2014;54(6):1717-36.
- 343 O'Boyle NM, Sayle RA. Comparing structural fingerprints using a literature-based similarity benchmark. *Journal of Cheminformatics*. 2016;8.
- 344 Jones G, Willett P, Glen RC. Molecular recognition of receptor-sites a genetic algorithm with a description of desolvation. *Journal of Molecular Biology*. 1995;245(1):43-53.
- 345 BindingDB (2021) , Available at: <http://www.bindingdb.org/bind/index.jsp> (Accessed: 16th May 2021).
- 346 Chen X, Liu M, Gilson MK. BindingDB: A web-accessible molecular recognition database. *Combinatorial Chemistry & High Throughput Screening*. 2001;4(8):719-25.
- 347 Thompson JD, Higgins DG, Gibson TJ. CLUSTAL-W –Improving the sensitivity of progressive multiple sequence alignment through sequence weighting, position-specific gap penalties and weight matrix choice. *Nucleic Acids Research*. 1994;22(22):4673-80.
- 348 Tirado-Rives, J.; Jorgensen W. L. Contribution of conformer focusing to the uncertainty in predicting free energies for protein-ligand binding. *J. Med. Chem*. 2006, 49, 5880-5884
- 349 Fischer J, Ganellin CR (2006) *Analogue-based Drug Discovery*. Google E-books [Online]. Available at: https://books.google.co.uk/books?id=FjKfqkaKkAAC&pg=PA464&redir_esc=y#v=onepage&q&f=false (Accessed: 22nd October 2020).
- 350 Peterson BZ, Tanada TN, Catterall WA. Molecular determinants of high affinity dihydropyridine binding in L-type calcium channels. *Journal of Biological Chemistry*. 1996;271(10):5293-6.
- 351 Perry I, Buttrum SM, Nash GB. Effect of activation on adhesion of flowing neutrophils to culture endothelium- Time course and inhibition by calcium-channel blocker (Nitrendipine). *British Journal of Pharmacology*. 1993;110(4):1630-4.
- 352 Eitze M, Boer R, Sanders KH, Boss H, Ulrich WR, Flockerzi D. Stereoselective Inhibition of Thromboxane Induced Coronary Vasoconstriction by 1,4-Dihydropyridine Calcium-Channel Antagonists. *Chirality*. 1990;2(4):233-40.
- 353 Hof RP, Ruegg UT, Hof A, Vogel A. Stereoselectivity At The Calcium-channel Opposite Action OF The Enantiomers Of A 1,4-dihydropyridine. *Journal of Cardiovascular Pharmacology*. 1985;7(4):689-93.
- 354 Thompson MJ, Borsenberger V, Louth JC, Judd KE, Chen BN. Design, Synthesis, and Structure-Activity Relationship of Indole-3-glyoxylamide Libraries Possessing Highly Potent Activity in a Cell Line Model of Prion Disease. *Journal of Medicinal Chemistry*. 2009;52(23):7503-11.
- 355 Bethesda (MD) (2021) *Clinical and Research Information on Drug-Induced Liver Injury*, USA: National Institute of Diabetes and Digestive and Kidney Diseases (NIDDK).
- 356 Abongwa M, Baber KE, Martin RJ, Robertson AP. The cholinomimetic morantel as an open channel blocker of the *Ascaris suum* ACR-16 nAChR. *Invertebrate Neuroscience*. 2016;16(4).
- 357 Araki R, Hayashi K, Sawa T. Dopamine D2-receptor Antagonist Droperidol Deepens Sevoflurane Anesthesia. *Anesthesiology*. 2018;128(4):754-63.

- 358 Bosman B. Testing of Lipoxygenase inhibitors, Cyclooxygenase Inhibitors, Drugs with Immunomodulating Properties and Some Reference Antipsoriatic- drugs in the Modified Mouse Tail Test, An Animal Model of Psoriasis. *Skin Pharmacology*. 1994;7(6):324-34.
- 359 Allchurch.G.H and Benstetter.M (2021) European Medicines Agency recommends revocation of marketing authorisations for bufexamac, Available at: <https://www.ema.europa.eu/en/news/european-medicines-agency-recommends-revocation-marketing-authorisations-bufexamac> (Accessed: 18th March 2021).
- 360 Allenmersh TG, Earlam S, Fordy C, Abrams K, Houghton J. Quality of life and survival with continuous hepatic artery fluoroxidine infusion for colorectal liver metastases. *Lancet*. 1994;344(8932):1255-60.
- 361 Tosini G, Ye K, Iuvone PM. N-Acetylserotonin: Neuroprotection, Neurogenesis, and the Sleepy Brain. *Neuroscientist*. 2012;18(6):645-53.
- 362 Lopachin RM, Gaughan CL, Lehning EJ, Weber ML, Taylor CP. Effects of ion channel blockade on the distribution of Na, K, Ca and other elements in oxygen-glucose deprived CA1 hippocampal neurons. *Neuroscience*. 2001;103(4):971-83.
- 363 Filloux FM, Fitts RC, Skeen GA, White HS. The dihydropyridine nitrendipine inhibits H-3 MK-801 binding to mouse-brain sections. *European Journal of Pharmacology-Molecular Pharmacology Section*. 1994;269(3):325-30.
- 364 Anderson K, Wherle L, Park M, Nelson K, Nguyen L. Salsalate, an old, inexpensive drug with potential new indications: a review of the evidence from 3 recent studies. *American health & drug benefits*. 2014;7(4):231-5.
- 365 Friedel HA, Buckley MMT. Torasemide- a review of its pharmacological properties and therapeutical potential. *Drugs*. 1991;41(1):81-103.
- 366 Monteiro JP, Alves MG, Oliveira PF, Silva BM. Structure-Bioactivity Relationships of Methylxanthines: Trying to Make Sense of All the Promises and the Drawbacks. *Molecules*. 2016;21(8).
- 367 Christopher M. Stringer; Michael J. Lopez; Christopher V. Maani. (2020) Tetracaine. StatPearls [Online]. Available at: <https://www.ncbi.nlm.nih.gov/books/NBK535437/> (Accessed: 24th of May 2021).
- 368 Tanwar G, Mazumder AG, Bhardwaj V, Kumari S, Bharti R, Yamini, et al. Target identification, screening and in vivo evaluation of pyrrolone-fused benzosuberene compounds against human epilepsy using Zebrafish model of pentylenetetrazol-induced seizures. *Scientific Reports*. 2019;9.
- 369 Wells JA, McClendon CL. Reaching for high-hanging fruit in drug discovery at protein-protein interfaces. *Nature*. 2007;450(7172):1001-9.
- 370 Jones S, Thornton JM. Principles of protein-protein interactions. *Proceedings of the National Academy of Sciences of the United States of America*. 1996;93(1):13-20.
- 371 Cheng AC, Coleman RG, Smyth KT, Cao Q, Soulard P, Caffrey DR, et al. Structure-based maximal affinity model predicts small-molecule druggability. *Nature Biotechnology*. 2007;25(1):71-5.
- 372 Clackson T, Wells JA. A hot-spot of binding-energy in a hormone receptor interface. *Science*. 1995;267(5196):383-6.

- 373 Maltarollo VG, Kronenberger T, Windshuegel B, Wrenger C, Goulart Trossini GH, Honorio KM. Advances and Challenges in Drug Design of PPAR delta Ligands. *Current Drug Targets*. 2018;19(2):144-54.
- 374 Amaro RE, Baudry J, Chodera J, Demir O, McCammon JA, Miao Y, et al. Ensemble Docking in Drug Discovery. *Biophysical Journal*. 2018;114(10):2271-8.
- 375 Perryman AL, Santiago DN, Forli S, Santos-Martins D, Olson AJ. Virtual screening with AutoDock Vina and the common pharmacophore engine of a low diversity library of fragments and hits against the three allosteric sites of HIV integrase: participation in the SAMPL4 protein-ligand binding challenge. *Journal of Computer-Aided Molecular Design*. 2014;28(4):429-41.
- 376 Villacanas O, Madurga S, Giralt E, Belda I. Explicit Treatment of Water Molecules in Protein-Ligand Docking. *Current Computer-Aided Drug Design*. 2009;5(3):145-54.
- 377 Roberts BC, Mancera RL. Ligand-protein docking with water molecules. *Journal of Chemical Information and Modeling*. 2008;48(2):397-408.
- 378 Ferrins L, Diaz R, Navarro M, Pollastri M. Hit-to-lead studies and pharmacophore identification within a novel class of antitrypanosomal agents. *Abstracts of Papers of the American Chemical Society*. 2017;254.
- 379 Gola J, Obrezanova O, Champness E, Segall M. ADMET property prediction: The state of the art and current challenges. *Qsar & Combinatorial Science*. 2006;25(12):1172-80.
- 380 Raies AB, Bajic VB. In silico toxicology: computational methods for the prediction of chemical toxicity. *Wiley Interdisciplinary Reviews-Computational Molecular Science*. 2016;6(2):147-72.
- 381 Miyawaki I. Application of zebrafish to safety evaluation in drug discovery. *Journal of Toxicologic Pathology*. 2020;33(4):197-210.
- 382 Swinney DC. Phenotypic vs. Target-Based Drug Discovery for First-in-Class Medicines. *Clinical Pharmacology & Therapeutics*. 2013;93(4):299-301.
- 383 Zheng W, Thorne N, McKew JC. Phenotypic screens as a renewed approach for drug discovery. *Drug Discovery Today*. 2013;18(21-22):1067-73.
- 384 Bruni G, Lakhani P, Kokel D. Discovering novel neuroactive drugs through high-throughput behavior-based chemical screening in the zebrafish. *Frontiers in Pharmacology*. 2014;5.
- 385 Stroud.C, Keren.I.N and Bain.L Enabling Novel Treatments for Nervous System Disorders by Improving Methods for Traversing the Blood–Brain Barrier: Proceedings of a Workshop.. Washington : National Academies Press . Available at :<https://www.ncbi.nlm.nih.gov/books/NBK507360/>.
- 386 d'Amora M, Giordani S. The Utility of Zebrafish as a Model for Screening Developmental Neurotoxicity. *Frontiers in Neuroscience*. 2018;12.
- 387 Kozol RA, Abrams AJ, James DM, Buglo E, Yan Q, Dallman JE. Function Over Form: Modeling Groups of Inherited Neurological Conditions in Zebrafish. *Frontiers in Molecular Neuroscience*. 2016;9.
- 388 [Khan.R.F and Alhewairini.S.S. \(2019\). Zebrafish \(Danio rerio\) as a Model Organism. In: Streba.L, Gheonea.D and Schenker.M Current Trends in Cancer Management. London: IntechOpen. Available at : <https://www.intechopen.com/chapters/64178>](#)

- 389 Mizgirev I, Revskoy S. Generation of clonal zebrafish lines and transplantable hepatic tumors. *Nature Protocols*. 2010;5(3):383-94.
- 390 Kari G, Rodeck U, Dicker AP. Zebrafish: An emerging model system for human disease and drug discovery. *Clinical Pharmacology & Therapeutics*. 2007;82(1):70-80.
- 391 Sehnert AJ, Huq A, Weinstein BM, Walker C, Fishman M, Stainier DYR. Cardiac troponin T is essential in sarcomere assembly and cardiac contractility. *Nature Genetics*. 2002;31(1):106-10.
- 392 Hoo JY, Kumari Y, Shaikh MF, Hue SM, Goh BH. Zebrafish: A Versatile Animal Model for Fertility Research. *Biomed Research International*. 2016;2016.
- 393 Delvecchio C, Tiefenbach J, Krause HM. The Zebrafish: A Powerful Platform for In Vivo, HTS Drug Discovery. *Assay and Drug Development Technologies*. 2011;9(4):354-61.
- 394 Kalueff AV, Stewart AM, Gerlai R. Zebrafish as an emerging model for studying complex brain disorders. *Trends in Pharmacological Sciences*. 2014;35(2):63-75.
- 395 Kim YJ, Nam RH, Yoo YM, Lee CJ. Identification and functional evidence of GABAergic neurons in parts of the brain of adult zebrafish (*Danio rerio*). *Neuroscience Letters*. 2004;355(1-2):29-32.
- 396 Rico EP, Rosemberg DB, Seibt K, Capiotti KM, Da Silva RS, Bonan CD. Zebrafish neurotransmitter systems as potential pharmacological and toxicological targets. *Neurotoxicology and Teratology*. 2011;33(6):608-17.
- 397 Parng C, Roy NM, Ton C, Lin Y, McGrath P. Neurotoxicity assessment using zebrafish. *Journal of Pharmacological and Toxicological Methods*. 2007;55(1):103-12.
- 398 Howe K, Clark MD, Torroja CF, Torrance J, Berthelot C, Muffato M, et al. The zebrafish reference genome sequence and its relationship to the human genome. *Nature*. 2013;496(7446):498-503.
- 399 Cornet C, Di Donato V, Terriente J. Combining Zebrafish and CRISPR/Cas9: Toward a More Efficient Drug Discovery Pipeline. *Frontiers in Pharmacology*. 2018;9.
- 400 Armstrong GAB, Liao M, You Z, Lissouba A, Chen BE, Drapeau P. Homology Directed Knockin of Point Mutations in the Zebrafish *tardbp* and *fus* Genes in ALS Using the CRISPR/Cas9 System. *Plos One*. 2016;11(3).
- 401 Clovis.Y. (2021). Worms, Flies or Fish? A Comparison of Common Model Organisms – Part 1: Models for Biomedical Research. Available: <https://invivobiosystems.com/disease-modeling/worms-flies-fish-comparison-common-model-organisms/>. Last accessed 28 September 2021.
- 402 Strange.K. Drug Discovery in Fish, Flies, and Worms. *ILAR J*. 2016;57 (2), 133–143
- 403 Kelly.R.J, Benson.A.S. Inconsistent ethical regulation of larval zebrafish in research. *J Fish Biol*. 2020;97, 324–327.
- 404 Veinotte CJ, Dellaire G, Berman JN. Hooking the big one: the potential of zebrafish xenotransplantation to reform cancer drug screening in the genomic era. *Disease Models & Mechanisms*. 2014;7(7):745-54.
- 405 Wijk.C.R, Hrekels.H.J.E, Hankemeier.T et al . (2016). Systems pharmacology of hepatic metabolism in zebrafish larvae. In: Henney.M.A, Alliance.A Drug

- Discovery Today: Disease Models. Canterbury: Certara QSP. Available at :<https://www.sciencedirect.com/science/article/pii/S1740675717300191#bib0195>.
- 406 Gilbert.S. (2016). *Zebrafish help researchers study human genes*. Available: <https://news.psu.edu/story/418819/2016/07/28/research/zebrafish-help-researchers-study-human-genes>. Last accessed 17th Sep 2021.
- 407 Mraz. M and Haas. K (2020) Antioxidant: Cu/Zn Superoxide dismutase (SOD1), Available at: [https://chem.libretexts.org/Courses/Saint_Marys_College_Notre_Dame_IN/CH2EM_342%3A_Bio-inorganic_Chemistry/Readings/Metals_in_Biological_Systems_\(Saint_Marys_College\)/Antioxidant%3A_Cu%2F%2FZn_Superoxide_dismutase_\(SOD1\)](https://chem.libretexts.org/Courses/Saint_Marys_College_Notre_Dame_IN/CH2EM_342%3A_Bio-inorganic_Chemistry/Readings/Metals_in_Biological_Systems_(Saint_Marys_College)/Antioxidant%3A_Cu%2F%2FZn_Superoxide_dismutase_(SOD1)) (Accessed: 25th June 2021).
- 408 Milani P, Gagliardi S, Cova E, Cereda C. SOD1 Transcriptional and Posttranscriptional Regulation and Its Potential Implications in ALS. *Neurology research international*. 2011;458427-.
- 409 Chan PH, Kawase M, Murakami K, Chen SF, Li YB, Calagui B, et al. Overexpression of SOD1 in transgenic rats protects vulnerable neurons against ischemic damage after global cerebral ischemia and reperfusion. *Journal of Neuroscience*. 1998;18(20):8292-9.
- 410 Wakai T, Sakata H, Narasimhan P, Yoshioka H, Kinouchi H, Chan PH. Transplantation of neural stem cells that overexpress SOD1 enhances amelioration of intracerebral. *Journal of Cerebral Blood Flow and Metabolism*. 2014;34(3):441-9.
- 411 Elshafey A, Lanyon WG, Connor JM. Identification of a new nonsense point mutation in exon-4 of the CU/Zn superoxide-dismutase (SOD!) GENE in a family with amyotrophic lateral sclerosis. *Human Molecular Genetics*. 1994;3(2):363-4
- 412 Gifondorwa.J.D, Robinson.B.M et al. Exogenous Delivery of Heat Shock Protein 70 Increases Lifespan in a Mouse Model of Amyotrophic Lateral Sclerosis. *J Neurosci*. 2007;27 (48), 13173–13180.
- 413 Turner BJ, Talbot K. Transgenics, toxicity and therapeutics in rodent models of mutant SOD1-mediated familial ALS. *Progress in Neurobiology*. 2008;85(1):94-134.
- 414 Lyon MS, Milligan C. Extracellular heat shock proteins in neurodegenerative diseases: New perspectives. *Neuroscience Letters*. 2019;711.
- 415 Chakraborty. K, Chatila.M et al. Chaperonin-Catalyzed Rescue of Kinetically Trapped States in Protein Folding. *Cell*. 2010;142 (1), 112-122.
- 416 Sherman.Y.M and Goldberg.L.A. Cellular Defenses against Unfolded Proteins. *Cell*. 2001;29 (1), 15–32.
- 417 Lyon.M.S and Milligan.C. Extracellular heat shock proteins in neurodegenerative diseases: New perspectives. *Neuroscience Letters*. 2019;711 (1), 134-462.
- 418 Morozov.V.A et al. Interplay between recombinant Hsp70 and proteasomes: proteasome activity modulation and ubiquitin-independent cleavage of Hsp70. *Cell Stress and Chaperones*. 2017;22 (1), 687–697.
- 419 Ramesh T, Lyon AN, Pineda RH, Wang C, Janssen PML, Canan BD, et al. A

- genetic model of amyotrophic lateral sclerosis in zebrafish displays phenotypic hallmarks of motoneuron disease. *Disease Models & Mechanisms*. 2010;3(9-10):652-62.
- 420 Sharp FR, Lowenstein D, Simon R, Hisanaga K. Heat-shock protein HSP72 induction in cortical and striatal astrocytes and neurons following infarction. *Journal of Cerebral Blood Flow and Metabolism*. 1991;11(4):621-7.
- 421 Welsh FA, Moyer DJ, Harris VA. Regional expression of heat-shock-protein-70 messenger-RNA following focal ischemia in rat brain. *Journal of Cerebral Blood Flow and Metabolism*. 1992;12(2):204-12.
- 422 Kinouchi H, Sharp FR, Hill MP, Koistinaho J, Sagar SM, Chan PH. Induction of 70-Kda heat shock protein and HSP70 messenger RNA following transient focal cerebral ischemia in the rat. *Journal of Cerebral Blood Flow and Metabolism*. 1993;13(1):105-15.
- 423 Sharp FR, Lu AG, Tang Y, Millhorn DE. Multiple molecular penumbras after focal cerebral ischemia. *Journal of Cerebral Blood Flow and Metabolism*. 2000;20(7):1011-32.
- 424 Yenari MA, Liu JL, Zheng Z, Vexler ZS, Lee JE, Giffard RG. Antiapoptotic and anti-inflammatory mechanisms of heat-shock protein protection. *Neuroprotective Agents*. 2005;1053:74-83.
- 425 O'Sullivan JC, Yao X-L, Alam H, McCabe JT. Diazoxide, as a postconditioning and delayed preconditioning trigger, increases HSP25 and HSP70 in the central nervous system following combined cerebral stroke and hemorrhagic shock. *Journal of Neurotrauma*. 2007;24(3):532-46.
- 426 Inacio.P. (2021). Arimoclomol Fails to Show Efficacy in Phase 3 Trial, Topline Data Show. Available: <https://alsnewstoday.com/news-posts/2021/05/11/arimoclomol-fails-phase-3-als-trial-does-not-show-efficacy-per-topline-data/>. Last accessed 17th Sep 2021.
- 427 Da Costa MMJ, Allen CE, Higginbottom A, Ramesh T, Shaw PJ, McDermott CJ. A new zebrafish model produced by TILLING of SOD1-related amyotrophic lateral sclerosis replicates key features of the disease and represents a tool for in vivo therapeutic screening. *Disease Models & Mechanisms*. 2014;7(1):73-81.
- 428 Sehnert AJ, Huq A, Weinstein BM, Walker C, Fishman M, Stainier DYR. Cardiac troponin T is essential in sarcomere assembly and cardiac contractility. *Nature Genetics*. 2002;31(1):106-10.
- 429 Doble A. The pharmacology and mechanism of action of riluzole. *Neurology*. 1996;47(6):S233-S41.
- 430 Bellingham MC. A Review of the Neural Mechanisms of Action and Clinical Efficiency of Riluzole in Treating Amyotrophic Lateral Sclerosis: What have we Learned in the Last Decade? *Cns Neuroscience & Therapeutics*. 2011;17(1):4-31.
- 431 Roh K, Roh S, Yang B-H, Lee J-S, Chai YG, Choi MR, et al. Effects of haloperidol and risperidone on the expression of heat shock protein 70 in MK-801-treated rat C6 glioma cells. *Progress in Neuro-Psychopharmacology & Biological Psychiatry*. 2008;32(8):1793-7.
- 432 Sharp FR, Jasper P, Hall J, Noble L, Sagar SM. MK-801 and ketamine induce heat shock protein-hsp72 in injured neurones in posterior cingulate and retrosplenial cortex. *Annals of Neurology*. 1991;30(6):801-9.

- 433 Olney JW, Labruyere J, Wang G, Wozniak DF, Price MT, Sesma MA. NMDA antagonist neurotoxicity- mechanism and prevention. *Science*. 1991;254(5037):1515-8.
- 434 Chen HJ, Liu ZW, Zhou ZH, Jiang MH, Qian LH, Wu SM. The regulatory effect of memantine on expression and synthesis of heat shock protein 70 gene in neonatal rat models with cerebral hypoxic ischemia. *Chinese Medical Journal*. 2003;116(4):558-64.
- 435 Sankaranarayanan A, Raman G, Busch C, Schultz T, Zimin PI, Hoyer J, et al. Naphtho 1,2-d thiazol-2-ylamine (SKA-31), a New Activator of KCa2 and KCa3.1 Potassium Channels, Potentiates the Endothelium-Derived Hyperpolarizing Factor Response and Lowers Blood Pressure. *Molecular Pharmacology*. 2009;75(2):281-95.
- 436 He YJ, Zorumski CF, Mennerick S. Contribution of presynaptic Na⁺ channel inactivation to paired-pulse synaptic depression in cultured hippocampal neurons. *Journal of Neurophysiology*. 2002;87(2):925-36.
- 437 Pratt J, Rataud J, Bardot F, Roux M, Blanchard JC, Laduron PM, et al. Neuroprotective actions of riluzole in rodent models of global and focal cerebral ischemia. *Neuroscience Letters*. 1992;140(2):225-30.
- 438 Verma SK, Arora I, Javed K, Akhtar M, Samim M. Enhancement in the Neuroprotective Power of Riluzole Against Cerebral Ischemia Using a Brain Targeted Drug Delivery Vehicle. *Acs Applied Materials & Interfaces*. 2016;8(30):19716-23.
- 439 Deeken JF, Loescher W. The blood-brain barrier and cancer: Transporters, treatment, and Trojan horses. *Clinical Cancer Research*. 2007;13(6):1663-74.
- 440 Miyawaki I. Application of zebrafish to safety evaluation in drug discovery. *Journal of Toxicologic Pathology*. 2020;33(4):197-210.
- 441 Wolburg H, Lippoldt A. Tight junctions of the blood-brain barrier: Development, composition and regulation. *Vascular Pharmacology*. 2002;38(6):323-37.
- 442 O'Brown NM, Pfau SJ, Gu C. Bridging barriers: a comparative look at the blood-brain barrier across organisms. *Genes & Development*. 2018;32(7-8):466-78.
- 443 Quinonez-Silvero C, Huebner K, Herzog W. Development of the brain vasculature and the blood-brain barrier in zebrafish. *Developmental Biology*. 2020;457(2):181-90.
- 444 Fleming A, Diekmann H, Goldsmith P. Functional Characterisation of the Maturation of the Blood-Brain Barrier in Larval Zebrafish. *Plos One*. 2013;8(10).
- 445 Xie J, Farage E, Sugimoto M, Anand-Apte B. A novel transgenic zebrafish model for blood-brain and blood-retinal barrier development. *Bmc Developmental Biology*. 2010;10.
- 446 Stewart A, Cachat JM, Suci C, Hart PC, Gaikwad S, Utterback E, et al. Intraperitoneal Injection as a Method of Psychotropic Drug Delivery in Adult Zebrafish. *Zebrafish Neurobehavioral Protocols*. 2011;51:169-79.
- 447 Cassar S, Adatto I, Freeman JL, Gamse JT, Iturria I, Lawrence C, et al. Use of Zebrafish in Drug Discovery Toxicology. *Chemical Research in Toxicology*. 2020;33(1):95-118.
- 448 Marques IJ, Lupi E, Mercader N. Mode systems for regeneration: *zebrafish*. *Development*. 2019;146(18).
- 449 Nogales FF. Pathology of the human secondary yolk sac. Haines and Taylor

- obstetrical and gynaecological pathology, Fourth edition. 1995:1677-88.
- 450 Donovan.F.M and Bordoni. B (2021) Embryology, Yolk Sac, 1 edn., StatPearls :
Treasure Island (FL). (link <https://www.ncbi.nlm.nih.gov/books/NBK555965/>)
- 451 Sant KE, Timme-Laragy AR. Zebrafish as a Model for Toxicological
Perturbation of Yolk and Nutrition in the Early Embryo. *Current Environmental
Health Reports*. 2018;5(1):125-33.
- 452 Chlebowski AC, Garcia GR, La Du JK, Bisson WH, Truong L, Simonich SLM, et
al. Mechanistic Investigations Into the Developmental Toxicity of Nitrated and
Heterocyclic PAHs. *Toxicological Sciences*. 2017;157(1):246-59
- 453 Lovato AK, Creton R, Colwill RM. Effects of embryonic exposure to
polychlorinated biphenyls (PCBs) on larval zebrafish behavior. *Neurotoxicology
and Teratology*. 2016;53:1-10.
- 454 Faria M, Garcia-Reyero N, Padros F, Babin PJ, Sebastian D, Cachot J, et al.
Zebrafish Models for Human Acute Organophosphorus Poisoning. *Scientific
Reports*. 2015;5.
- 455 Cayman Chemical (2020) SAFETY DATA SHEET:- acc. to OSHA HCS,
Available at: <https://www.caymanchem.com/msdss/17549m.pdf> (Accessed:
18th of June 2021).
- 456 Cayman Chemical (2018) SAFETY DATA SHEET, Available at:
<https://www.caymanchem.com/msdss/14328m.pdf> (Accessed: 18th of June
2021).
- 457 Drugs.ncat. (2021). N-METHYL-D-ASPARTIC ACID. Available:
<https://drugs.ncats.io/substance/1903B9Q6PI>. Last accessed 29th September
2021.
- 458 Patneau.D.K and Mayer.M.L. Structure-activity relationships for amino acid
transmitter candidates acting at N-methyl-D-aspartate and quisqualate
receptors. *J Neurosci*. 1990;10 (7), 2385–2399.
- 459 Intercollegiate Stroke Working Party. *National clinical guideline for stroke*. 2016;
5th edn, London: Royal College of Physicians.
- 460 Chan.K.M et al. Detection of Necrosis by Release of Lactate Dehydrogenase
(LDH) Activity. *Methods Mol Biol*. 2013;979 (1), 65–70.
- 461 Jin.M.F, Ni.H and Li.L. Leptin Maintained Zinc Homeostasis Against Glutamate-
Induced Excitotoxicity by Preventing Mitophagy-Mediated Mitochondrial
Activation in HT22 Hippocampal Neuronal Cells. *Front Neurol*. 2018;1 (9)322
- 462 Nedeltchev K, der Maur TA, Georgiadis D, Arnold M, Caso V, Mattle HP, et al.
Ischaemic stroke in young adults: predictors of outcome and recurrence.
Journal of Neurology Neurosurgery and Psychiatry. 2005;76(2):191-5.
- 463 Sanchez-Mendoza EH, Hermann DM. Correlates of Post-Stroke Brain
Plasticity, Relationship to Pathophysiological Settings and Implications for
Human Proof-of-Concept Studies. *Frontiers in Cellular Neuroscience*. 2016;10.
- 464 Tornero D, Wattananit S, Madsen MG, Koch P, Wood J, Tatarishvili J, et al.
Human induced pluripotent stem cell-derived cortical neurons integrate in
stroke-injured cortex and improve functional recovery. *Brain*. 2013;136:3561-77.
- 465 Rash B.G, Grove E.A. Area and layer patterning in the developing cerebral
cortex. *Curr Opin Neurobiol*. 2016;16 (1), 25-34.
- 466 Bowes.J. et al. Reducing safety-related drug attrition: the use of in vitro
pharmacological profiling. *Nature reviews drug discovery*.2012;11, 909–922.

467 Fee. L. S (2011) Of Mice and Men, a Common Cortical Connection, Available
at:
https://ucsdnews.ucsd.edu/pressrelease/of_mice_and_men_a_common_cortical_connection/ (Accessed: 29th June 2021).

468 Imaizumi Y, Okano H. Modeling human neurological disorders with induced pluripotent stem cells. *Journal of Neurochemistry*. 2014;129(3):388-99.

469 Eugenin.E.A, King.J.E, Hazleton.J. Differences in NMDA Receptor Expression During Human Development Determine the Response of Neurons to HIV-Tat-mediated Neurotoxicity. *Neurotox Res*. 2011;19 (1), 138–148.

470 Anderson.M *et al.* Functional NMDA receptors with atypical properties are expressed in podocytes. *Am J Physiol Cell Physiol* 300. 2011;1, C22-C32.

471 Xu B , Xu ZF, Deng Y. Effect of manganese exposure on intracellular Ca²⁺ homeostasis and expression of NMDA receptor subunits in primary cultured neurons. *Neurotoxicology*. 2012;30,941–949.

472 Smith.M.S, Wunder.B.M, Norris.A.D and Shellman. G.Y. A Simple Protocol for Using a LDH-Based Cytotoxicity Assay to Assess the Effects of Death and Growth Inhibition at the Same Time. *PLoS One*. 6 2011;(11), e26908.

473 Burrows.J.D (2020) 'The pre-clinical development and characterisation of two novel antioxidant and anti-excitotoxic therapies for multiple sclerosis' pp. 56-58.

474 Portugal J, Waring MJ. Assignment of DNA-binding sites for 4',6'-diamide-2phynylindole and bisbenzimidazole (Hoechst-33258)- a comparative footprint study. *Biochimica Et Biophysica Acta*. 1988;949(2):158-68.

475 Thermo Fisher Scientific (2019) Propidium Iodide, Available at: <https://www.thermofisher.com/uk/en/home/life-science/cell-analysis/fluorophores/propidium-iodide.html> (Accessed: 31st July 2021).

476 BIOASSAY RECORD. DRUGMATRIX: Calcium Channel Type L, Benzothiazepine radioligand binding (ligand: [3H] Diltiazem). Available: <https://pubchem.ncbi.nlm.nih.gov/bioassay/625215#section=Modify-Date>. Last accessed 29th September 2021. (CHEMBL1909102)

477 Warltier.D.C *et al.* The slow-channel calcium blocking agent, nitrendipine, and coronary collateral blood flow. *J Cardiovasc Pharmacol*. 1983;5 (2), 272-7.

478 Skeen G.A, Twyman R.E, White H.S. The dihydropyridine nitrendipine modulates N-Methyl-D-Aspartate receptor channel function in mammalian neurons. *Molecular Pharmacology*. 1993;44(2):443-50.

479 Horn.J, Haan.R, Vermeulen.M and Limburg.M. Very Early Nimodipine Use in Stroke (VENUS): a randomized, double-blind, placebo-controlled trial. *Stroke*. 2001;32 (2), 461-5.

480 Staessen J.A, Fagard.R, Thijs.L *et al.* (1997). Randomised double-blind comparison of placebo and active treatment for older patients with isolated systolic hypertension. The Systolic Hypertension in Europe (Syst-Eur) Trial Investigators. *Lancet*. 1997;350 (9080), 757-64.

481 Schrader J, Luders S, Kulschewski A, Hammersen F, Plate K, Berger J, *et al.* Morbidity and mortality after stroke, eprosartan compared with nitrendipine for secondary prevention - Principal results of a prospective randomized controlled study (MOSES). *Stroke*. 2005;36(6):1218-24.

482 Kaja.S, Payne.J.A *et al.* An optimized lactate dehydrogenase release assay for screening of drug candidates in neuroscience. *J Pharmacol Toxicol Methods*.

- 2015;73, 1-6.
- 483 Sahu. P.M, Nikkilä.O, Lågas.S,Kolehmainen.S and Castrén.E. Culturing primary neurons from rat hippocampus and cortex. *Neuronal Signal*. 2019;3 (2), NS20180207.
- 484 Lobner D. Comparison of the LDH and MTT assays for quantifying cell death: validity for neuronal apoptosis? *Journal of Neuroscience Methods*. 2000;96(2):147-52.
- 485 Llovera G, Roth S, Plesnila N, Veltkamp R, Liesz A. Modeling Stroke in Mice: Permanent Coagulation of the Distal Middle Cerebral Artery. *Jove-Journal of Visualized Experiments*. 2014(89).
- 486 Neuroems (2014) *Blood Flow Through the Brain, pt. 3 (Circle of Willis) Anatomy & Physiology*, Available at: <http://neuroems.com/2014/04/18/blood-flow-through-the-brain-pt-3-circle-of-willis/> (Accessed: 10th April 2021).
- 487 Singh J, Elbarbry F, Lan K, Grabowski T. Animal Pharmacokinetic/Pharmacodynamic Studies (APPS) Reporting Guidelines. *European Journal of Drug Metabolism and Pharmacokinetics*. 2018;43(5):483-94.
- 488 Gad SC, Cassidy CD, Aubert N, Spainhour B, Robbe H. Nonclinical vehicle use in studies by multiple routes in multiple species. *International Journal of Toxicology*. 2006;25(6):499-521.
- 489 Bradford MM. Rapid and sensitive method for quantitation of microgram quantities of protein utilizing principle of protein-dye binding. *Analytical Biochemistry*. 1976;72(1-2):248-54.
- 490 Smith PK, Krohn RI, Hermanson GT, Mallia AK, Gartner FH, Provenzano MD, et al. Measurement of protein using bicinchoninic acid. *Analytical Biochemistry*. 1985;150(1):76-85.
- 491 Pereira EM, de Mattos CS, dos Santos OC, Ferreira DC, de Oliveira TLR, Laport MS, et al. Staphylococcus hominis subspecies can be identified by SDS-PAGE or MALDI-TOF MS profiles. *Scientific Reports*. 2019;9.
- 492 Llovera G, Roth S, Plesnila N, Veltkamp R, Liesz A. Modeling Stroke in Mice: Permanent Coagulation of the Distal Middle Cerebral Artery. *Jove-Journal of Visualized Experiments*. 2014(89).
- 493 Ford G, Xu ZF, Gates A, Jiang J, Ford BD. Expression Analysis Systematic Explorer (EASE) analysis reveals differential gene expression in permanent and transient focal stroke rat models. *Brain Research*. 2006;1071(1):226-36
- 494 Shimazu.T, Inoue.I, Araki.N et al . (2005). A peroxisome proliferator-activated receptor-gamma agonist reduces infarct size in transient but not in permanent ischemia. *Stroke*. 36 (2), 353-9.
- 495 Berger C, Stauder A, Xia F, Sommer C, Schwab S. Neuroprotection and glutamate attenuation by acetylsalicylic acid in temporary but not in permanent cerebral ischemia. *Experimental Neurology*. 2008;210(2):543-8.
- 496 Steinberg GK, Yoon EJ, Kunis DM, Sun GH, Maier CM, Grant GA. Neuroprotection by N-Methyl-D-Aspartate antagonist in focal cerebral-ischemia is dependent on continued maintenance dosing. *Neuroscience*. 1995;64(1):99-107.
- 497 Ma R, Xie Q, Li Y, Chen ZP, Ren MH, Chen H, et al. Animal models of cerebral ischemia: A review. *Biomedicine & Pharmacotherapy*. 2020;131.

- 498 McBride DW, Zhang JH. Precision Stroke Animal Models: the Permanent MCAO Model Should Be the Primary Model, Not Transient MCAO. *Translational Stroke Research*. 2017;8(5):397-404.
- 499 Fluri F, Schuhmann MK, Kleinschnitz C. Animal models of ischemic stroke and their application in clinical research. *Drug Design Development and Therapy*. 2015;9:3445-54.
- 500 Macrae IM. Preclinical stroke research - advantages and disadvantages of the most common rodent models of focal ischaemia. *British Journal of Pharmacology*. 2011;164(4):1062-78.
- 501 Randomised, double-blind, placebo-controlled trial of nimodipine in acute stroke. *Trust Study Group*. *Lancet* (London, England). 1990;336(8725):1205-9.
- 502 Wahlgren NG, Macmahon DG, Dekeyser J, Indredavik B, Ryman T. Intravenous nimodipine west-European stroke trial (INWEST) of nimodipine in the treatment of acute ischaemic stroke. *Cerebrovascular Diseases*. 1994;4(3):204-10.
- 503 Yamaguchi T, Sano K, Takakura K, Saito I, Shinohara Y, Asano T, et al. Ebselen in acute ischemic stroke - A placebo-controlled, double-blind clinical trial. *Stroke*. 1998;29(1):12-7.
- 504 Franke CL, Palm R, Dalby M, Schoonderwaldt HC, Hantson L, Eriksson B, et al. Flunarizine in stroke treatment (FIST): A double-blind, placebo-controlled trial in Scandinavia and the Netherlands. *Acta Neurologica Scandinavica*. 1996;93(1):56-60.
- 505 Schreiber JA, Schepmann D, Frehland B, Thum S, Datunashvili M, Budde T, et al. A common mechanism allows selective targeting of GluN2B subunit-containing N-methyl-D-aspartate receptors. *Communications Biology*. 2019;2.
- 506 Wahlgren NG, Macmahon DG, Dekeyser J, Indredavik B, Ryman T. Intravenous nimodipine west-European stroke trial (INWEST) of nimodipine in the treatment of acute ischaemic stroke. *Cerebrovascular Diseases*. 1994;4(3):204-10.
- 507 Juskaite V, Ramanauskiene K, Briedis V. Design and Formulation of Optimized Microemulsions for Dermal Delivery of Resveratrol. *Evidence-Based Complementary and Alternative Medicine*. 2015;2015
- 508 Sercombe L, Veerati T, Moheimani F, Wu SY, Sood AK, Hua S. Advances and Challenges of Liposome Assisted Drug Delivery. *Frontiers in Pharmacology*. 2015;6.
- 509 Lee TWY, Boersen NA, Hui HW, Chow SF, Wan KY, Chow AHL. Delivery of Poorly Soluble Compounds by Amorphous Solid Dispersions. *Current Pharmaceutical Design*. 2014;20(3):303-24.
- 510 Goh WJ, Zou S, Ong WY, Torta F, Alexandra AF, Schiffelers RM, et al. Bioinspired Cell-Derived Nanovesicles versus Exosomes as Drug Delivery Systems: a Cost-Effective Alternative. *Scientific Reports*. 2017;7.
- 511 Farjadian F, Ghasemi A, Gohari O, Roointan A, Karimi M, Hamblin MR. Nanopharmaceuticals and nanomedicines currently on the market: challenges and opportunities. *Nanomedicine*. 2019;14(1):93-126.
- 512 LKT Laboratories (2021) *NITRENDIPINE*, Available at: <https://lktlabs.com/product/nitrendipine/> (Accessed: 16072021).
- 513 Cayman chemical (2015) *NITRENDIPINE*, Available

- at: <https://www.caymanchem.com/pdfs/17549.pdf> (Accessed: 16/07/2021).
- 514 Bartsch W, Sponer G, Dietmann K, Fuchs G. Acute toxicity of various solvents in mouse and rat – LD50 of ethanol, diethylacetamide, dimethylformamide, dimethylsulfoxide, glycerine, n-methylpyrrolidone, polyethylene-glycol 400, 1,2-propanediol and tween 20. *Arzneimittel-Forschung/Drug Research*. 1976;26(8):1581-3.
- 515 Kelava T, Cavar I, Culo F. Influence of small doses of various drug vehicles on acetaminophen-induced liver injury. *Canadian Journal of Physiology and Pharmacology*. 2010;88(10):960-7.
- 516 Schwabe U, Ukena D, Lohse MJ. Xanthine derivatives as antagonists at A1 and A2 adenosine receptors. *Naunyn-Schmiedeberg's Archives of Pharmacology*. 1985;330(3):212-21.
- 517 Selleckchem. (2021) *Dyphylline*. Available: [https://www.selleckchem.com/products/Dyphylline\(Dilor\).html](https://www.selleckchem.com/products/Dyphylline(Dilor).html). Last accessed 28th September 2021.
- 518 Parr JS, Khalifah RG. Inhibition of carbonic anhydrases-I and anhydrases II by N-unsubstituted carbamate esters. *Journal of Biological Chemistry*. 1992;267(35):25044-50.
- 519 Matsuda A, Hattori H, Tanaka M, Sasaki T. Nucleosides and nucleotides .152. 1-(3-C-ethynyl-beta-D-ribo-pentofuranosyl)uracil as a broad spectrum antitumor nucleoside. *Bioorganic & Medicinal Chemistry Letters*. 1996;6(16):1887-92.
- 520 Sigma-Aldrich. (2002). *5-Fluorouracil Product information*. Available: <https://www.sigmaaldrich.com/deepweb/assets/sigmaaldrich/product/documents/196/138/f6627pis.pdf>. Last accessed 28th September 2021.
- 521 Gad SC, Cassidy CD, Aubert N, Spainhour B, Robbe H. Nonclinical vehicle use in studies by multiple routes in multiple species. *International Journal of Toxicology*. 2006;25(6):499-521.
- 522 Erhirhie EO, Ihekwereme CP, Ilodigwe EE. Advances in acute toxicity testing: strengths, weaknesses and regulatory acceptance. *Interdisciplinary toxicology*. 2018;11(1):5-12.
- 523 Thackaberry EA, Wang X, Schweiger M, Messick K, Valle N, Dean B, et al. Solvent-based formulations for intravenous mouse pharmacokinetic studies: tolerability and recommended solvent dose limits. *Xenobiotica*. 2014;44(3):235-41.
- 524 Chemical Book (2017) Chemical properties, Available at: <https://www.chemicalbook.com/> (Accessed: 19th of July 2021).
- 525 Nair AB, Jacob S. A simple practice guide for dose conversion between animals and human. *Journal of basic and clinical pharmacy*. 2016;7(2):27-31.
- 526 Jouyban A, Fakhree MAA, Shayanfar A. Review of Pharmaceutical Applications of N-Methyl-2-Pyrrolidone. *Journal of Pharmacy and Pharmaceutical Sciences*. 2010;13(4):524-35.
- 527 Saillenfait AM, Gallissot F, Morel G. Developmental toxicity of N-methyl-2-pyrrolidone in rats following inhalation exposure. *Food and Chemical Toxicology*. 2003;41(4):583-8.
- 528 Walter J, Plesnila N, Terpolilli NA. Influence of organic solvents on secondary brain damage after experimental traumatic brain injury. *Journal of Neurotrauma*. 2018;35(16):A217-A.

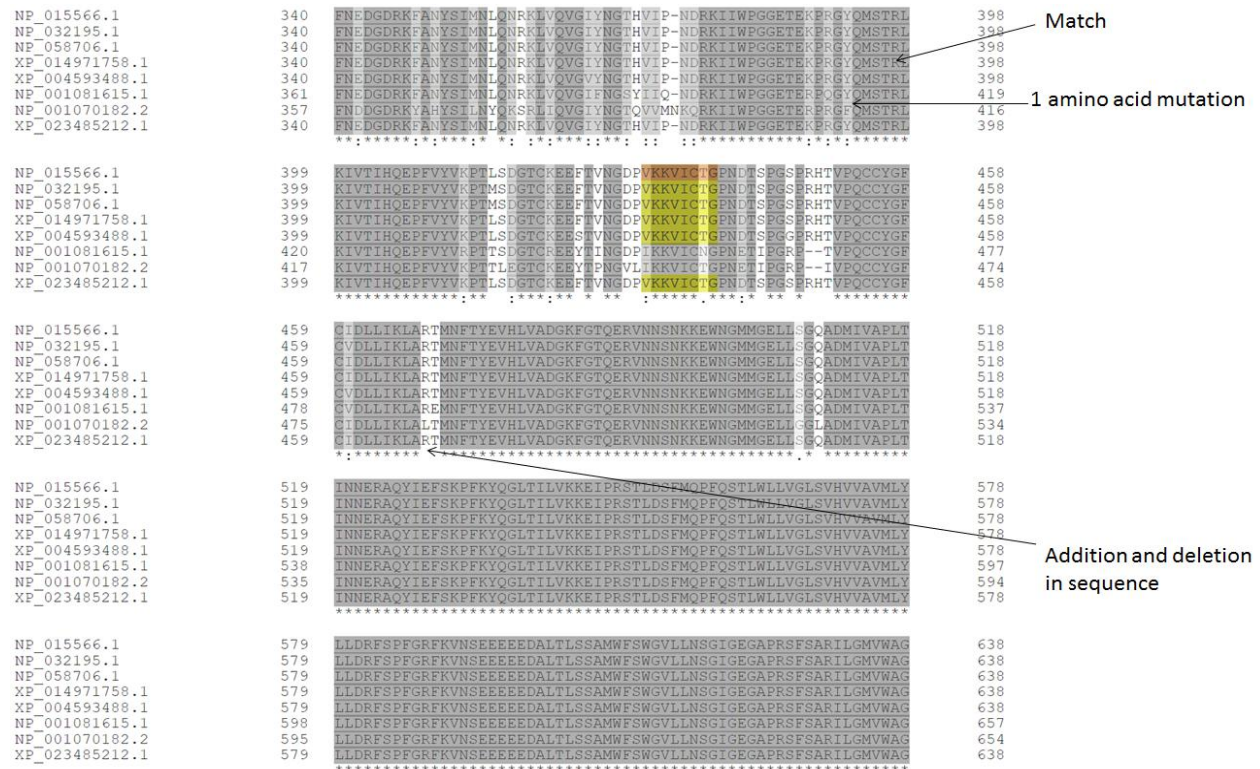
- 529 Bian J, Cao D, Shen J, Jiang B, Chen D, Bian L. N-methyl pyrrolidone promotes ankle fracture healing by inhibiting inflammation via suppression of the mitogen-activated protein kinase signaling pathway. *Experimental and Therapeutic Medicine*. 2018;15(4):3617-22.
- 530 Hua GX, Zhang QZ, McManus D, Slawin AMZ, Woollins JD. Improvement of the Fe-NTA sulfur recovery system by the addition of a hydroxyl radical scavenger. *Phosphorus Sulfur and Silicon and the Related Elements*. 2007;182(1):181-98.
- 531 Kouhzaei S, Rad I, Khodayari K, Mobasheri H. The Neuroprotective Ability of Polyethylene Glycol is Affected by Temperature in Ex Vivo Spinal Cord Injury Model. *Journal of Membrane Biology*. 2013;246(8):613-9.
- 532 Hendeles L, Weinberger M. Dyphylline – untheophylline xanthine bronchodilator. *Drug Intelligence & Clinical Pharmacy*. 1977;11(7):424-.
- 533 Drug bank (2021) Dyphylline, Available at: <https://go.drugbank.com/drugs/DB00651> (Accessed: 23rd July 2021).
- 534 Schwabe U, Ukena D, Lohse MJ. Xanthine derivatives as antagonists AT A1 AND A2 adenosine receptors. *Naunyn-Schmiedebergs Archives of Pharmacology*. 1985;330(3):212-21.
- 535 Chen JF, Eitzschig HK, Fredholm BB. Adenosine receptors as drug targets - what are the challenges? *Nature Reviews Drug Discovery*. 2013;12(4):265-86.
- 536 Borea PA, Gessi S, Merighi S, Vincenzi F, Varani K. Pharmacology of adenosine receptors: the state of the art. *Physiological Reviews*. 2018;98(3):1591-625.
- 537 Stockwell J, Chen ZC, Niazi M, Nosib S, Cayabyab FS. Protein phosphatase role in adenosine A1 receptor-induced AMPA receptor trafficking and rat hippocampal neuronal damage in hypoxia/reperfusion injury. *Neuropharmacology*. 2016;102:254-65.
- 538 Levers TE, Edgar JM, Price DJ. The fates of cells generated at the end of neurogenesis in developing mouse cortex. *Journal of Neurobiology*. 2001;48(4):265-77.
- 539 Bederson JB, Pitts LH, Germano SM, Nishimura MC, Davis RL, Bartkowski HM. Evaluation of 2,3,5-triphenyltetrazolium chloride as a stain for detection and quantification of experimental cerebral infarction in rats. *Stroke*. 1986;17(6):1304-8.
- 540 Chou R, Peterson K, Helfand M. Comparative efficacy and safety of skeletal muscle relaxants for spasticity and musculoskeletal conditions: a systematic review. *Journal of Pain and Symptom Management*. 2004;28(2):140-75.
- 541 Han R, Yang YM, Dietrich J, Luebke A, Mayer-Proschel M, Noble M. Systemic 5-fluorouracil treatment causes a syndrome of delayed myelin destruction in the central nervous system. *Journal of biology*. 2008;7(4):12-.
- 542 Weng Q, Tan B, Wang J, Wang J, Zhou H, Shi J, et al. 5-Fluorouracil causes severe CNS demyelination by disruption of TCF7L2/HDAC1/HDAC2 complex in adolescent mice. *Toxicology*. 2014;325:144-50.
- 543 Skeen GA, White HS, Twyman RE. The dihydropyridine nitrendipine reduces N-methyl-D-aspartate (NMDA)-evoked currents of rodent cortical neurons through a direct interaction with the NMDA receptor associated ion channel. *Journal of Pharmacology and Experimental Therapeutics*. 1994;271(1):30-8.

- 544 Qian W-J, Kaleta DT, Petritis BO, Jiang H, Liu T, Zhang X, et al. Enhanced Detection of Low Abundance Human Plasma Proteins Using a Tandem IgY12-SuperMix Immunoaffinity Separation Strategy. *Molecular & Cellular Proteomics*. 2008;7(10):1963-73.
- 545 Thermofisher (2021) SulfoLinK, Immobilization Kit for Peptides, Available at: <https://www.thermofisher.com/order/catalog/product/44999#/44999> (Accessed: 14th August 2021).
- 546 Syedbasha M, Linnik J, Santer D, O'Shea D, Barakat K, Joyce M, et al. An ELISA Based Binding and Competition Method to Rapidly Determine Ligand-receptor Interactions. *Jove-Journal of Visualized Experiments*. 2016(109).
- 547 Englebienne P, Van Hoonacker A, Verhas M. Surface plasmon resonance: principles, methods and applications in biomedical sciences. *Spectroscopy-an International Journal*. 2003;17(2-3):255-73.
- 548 Holloway PM, Gavins FNE. Modeling Ischemic Stroke In Vitro: Status Quo and Future Perspectives. *Stroke*. 2016;47(2):561-9.
- 549 Glasgow NG, Johnson JW. Whole-Cell Patch-Clamp Analysis of Recombinant NMDA Receptor Pharmacology Using Brief Glutamate Applications. *Patch-Clamp Methods and Protocols*, 2nd Edition. 2014;1183:23-41.
- 550 Jiang X, Andjelkovic AV, Zhu L, Yang T, Bennett MVL, Chen J, et al. Blood-brain barrier dysfunction and recovery after ischemic stroke. *Progress in Neurobiology*. 2018;163:144-71.
- 551 Moser AC, Hage DS. Immunoaffinity chromatography: an introduction to applications and recent developments. *Bioanalysis*. 2010;2(4):769-90.
- 552 Manjunath K, Venkateswarlu V. Pharmacokinetics, tissue distribution and bioavailability of nitrendipine solid lipid nanoparticles after intravenous and intraduodenal administration. *Journal of Drug Targeting*. 2006;14(9):632-45.
- 553 Bagchi S, Chhibber T, Lahooti B, Verma A, Borse V, Jayant RD. In-vitro blood-brain barrier models for drug screening and permeation studies: an overview. *Drug Design Development and Therapy*. 2019;13:3591-605.
- 554 Jouan E, Le Vee M, Mayati A, Denizot C, Parmentier Y, Fardel O. Evaluation of P-Glycoprotein Inhibitory Potential Using a Rhodamine 123 Accumulation Assay. *Pharmaceutics*. 2016;8(2).

Appendix

Appendix A.

The complete sequence alignment of NMDAR GluNR1 sequence with other species.



Key	ID	Species	Species NMDA NR1 Full sequence Alignment	% Identity
1	NP_015566.1	Homo sapiens (Human)	Human vs Mouse	99.04
2	NP_032195.1	Mus musculus (Mouse)	Human vs Rat	99.25
3	NP_058706.1	Rattus norvegicus (Rat)	Human vs Pica	91.16
4	XP_014971758	Macaca mulatta (Monkey)	Human vs Monkey	99.50
5	XP_004593488.1	Ochotona princeps (Pika)	Human vs Frog	82.47
6	NP_001081615.1	Xenopus laevis (Frog)	Human vs Zebrafish	78.76
7	NP_001070182.2	Danio rerio (Zebra fish)	Human vs Horse	99.36
8	XP_023485212.1	Equus caballus (Horse)		

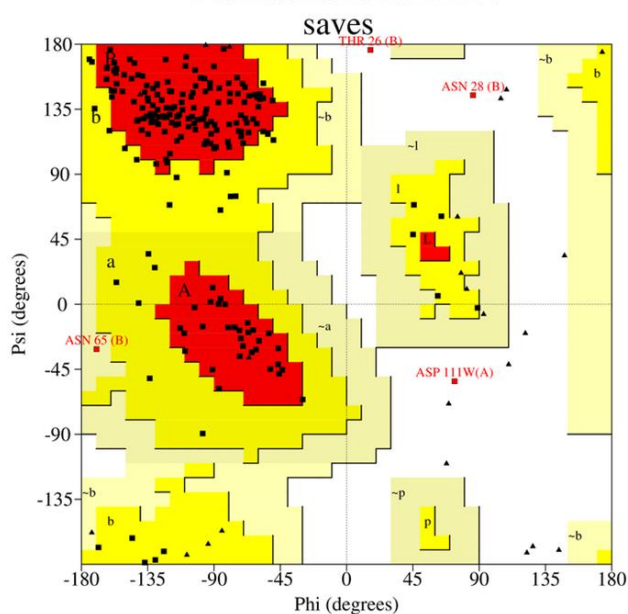
Appendix B

Overall Templates						
PDB Code	Similarity (%)	Identity (%)	Resolution	VH	VL_LAMBDA	Redundant Hits
3ks0	79.8	54.9	2.7	H:1-117	L:1-110	
1etz	77.5	54.9	2.6	B:1-126	L:1-110	
1p4i	76.3	54.3	2.8	H:1-112	L:2-110	
1p4b	76.3	53.8	2.35	H:1-112	L:2-110	
1gig	75.7	53.2	2.3	H:1-122	L:1-110	2vis;2vit;2vir
1nc2	75.2	52.6	2.1	B:1-118	A:1-110	1nc4
1nfd	73.4	53.7	2.8	F:1-120	E:1-108	
2op4	72.3	47.4	2.85	H:1-122	L:1-110	2ntf
1a6v	71.1	47.4	1.8	H:1-118	L:1-110	
1a6w	71.1	47.4	2	H:1-120	L:1-109	
1a6u	71.1	47.4	2.1	H:1-120	L:1-108	
2y06	71.1	46.8	2.5	H:1-120	L:1-110	
1ngq	71.1	46.2	2.4	H:1-120	L:1-110	1ngp
1nj9	71.1	46.2	2.35	B:1-116	L:1-110	
1yuh	71.1	46.2	3	B:1-118	L:1-109	
2zpk	71.1	44.5	1.8	H:1-115	L:1-109	
1ind	70.5	48	2.2	H:1-114	L:1-109	1ine
2xzq	70.5	46.2	2.4	H:1-120	L:1-110	
2y07	70.5	46.2	2.4	H:1-120	L:1-110	
4a6y	70.5	45.7	2.9	B:1-119	A:1-110	
1q0x	70.5	44.5	1.6	H:1-119	L:1-110	1q0y
1f4x	69.9	48	2.3	H:1-117	L:1-110	1f4w;1f4y
1y0l	69.9	47.4	2.5	B:1-123	L:1-110	3cfk
1y18	69.9	47.4	2.8	B:1-123	L:1-110	
2y36	69.9	45.6	2.7	H:1-120	L:1-110	
3ffd	69.4	51.4	2	A:1-118	B:1-116	
1pg7	69.4	45.7	2.5	X:1-120	W:1-110	
3rhw	69.4	45.1	3.26	F:1-122	K:1-110	3rif;3ri5
1sm3	69.3	48.6	1.95	H:1-117	L:1-109	
1mfd	68.8	41	2.1	H:1-118	L:1-110	1mfb;1mfc
1mfa	68.8	40.4	1.7	H:1-117	L:1-110	
2otu	68.2	51.4	1.68	D:1-118	A:2-115	2gsg;2otw
2qhr	68.2	50.3	2	H:1-123	L:1-116	
1jn6	68.2	45.1	2.7	B:1-119	A:1-110	1jnh
1mfe	68.2	41	2	H:1-117	L:1-109	
3s96	67.7	48.5	1.9	A:1-119	B:1-116	
4dcq	67.1	48.5	1.94	B:1-119	A:1-115	

Appendix C

a) 5ACO_M0012

Ramachandran Plot



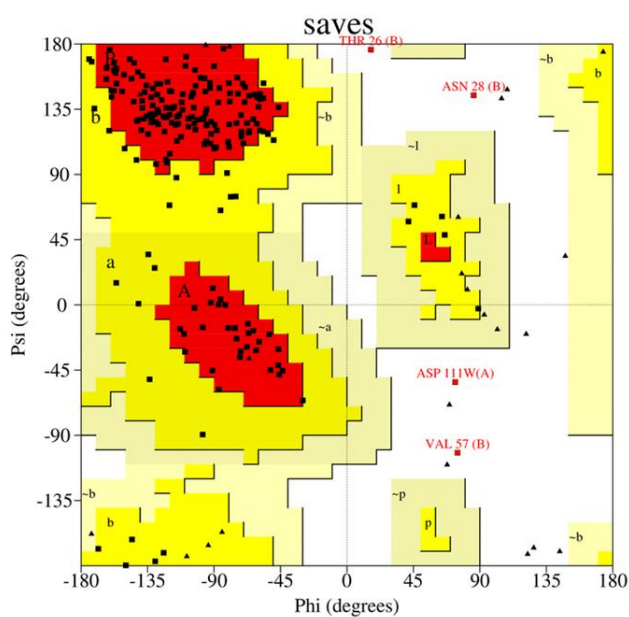
Plot statistics

Residues in most favoured regions [A,B,L]	159	82.0%
Residues in additional allowed regions [a,b,l,p]	31	16.0%
Residues in generously allowed regions [-a,-b,-l,-p]	1	0.5%
Residues in disallowed regions	3	1.5%
Number of non-glycine and non-proline residues	194	100.0%
Number of end-residues (excl. Gly and Pro)	3	
Number of glycine residues (shown as triangles)	24	
Number of proline residues	14	
Total number of residues	235	

Based on an analysis of 118 structures of resolution of at least 2.0 Angstroms and R-factor no greater than 20%, a good quality model would be expected to have over 90% in the most favoured regions.

b) 5ACO_M0016

Ramachandran Plot



Plot statistics

Residues in most favoured regions [A,B,L]	159	82.0%
Residues in additional allowed regions [a,b,l,p]	31	16.0%
Residues in generously allowed regions [-a,-b,-l,-p]	0	0.0%
Residues in disallowed regions	4	2.1%
Number of non-glycine and non-proline residues	194	100.0%
Number of end-residues (excl. Gly and Pro)	3	
Number of glycine residues (shown as triangles)	24	
Number of proline residues	14	
Total number of residues	235	

Based on an analysis of 118 structures of resolution of at least 2.0 Angstroms and R-factor no greater than 20%, a good quality model would be expected to have over 90% in the most favoured regions.

Figure 3.5 Cross validation of best homolog model 5ACO_M0012 and 5ACO_M0016

Using the PROCHECK server to demonstrate that the quality of the homology model is good enough for the docking studies.

Appendix D

Table 1. Active site residues extracted from the crystal structures of NMDAR using DS software.

PDB ID Crystal Structure	Binding site	Amino acids (No)
5U8C	BS1	TYR(18),THR(33),VAL(34),ASN(35),PHE(230)GLN(234),LYS(282),THR(283),TRP(284),286(ARG),TYR(287)
	BS2	THR(33),ASP(37),PRO(38),VAL(39),LYS(40),ASP(69),THR(283),TRP(284),PHE(276)
	BS3	ILE(11),HIS(12),GLN(13),GLU(14),VAL(19),PRO(47),ASN(48),ASP(49),ARG(56),THR(58),GLN(61),LEU(86),VAL(87),ALA(88),ASP(89),GLY(90),LYS(91)PHE(92),VAL(176)LYS(177)GLN(178),SER(179),GLU(204),SER(205),ALA(206)GLU(208),ILE(210),TRP(223),VAL(227),GLU(231)
1PB8	BS1	GLU(14),TYR(18),GLU(31),PHE(32),THR(33),VAL(34),VAL(39),LYS(41),TYR(64),PHE(230),GLU(231),GLN(234),LYS235,THR283,284(TRP),287(TYR)288(GLN)292(SER)
	BS2	THR(33),PRO(38),VAL(39),LYS(40),ASP(69),TRP(284),PHE276,LEU280
	BS3	ARG(5),ILE(43),TYR(82),GLU(83),
2A5T	BS1	THR(33),VAL(34),ASN(35),LYS(282),THR(283),TYR(287),ASP(27)
	BS2	LYS(40),ASP(69),ILE(72),LYS(73),PHE(276),THR(33),PRO(38),VA;(39),LYS(40),ASP(69),THR(283),TRP(284)
	BS3	ILE(2),HIS(12),GLN(13),GLU(14),VAL(19),PRO(47),ASN(48),GLN(61),LEU(86),VAL(87),ALA(88),HLY(90),LYS(91),PHE(92)VAL(176),LYS(177),GLU(204),SER(205),ALA(206),GLU(208),ILE(210),TRP(223),VAL(227),GLU(231)
4KFQ	BS1	TYR(18),GLU(31),PHE(32),THR(33),VAL(34),ASN(35),ASP(37),VAL(39),LYS(41)TYR(64)PHE(230),ASP(279),LYS(282),THR(283),TRP(284),ARG(286)TYR(287),GLN(288)
	BS2	LYS(40),ASP(69),ILE(72),LYS(73),ARG(76),PHE(276)
	BS3	THR(22),MET(23),SER(24),GLY(26),ARG(56),PRO(60)
5H8F	BS1	SER(169),PHE(172),TYR(19),TRP(285),TYR(288)
	BS2	LYS(41),ASP(70),ILE(73),LYS(74),PHE(277)
	BS3	ILE(12),HIS(13),GLN(14),GLU(15),PRO(48),ASN(49),ASP(50)THR(51),SER(52),PRO(53),GLY(54),SER(55),PRO(56),ARG(57),LEU(87),VAL(88),ALA(89),ASP(90),GLY(91),LYS(92),PHE(93),VAL(177),LYS(178),GLN(179),SER(180),GLU(205),SER(206),ALA(207),ALA(208),GLU(209),ILE(211),TRP(224),VAL(228),232(GLU)
5H8Q	BS1	SER(169),PHE(172),TYR(19),TRP(285),TYR(288)
	BS2	THR(34),VAL(35),ASN(36),ASP(38),PRO(39),VAL(40),LYS(41),ASP(70),ILE(73),LYS(74),PHE(277),ASP(280),LEU(281),LYS(283),THR(284),TYR(285)
	BS3	ILE(12),HIS(13),GLN(14),GLU(15),VAL(20),PRO(48),ASN(49),ASP(50),THR(51),SER(52),PRO(53),GLY(54),SER(55)ARG(57),GLN(62),LEU(87),VAL(88),ALA(89),ASP(90),GLY(91),LYS(92),PHE(93),VAL(177),LYS(178),GLN(179),SER(180),GLU(205),SER(206),ALA(207),ALA(208),GLU(209),ILE(211),TRP(224),VAL(228),GLU(232),LYS(236)
5H8H	BS1	TYR(19),GLU(32),PHE(33),THR(34),VAL(35),ASN(36),ASP(38),VAL(40),TYR(65),PHE(231),GLN(235),ASP(280),284(THR),TRP(285)
	BS2	LYS(41),ASP(70),ILE(73),LYS(74),PHE(277),LEU(281)
	BS3	ILE(12),HIS(13),GLN(14),GLU(15),VAL(20),PRO(48),ASN(49),ASP(50),THR(51),SER(52),PRO(53),GLY(54),SER(55)ARG(57),GLN(62),LEU(87),VAL(88),ALA(89),ASP(90),GLY(91),LYS(92),PHE(93),VAL(177),LYS(178),GLN(179)

Appendix E.

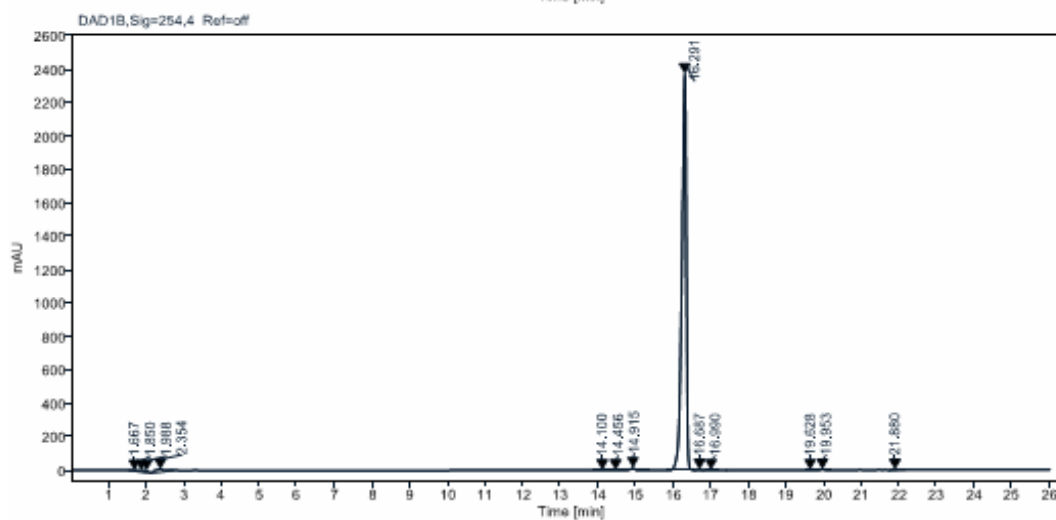
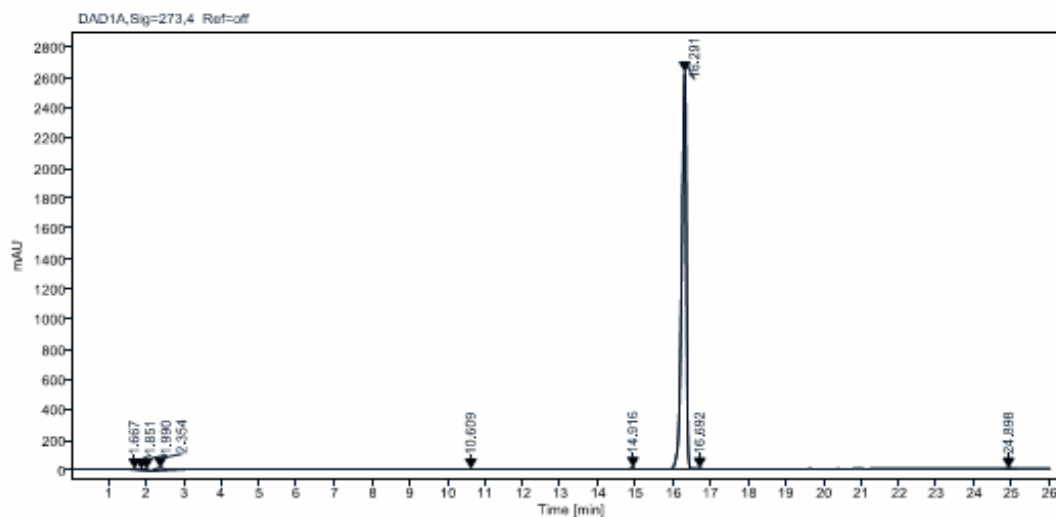
Binding energy of Nitrendipine (4507) enantiomers (R) and (S)

Binding Site 1								
Ligand Name	Binding Energy (kcal/mol)	Total Binding Energy (kcal/mol)	Ligand Energy (kcal/mol)	Protein Energy (kcal/mol)	Complex Energy (kcal/mol)	Entropic Energy (kcal/mol)	Ligand Conformational Energy (kcal/mol)	Ligand Conformational Entropy (kcal/mol-K)
S-Nitrendipine	-5.58760	-1.9252	29.10881	-32010	-31986.34012	19.81880	3.6624	0.61479
S-Nitrendipine	-9.55453	-6.5476	25.23926	-32010	-31994.17660	19.86700	3.0069	0.82263
S-Nitrendipine	-9.55453	-6.5476	25.23926	-32010	-31994.17660	19.86700	3.0069	0.82263
S-Nitrendipine	-9.55453	-6.5476	25.23926	-32010	-31994.17660	19.86700	3.0069	0.82263
S-Nitrendipine	-4.19033	-3.0933	24.67514	-32010	-31989.37652	19.86920	1.0970	0.82263
S-Nitrendipine	-1.88438	1.5836	27.63154	-32010	-31984.11417	19.81530	3.4680	0.82263
S-Nitrendipine	-1.88438	1.5836	27.63154	-32010	-31984.11417	19.81530	3.4680	0.82263
S-Nitrendipine	-4.14550	-2.9426	29.50823	-32010	-31984.49860	19.85190	1.2029	0.82263
S-Nitrendipine	-4.14550	-2.9426	29.50823	-32010	-31984.49860	19.85190	1.2029	0.82263
S-Nitrendipine	-4.14550	-2.9426	29.50823	-32010	-31984.49860	19.85190	1.2029	0.82263
R-Nitrendipine	2.73103	4.1771	25.30832	-32010	-31981.82198	19.88460	1.4461	0.83957
R-Nitrendipine	2.73103	4.1771	25.30832	-32010	-31981.82198	19.88460	1.4461	0.83957
R-Nitrendipine	2.73103	4.1771	25.30832	-32010	-31981.82198	19.88460	1.4461	0.83957
R-Nitrendipine	2.73103	4.1771	25.30832	-32010	-31981.82198	19.88460	1.4461	0.83957
R-Nitrendipine	-2.46711	-0.40583	24.66844	-32010	-31987.66000	19.85600	2.0613	0.83957
R-Nitrendipine	-6.84729	-5.1536	25.54855	-32010	-31991.16007	19.84980	1.6937	0.83957
R-Nitrendipine	-6.84729	-5.1536	25.54855	-32010	-31991.16007	19.84980	1.6937	0.83957
R-Nitrendipine	-6.84729	-5.1536	25.54855	-32010	-31991.16007	19.84980	1.6937	0.83957
R-Nitrendipine	-6.84729	-5.1536	25.54855	-32010	-31991.16007	19.84980	1.6937	0.83957
R-Nitrendipine	-6.84729	-5.1536	25.54855	-32010	-31991.16007	19.84980	1.6937	0.83957

Binding site 2								
Ligand Name	Binding Energy (kcal/mol)	Total Binding Energy (kcal/mol)	Ligand Energy (kcal/mol)	Protein Energy (kcal/mol)	Complex Energy (kcal/mol)	Entropic Energy (kcal/mol)	Ligand Conformational Energy (kcal/mol)	Ligand Conformational Entropy (kcal/mol-K)
S-Nitrendipine	5.20953	7.5565	25.61421	-32010	-31979.03759	19.87440	2.3470	0.62495
S-Nitrendipine	5.20953	7.5565	25.61421	-32010	-31979.03759	19.87440	2.3470	0.62495
S-Nitrendipine	5.90912	8.2561	24.22743	-32010	-31979.72478	19.86460	2.3470	0.62495
S-Nitrendipine	5.90912	8.2561	24.22743	-32010	-31979.72478	19.86460	2.3470	0.62495
S-Nitrendipine	5.90912	8.2561	24.22743	-32010	-31979.72478	19.86460	2.3470	0.62495
S-Nitrendipine	5.21160	7.5586	25.61444	-32010	-31979.03529	19.87440	2.3470	0.62495
S-Nitrendipine	5.30398	7.6510	24.86735	-32010	-31979.69000	19.88390	2.3470	0.62495
S-Nitrendipine	5.30398	7.6510	24.86735	-32010	-31979.69000	19.88390	2.3470	0.62495
S-Nitrendipine	3.28645	5.1010	26.25220	-32010	-31980.32268	19.82670	1.8146	0.62495
S-Nitrendipine	9.03951	11.387	28.68980	-32010	-31972.13202	19.87210	2.3470	0.62495
R-Nitrendipine	10.28228	11.923	25.64594	-32010	-31973.93311	19.85360	1.6410	0.81372
R-Nitrendipine	11.54242	14.730	28.59654	-32010	-31969.72237	19.83810	3.1875	0.81372
R-Nitrendipine	11.54242	14.730	28.59654	-32010	-31969.72237	19.83810	3.1875	0.81372
R-Nitrendipine	11.54242	14.730	28.59654	-32010	-31969.72237	19.83810	3.1875	0.81372
R-Nitrendipine	9.76580	11.407	25.23083	-32010	-31974.86470	19.85150	1.6410	0.81372
R-Nitrendipine	9.76580	11.407	25.23083	-32010	-31974.86470	19.85150	1.6410	0.81372
R-Nitrendipine	9.76580	11.407	25.23083	-32010	-31974.86470	19.85150	1.6410	0.81372
R-Nitrendipine	10.12087	11.762	24.93428	-32010	-31974.80618	19.85020	1.6410	0.81372
R-Nitrendipine	10.12087	11.762	24.93428	-32010	-31974.80618	19.85020	1.6410	0.81372
R-Nitrendipine	5.14333	7.6994	26.95554	-32010	-31977.76246	19.84900	2.5561	0.81372

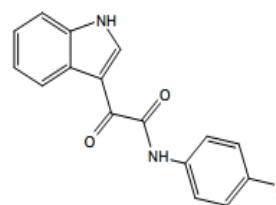
Synthesis of *N*-(4-fluorobenzyl)-2-(1*H*-indole-3-yl)-2-oxoacetamide

Single Injection Report

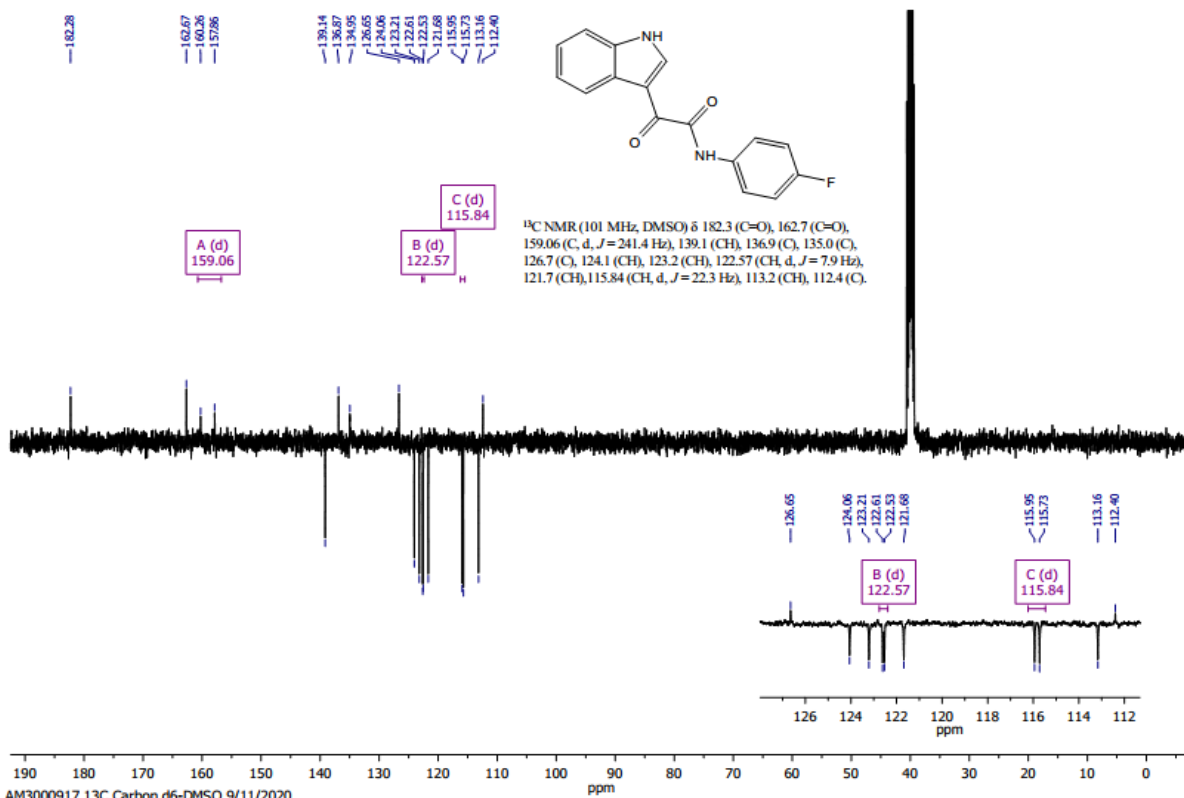
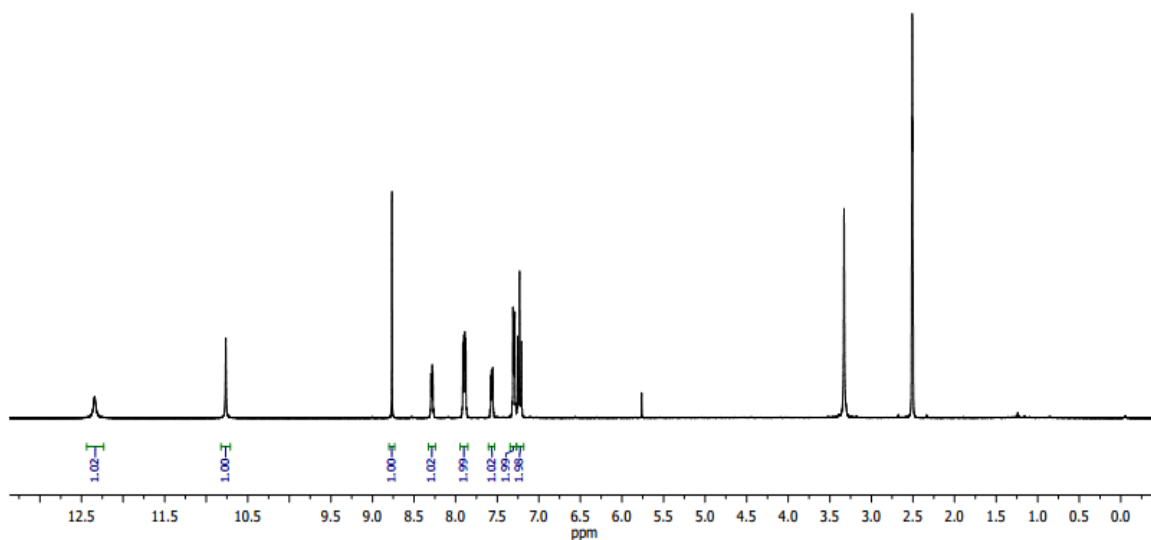


Signal: Ref=off					
RT [min]	Type	Width [min]	Area	Height	Area% Name
1.667	BV	0.2634	47.7660	3.2704	0.2046
1.851	vv	0.1474	67.1017	7.4799	0.2874
1.990	VB	0.1625	68.4144	10.5122	0.2931
2.354	BB	0.9100	403.0403	16.5580	1.7264
10.609	BV	1.0416	73.2359	2.0434	0.3137
14.916	vv	0.4560	76.3983	10.3474	0.3273
16.291	BV	0.7380	22533.2593	2628.9282	96.5211
16.692	vv	0.2910	59.9259	5.7185	0.2567
24.898	BV	0.4250	16.2819	1.7399	0.0697
		Sum	23345.4238		
Signal: Ref=off					
RT [min]	Type	Width [min]	Area	Height	Area% Name
1.667	BV	0.2819	61.0574	4.1613	0.2992
1.850	vv	0.1479	79.2176	8.8186	0.3882
1.988	VB	0.1635	79.5057	12.1883	0.3896
2.354	BB	0.5900	316.3372	16.8391	1.5503
14.100	BV	0.4014	24.3421	1.9888	0.1193
14.456	vv	0.4033	34.1239	1.9724	0.1672
14.915	VB	0.6708	131.1541	16.8688	0.6428
16.291	BV	0.7149	19532.0775	2369.6466	95.7226
16.687	vv	0.2674	50.8838	4.7220	0.2494
16.990	VB	0.4068	37.7589	2.5682	o. 1850
19.628	BV	0.2433	11.2584	1.7910	0.0552
19.953	VB	0.4517	28.7763	4.6951	0.1410
21.880	BB	0.4083	18.3875	2.2943	0.0901
		Sum	20404.8805		

AM3000917 1H Proton d6-DMSO 9/11/2020



¹H NMR (400 MHz, DMSO) δ 12.34 (1H, br s, NH), 10.76 (1H, s, NH), 8.77 (1H, s, CH), 8.32 – 8.25 (1H, m, CH), 7.96 – 7.84 (2H, m, 2 × CH), 7.63 – 7.50 (1H, m, CH), 7.33 – 7.27 (2H, m, 2 × CH), 7.27 – 7.19 (2H, m, 2 × CH).



AM3000917 13C Carbon d6-DMSO 9/11/2020

Appendix I

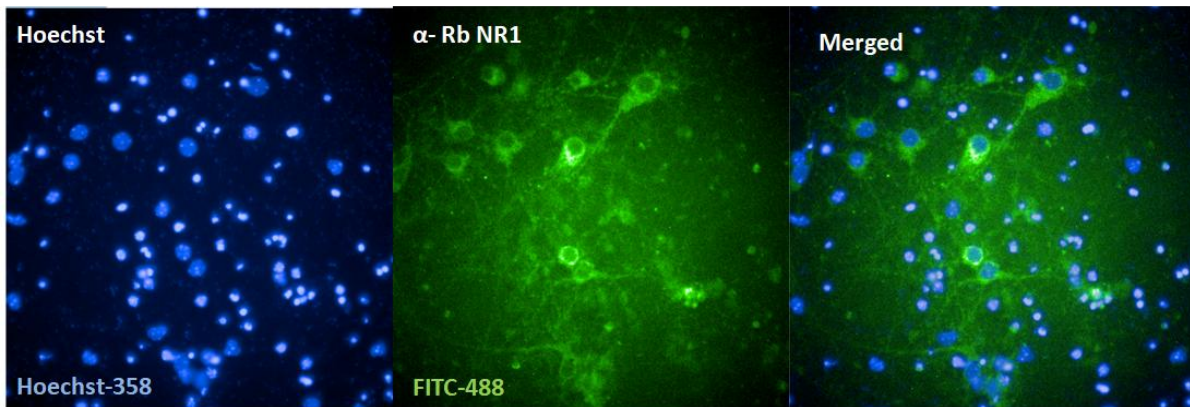


Figure 5.11 The immunocytochemistry and immunofluorescence evaluation of mouse primary cortical neurons

Targeting NMDA NR1 with the purified monoclonal rabbit antibody and 488-conjugated with the anti-goat igG secondary antibody (green) at 1:1000 and counterstained with Hoechst 33342 solution (blue), which shows the nucleus within the cells. Incell 2000 was used to obtain the images of the neuron. The cells were fixed with paraformaldehyde (4%) and permeabilised using Triton X-100 (0.1%).

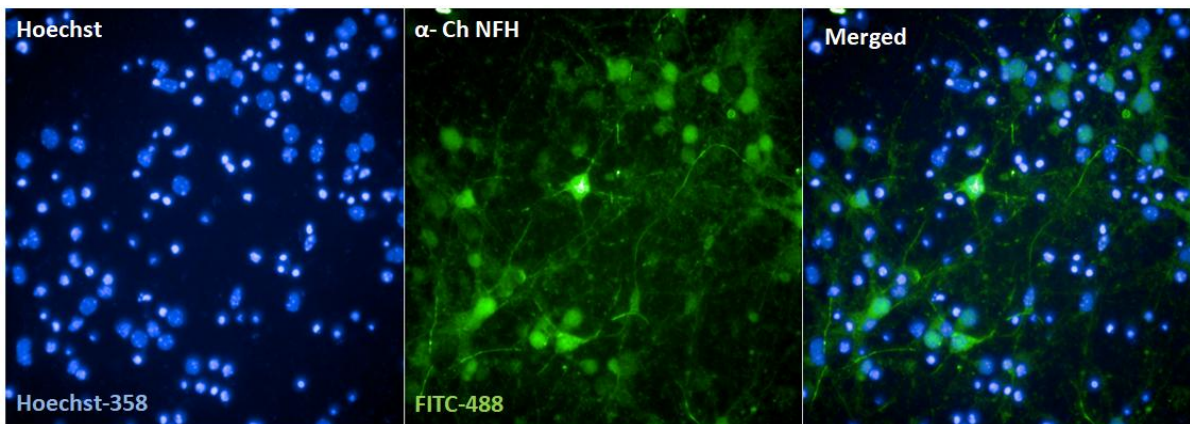


Figure 5.12 The immunocytochemistry to determine the axon density in mouse primary cortical neurons

The mouse cortical neurons on day 10 were initially fixed and stained for using neurofilament-H (green) at 1:1000 and counterstained with hoechst 33342 solution (blue), which shows the nucleus within the cells. Incell 2000 was used to obtain the images of the neuron. The images illustrate the abundant axon networks in the culture. The cells were fixed with paraformaldehyde (4%) and permeabilised using Triton X-100 (0.1%).

Appendix J

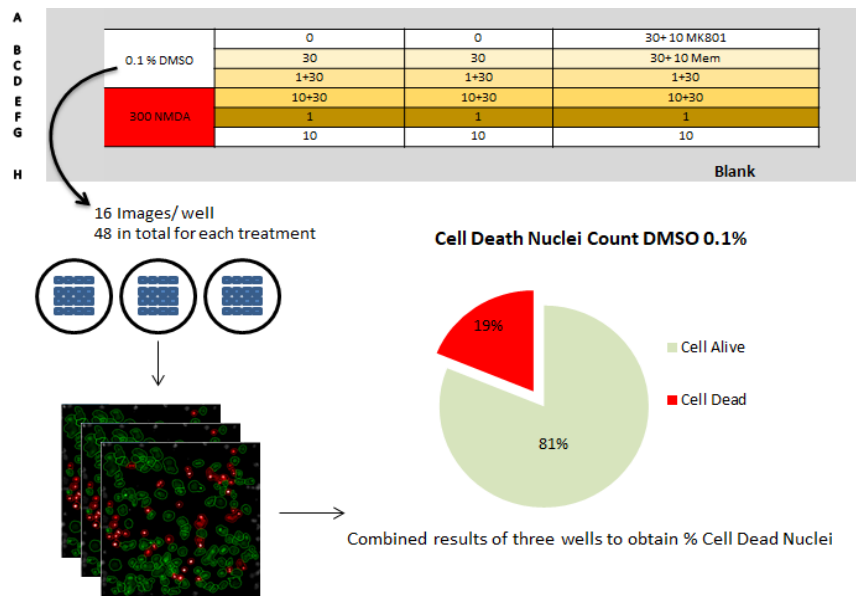


Figure 5.13. Image analysis of the NMDAR toxicity assay.

There were a total of three wells/treatments and by using InCell 200 16 images were taken from each well. Using Columbus, the number of alive and dead nuclei was then identified and filters were applied to exclude the nuclei on the edge of the images and areas of cell overlap to ensure better consistency throughout the data. Next the total number of alive and dead nuclei in each well were then combined and normalised to the total number of cells per well.

Appendix K

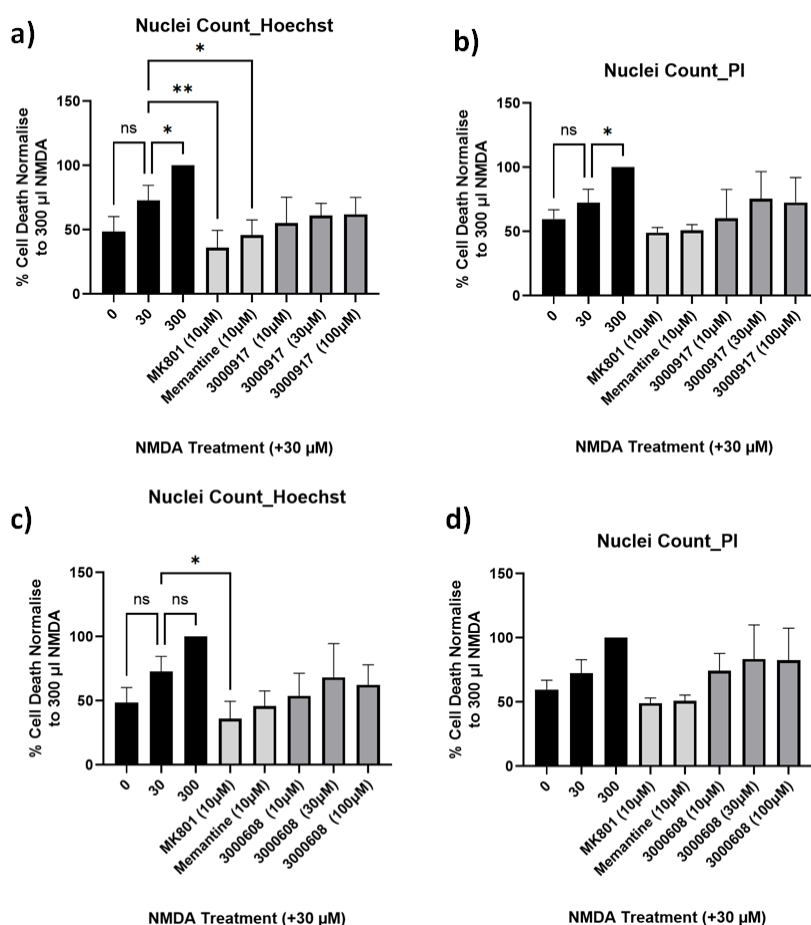


Figure 5.14. The dose response performed with NMDAR induced cytotoxicity for compounds 3000917 and 3000608 demonstrate no neuroprotection.

5.14a) Hoechst staining of dose response of 3000917 at 10 µM, 30 µM and 100 µM. One-way ANOVA, 0 vs 30 non significant, 30 vs 300 * $p=0.0273$, 30 vs. MK801 ** $p=0.0049$ value and 30 vs. Memantine * $p=0.0487$ **5.14b)** Nuclei standing with PI for 3000917. One-way ANOVA. 30 vs 300 * $p=0.0400$. **5.14c)** The dose response of compound 3000608 using hoechst staining. One-way ANOVA, 30 vs MK801 * $p=0.0013$ **5.14d)** PI staining for 300608. One-way ANOVA. For treatments 0, 30 and 300 $n=4$, The technical repeats for 0 µM and 30 µM is 6 wells per condition/experiment. The technical repeats for 300 µM, MK801, memantine and compound concentrations $n=3$, treated cells were 3 wells per condition/experiment. All data demonstrated as mean \pm SD.

[Type text]